Diffraction and database analyses of photoactive biphenyl compounds and novel carbaborane structures

Mackinnon, Angus

DIFFRACTION AND DATABASE ANALYSES OF PHOTOACTIVE BIPHENYL COMPOUNDS AND NOVEL CARBABORANE STRUCTURES.

Angus MacKinnon

Thesis submitted in part fulfilment of the requirements for the degree of

Doctor of Philosophy
at the
University of Durham

Department of Chemistry
September 1999.

The work described in this thesis was carried out in the Department of Chemistry at the University of Durham between October 1995 and September 1998, under the supervision of Prof. Judith A. K. Howard. All the work is my own, unless otherwise stated, and has not been submitted previously for a degree at this, or any other University.

Angus MacKinnon

ABSTRACT.

The research involved in this thesis is mainly concerned with crystallography and the analysis using crystallographic techniques and methods.

The work in this thesis is centered mainly on two types of chemical compounds, photoactive compounds and carbaboranes.

The first is the photoactive compounds of biphenyl, its derivatives and similar compounds; these compounds have been studied by diffraction and database analysis. The photochemistry and subsequent structural analysis of biphenyls has been studied in collaboration with Professor Peter Wan at the University of Victoria, Canada. In this study Professor Wan and his group conducted all synthesis and spectroscopic analysis, including the photochemical analysis.

In a similar study although not with biphenyls, the α-azidocinnamates were investigated in collaboration with Professor Meth-Cohn of the University of Sunderland. Professor Meth-Cohn and his group conducted all synthesis and spectroscopic analysis.

The biphenyl type compounds have also been studied using database analysis to examine the bond lengths, torsion angles, inter-/intra–molecular interactions and general packing conformations and interactions within these structures and this analysis was used to study several conformational anomalies that exist in biphenyl derivative compounds.

The second chemical type is carbaboranes; these compounds have been examined in collaboration with Professor Wade's group at the University of Durham. The analysis of carbaboranes centers mainly on hydrogen bonding however also expands into several novel carbaborane structures. Professor Wade and his group carried out the synthesis and spectroscopic analysis.

CONTENTS

CHAPTER 1: INTRODUCTION **1**

1.1 INTRODUCTION. 1

1.2 REFERENCES 3

CHAPTER 2: DIFFRACTION, X-RAYS, NEUTRONS AND STRUCTURE DETERMINATION **4**

2.1 SINGLE CRYSTAL DIFFRACTION 4

2.2 X-RAY DIFFRACTION EXPERIMENTATION, EQUIPMENT AND TECHNIQUES. 7

2.3 THE RIGAKU AFC6S 11

2.4 THE SIEMENS SMART-CCD DIFFRACTOMETER 15

2.5 THE ABSORPTION CORRECTION 19

2.6 THE DECAY CORRECTION 20

2.7 THE EXTINCTION CORRECTION 21

2.8 SPACE GROUP DETERMINATION 22

2.9 SOLVING THE STRUCTURE 23

2.10 REFINEMENT 25

2.11 NEUTRON DIFFRACTION 26

2.12 REFERENCES 32

CHAPTER 3: THE CAMBRIDGE STRUCTURAL DATABASE: AN INTRODUCTION. **33**

3.1 INTRODUCTION 33

3.2 THE CAMBRIDGE STRUCTURAL DATABASE SYSTEM (CSDS) 35

3.3 SOFTWARE 37

3.4 RESEARCH APPLICATIONS OF THE CSDS 41

3.5 THE SEARCHES CONDUCTED ON THE CSDS (EXPERIMENTAL SECTION) 43

3.6 REFERENCES 48

CHAPTER 4: AN INTRODUCTION TO ASPECTS OF PHOTOCHEMISTRY **50**

4.1 INTRODUCTION 50

4.2 ACID BASE PROPERTIES 55

4.3 PROTON TRANSFERS 56

4.4 MOLECULAR GEOMETRY, FLUORESCENCE EMISSION SPECTRA AND SPECTROSCOPIC BEHAVIOR. 58
4.5 ALTERING MOLECULAR GEOMETRY OF BIPHENYLS 59
4.6 REFERENCES 60

CHAPTER 5: BIPHENYL AND DERIVATIVE COMPOUNDS 61
5.1 INTRODUCTION 61
5.2 THE ULTRA VIOLET SPECTRA OF BIPHENYL TYPE COMPOUNDS 65
5.3 PHOTOCHEMICAL ASPECTS OF BIPHENYL AND DERIVATIVES 66
5.4 THE X-RAY DIFFRACTION STRUCTURE OF BIPHENYL AND DERIVATIVE COMPOUNDS 67
5.5 REFERENCES 82

CHAPTER 6: SOLID STATE AND SOLUTION PHASE PHOTOCYCLIZATION OF α,α-2-(2'HYDROXYPHENYL) BENZYL ALCOHOL 84
6.1 INTRODUCTION 84
6.2 BACKGROUND 87
6.3 EXPERIMENTAL DETAILS 88
6.4. RESULTS AND DISCUSSION 92
6.5 NEUTRON DIFFRACTION STUDY 100
6.6 SUMMARY 104
6.7 REFERENCES 105

CHAPTER 7: A STUDY OF PHOTOREACTIVE BIARYL MOLECULES 107
7.1 AN INTRODUCTION TO BIARYL METHANOLS WITH NAPHTHALENE RING(S) 107
7.2 PHOTOCYCLIZATION IN THE SOLID STATE. 109
7.3 2-[2'-(HYDROXYMETHYL)-1'-NAPHTHYL]PHENOL] (1) 111
7.4 2-HYDROXY-2'-HYDROXYMETHYL-1,1'-BINAPHTHYL (2) 115
7.5 1-[2'-(HYDROXYMETHYL)PHENYL]-2-NAPHTHOL (3) 118
7.6 SUMMARY AND DISCUSSION 122
7.7 REFERENCES 125

CHAPTER 8: QUINONE METHIDES **126**
8.1 INTRODUCTION 126
8.2 PHOTOGENERATION OF QUINONE METHIDES FROM HYDROXYBENZYL ALCOHOLS 128
8.3 TRIPHENYL ALCOHOL (2) 129
8.4 SYNTHESIS AND ANALYSIS OF THE STRUCTURES OF (1), (2), (3) AND (4) 130
8.5 STRUCTURAL X-RAY DIFFRACTION ANALYSIS 132
8.6 PHOTOLYSIS IN AQUEOUS METHANOL 136
8.7 PROPOSED MECHANISM FOR (1) TO (6) 137
8.8 PROPOSED MECHANISM FOR (4) TO (8) 139
8.9 PROPOSED MECHANISM FOR (2) TO (7) 140
8.10 REFERENCES 141

CHAPTER 9: A REINVESTIGATION OF THE PHOTOCHEMISTRY OF A-AZIDOCINNAMATES **142**
9.1 INTRODUCTION 142
9.2 RESULTS AND DISCUSSION 144
9.3 EXPERIMENTAL 151
9.4 GENERAL METHOD FOR THE PHOTOLYSES OF α-AZIDOCINNAMATES 152
9.5 REFERENCES 154

CHAPTER 10: THE TWISTING OF *ORTHO, ORTHO'*-BIPHENYL COMPOUNDS, AN ANALYSIS USING THE CSD **155**
10.1 INTRODUCTION 155
10.2 RESULTS AND DISCUSSION USING THE CSD 159
10.3 SUMMARY 170
10.4 REFERENCES 174

CHAPTER 11: THE TWISTING OF BIPHENYL WITH HYDROGEN ATOMS AT THE *ORTHO* POSITION **175**
11.1 INTRODUCTION. 175
11.2 THE STRUCTURE CORRELATION METHOD 176
11.3 NON *ORTHO* SUBSTITUTED BIPHENYLS AND THE STRUCTURE CORRELATION METHOD 178

11.4 DATABASE STUDY OF NON-*ORTHO* SUBSTITUTED BIPHENYLS 180
11.5 SUMMARY OF NON-ORTHO SUBSTITUTED BIPHENYLS 190
11.6 REFERENCES 192

CHAPTER 12: THE OVERALL EFFECT OF *PARA* AND *META* SUBSTITUTION ON BIPHENYLS. 193
12.1 INTRODUCTION 193
12.2 NO *PARA* SUBSTITUENTS PRESENT ON THE RINGS 195
12.3 BIPHENYLS WITH ONE *PARA* SUBSTITUENT 202
12.4 DI-*PARA* SUBSTITUTION ON BIPHENYLS 208
12.5 META SUBSTITUTED BIPHENYLS 213
12.6 SUMMARY OF *ORTHO, META* AND *PARA* SUBSTITUTION ON BIPHENYLS 216

CHAPTER 13: THE INTRA-MOLECULAR BOND LENGTHS OF SUBSTITUTED BIPHENYLS 219
13.1 INTRODUCTION 219
13.2 THE C-C LINKAGE BOND 221
13.3 THE INTRA RING BOND DISTANCES 222
13.4 THE BOND DISTANCES OF BIPHENYL 223
13.5 THE EFFECT OF *PARA* SUBSTITUTION ON THE INTRA RING DISTANCES OF BIPHENYLS 224
13.6 THE EFFECT OF *META* SUBSTITUTION ON THE INTER RING DISTANCES OF BIPHENYLS 227
13.7 THE EFFECT OF *ORTHO* SUBSTITUTION ON THE INTRA BOND LENGTHS OF BIPHENYLS 233
13.8 OTHER RING SUBSTITUTION 234
13.9 SUMMARY AND CONCLUSION 235
13.10 REFERENCES 237

CHAPTER 14: AN INTRODUCTION TO CARBABORANES 238
14.1 INTRODUCTION 238
14.2 THE BONDING OF BORON HYDRIDE CLUSTERS 239
14.3 THE ELECTRONIC DISTRIBUTION 242
14.4 NOMENCLATURE 243

14.5 PROPERTIES OF CARBORANES 244
14.6 CARBORANE SYNTHESIS 246
14.7 APPLICATIONS OF CARBORANES 247
14.8 CARBORNES IN THIS THESIS 248
14.9 REFERENCES 249

CHAPTER 15: DEFINITIVE CRYSTAL STRUCTURES OF ORTHO, META AND CARBORANES:SUPRAMOLECULAR STRUCTURES DIRECTED SOLELY BY C-H···O HYDROGEN BONDING. 251
15.1 INTRODUCTION 251
15.2 CHARACTERISATION 253
15.3 PRELIMINARY CHARACTERISATION 254
15.4 THE X-RAY DIFFRACTION ANALYSIS OF THE *ORTHO*, *META* AND *PARA* CARBORANE MOLECULES WITH HMPA. 256
15.5 CONCLUSION 262
15.6 REFERENCES 263

CHAPTER 16: HYDROGEN BONDING IN HETEROAROMATIC CARBORANES 264
16.1 INTRODUCTION 264
16.2 THE STRUCTURE OF 1-(2-PYRIDYL)-*ORTHO*-CARBORANE 266
16.3 THE STRUCTURE OF 1-(3'-PYRIDYL)-*ORTHO*-CARBORANE 268
16.4 THE STRUCTURE OF 1-(2'-THIOPHENYL)-*ORTHO*-CARBORANE. 270
16.5 THE STRUCTURE OF 1-(2-PYRIDYL)-Z(TRIMETHYLSTANNYL) *ORTHO*CARBORANE /$SNME_3$ 274
16.6 SUMMARY 277
16.7 REFERENCES 279

CHAPTER 17 NON HYDROGEN BONDING CARBORANES. 280
17.1 INTRODUCTION 280
17.2 THE DEBORANATION OF *ORTHO*-CARBORANE BY AN IMINOPHOSPHPHORANE: A NOVEL CARBORANE AND THE BORENIUM ADDUCT. 281
17.3 CARBORANES WITH NO INTER-MOLECULAR INTERACTIONS PRESENT. 286

17.4 SUMMARY 290
17.5 REFERENCES 291

CHAPTER18: AN INVESTIGATION INTO SYMMETRICAL TRIAZINES 292
18.1 INTRODUCTION 292
18.2 SYMMETRICALLY SUBSTITUTED TRIAZINES 294
18.3 PROPERTIES OF TRIAZINE COMPOUNDS 296
18.4 DIFFRACTION OF TRIAZINES 298
18.5 HIGH PRESSURE EXPERIMENTS 303
18.6 SUMMARY 304
18.7 REFERENCES 306

POST GRADUATE COLLOQUIA, LECTURES AND SEMINARS FROM INVITED SPEAKERS 307

ACKOWLEDGEMENTS 316

LIST OF FIGURES

Figure 2.1 The Bragg diffraction for 3-Dimensional space 6

Figure 2.2 The spectrum of wavelengths against intensity of a typical the X-ray tube 6

Figure 2.3 Simple schematic representation of a 4-Circle diffractometer 7

Figure 2.4 Extinction: a) Primary and b) Secondary 21

Figure 3.1 The drawing stage of a fragment in QUEST3D (Here showing a biphenyl fragment) 38

Figure 3.2 Various graphical outputs of the VISTA program: a) histogram, b) radial scatterplot and c) combined radial histogram and scatterplot 39

Figure 3.3 PLUTO screen (showing the inter-molecular interactions in the structure with the Refcode BPHCOY10) 40

Figure 3.4 An example of the biphenyl fragment for the CSDS 43

Figure 3.5 Problematic searching fragments 44

Figure 3.6 The *o,o'*-substituted biphenyls fragment 45

Figure 3.7 The non *ortho*-substituted biphenyl fragment 45

Figure 3.8 The Heteroaromatic fragment, where AA refers to any atom 46

Figure 3.9 The biphenyl fragment 46

Figure 4.1 Representation of structures (1), (2), (3) and (4) 53

Figure 5.1. The chemical structure of the biphenyl molecule 62

Figure 5.2 Showing the steric crowding of the *ortho* substituents on planar biphenyls 64

Figure 5.3 Thermal ellipsoid plot of biphenyl at 40 K, showing 50% probability 68

Figure 5.4 The space filled view of the X-ray diffraction structure of biphenyl (1) 69

Figure 5.5a The packing structure of biphenyl (1), showing the layered structure 69

Figure 5.5b Packing structure of biphenyl (1), viewed perpendicular to the plane of the rings 70

Figure 5.5c Packing of biphenyl (1), showing the relative orientation of the ring planes 70

Figure 5.6 The structure of 4, 4'-bipyridyl (2), with disordered H_2O present 72

Figure 5.7 The packing of 4, 4'-bipyridyl/H_2O, showing the inter-molecular interaction between the water and bipyridyl nitrogens. 72

Figure 5.8 The represented structure of 4-biphenylcarboxilic acid (3) 73

Figure 5.9 The thermal ellipsoid plot at 50% probability of the independent units of biphenylcarboxylic acid (3) 74

Figure 5.10 The expanded structure of 4-biphenylcarboxylic acid (3) showing all the hydrogen bonding present in the structure 75
Figure 5.11 The packing structure of 4-biphenylcarboxylic acid (3) 75
Figure 5.12 The structure of 4,4'-dihydroxybiphenyl (4), with 50% thermal ellipsoids. 76
Figure 5.13 The packing of 4,4'-dihydroxybiphenyl, showing the layered structure. 77
Figure 5.14 The hydrogen bonding structure of 4,4'-dihydroxybiphenyl (4) 77
Figure 5.15 The thermal ellipsoid plot of 2-hydroxy-3'-methoxybiphenyl (5), with 50% probability 78
Figure 5.16 The packing of structure of (5), looking down through on the layered structure 79

Figure 6.1 Scheme 1 representing the photoreaction (1) to (2) and (4) 84
Figure 6.2 Structural representation of (5),(6),(7) and (8) 85
Figure 6.3 The scheme for the Photolysis of (1) to (10) 90
Figure 6.4 The thermal ellipsoid plot of (5), with 50% probability 95
Figure 6.5 The hydrogen bonded structure of (5) 95
Figure 6.6 The thermal ellipsoid plot of (7), with 50% probability 97
Figure 6.7 Scheme 2, possible mechanism representing (5) to (7) 98
Figure 6.8 The thermal ellipsoid plot of (5), with neutron data, 50% probability 102
Figure 6.9 The dimers of (5) plotted with neutron diffraction data 102

Figure 7.1 The Biaryl molecules (1) 2-[2'-(Hydroxymethyl)-1'-Naphthal]phenol, (2) 2-Hydroxy-2'-hydroxymethyl-1,1'-Binaphthyl and (3) 1-[2'(Hydroxymethyl)phenyl]-2-naphthol 107
Figure 7.2 The reaction scheme to produce compound (1) 108
Figure 7.3 The reaction scheme to produce compound (2) 110
Figure 7.4 The structure of 2-[2'-(hydroxymethyl)-l'-naphthyl]phenol (1), with 50% thermal ellipsoid plot 112
Figure 7.5 The probable side product (17) 113
Figure 7.6 The photocyclization reaction of (1) to (15) 114
Figure 7.7 The structure of 2-Hydroxy-2'-Hydroxymethyl-1,1'-Binaphth (2), with 50% thermal ellipsoids, showing the disordered O12 and O12B 116
Figure 7.8 The photocyclization reaction from (2) to (24) 117
Figure 7.9 The reaction scheme to product (3) 119

Figure 7.10 The two independent structures of 1-[2'-(hydroxymethyl)phenyl]-2-naphthol (3), with 50% thermal ellipsoids 120
Figure 7.11 The photocyclization reaction of (3) to (23) 121

Figure 8.1 Photolysis reaction of (1), R=Ph and (3), R=H 126
Figure 8.2 The structures of (2) and (4) 127
Figure 8.3 [4+2] Diels-Alder photoreaction of (1) to (5) 128
Figure 8.4 The synthesis of (4) 130
Figure 8.5 The structure of α-phenyl-*o*-hydroxybenzyl alcohol (1), with 50% thermal ellipsoids. 132
Figure 8.6 The structure of (2), showing the intra-molecular interaction, with 50% thermal ellipsoids 133
Figure 8.7 The dimeric structure of (2) 134
Figure 8.8 The structure of (4), with 50% thermal ellipsoid plots 135
Figure 8.9 The reaction of (1) to (6) 138
Figure 8.10 the mechanism for (4) to (8) 139
Figure 8.11 The proposed mechanism of (2) to (7) 140

Figure 9.1 Scheme 1, representing the photreaction mechanism from (1) to (4) 143
Figure 9.2 X-ray Structure of compound (3Aa), with thermal ellipsoid probability 50% 146
Figure 9.3 Scheme 2, the mechanism for (3) to (5) 147
Figure 9.4 Scheme 3 147
Figure 9.5 X-ray structure of compound (5), with thermal ellipsoid probability of 50% 148
Figure 9.6 Scheme 4, the reaction of (3A) to (3B) and to (4) 149
Figure 9.7 Scheme 5 150

Figure 10.1 The positions of biphenyl, 1=*ipso*, 2=6=*ortho*, 3=5=*meta*, 4=*para*. 156
Figure 10.2 The *cis* and *trans* conformations of o-o'-substituted biphenyls, looking down the C-C axis. X and H represent the substituted side and non-substituted sides respectively. 157
Figure 10.3 Dihedral angle distribution of all *o-o*'-biphenyls 160
Figure 10.4 Biphenyls that contain *ortho* substituents only 162
Figure 10.5 Biphenyls containing *ortho* and *meta* substituents 163
Figure 10.6 The dihedral angle range *o,o*-substituted biphenyls with *meta* and *para* substituents 164

Figure 10.7 Carbon atom(s) at the *ortho* position(s) of *o,o'*-substituted biphenyls 166
Figure 10.8 Oxygen atom(s) at the *ortho* position(s) of *o,o'*-substituted biphenyls 168

Figure 11.1. The non *ortho* substituted biphenyl, here A, B, C, D, E and F are any atoms (including Hydrogen). 179
Figure 11.2 All non-*ortho* substituted biphenyls. 181
Figure 11.3 the Distribution of torsion angles for 0, 1 and 2 *para* substituted biphenyls 182
Figure 11.4 Bi-*para* substituted biphenyl, where P may equal P' 182
Figure 11.5 Biphenyls containing two *para* substituents. 183
Figure 11.6 Biphenyls with two *para* but no *meta* substituents 184
Figure 11.7 Biphenyls with one *para* and no *meta* substituents 185
Figure 11.8 Biphenyls with one *para* substituent with *meta* substituents on the same ring 186
Figure 11.9 The *meta* substitution positions of biphenyl 187
Figure 11.10 The distribution of torsion angles for biphenyls containing *meta* substituents 188

Figure 12.1 Biphenyls with *para* substituents 194
Figure 12.2 No *para* substituted biphenyls with and without *meta* substituents. 195
Figure 12.3 Non *para* and *meta* biphenyls with one *ortho* substituent 197
Figure 12.4 Non *para* substituted biphenyls with two *ortho* substituents on different rings 198
Figure 12.5 Biphenyls with *meta* but no *ortho* or *para* substituents 199
Figure 12.6 Biphenyls with *meta*, one *ortho* and no *para* substituents 200
Figure 12.7 Biphenyls with one p*ara* substituent 203
Figure 12.8 Biphenyls with one *para* and *meta* , but no *ortho*, substituents 205
Figure 12.9 Biphenyls with one *ortho* substituent containing *meta* and one *para*. 206
Figure 12.10 Mono *para* substituted biphenyl with *meta* and two *ortho* substituents 207
Figure 12.11 Two *para* substituted biphenyls 208
Figure 12.12 Two *para* substituted biphenyls with no *ortho* or *meta* substituents 209
Figure 12.13 Bi-*para* biphenyls with *meta* substituents, with all four *ortho* positions occupied. 212
Figure 12.14 Biphenyls with one *meta* substituent 213
Figure 12.15 Biphenyls with two *meta* substituents 214
Figure 12.16 The percentage of biphenyls with 1-4 *meta* substituents within given ranges of torsion angles. 215

Figure 13.1 Biphenyl with the bond between the two rings illustrated 216

Figure 13.2 Biphenyl intra bond distances, when X=Y; α=α', β=β' and γ=γ' 224
Figure 13.3a Representation of the mean values for non-*para* substituted biphenyls, (All figures in Å) 226
Figure 13.3b Representing the mean values for mono *para* substituted biphenyls (All figures in Å), where X ≠H 226
Figure 13.3c Representing the mean values for doubly *para* substituted biphenyls (All figures in Å), where X ≠ H and X' ≠ H (note X may not equal X') 226
Figure 13.4 Representing the mean values for non-*meta* substituted biphenyls (All figures in Å) 227
Figure 13.5 Representing the mean values for mono-*meta* substituted biphenyls (All figures in Å) 228
Figure 13.6 Representing the mean values for bi-*meta* substituted biphenyls, with the *meta* substituents on the same ring (All figures in Å) 229
Figure 13.7 Representing the mean values for bi-*meta* substituted biphenyls, with the *meta* substituents on different ring (All figures in Å) 229
Figure 13.8 Representing the mean values for tri-*meta* substituted biphenyls (All figures in Å) 230
Figure 13.9 Representing the mean values for tetra-*meta* substituted biphenyls (All figures in Å) 230

Figure 14.1 The bonding in diborane 240
Figure 14.2 The removal of a BH^{2+} vertex 240
Figure 14.3 The isomers of $B_{10}C_2H_{12}$. a = *ortho*, b = *meta* and c = *para* 241
Figure 14.4 The numbering scheme of boron hydride cages, with a = the *closo* cage and b = *nido*. 243

Figure 15.1 Molecular structure of the dimer unit of *ortho*carborane/HMPA, with 50% thermal ellipsoid probability 256
Figure15.2 The packing of *ortho*carborane/HMPA 257
Figure 15.3 Molecular structure of *meta* carborane/HMPA, 50% thermal ellipsoid plot 258
Figure 15.4 The polymeric structures of *meta* carborane with HMPA. 258
Figure 15.5 X-ray structure of *para*carborane/HMPA, 50% thermal ellipsoid plot 259
Figure 15.6 The polymeric structures of *para* and *meta* carboranes with HMPA. 260

Figure 16.1 The structure of 1-(2-pyridyl)-*ortho*carborane 266
(for clarity hydrogen atoms not shown)
Figure 16.2 The crystal structure of 1-(2-pyridyl)-*ortho*carborane, with 50% probability) 267
Figure 16.3 Packing diagram of 1-(2-pyridyl)-*ortho*carborane 267
Figure 16.4 The structure of 1-(3'-pyridyl)-*ortho*-carborane (hydrogen atoms not shown) 268
Figure 16.5 The structure of 1-(3'-pyridyl)-*ortho*-carborane 269
Figure 16.6 The Packing of 1-(3'-pyridyl)-*ortho*-carborane 269
Figure 16.7 The structure of 1-(2'-thiophenyl)-*ortho*-carborane 270
(hydrogen atoms not shown)
Figure 16.8 The Envisaged hydrogen bonding of 1-(2'-thiophenyl)-*ortho*-carborane 270
(a) intra-molecular and (b) inter-molecular hydrogen bonding
Figure 16.9 The structure of 1-(2'-thiophenyl)-*ortho*-carborane 271
Figure 16.10 The packing structure of 1-(2'-thiophenyl)-*ortho*-carborane viewed 272
down the rings
Figure 16.11 The packing structure of 1-(2'-thiophenyl)-*ortho*-carborane 273
view of rings side on
Figure 16.12 The structure of 1-(2-pyridyl)-2-(trimethylstannyl) *ortho*carborane /$SnMe_3$ 274
Figure 16.13 The X-ray diffraction structure of 275
1-(2-pyridyl)-2-(trimethylstannyl *ortho*carborane
/SnMe3, with a probability of 50%.
Figure 16.14 The packing structure of 1-(2-pyridyl)-2-(trimethylstannyl) 276
*ortho*carborane /$SnMe_3$

Figure 17.1 Scheme 1, The reaction of (1) to (2) 282
Figure 17.2 Scheme 2, The reaction scheme from structure (1) to (3), (4), (5) and (6) 282
Figure 17.3 X-ray diffraction structure of (3), with 50% probability 284
Figure 17.4 the X-ray structure of (6), with 50% probability 285
Figure 17.5 1,2-bis({1,2-diphenyl})*ortho*carborane (7) and 286
1,2-bis({1,2-di-2'-picolyl}ethyl)*ortho*carborane (8)
Figure 17.6 The asymmetric unit of (7) 287
Figure 17.7 The structure of (7) 287
Figure 17.8 The structure of 1,4-di(phenyl*ortho*carboranyl)benzene (9) 288
Figure 17.9 The X-ray diffraction structure of (9) 289
Figure 17.10 The X-ray structure of (10) 289

Figure 18.1 The three triazine isomers, a) 1,2,3-triazine, b) 1,2,4-triazine and c) 1,3,5-triazine 292

Figure 18.2 The two possible isomers of 1, 3, 5-triazines 298

Figure 18.3 The structure of 2,4,6-tris-(2'-diphenyl-*ortho*-carboranyl)- 1,3,5-triazine, single unit, with thermal ellipsoid probability of 50 % 299

Figure 18.4 The structure of 2,4,6-tris-(2'-diphenyl-*ortho*-carboranyl)- 1,3,5-triazine expanded for the whole molecule, clearly showing the three fold symmetry. 299

Figure 18.5 The structure of 2,4,6-tris-(12'-phenyl-*para*-carboryl)-1,3,5-triazine with 50% thermal ellipsoids. Disordered solvent is not shown. 302

LIST OF TABLES

Table 5.1 The bond distances of biphenyl at 40 ± 2 K 70

Table 5.2 The Crystallographic data for structures (1)-(5) :* is without the disordered solvent 80

Table 6.1 X-ray crystal data for structures (5) and (7) 94

Table 6.2 The Neutron diffraction data for (5) 103

Table 7.1 X-ray Diffraction data for (1), (2) and (3) 124

Table 9.1 Products from the photolysis of azidocinnamates, P =Light petroleum, A = Acetone, Py = Pyrex and Q = Quartz . 145

Table 9.2 Diffraction data for compounds (3A) and (5) 153

Table 10.1 Summary of Biphenyl conformations with positional variation of substituents 172

Table 10.2 Summary of Biphenyl conformations with substitutional variation 173

Table 11.1 The dihedral angle distribution of *para* substituted non-*ortho* biphenyls 191

Table 11.2 The dihedral angle distribution of *meta* substituted non-*ortho* substituted biphenyls 191

Table 12.1 The distribution of *meta* substituted biphenyls 217

Table 12.2 The distribution of *ortho* substituted biphenyls 218

Table 13.1 Mean bond lengths of *para* substituted biphenyls (All figures in Å) 225

Table 13.2 The average bond lengths of the symmetrically substituted *meta* biphenyls with zero and four substituents. 231

Table 13.3 The average bond lengths of the asymmetrically substituted biphenyls 232

Table 14.1 The cage structure types and related number of skeletal electron pairs 243

Table 15.1 Selected inter-molecular bond lengths and angles of *meta* and *para* carboranes/HMPA 260

Table 15.2 Summary of crystallographic data of the three datasets 261

Table 16.1 Crystallographic data for the structures in this chapter 278

Table 17.1 Selected bond lengths of (3) 283

Table 18.1 Summary of selected bond lengths and torsion angles 300

Table 18.2 X-ray diffraction data 305

ABREVIATIONS

BNCT	=	Boron Neutron Capture Therapy
CCD	=	Charge Couple Device
CFOM	=	Combined Figure of Merit
CSD	=	Cambridge Structural Database
CSDS	=	Cambridge Structural Database system
ESD	=	Estimated Standard Deviation
ESIerPT	=	Inter-molecular Excited State Proton Transfer
ESIraPT	=	Intra-molecular Excited State Proton Transfer
ESPT	=	Excited State Proton Transfer
GC	=	Gas Chromatography
HMPA	=	Hexamethylphosphoramide
HMO	=	Hückel Molecular Orbital
HOMO	=	Highest Occupied Molecular Orbital
ICSD	=	Inorganic Crystal Structure Database
ILL	=	Institut Max von Laue – Paul Langevin
IR	=	Infra Red
LFP	=	Laser Flash Photolysis
LUMO	=	Lowest Unoccupied Molecular Orbital
MM	=	Molecular Mechanics
MO	=	Molecular Orbital
MS	=	Mass Spectroscopy
NDB	=	Nucleic acid Data Bank
NMR	=	Nuclear Magenetic Resonance
PDB	=	Protein Data Bank
PR	=	Pulse Radiolysis
PT	=	Proton Transfer
QM	=	Quinone Methide
THF	=	Tetrahydrofuran
TLC	=	Thin Layer Chromatography
UV	=	Ultra Violet
UV-Vis	=	Visible Ultra Violet

CHAPTER 1

1.1 INTRODUCTION.

The topics within this thesis are concentrated on structural analysis using a variety of methods. Their methods all involve diffraction either by X-rays or neutrons. For any of the work in this thesis to have taken place the discovery, use and experimentation of X-rays has had to be conducted and advanced. This is an ongoing process with great advancements been made and this has been the case for almost a century.

The discovery of X-rays and their diffraction led to the major advancement in science (medicine, physics, chemistry and many many more), most importantly to this thesis these advancements have fundamentally affected the field of chemistry. If it was not for the developments of diffraction techniques and subsequently the emergence of crystallography then we would still have distinct problems in structural analysis. The development of techniques including NMR and spectroscopy is largely dependent on validation using crystallographic data. Stereochemical knowledge of optically active compounds owe much to crystallography. It was Bijvoet using anomalous scattering of X-rays to demonstrate the absolute structure of ± glyceraldehyde that confirmed the structure that Fischer had previously assigned to it. In essence, most structural analysis of the modern era owes a great deal to the scientists who pioneered and advanced the field of crystallography.

The use of X-rays and their diffraction is relatively modern. The first ever Nobel Prize in Physics was awarded to Wilhelm Conrad Röntgen in 1901 for his discovery and characterization of what were then called "Röntgenrays". The results of Conrad Röntgen's first experiments to determine the properties of this new radiation were initially described in his paper on the 28th December, 1895 (Röntgen, 1895). Röntgen called these new 'rays' "X-rays" to distinguish them from other types of 'rays'. Initially Röntgen could find little to link these new rays to the properties of visible light, despite some obvious similarities. Many of these differences (i.e. diffraction and refraction) were due to the small wavelength. However, he did find evidence of interference and became convinced of 'longitudinal vibrations' (Röntgen, 1895). The discovery of these new X-rays/Röntgenrays created a lot of public interest as well as in the scientific community (M^{c}Clure's Magazine, 1896). The nature of these rays were largely a mystery until Max Theodor Felix von Laue began to discover the properties of these X-rays/Röntgenrays. In 1914 Max Theodor Felix von Laue became a Nobel Laureate for his discovery of the diffraction of these "Röntgenrays" by a crystal. The significance of this work was twofold; it confirmed that X-rays/Röntgenrays displayed wave character and that a crystal is a symmetrical three-dimensional array of atoms that can act as a diffraction grating. This work was greeted with great interest and even before von Laue had received his Nobel Prize, work was already ongoing to use the diffraction phenomenon in the

elucidation of crystal structure. Debye was prominent in his assertion that the X-rays were being scattered by electrons. Debye and Scherrer attempted to determine the ionic charges in LiF (Debye and Scherrer, 1918), followed by a similar study by Bragg on NaCl (Bragg *et al*, 1922). Bragg also endeavored to use diffraction data to obtain an experimental description of the covalent bonding in diamond by calculating the diffracted intensities, which would result from the localized two-electron bonds in accord with the Lewis model (Bragg *et al*, 1921).
It is thus apparent that, right from the start, X-ray diffraction was recognized not only as a tool for the molecular structure determination in the sense of definite atomic positions, but also for the determination of the electronic structure, and therefore it would be of huge benefit for not only chemistry, but for all science.

In the modern laboratory the use of diffraction with X-rays has distinct advantages over other analytical techniques, including that of neutron diffraction. X-rays are easily produced in large quantities by relatively inexpensive equipment that is becoming increasingly easier to use. The diffractometers used can be adapted to include high pressure cells, laser excitation equipment and ultra low cooling devices, *etcetera*. The chemical samples used can be relatively small, a crystal for X-ray diffraction can be 100 times smaller than that used for neutron diffraction work and the crystal may be of much lower quality. The main advantage of X-ray analysis over other analytical techniques is that from a sample of a single crystal, where little is known about the structure, the result will be a definitive crystal structure where little is open to interpretation. Another advantage is that the sample can easily be recovered, unless it is air sensitive (where the recovery is much more difficult) or susceptible to X-ray damage (where the crystal will be destroyed).

In this body of research the majority of the analysis has been with X-ray diffraction data or the analysis of previous work done by X-ray diffraction. There has been some neutron diffraction work to compliment the X-ray data and also other analytical techniques have been conducted so as to obtain additional information, again to corroborate the X-ray diffraction.
For the structure and synthetic work of the photochemicals and the carboranes in this thesis, the defining part of the study has been with the use of X-ray diffraction. In the database study, the analysis takes a slightly different form, with the Cambridge Structural Database (CSD) being used to examine a collection of structures that have been found previously with X-ray or neutron analysis. The majority are X-ray studies since structure solving by this technique is much more common than that of neutron analysis.

The work in this thesis can be divided into several parts; although these parts are not strictly separate and some overlap (considerably), there are definite sections in this work, with photochemistry, biphenyls and carboranes.

Firstly the photochemical analysis of simple organic compounds, which is collaborative work that relies on several analytical techniques including the X-ray and neutron diffraction analysis to give definitive answers on the structural implications of the photochemical reaction involved. This work has been done in collaboration with Prof. Peter Wan and his group in the University of Victoria, Victoria, British Columbia, Canada, with the study of the photochemistry of α-Azidocinnamates in collaboration with Prof. Otto Meth-Cohn and Dr Nicola Williams of the University of Sunderland, UK. The second part is the database work done with the CSD. This section was inspired by the work in the first section on biphenyl and derivative compounds, although the database study became more involved and encompassed many more aspects than were associated initially with the photochemical analysis. The third part is independent from the first two parts and involves the structural determination of carborane cage structures, with specific reference to their hydrogen bonding.

1.2 REFERENCES

1. Bragg, W. L.; James, R. W.; Bosanquet, C. H., *Phil. Mag*, **1921**, 44, 433.
2. Bragg, W. L. Proc. Roy. Soc. (London), **1922**, 33, 301.
3. Debye, P.; Scherrer, P. Phys. Z, **1918**, 19, 474.
4. Interview with Conrad Röntgen in *M^cClure's Magazine*, April, **1896**.
5. Röntgen, C., *Wurzburg Physico-Medical Society*, **1896**.

CHAPTER 2

DIFFRACTION, X-RAYS, NEUTRONS AND STRUCTURE DETERMINATION

2.1 SINGLE CRYSTAL DIFFRACTION

This chapter is designed to give a brief introduction to the theory of X-ray diffraction and procedure, with specific attention paid to details that are relevant to experiments and procedures contained in this thesis. Specific reference will be made to instrumentation and equipment used.
Soon after von Laue's initial experiment to show that a single crystal could diffract X-rays, the Braggs discovered that the angular distribution of the X-radiation scattered by a single crystal was predictable. Bragg showed that all diffracted beams produced by an appropriate orientation of a crystal in an X-ray beam could be regarded geometrically as if they were being reflected from sets of parallel planes passing through lattice points. This diffraction can be compared to reflection of light by a mirror, with the angles of incidence and reflection being equal and that the incoming and outgoing X-ray beams and the normal to the reflecting planes must themselves all lie in one plane (see Figure 2.1). The reflection by adjacent planes in the set gives interference effects, to define a plane three integers need to be specified to give its orientation with respect to the three-unit cell edges, these are the Miller indices h, k, and l. The spacing between the successive planes is determined by the lattice geometry, and thus is a function of the unit cell parameters. For reflection by two adjacent parallel planes, the path difference can be denoted by Equation 2.1;

$$\text{Path Difference} = n\lambda = 2d_{hkl}\sin\theta \qquad \text{Equation 2.1}$$

This was developed by W. L. Bragg soon after he had demonstrated that X-rays could be diffracted and is commonly referred as the Bragg equation. In practice the value of n can always be set to one by considering planes with smaller spacing, (i.e. n=2 for the planes hkl is equivalent to n=1 for $2h$, $2k$, $2l$). So Equation 2.1 can now be represented in the form, Equation 2.2;

$$\lambda = 2d_{hkl}\sin\theta \qquad \text{Equation 2.2}$$

It is in this form that the Bragg equation is usually represented. The Bragg equation allows each observed reflection (diffracted beam) to be labeled uniquely with its three indices and for its net scattering angle, (2θ), to be calculated from the unit cell geometry, of which each d_{hkl} spacing is a function. The distance of each spot from the centre of an X-ray diffraction pattern is proportional to $\sin\theta$ and hence to $1/d_{hkl}$ for some set of lattice planes. The reciprocal nature of the geometrical relationship between a crystal lattice and its diffraction pattern, is seen in Figure 2.1.

As seen with the analogy between X-ray diffraction and optical reflection, it is possible to compare the X-ray diffraction to optical phenomena, and this can be taken further for optical microscopes and telescopes. Enlargement of images is by collecting and recombining the visible radiation scattered by the objects using a series of magnifying lenses or/and mirrors. The resolution of the microscopes is limited to the wavelength of visible light (6×10^{-7} m). To look at objects smaller than this it is necessary to use radiation that has a shorter wavelength. High-energy electrons are used in electron microscopes to view atoms and X-rays are used to determine the structures of the molecules that make up crystals (10^{-8}-10^{-10} m). X-radiation is not found to naturally occur in the quantities needed for X-ray diffraction analysis, although some atoms will radiate X-radiation. This is in contrast to light in the visible spectrum, where there is enough radiation available to facilitate optical microscopy. So X-rays have to be manufactured by artificial means for use. X-rays are produced when a beam of high-energy electrons strikes a metal target. Two types of radiation are emitted; a continuous X-ray spectrum and sharp emission lines with wavelengths characteristic of the metal from which the target is made (Figure 2.2). It is the emission lines that are employed in X-ray diffraction experiments. They are produced because some of the electrons that strike the target have sufficient energy to eject electrons from the inner shells of the metal atoms. Electrons from higher energy shells drop down to occupy the vacated inner shells. These electrons must lose the energy difference between the two energy levels and so there is an emission of a specific energy, which is the difference between the outer and inner shells, in the form of X-rays giving rise to the sharp peaks observed in the X-ray spectrum. The continuous X-ray spectrum is made up of white radiation. This white radiation occurs due to electrons being slowed down or stopped by collisions. Some of the lost energy is converted to electromagnetic radiation. The intensity is the relative number of photons produced and is directly related to the number of high energy electrons striking the metal target.

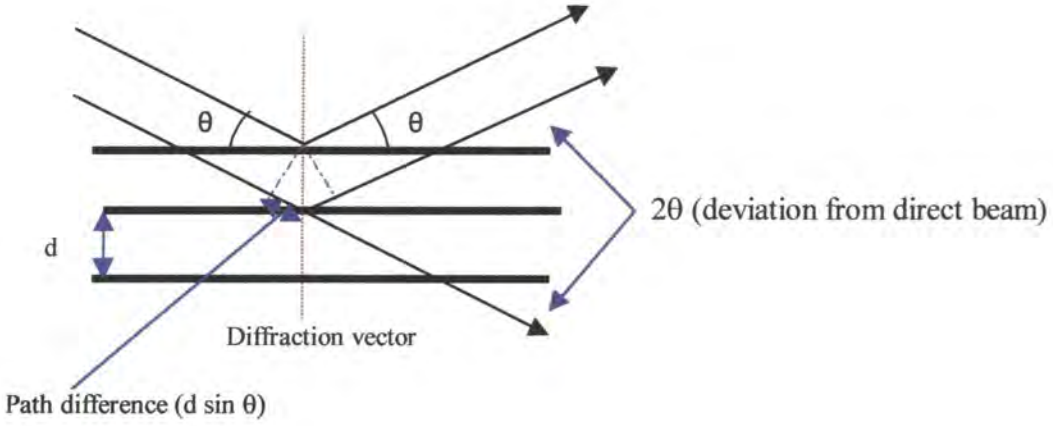

Figure 2.1 The Bragg diffraction for 3-Dimensional space

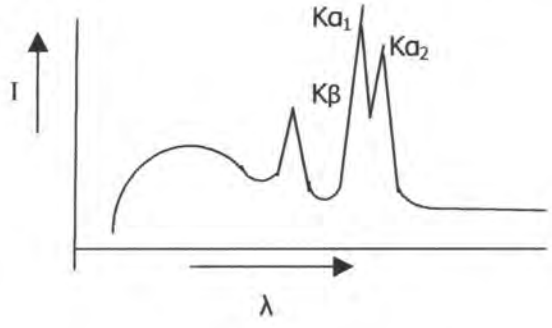

Figure 2.2 The spectrum of wavelengths against intensity of a typical X-ray tube

2.2 X-RAY DIFFRACTION EXPERIMENTATION, EQUIPMENT AND TECHNIQUES.

To determine the molecular structures from single crystals using X-ray diffraction data is a reasonably complicated process, which involves several steps. The following text will give a brief overview, in general terms, the steps to obtain the structural results described in this thesis (with particular reference to the instrumentation used). More comprehensive accounts of structure solution and the theory behind it can be found in any of the standard crystallography texts (see Crystal Structural Analysis: A Primer, Glusker and Trueblood, 1985).

The two instruments used in the collection of X-ray data reported in this thesis are a Siemens SMART CCD diffractometer and a Rigaku four circle diffractometer. A schematic representation of an Eulerian four circle diffractometer like the RIGAKU AFC6S is shown in Figure 2.3, which illustrates the four circles. The 4-circle diffractometer consists of a radiation source; a computer controlled goniostat that consists of four concentric circles and a detector. Three of the circles (ϕ, χ and ω) are used to orientate the crystal in space. For the SMART CCD the χ circle is fixed. The fourth (2θ) is used to move the detector. All datasets were obtained using a Molybdenum Kα X-radiation source and low temperature data collections were performed using an Oxford Cryosystems nitrogen Cryostream device (Cosier and Glazer, 1986) attached to the diffractometer. The area detector is similar but has the χ circle replaced by an area detection unit.

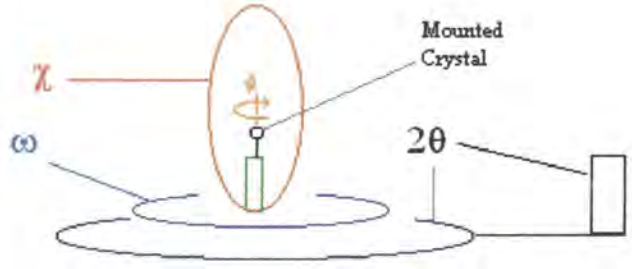

Figure 2.3 Simple schematic representation of a 4-circle diffractometer

2.2.1 Crystal Selection and Mounting

The first step in the experimental procedure is always to examine the crystals, since if the crystals are unusable then the experiment cannot proceed further. A polarizing microscope is the best way of examination. Crystals, which do not have straight edges, which have large numbers of smaller crystals (or crystallites) attached to them, or which have re-entrant angles, are generally disregarded. Ideal samples are, therefore, have clear and well defined faces and, if possible, approximately equal dimensions (i.e. not needles or plates) in order to minimize differential absorption effects. This is ideal, but in practice the quality of obtainable crystals are often not of such a standard and so quite often crystals that are not ideal are selected.

The overall sizes, as well as the relative dimensions, of the crystals are also important. The scattering power of a crystal depends on its volume as well as on contents. However, as crystal size increases so does the amount of absorption and these two effects had to be balanced. In practice, an upper limit on crystal size is imposed by the diameter of the X-ray beam produced by the instrument being used. Usually the sample is picked to have linear dimensions of between 0.1 mm and 0.5 mm.

The specific way in which the compounds are mounted depends on whether the sample is air and/or moisture sensitive. Air stable compounds are usually glued to the end of a fine glass filament using small amounts of a fast setting epoxy resin. The filament is then inserted into a brass pip and usually secured with wax. The pip is fitted into a well in the top of a goniometer head and held in place using a grub screw. The goniometer head is then located on its mount on the ϕ circle of the diffractometer and screwed firmly into place. However, air and moisture sensitive crystals have to be kept in a suitable environment during the experiment. The way this was done with such samples in this thesis is using the oil drop method (Stalke and Kottke, 1993). This involves coating the crystals in a highly viscous perfluoropolyether oil whilst they were still in a nitrogen environment. The oil forms a thin film around the crystals allowing them to be removed from the nitrogen atmosphere and attached to glass filaments. The viscosity of the oil is such that no additional adhesive is required to do this The oil forms a barrier around the crystal from the air and moisture thereby keeping the sample crystalline so as to diffract. The mounted sample is then put onto the diffractometer and rapidly cooled, causing the oil to harden and form a rigid barrier around the crystal which protects the sample from the atmosphere. The oil is amorphous and so will increase the amount of diffuse scattering from the sample, especially since

it covers the whole crystal, and consequently detracts from the quality of the data, so the method involving glue (epoxy resin) is preferred when possible. Although the resin is also amorphous it is preferred to the oil, for air/moisture sensitive materials because when it is used, the amount used can be kept to a minimum. The epoxy resin method is preferred because the crystal sample can be cooled at a much slower rate, rather than the flash freezing necessary for the oil method and therefore minimises damage on cooling.

Finally, the mounted crystal is optically centered in the X-ray beam. A crystal which is correctly centered will remain in the path of the X-ray beam when the ϕ and χ axes of the diffractometer are rotated.

2.2.2 Cooling Devices

Collecting the data at reduced temperatures helps to increase the number of observable data and increases the precision of all the measured reflections, it also reduces the amount of atomic motion. The type of cooling device used for both the SMART CCD and the RIGAKU AFC6S uses a cold inert gas flow. Cryostream nitrogen gas-stream cryostats (Cosier and Glazer, 1986) were used for all the X-ray diffraction data reported herein. These cryostats are designed to have a working range that is stable over the temperature range from approximately 100 K to room temperature. The diffractometers in this thesis are both fitted with these types of cryostats.

Liquid nitrogen is drawn up from an unpressurised Dewar vessel through a vacuum insulated supply line and into an evaporation coil by a diaphram pump. Most of the liquid is evaporated to gaseous nitrogen at its boiling point (77.4 K), passed through a heat exchanger to bring it to just below room temperature and then passed through the diaphram pump. The nitrogen gas is then pumped back through the heat exchanger at a constant flow rate, controlled by the pump and a flow regulating valve. The gas then passes from the cold end of the heat exchanger over a heater, which allows the temperature to be controlled, and on to the sample. A temperature sensor is situated at the tip of the delivery nozzle. There is usually some temperature gradient between the position of this sensor and the crystal so the device needs to be calibrated. The original calibration was carried out by observing the phase transition between the tetragonal and orthorhombic phases of KDP (KH_2PO_4) which occurs at 122 K (Nelmes *et al.*, 1987). The particular feature of this gas flow cryostat is the positioning of the pump, between the liquid supply and the gas output. The heat exchanger is required as the pump operates at room temperature. Generally flow rate is

set at around 0.5 lhr^{-1}, which is reasonably economical and ensures a stable temperature. To reduce the problem of frosting the cold gas the stream is surrounded by a flow of dry air.

2.3 THE RIGAKU AFC6S

For the Rigaku AFC6S diffractometer the X-ray source is a copper X-radiation tube ($\lambda_{K\alpha}$= 1.5418 Å) this is useful for measuring samples that are weakly diffracting and to determine absolute configurations in light atom structures by anomalous dispersion studies. To monochromate the beam a (111) graphite crystal plane is used with a (0.2mm, 0.5mm or 0.8mm check) lead collimator. The sample is mounted onto a goniometer head, which is screwed onto the ϕ-shaft and the crystal is centered using the instrument's in-built microscope. The crystal is now ready to be centered in the X-ray beam and once this is done the sample is ready for X-ray diffraction analysis.

For safety a lead glass-panelled interlocking door prevents the user accessing the instrument and allows the X-ray beam shutter to open if the door becomes opened then the X-ray shutter will be automatically closed. Computer controlled software is then used to move the circles in order to search for diffraction from the sample. To avoid damage to the detector by non-diffracted X-rays a lead beam-stop is situated in the direct-line of the incident beam in between the sample and the detector. The Oxford Cryosystems Cryostream cooling device (Cosier & Glazer, 1986) as described previously is positioned diagonally above the sample such that collision with the χ circle of the Eulerian cradle is avoided. The diffracted X-ray beams themselves are detected using a KBr scintillation counter. The Rigaku AFC6S diffractometer uses MSC/AFC Diffractometer Control Software (Molecular Structure Corporation, 1991).

2.3.1 Searching and Indexing the diffracted beams

To proceed with the diffraction experiment the Rigaku AFC6S diffractometer needs to find the correct orientation of the crystal. To obtain a reliable preliminary orientation matrix for a given crystalline sample in an X-ray experiment, between 10 and 20 suitable reflections are usually required. The diffractometer is set to search for 20 suitable reflections by systematically 'zigzagging' through reciprocal space. These 20 reflections are indexed together or, if initial indexing fails, in smaller groups. If fewer than 20 reflections are found then the software can attempt indexing with the number that have been found, but because the indexing is less precise with fewer reflections, usually any less than 12 reflections would be considered too few. If the indexing procedure fails, it is possible to select the peaks to be indexed manually using given

criteria (e.g. good profiles or high intensity). The 'auto-indexing' or 'real space method' strategy ((Clegg, 1984), (Sparks, 1976 and 1982)) is used to determine the orientation matrix and cell parameters of a given crystal. This method does not work in reciprocal space but in real space. The three shortest non coplanar vectors are arbitrarily assigned the indices 100, 010 and 001 such that a preliminary orientation matrix and unit cell can be generated. Although this unit cell (a', b', c') will probably not be the 'true' cell, it must be a sub-cell, since all vectors in the true lattice are also vectors in a lattice described by a sub-cell. The program then tests the cell by generating vectors, (t = ua' + vb' +wc', where u,v,w are integral values) up to a specified maximum length and calculating the product, t.n for each of the 3n vectors, where n is an integer. If t.x is an integral (within a small tolerance) for all reflections in the given list, then this x vector will be a true lattice vector. Otherwise, it is not a lattice vector and a new x vector must be chosen and the whole procedure repeats until 3 x vectors are found which satisfy this condition.

If the indexing is successful then the deduced cell parameters are refined and checked to make sure that the given cell is not a sub-cell of the true cell and to determine which Bravais lattice type and Laue class the crystal structure probably belongs. Collecting symmetry equivalents is advantageous since it improves statistics on merging, reduces systematic errors, improves precision and gives an indication of internal consistency of data and the absolute configuration and improves the matrix. It is always good practice to collect symmetry equivalents and Friedel equivalents although there are inherent limits in angular range by collision limits. Once the crystal symmetry has been satisfactorily ascertained a data collection can be undertaken. If the symmetry is in any doubt whatsoever, a data collection suitable for a triclinic crystal should be performed, since with this all quadrants of reciprocal space will be measured, and therefore all unique data collected (within a given 2θ range and machine limits) regardless of its symmetry. So for this reason it can prove advantageous to collect a triclinic cell, even if the symmetry is ultimately much higher than triclinic. If collection time were not a factor, then the data collection suitable for triclinic crystals would always be performed, so that one always had more data than needed, but this takes much more time and data storage takes up more room, so symmetry considerations are used to reduce the collection time and data storage space.

2.3.2 Data Collection Strategies

Since measured precision is proportional to the square root of the time of measurement and one can increase this precision by either collecting scans more slowly or repeatedly. Since weak reflections tend to have particularly poor precision, the level of precision tends to be often very disparate. Each control software package therefore attempts to scan reflections to at least a given minimum level of precision and to make the overall precision more uniform. The RIGAKU AFC6S diffractometer tries to ensure this by first scanning a given reflection and in the process determining the measurement's precision. If this precision falls below the minimum precision threshold then the reflection is rescanned until either this threshold has been reached or the maximum number of rescans permitted, as specified by the user, is reached. The actual time per scan remains constant throughout the experiment. The types of scan available are $2\theta/\omega$ scans, θ/ω and ω scans. The $2\theta/\omega$ type of scan involves the concurrent rotation of both the detector and sample whereas in the latter type of scan only the sample is rotated. It is common practice for $2\theta/\omega$ scans to be used instead of ω-scans unless the scans are very broad or one or more of the cell axes is large, since in such cases peaks are close in θ and so may overlap the next reflection. θ/ω scans may also be taken and these are a compromise of reciprocal space of ω and $2\theta/\omega$ scans. The scan width can be either fixed or varied. The width should be defined to include only where the X-radiation amplitude is greater than the background level. In cases where the variable width is used, two constant parameters, A and B, from the function $(\omega^{o}) = A + B\tan\theta$ must be evaluated. Parameter A is determined experimentally from high angle data and parameter B is fixed at a value based on the difference between $K\alpha_1$ and $K\alpha_2$ wavelengths. The function itself allows one to account for peak broadening at increasingly higher 2θ values due to increased wavelength dispersion. The quantity and frequency of reflections must be measured. It is useful to be able to detect any problem occurring during data collection, and to do this there should be a periodic survey over as large an area of reciprocal space as possible. This is done by choosing three reflections of intermediate strength, each with one alternately large Miller index and are measured every 150 or 100 reflections detected on the Rigaku AFC6S diffractometer.

2.3.3 Data Reduction

Once there is data obtained from the diffractometer it needs to be reduced. For the Rigaku AFC6S diffractometer this is done using the TEXSAN software (Molecular Structure Corporation, 1991). The collected intensities are converted into structure factors *via* a Lorentz and polarization corrections. The Lorentz correction is a geometric correction and is determined by the time taken for a given reflection (defined for this purpose as a reciprocal lattice point with finite size) to pass through the surface of the sphere of reflection. It takes the form of Equation 2.3;

$$L=(\sin 2\theta)^{-1} \qquad \text{Equation 2.3}$$

The polarization correction (which is geometric) accounts for the partial polarization of both the incident X-ray beam by the graphite monochromator and that invoked during diffraction within the sample. The amount of polarization is dependent on the value of 2θ and is given by Equation 2.4

$$P = (1 + \cos^2 2\theta) / 2 \qquad \text{Equation 2.4}$$

2.4 THE SIEMENS SMART-CCD DIFFRACTOMETER

The Seimens SMART-CCD is different to the Rigaku AFC6S diffractometer in that it is not a 4-circle instrument. This instrument employs an area detection device to effectively be a 3-circle diffractometer. The SMART CCD has only three Eulerian circles since the value of χ is fixed at 54.74°. The sample is mounted onto the ϕ-shaft, positioned at the centre of these circles and centered using the in-built microscope. A 512 x 512 pixel scintillation area detector, which employs a charge coupled-device (CCD) to amplify the output, measures the diffraction. The diffraction data is collected on a series of frames and each frame covers an area (hence the term area detector) in contrast to the standard 4-circle diffractometers which collect data over a series of single points. The area detector records the diffracted intensity information over a large area of 2-dimensional space which is then stored digitally as a 'frame' of diffracted intensity information. The actual area covered by the detector per frame is dependent on the distance of the detector from the sample. The detector itself has a 90 mm radius circular fiberoptic taper bonded to a one inch CCD chip. Since the area covered usually records more than one reflection at a time (per frame) then this dramatically speeds up data collection. The instrument employs (111) graphite monochromated molybdenum Kα X-radiation that is collimated using a 0.2mm, 0.5mm or 0.8mm lead aperture. A lead beam-stop is fixed in the direct line of the incident X-ray beam and a glass-paneled interlock prevents user intervention when the X-ray shutter is open, in much the same manner as with the Rigaku AFC6S diffractometer. The Oxford Cryosystems Cryostream cooling device (Cosier & Glazer, 1986) is positioned diagonally above the sample in a similar manner to the other diffractometer previously described

2.4.1 Data searching and indexing.

These procedures are carried out using the computer control software, SMART (Seimens SMART, 1995). Since this instrument has a two-dimensional detector, it covers a large area of reciprocal space in the measurement of each frame of data. This feature allows for the determination of the X-ray quality of the crystal *via* an 'electronic' rotation photograph very quickly. If the X-ray quality looks satisfactory, one continues by searching for reflections. A certain number of frames of data (typically 10-20) are measured at a given X-ray exposure time

(typically 5-20 seconds) over three different regions of reciprocal space two of which are mutually orthogonal. Reflections appearing in these frames are then selected by a 'thresholding' procedure which puts into a list all reflections which exceed a minimum I/σ value which is specified by the user. An attempt is then made to index these reflections. Usually, a minimum of about 20 reflections is necessary for successful indexing, although the number of reflections for good to reasonable diffracting crystals is generally larger (usually 40-100+). The algorithm used for this procedure is similar to that described previously (Sparks, 1976 and 1982). If initial indexing fails, one can try sorting this list of reflections with respect to a given parameter, e.g. mean intensity, 2θ range, etc and then selecting reflections at one end of this scale e.g. of the highest intensity, smallest 2θ range, etc, for re-indexing. Alternatively, one can either simply collect more frames of data and index on a greater number of reflections or remove all of the existing reflections in the list and select reflections manually from the frames. This would be done on the basis of good sharp peak profiles and moderate intensities and then, this subset would be attempted to be re-indexed, or alternatively recollecting the data with a greater exposure time per frame, which will expose the weaker peaks more from the background.

2.4.2 Data Collection Procedures

When indexing has proved successful, a least-squares procedure is used to refine the orientation matrix, this updates the cell parameters and crystal offsets. Higher symmetry can also checked for at this point using the 'Bravais' option. It is then necessary to set up a data collection routine. Since it is an area detector, data collection strategies on the Seimens SMART-CCD diffractometer are much simpler than those required for the Rigaku AFC6S and four-circle diffractometers in general. An ω-scan is sufficient and a scan width need not be employed because such a large area of reciprocal space is covered in each frame, although a step size must be selected. For routine data collections (with Mo Kα X-radiation) typically this value is set to 0.3 in ω. Although this value can be reduced to a smaller magnitude if the reflections are obviously sharper than the average or if a greater accuracy is required. In these circumstances, the number of scans should be increased to collect the same amount of space. Standard reflections, like those collected on the Rigaku, cannot be collected on an area detector system, but

this does not really matter since data collection on the Seimens SMART-CCD is so fast (typically 8-20 hours, and often nearer to 8 when the crystal diffracts well) crystal decay usually proves not to be a significant factor. A full hemisphere of reciprocal space is surveyed by collecting frames of data, in batches at predetermined angular settings, to a maximum value of 2θ. This value (often 50°) depends on the distance between the crystal and the detector (which is typically 6 cm). The user selects the length of time in which each frame is collected and this decision is governed by the diffracting capability of the sample. The poorer the diffraction of the sample the longer each frame needs and the precision of the collection is directly related to this. For a standard data collection, this time is typically set to 10-40 seconds depending on the apparent diffracting strength of the sample.

Once the data collection is complete, the user uses parameters that were used initially to index the cell and collects reflections over all areas of reciprocal space, to a maximum of 512 permitted by the software. This array of reflections is used to determine the unit cell parameters more accurately.

2.4.3 Reduction of the Data

The collected frames do not directly contain reflections ready for analysis, the frames contain data of the reflections and this must be processed into a form of individual reflection data. This process is conducted using the program SAINT (Seimens SAINT, 1995). Each three-dimensional peak profile is placed in a three-dimensional box of a given size, as specified by the user, where the box comprises a grid of 9 x 9 x 9 points. Analyzing a variety of reflections, prior to the data reduction allows the box size to be chosen. These reflections are analyzed in terms of their width in the x and y directions and the full-width-half-maximum of the ω-rocking curve width (the z-direction). The largest widths in each direction are taken as the dimensions of the box and this is constant for each data set. The integration proceeds in two stages.

The first stage, only the strong reflections (as determined by a specified I/(θ)(I) threshold) are considered. For each profile, the most intense point in the three-dimensional box is determined in order to calculate the background which is assumed to be lower than 2% of this maximum intensity. The points that are above this 2% threshold are considered as a signal and are normalized. The profiles of all of the strong reflections are stored in a temporary file.

The second stage of integration is then performed, in which all weak reflections are considered. The profile of each of these reflections is approximated to that of the nearest strong reflection profile stored. The weak reflection is then normalized in accordance to this profile. After integration, a Lorentz correction is applied (see previous section) before conversion of the resulting intensities to structure factor amplitudes.

The level of decay is then analyzed by comparing reflection intensities with the same hkl indices and the same ϕ-values from the beginning and the end of the data collection. A linear decay correction is applied when decay of a measurable value has occurred during the course of the experiment.

2.5 THE ABSORPTION CORRECTION

In general all datasets collected with copper or molybdenum radiation that have heavier atoms than silicon should have an absorption correction applied. The absorption correction compensates for attenuation of the X-ray beam as it passes through the crystal. Reflection intensity is reduced by absorption and this is directly related to the volume of the crystal (V). The linear absorption coefficient (μ) is based on unit cell contents and the types of atoms present in the unit cell. The correction factor (A) is the reciprocal of this value and is represented by Equation 2.4, where t is the path length;

$$A = \frac{1}{V}\int e^{-\mu t} dV \qquad \text{Equation 2.5}$$

This is a simple absorption correction and only directly applies to solids such as spheres and cylinders. More complex shapes use either numerical or empirical absorption correction. Numerical corrections involve determining the Miller indices of the bounding faces of the crystal and their precise dimensions. A mathematical representation of the crystal can be constructed from this information, which is then divided up into a Gaussian grid. The contributions made by each of the grid points to the total absorption are evaluated and summed so that they approximate the integral above.

Also common are the empirical absorption corrections. In this thesis the semi-empirical correction involving ψ scans is often used. In this type of absorption correction the correction works by scanning reflections that have χ values close to 90° as the crystal is rotated about the diffraction vector, ψ. For reflections with χ values close to 90° this is achieved almost exclusively by rotating the ϕ axis of the diffractometer. Since the path length of the X-ray beam through the crystal varies with ψ, the measured intensity of the reflection at different ψ angles will be different due to absorption. The numerical and semi-empirical ψ scan absorption corrections have been used for datasets in this thesis. The magnitude and any relevant details of the correction applied are given in the relevant experimental sections.

2.6 THE DECAY CORRECTION

When there are variations in the intensities of reflections over time caused by radiation damage or other deterioration of the crystal, the 'decay' correction is used to compensate for this. The correction is based on changes in the intensities of the standard reflections, which are re-measured at regular intervals throughout the data collection. Simple decay corrections use straight line functions to describe this variation. The general assumption of isotropic decay is mostly valid but may be checked by examining the variation in the individual standards. The purpose of a decay correction is to place intensity measurements taken at different stages of the data collection on the same basis: for example, if the standards have fallen to half their initial value by the end of the data collection and a linear correction is applied, the last reflection would be multiplied by a factor double that for the first one.

2.7 THE EXTINCTION CORRECTION

Extinction modifies the beam as it passes through a single block of the crystal, the effect of this is that it reduces the intensity of strong reflections at low 2θ angles and is especially pronounced in the more perfect crystals. There are two types of extinction, primary and secondary. Primary extinction occurs when a portion of the diffracted beam is diffracted a second time by the same set of Miller planes, causing a phase lag. This introduced lag, a 'double' diffraction causes destructive interference and can reduce or increase the intensity of the diffracted beam (see Figure 2.4a).

Secondary extinction occurs when separate mosaic blocks within a crystal are aligned identically with respect to the incident X-ray beam. The mosaic blocks close to the surface of the crystal diffract a portion of the incident beam. The remainder penetrates deeper into the crystal and is diffracted by other identically aligned mosaic blocks (see Figure 2.4b). This leads to the blocks deeper within the crystal contributing less diffracted intensity because they are shielded from the already diffracted incident intensity.

The quantities that dictate the magnitude of extinction effects, the mosaic spread and the domain radius, are usually unknown and empirical extinction corrections are often applied during structure refinement.

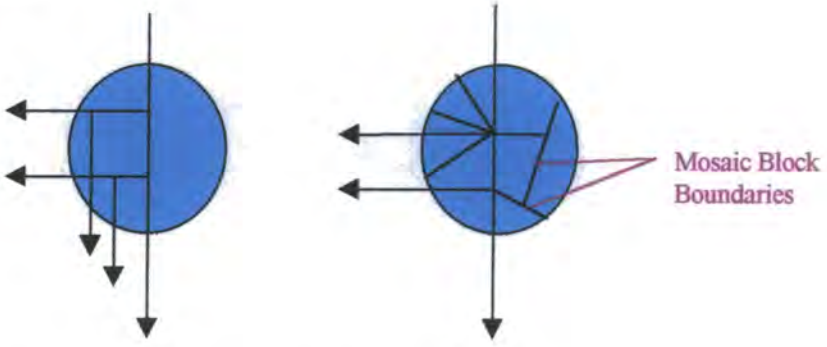

Figure 2.4 Extinction: (a) Primary and (b) Secondary

2.8 SPACE GROUP DETERMINATION

The space group symmetry of the crystal needs to be found. Currently it is with the use of computer software that space groups are determined using criteria, (including the Laue symmetry, the Bravais lattice type, the cell parameters and the systematic absences).

To distinguish whether the space group is centrosymmetric or non-centrosymmetric, the normalized structure factors are calculated (Wilson, 1942 and 1949). Normalized structure factors are corrected for diffracted intensities that decrease as $\sin\theta/\lambda$ increases. Their derivation is from Equation 2.6;

$$|E_{hkl}| = \frac{|F_{hkl}|}{\sqrt{|F|_{\theta hkl}{}^2}} \qquad \text{Equation 2.6}$$

Where $|F|_{\theta hkl}$ is the mean value of all structure factors that have a scattering angle of θ_{hkl}. Since $|E_{hkl}|$ values are independent of scattering angle the underlying intensity distributions present within datasets become apparent when they are analyzed. Since theoretical probability distributions of the $|F_{hkl}|$ and $|E_{hkl}|$ are different where the structure is centric or acentric, comparison of the mean of the experimental $|E_{hkl}|$ with the theoretical values for centric and acentric structures may determine whether an inversion center is present. Software typically uses $|E_{hkl}|$-1 since it has been found that for a centric distribution the value of this function calculated using all data is close to 0.97 while for an acentric distribution the value is closer to 0.74. If the experimental value is closer to 0.97 then it is probably centric and closer to 0.74 indicates acentric. In some cases with heavy atoms in the structure the presence of the heavy atom may distort the statistics of intensity distribution and so the $|E_{hkl}|$-1 value may be misleading

All the space group determinations described in this thesis were carried out using the XPREP program within the SHELXTL program (Sheldrick, 1991).

2.9 SOLVING THE STRUCTURE

Once the correct space group of a crystal has been determined, the full structural solution is sought. This is not as simple as may be initially thought, since one measures the intensity of data, i.e. amplitude, one can easily deduce structure factor amplitudes from the observed data (i.e. $I = F^2$). However one has no idea of the relative phases of these amplitudes because it is $|F^2|$ rather than $|F|$ being deduced. Since there is no knowledge of the phases, the data are rendered useless since the structure factors can only be converted into an electron density distribution *via* a Fourier transform, which can only be solved if one knows the phases involved. This is the so-called 'phase-problem'. The phase problem has not been solved, but this does not matter since there have been methods developed to get around the problem and allow for the solution of crystal structures. The two main methods, Patterson methods and Direct Methods are used routinely in the solving of a structure by X-ray analysis ((Giacovazzo *et al.*, 1992) and (Sayre, 1952)).

2.9.1 Patterson methods

The Patterson method was the first way the phase problem was overcome and is the oldest structure solving method.

Patterson methods are used to determine the phases of the structure factor amplitudes. A Patterson function is the Fourier Transform of the square of the modulus of the structure factors. Patterson functions can be calculated without any phase information. However, the peaks in a Patterson map do not correspond directly to atomic positions. Instead, they represent inter-atomic vectors. The height of each Patterson peak corresponds to the product of the atomic numbers of the atoms linked by the vector. Patterson methods are therefore particularly effective when just a few heavy atoms are present. In these situations the heavy atoms usually dominate the scattering and the Patterson peaks which represent the vectors between them are the most prominent features in the Patterson map. Once the peaks representing the vectors between the heavy atoms have been identified, it is possible to determine the positions of the heavy atoms. This information is used to derive a set of 'heavy atom' phases, which are combined with the structure amplitudes and converted into an electron density distribution. These electron density maps are then used to

determine the positions of other atoms within the crystallographic unit cell and so the process can be repeated until all the non-hydrogen atoms are located.

Unfortunately, Patterson methods cannot normally be used to solve 'light atom only' structures because there is very little texture in the Patterson maps derived from such compounds. In the beginning heavy atom substitution was the only way to overcome these difficulties and so the large range of organic molecules with no heavy atoms present were rarely solved, and for these compounds the direct phasing methods, which do not rely on heavy atoms, are important.

2.9.2 Direct Methods

In 1985 Herb Hauptman and Jerome Karle won the Nobel Prize for their work on the "Direct Method" (Karle, *et al*, 1958). These methods have surpassed the Patterson method as the most frequently used approaches for structure determination, at the present point in time.

This method relies on the fact that structure factor magnitudes and phases are correlated through a prior partial knowledge of the nature of the electron density distribution (Sayre, 1952).

The convolution of the structure factor magnitudes and phases give the complete structure factor. We inherently possess some information about the electron density, e.g. $\rho(x) \geqslant 0$, $\rho^3(x)dV$ must equal a maximum, and many of the atoms in a given structure may be very similar (this applies especially to organic compounds). Such information is expressed as mathematical constraints on the function, $\rho(x)$, and since $\rho(x)$ is related to the structure factor $|F(h)|$, corresponding structure factor constraints are formulated. Since the structure factor magnitudes are already known, these constraints apply mainly to the phases.

A given number of strong reflections are arbitrarily assigned phases and the constraints are applied such that, in favorable cases, all phases may then be determined. Obviously the more constraints available the easier the determination of the un-assigned phases.

Since the initial partial assignment of phases is completely arbitrary, the procedure will seldom give the correct solution. Moreover, it is not instinctively obvious which is the correct solution. Hence, this procedure is repeated, typically 30-200 times and for each solution a combined figure of merit (CFOM) is calculated in order to identify the best solution. Once a good solution has been found the phases of this are used to generate an electron density map. From this electron density map many atomic positions can be determined; this acts as a starting model. The phases that are known are used to approximate the unknown phases. Using difference Fourier synthesis and least squares refinement, leads to a new electron density map and the assignment of

undetermined atomic positions, this is then repeated until all the atoms have been found and the model is chemically correct. This method has the advantage that it does not necessitate the presence of heavy atoms.

2.10 REFINEMENT

The refinement of structures in this thesis is done using computer software, specifically the SHELXL-93 software (Sheldrick, 1993). This software uses a model of the structure and by performing a least squares calculation brings the calculated structure factors closer to the observed data. The least square method of refinement is a statistical method that obtains the best fit from the data. It minimizes the sum of the squares of the deviations of the experimentally observed values from their respective ones. When refining the data for a crystal structure the atomic coordinates and other parameters are made to fit the observed intensities.

2.11 NEUTRON DIFFRACTION

Neutron diffraction is an experimental method which provides accurate positional data for hydrogen atoms in molecular crystals and it is for this reason that it is widely used in the determination of the geometries of hydrogen bonding interactions. This is despite the relatively large costs involved in obtaining neutrons, in comparison to other analytical techniques and X-ray diffraction. In recent times there has been a great deal of interest in the so called hydrogen bonding, in particular the "weak" hydrogen bonds, such as C-H···O, O-H···π, O-H···F, etc. The weak hydrogen bond has generated quite a lot of controversy, with the boundaries of what is and what is not a hydrogen bond, but this controversy has also generated an increased interest in neutron diffraction experiments.

2.11.1 Neutrons and their characteristics

Neutrons are an unique probe of condensed matter and the information obtained from neutron scattering experiments is crucial to an understanding of a system, either on its own or in combination with other physical measurements.

Neutrons allow the simultaneous measurement of structure and dynamics. This results from the fact that thermal neutrons naturally have appropriate properties for each type of measurement. For example, thermal neutrons have wavelengths similar to atomic spacing, typically in the range 0.5-10 Å or so. This allows thermal neutron scattering techniques to examine structural features in the range 0.1-1000 Å. At the same time thermal neutrons have energies similar to the energies of atomic movements, in the meV to eV range. This allows the probing of quantum tunnelling effects, molecular translations and rotations, molecular vibrations, lattice vibrations and electronic transitions within atoms. There are methods of measuring dynamical properties during a structural experiment (or vice versa) using other forms of radiation, for example, by performing Raman scattering on a sample in an X-ray beam. Such measurements, however, require the provision of two sources, in this case an X-ray source and a laser, whereas the corresponding measurement with neutrons could be done with just one source (but with two slightly different methods of examining the scattered neutrons).

Neutrons interact weakly with matter and are therefore non-destructive, even to complex or delicate materials and this gives a distinct advantage for X-ray sensitive materials. Accordingly, neutrons are a bulk probe, allowing the interior of materials to be probed, not merely the surface

layers probed by techniques such as X-rays, electron microscopy or optical methods. Neutrons have a magnetic moment, allowing magnetic structure (the distribution of magnetic moments within a material) and magnetic dynamics (how these moments interact with each other) to be studied in a way not possible with other forms of radiation. Neutrons scatter from materials *via* interaction with the nucleus rather than the electron cloud. This means that the scattering power of an atom is not strongly related to its atomic number, unlike with X-rays and electron scattering. This has three advantages:

(i) it is easier to sense light atoms, such as hydrogen, in the presence of heavier ones, which is of relevance to this thesis.

(ii) neighboring elements in the periodic table generally have substantially different scattering cross sections; for elements that have a similar atomic number, and hence similar number of electrons, this method is extremely useful in distinguishing the separate elements.

(iii) the nuclear dependence of scattering allows isotopes of the same element to have substantially different scattering lengths for neutrons, thus allowing the technique of isotopic substitution to be used to yield structural and dynamical details. The use of contrast variation where the scattering density of a mixture is matched to part of the system is particularly powerful and has been a key to many successful applications of the technique of neutron scattering in chemistry and biology.

2.11.2 Neutron Production

The development of single crystal neutron diffraction has been developed within the constraints set by the nature of the radiation itself and no neutron diffraction experiment could be carried out before 1932 (Wilson), when the existence of the neutron was merely suspected with its properties and means of production not understood. Diffraction techniques had already been developed and were equally applicable to both neutron and X-ray radiation. The early diffraction theory pioneered by workers such as Laue were also valid for neutron diffraction. Neutron diffraction therefore came into being with considerable theoretical and experimental advances already in existence.

2.11.3 The development of reactor sources

Techniques of neutron diffraction had to wait for the advent of nuclear reactors in which neutron flux would be much increased. In recent times the availability of reactors has become widespread and an increasing range of science devised for using the neutron beams produced. Traditionally neutron beams were extracted from multi-purpose reactors whose design spanned many uses. In order to achieve the desired neutron flux it was necessary to consider the construction of nuclear reactors solely for the production of beams for neutron scattering. In 1965 the High Flux Beam Reactor at Brookhaven National Laboratory, USA was the first of this type. Also a similarly high flux reactor was built at the Oak Ridge National Laboratory, at the same time, which was not dedicated to neutron production but also encompassed isotope production. In 1972 at Grenoble, France, a specially designed reactor was commissioned solely for neutron scattering and to support the work at this reactor a completely new institute was created. The Institut Max von Laue-Paul Langevin (ILL) was the world's first purpose-built neutron scattering centre. The ILL was unique in another way, in that the reactor was built as an international collaboration between France and Germany, with the UK joining the Institute as a full-1/3 partner soon afterwards, in 1973. The flux available has increased by a factor of some 103 between the early general purpose reactors and today's best research reactors. In order to attain increasing neutron fluxes it is necessary to turn to alternative technology to that of reactor design and construction. Fortunately, there is an alternative means of production of neutron beams based on accelerators rather than reactors. By their nature, accelerator-based sources can be pulsed, opening up a new type of scattering experiment.

2.11.4 Spallation sources

The characteristics of a pulsed spallation source are very different to those of a reactor neutron source. The production mechanism itself is a dynamic process, being based on an accelerator rather than a steady state reactor. The term "spallation" comes from a mining term meaning to chip. Massive particles are accelerated to high velocities (energies) in the accelerator before impacting on a heavy metal target (at ISIS H^- ions are accelerated, see section 2.11.5). These impacts produce neutrons (typically tens of neutrons for each incident accelerated particle). The neutrons produced have energies typically of the order of MeV, this is much too high to be of use

in condensed matter studies. In order to perform diffraction and other scattering experiments using these neutrons they must first be slowed down. This deceleration is achieved by passing the fast neutrons through moderators, which exploit the large collision cross-section for neutrons associated with the hydrogen atom.

The good fortune for neutron scattering is that hydrogen is the most abundant element around and for the purposes of moderation, does not have to be in elemental form. This means that neutron moderators can be constructed from common materials such as water, hydrocarbons or from hydrogen itself.

When a beam of fast neutrons is passed into a moderator, the neutrons undergo collisions with the hydrogen in the moderating material, in the manner of a random walk. Since the fast neutrons have a much higher temperature than the molecules in the moderator, they tend to lose more energy than they gain in such collisions - and are thus slowed down. The extent to which these neutrons are slowed down depends on two factors - the temperature and the size and shape of the moderator. Obviously the higher the temperature of the moderator, the higher the energy of the "thermalised" neutrons. Very large moderators can slow down the majority of the fast neutrons, whereas a small moderator tends to allow more fast neutrons to escape before becoming thermalised, and so a spectrum of slowed neutrons is produced. The characteristics of each of these moderators are exploited in the various types of neutron source. "Full" moderation using large moderators tends to be used at reactors or steady state sources, whereas "under" moderation is of particular value at a pulsed source.

2.11.5 The ISIS pulsed spallation neutron source

The ISIS source, at the Rutherford Appleton Laboratory in Oxfordshire, UK, is the world's most intense pulsed neutron source and its neutron production mechanism is similar to that used in all such sources. The production of particles energetic enough to produce efficient spallation at ISIS involves three stages. First, an ion source produces hydrogen ions (H^-), which are accelerated in a pre-injector column to 665 keV. In the linear accelerator, the second stage, the hydrogen ions pass through four accelerating cavities to reach an energy of 70 MeV. At injection into the third acceleration stage, the synchrotron, the electrons are stripped from the hydrogen ions by a very thin alumina foil, producing a circulating beam of protons. The proton synchrotron, of 52m diameter, accelerates 2.5×10^3 protons per pulse to 800 MeV, before they are extracted and sent

to the target station. This happens 50 times a second. The spallation target is made from a heavy metal such as depleted uranium or tantalum. The highly energetic protons produce neutrons by chipping nuclear fragments from the heavy metal nucleus. For an 800 MeV proton beam some 25 neutrons are typically produced by each proton hitting the uranium target.

Around the target there is an array of small hydrogenous moderators to slow down the neutrons to thermal or close to thermal energies, as described above. The characteristics of the pulsed neutrons produced by a pulsed spallation source such as ISIS are different from those produced at a reactor, leading to different ways of carrying out neutron scattering experiments. The pulsed nature of the source makes it mandatory to exploit time-of-flight techniques on white neutron beams. The production time can be precisely defined when the proton beam hits the target, by recording the arrival time of each neutron at the detector, providing the flight path is known.

The use of white beams, sorted using the time-of-flight technique, allows fixed scattering geometries to be adopted which greatly simplifies the use of complex and extreme sample environments. In the particular case of single crystal diffraction, the wavelength-sorted white beam has particular benefits in many types of measurement. The measurements of scattering on a pulsed source cover a wide spectral range in both energy and momentum transfer. Access to data over as wide a dynamic range as possible facilitates the study of increasingly complex systems.

2.11.6 Neutron detection

The characteristics that lend neutrons their advantageous properties for the probing of matter also give some of the problems associated with neutron scattering experiments. Neutrons are penetrative into matter because their interactions are relatively weak. This is related to the fact that neutrons are uncharged and therefore interact with the nucleus through the strong nuclear force rather than with the electrons *via* electrostatic interactions. They also interact with the electrons *via* the magnetic moment of the neutron, but this interaction is generally not so strong as that between electromagnetic radiation (photons) and the electrons. The principle of efficient detection is that the incoming particle must interact with the detecting medium in as short a distance as possible, yielding a clear and unambiguous signal to indicate that it has in fact been detected. The subsequent electronic coding, if any, of this signal must be accomplished in as short a time as possible and the detection system placed in a state of readiness for detection of the next event. The situation for neutron scattering experiments is frequently complicated by the fact

that a single detection element (an isolated 'detector') may not be adequate for the particular experiment. This is frequently the case in single crystal studies when the use of a position-sensitive two-dimensional area detector may be desirable.

Two main methods, gas and scintillator detectors detect neutrons. Gas detectors use a volume of gas, typically ^{3}He and BF_3, for detection. The scintillator detector uses a medium, typically solid, containing ^{6}Li or GD.

2.11.7 Summary of single crystal neutron diffraction

Single crystal neutron diffraction is an extremely powerful technique for accurate chemical crystallography. Good neutron single crystal data will: yield high precision atomic and vibrational parameters, including higher order thermal effects; permit detailed analysis of conformations, molecular energetics etc. It is clear that there are several high profile areas in which such neutron structure determination can have an impact, for example; pharmaceuticals, where many drug molecules are in the accessible cell range. Detailed neutron data can be vital to the understanding of molecular conformation, especially with regard to the often very small energy differences between active and inactive polymorphs. Neutrons also sample the bulk of such materials, again vital in the study of polymorphism in relation to production processes. Organometallic materials, frequently have important hydrogen atoms located close to a heavy metal atom, rendering neutron diffraction an incredibly useful way of adequately determining the structure. Organic structures, where neutrons have a vital role to play in the study of basic bonding, charge density studies, hydrogen bonding and in non-destructive phase transitions, particularly those involving hydrogen atom shifts.

2.12 REFERENCES;

1. Clegg, W., *J. Appl. Cryst.*, **1984**, 17, 334.
2. Cosier, J.; Glazer, A. M., *J. Appl. Cryst.*, **1986**, 19, 105.
3. Giacovazzo, C.; Monaco H. L.; Viterbo, D.; Scordari, F.; Gilli, G.; Zanotti, G.; Catti, M., *Fundamentals of Crystallography*, **1992**, Oxford University Press.
4. Glusker, J.P.; Trueblood, K.N., *Crystal Structure Analysis: A Primer*, **1985**, Oxford University Press.
5. Karle, J.; Hauptman, H.; Christ, C. L., *Acta Cryst.*, **1958**, 11, 757.
6. Kottke, T.; Stalke, D., *J. Appl. Crystallogr.* **1993**, 26, 615.
7. Molecular Structure Corporation, **1991**, TEXSAN, TEXRAY Structure Analysis Package, 3200 Research Forest Drive, The Woodlands, TX77381, U.S. A.
8. Nelmes, R. J.; Tun, Z.; Kuhs, W. F., *Ferroelectrics.*, **1987**, 71, 125.
9. Sayre, D., *Acta Cryst.*, **1952**, 5, 60.
10. Siemens SAINT Version 4.050, Siemens Analysitical X-ray Instruments, Madison, U.S.A., **1995**.
11. Siemens SMART Version 4.050, Siemens Analytical X-ray Instruments, Madison, U.S.A., **1995**.
12. Sheldrick, G. M., SHELXL 93. Program for the Refinement of Crystal Structures, **1995**, University of Göttingen, Germany.
13. Sheldrick, G. M., SHELXTL-Plus. Release 4.1., **1991**, Seimens Analytical X-ray Instruments Inc., Madison, Wisconsin, U. S. A.
14. Sparks, R. A., *Computational Crystallography*. Ed. Sayre, D., Claredon Press, Oxford, **1982**, 1.
15. Sparks, R. A., *Crystallographic Computing Techniques*. Ed. Ahmed, F.R., Munsskgaard, Copenhagen, **1976**, 452.
16. Wilson, A. J. C., *Nature*, **1942**, 150, 152.
17. Wilson, A. J. C., *Acta Cryst.*, **1949**, 2, 318.
18. Wilson, C. C. Unpublished Work.

CHAPTER 3:

THE CAMBRIDGE STRUCTURAL DATABASE: AN INTRODUCTION.

3.1 INTRODUCTION

In recent years the solving of a crystal structure by diffraction analyses has become a reasonably quick and uncomplicated procedure but, for the first half of this century, the solving of the molecular structure of a compound by crystallographic means was a complicated and time-consuming business. To solve a structure was extremely laborious and involved tedious manual methods to collect, solve and then finally refine the diffraction data and it was not uncommon for a single structure determination to take several years to complete. As a consequence of this there were only a few new crystal structures being published each year. This relatively low number of published structures made it possible for individual researchers to examine the whole of the primary crystallographic literature and perform systematic analyses of related and similar structures by hand. There were a large number of studies conducted during the 1950's and 60's dealing with topics such as bond lengths, molecular conformations (Sutton, 1963) and hydrogen bonding (Pimental, 1960).

As improvements were made in diffractometer design and manufacture and the levels of automation increased, more researchers were able to collect diffraction data in less time and so the number of crystal structure determinations being reported annually increased steadily from the late 1950's onwards. Because of the ever increasing number of structures it became increasingly difficult for individuals to conduct comprehensive searches of the primary literature and secondary publication.

A major advancement in crystallography came in the form of computation. By the 1960's affordable computer technology was becoming more and more powerful. This then led onto fully automated data collections with the collections being able to be conducted 24 hours a day with the use of computer controlled diffractometers. The speed of computers meant that the large number of repetitive mathematical procedures associated with structure solution and refinement were able to be performed many times faster than previously possible.

Even more structures were able to be solved when the new direct phasing methods (Sayre, 1952) for solving crystal structures were developed. These new direct methods were good at solving small organic compounds, which were a huge range of structures that had hitherto been unsolvable.

With these advancements the number of crystal structures being reported each year naturally increased quite considerably (from 224 in 1960 to 1258 in 1970). This meant that manual systematic analyses of the crystallographic data became impossible and with this a great deal of the chemical information that was contained therein was in danger of becoming increasingly underexploited. Ironically the computational methods that they themselves had been largely responsible for had to be used to overcome this problem. The structural data began to be compiled into computerized databases that could be searched systematically using software developed specifically for that purpose.

There are currently five fully retrospective computerized crystallographic databases in use today, in order of size these are;

1) Cambridge Structural Database (CSD, >200,000 entries), for organic and organometallic structures.

2) Inorganic Crystal Structure Database (ICSD, 55,000 entries),

3) Metals Data File (CRYSTMET, 45,000 entries),

4 Protein Data Bank (PDB, 6,500 entries),

5) Nucleic Acids Data Bank (NDB, 731 entries)

All of the database analyses conducted in this thesis have been conducted with organic molecules, as a result of this the CSD has been used in these analyses and in general much more than the other four databases. So the databases 2-5, will not be further explained and the CSD will be detailed for relevance to this thesis.

3.2 THE CAMBRIDGE STRUCTURAL DATABASE SYSTEM (CSDS)

The Cambridge Structural Database system CSDS (Allen, 1991) is easily the largest of the current databases and will be so for the foreseeable future. The database that is run by the CCDC was initially set up in 1965 and at present it contains the crystallographic structures of over 200,000 organic and organometallic compounds. Although the CSDS is a database for organic structures, the CSDS definitions of what structures are acceptable to be included is broad: it contains structures if they contain at least one C-C or C-H bond, within whatever collection of atoms and bonds entered as the structure (i.e. carboranes, all the examples of which are in this thesis are considered to be organic molecules by the CSDS) the result of this is that the CSD contains structural information on a huge range of different structures, from large metal clusters to simple alkanes, and everything in between. These data are accessed using CSDS search and retrieval software, which is being developed and updated constantly. There are four new versions of the CSDS annually and this allows researchers to keep reasonably up to date with the new structures being developed. These improvements to the CSD is changing the way in which the database is being used, there is an increasing number of non-crystallographers using it for increasingly more complex structural analyses, and the days of a synthetic chemist getting a crystallographer to search a reference on the CSD are thankfully becoming a thing of the past.
Structural data is recorded in the CSD in three ways. These three can be categorized easily in terms of their "dimensionality" (CSDS Manuals 1994 & 1995).

3.2.1 One dimensional

One-dimensional data contains bibliographic and chemical text: typically information contained are compound name(s), molecular formula(e), literature citation and cell parameters. Basically this is all the information that can be kept in simple text format.

3.2.2 Two Dimensional

Two-dimensional data contains chemical connectivity representation. This information is encoded in the form of two connectivity tables. The first of these stores atom properties and the second stores bond properties.

3.2.3 Three Dimensional

Three-dimensional data consists of atomic coordinates, cell dimensions, space group and symmetry operators for each entry. This information is used to establish a crystallographic connectivity using standard covalent radii. The chemical and crystallographic connectivities are then mapped onto one another so that atom and bond properties can be matched to the three dimensional structure.

All of the dimensional data is extracted from the primary literature. Over 500 journals are currently represented in the CSD. To maintain data quality each is subjected to a series of computerized checks to ensure that the information contained in the database is consistent and accurate.

3.3 SOFTWARE

The CSD uses several software packages to access and analyse the data it stores, details follow of these programmes.

3.3.1 QUEST3D

QUEST3D is the main program of the CSDS; all subsequent uses and programs require the files outputted from QUEST3D: simply put, QUEST3D is the starting point for searching the CSDS. The use of QUEST3D is to define and execute text, numeric and two dimensional chemical fragment searches. More complicated composite searches can be performed by linking these definitions together using the Boolean logical operators AND, OR and NOT. Probably the most common use and certainly for the work conducted in this thesis is the search using a two dimensional model of the chemical fragment. This includes drawing the molecular fragment with the drawing facilities of the QUEST3D program, often specific parts (angles, bonds, etc) are selected on the fragment to obtain a numerical parameter for those parts of the molecule. The fragment is then defined and the search conducted, over the whole of the CCDC. Entries that satisfy the input search criteria are displayed on the screen. The user can visually manipulate this output (e.g. rotate, translate and magnify) and can view it in a one, two, two/three and three dimensional display before deciding on whether to keep or reject the specific entry. The saved entries have their information stored in the form of several files, which can be read using complementary CSDS programs. Some of the stored files are saved only optionally and the user determines which of these files they wish to keep before running the search. The files saved are dependent on the subsequent CSDS programs the user wants to use with the search results. Features of the CSDS include filters, to filter out data that does not fit crystal or chemical parameters, i.e. one can choose to search only in organometallic compounds or can search for structures with an R-factor lower than a specified value. Also a fragment can be drawn and the NOT logical operator will filter out any crystal structures containing this fragment. It is also possible to select a cap on the number of structures found rather than search the whole database. An example of a QUEST search is seen in Figure 3.1.

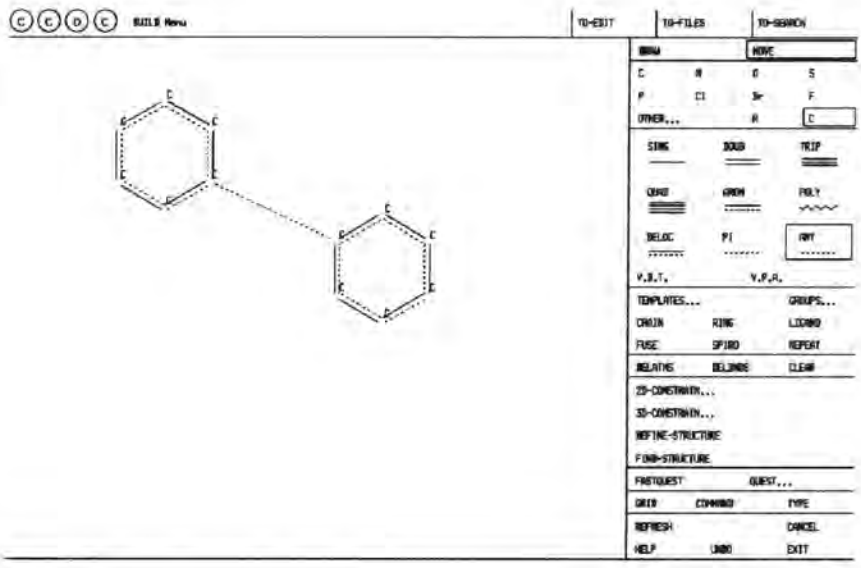

Figure 3.1 The drawing stage of a fragment in QUEST3D (here showing a biphenyl fragment)

3.3.2 VISTA

This is a program which reads the geometrical table(s) generated by the QUEST3D program and provides the user(s) with facilities for the graphical representation of the data, in the form of histograms, scattergrams, polar plots, etc. An important feature of VISTA is statistical analyses of the numerical data; this allows the user to "play" with the figures and to mould the data to their specific needs. Vista has been used extensively in the database chapters of this thesis and has proved invaluable in analysing the structures from the searches conducted. An example of analysis types is given in Figure 3.2.

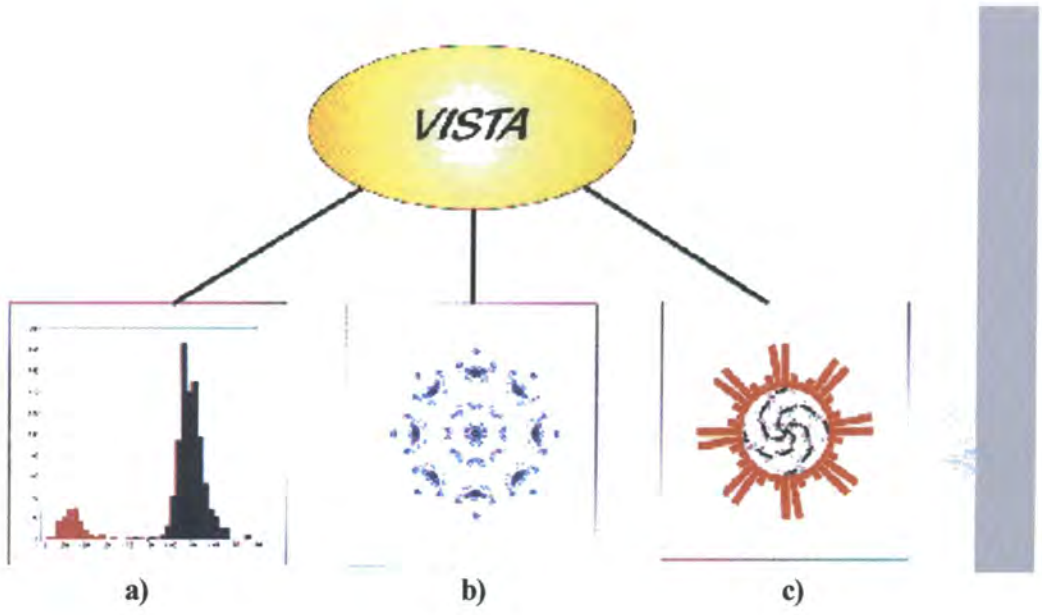

Figure 3.2 Various graphical outputs of the VISTA program: a) histogram, b) radial scatterplot and c) combined radial histogram and scatterplot

3.3.3 PLUTO

This is a crystallographic graphics program that can be used to visualize saved entries in several ways. Molecular structures can be rotated, translated and magnified to obtain the desired view. The structure can then be saved as a PostScript file in a variety of ways. PLUTO is a useful way of examining the structures in the CSDS and is commonly used for the exploration of crystal packing and the non-bonded interactions. This is a useful way of examining these features in the crystal structure, an example of PLUTO is given in Figure 3.3.

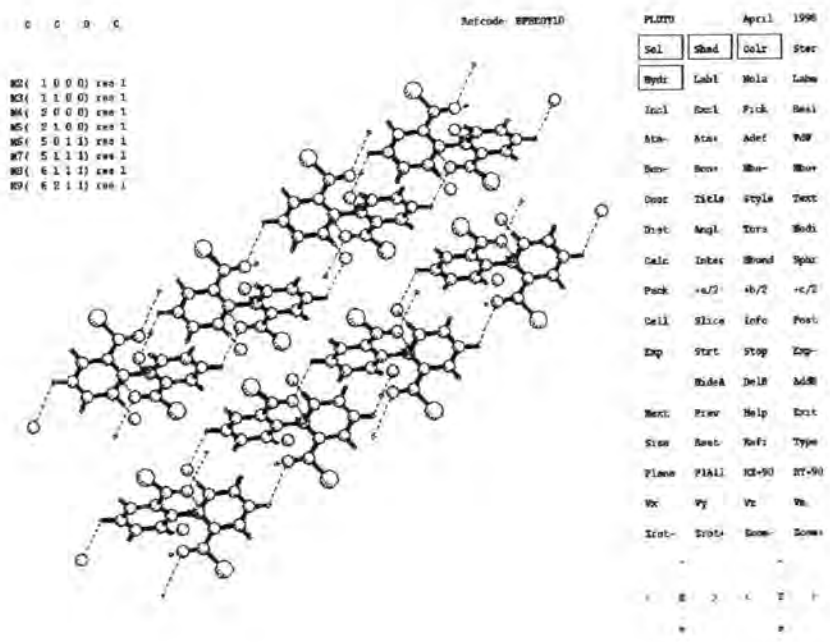

Figure 3.3 PLUTO screen (showing the inter-molecular interactions in the structure with the Refcode BPHCOY10)

3.4 RESEARCH APPLICATIONS OF THE CSDS

The CSDS has a worldwide distribution and many chemists and crystallographers use it as a tool to compare the cell parameters of an unknown material with those of compounds that have already been crystallographically characterized. It is also commonly used to search the CSD for fragments of compounds they are interested in and obtain bibliographic and structural information on them. However, the CSDS has many other applications.

3.4.1 Crystallographic Studies

The CSDS can be used to study crystallographic systematics. The reliability of the estimates of precision (Estimated Standard Deviation, ESD) used by crystallographers was attempted to be determined using data abstracted from the CSDS (Kennard and Taylor, 1986), while others have used the CSDS to compile space group frequency tables (Mighell, Himes and Rodgers, 1983) and attempted to rationalize the results (Wilson, 1988, 1990, 1991 and 1993) and (Brock and Dunitz, 1994).

3.4.2 Mean Molecular Dimensions

There have been several studies of the CSDS in an effort to determine the mean lengths of a large number of different types of chemical bonds. The derivation of simple descriptive statistics for standard geometrical parameters is a relatively straightforward application of the CSDS. As an aid to structural chemists and modelers, two major compilations of bond lengths were produced for both organic (Allen *et al.*, 1987) and organometallic (Orpen et. al., 1989) compounds. A study of inter-molecular bond angles and conformation in peptides has also been performed (Ashida *et al.*, 1987).

3.4.3 The Structure Correlation Method

The structure correlation method is based on the assumption that observed structures tend to lie mainly in regions of low potential energy. If a range of independent parameters describing a structure of a fragment in different environments can be correlated then the correlated functions map a minimum energy path.

The CSDS has been used extensively to analyze molecular conformation. Conformational preferences can be detected using the structure correlation method. The conformations of five, six, seven and eight membered carbocycles have already been extensively examined ((Allen, Doyle and Taylor, 1991) (Allen, Doyle and Auf der Heyde, 1991), (Allen, Howard and Pitchford, 1993), (Allen, Howard, Pitchford and Vinter, 1994), (Allen, Garner, Howard and Pitchford, 1994) & (Brock and Minton, 1989)). Other studies have examined the conformations of certain bioorganic (Murray-Rust and Motherwell, 1978 and Murray-Rust and Bland, 1978) and organometallic fragments. Biphenyl compounds are six membered rings and these are of particular interest in this thesis, see chapters 5 and 10-13.
The structure correlation method and how it relates to this thesis is discussed in more detail in chapter 11.

3.4.4 Non-bonded Interactions

There has been and is a great deal of interest in hydrogen bonding and all inter/intra molecular interactions in general and so a large number of non-bonded interactions have been studied using the CSDS. These investigations typically involve analyses of non-bonded contact frequencies, distances and angles in relevant fragments. The CSDS is well structured for the study of non-bonded interactions, and caters for these types of studies. Notable studies include an investigation of C-H...O hydrogen bonding using neutron derived structural data (Taylor and Kennard, 1982), a comprehensive survey of interactions between halogens and nucleophiles (Lommerse *et. al.*, 1996) and database studies of C-H···O, X···O_2N and C-F···H interactions (V.J.Hoy, 1997).

3.4.5 Knowledge based Libraries

Many of the analyses of the CSDS have followed similar paths and for ease and to allow the non-experienced database searcher more access, the CCDC began to explore associated software, in 1995. The initial topic picked for this venture was that of intermolecular interactions, this was called IsoStar and was released with the 1997 October Unix edition of the CSD. There is a similar type of library with the PDB, molecular scene analyses and torsional distributions have been studied in both the CSDS and the PDB for modeling protein-ligand docking.

3.5 THE SEARCHES CONDUCTED ON THE CSDS (EXPERIMENTAL SECTION)

3.5.1 General

In Chapters 10, 11 and 12 there are database studies using the CSDS. These have concentrated mainly on the torsion angle distribution of biphenyls and similar compounds. In the following section the details of these searches will be described with specific focus on the non-routine parts of these searches.

First of all the one thing that most searches have in common is the biphenyl or biphenyl type fragments, see Figure 3.4 and this structure is input into the QUEST3D software by drawing the fragment as seen in Figure 3.4.

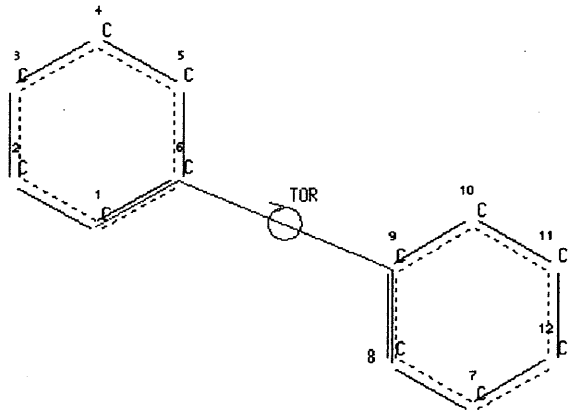

Figure 3.4 An example of the biphenyl fragment for the CSDS

The bond lengths C1-C6 and C8-C9 and the dihedral angle C1-C6-C9-C8, as indicated in Figure 3.4 are specified to be used as data for analyses with the VISTA and PLUTO programs. Since the number of structures found in these searches is often relatively low, structures that are disordered, are not screened out, but included since the torsion angle should be roughly the same regardless of some disorder, as long as the rings themselves are not disordered which is checked with all structures. This may create some anomalies when defining specific position with hydrogen atoms, since often disordered structures lack hydrogen atoms. The subset may not contain the disordered structure because there is a lack of hydrogen atoms located at that position, this has the consequence that the total number of

structures in the parent set may be greater than the sum of the subsets. The searches were conducted with the rings being unconnected from each other, other than the C-C linkage between the two rings. So connections between the rings other than the C-C bond were screened out, Figure 3.5 shows such type structures.

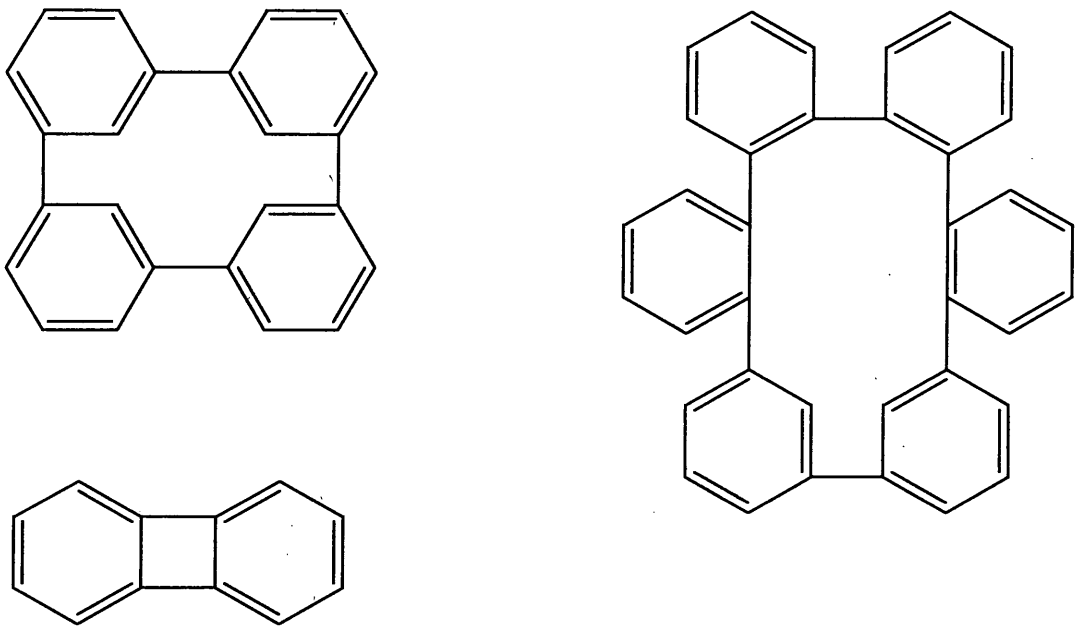

Figure 3.5 Problematic searching fragments

As a result of structures like those seen in Figure 3.5 the data was viewed and assessed individually. This can prove to laborious, but attempts to screen out all unwanted structures resulted in good structures being rejected.

3.5.2 *o-o'*-biphenyls

Here there were many structures that had to be rejected because of connections other than the single C-C linkage bond between the rings. The search conducted of the *o,o'*-biphenyl fragment, Figure 3.5, with any atom attached to 2 and 2' and with 6 and 6' being hydrogen substituted. This created the overall *o,o'*-biphenyl set in which all separate subsets were searched. The structural data were then edited to discard any structures that had the same

dihedral angle counted more than once. Structures with more than one biphenyl in the asymmetric unit were deemed to have each biphenyl counted as a separate entity so all the dihedral angles are counted in the statistical analyses even when both the angles are of very similar values, see Figure 3.6.

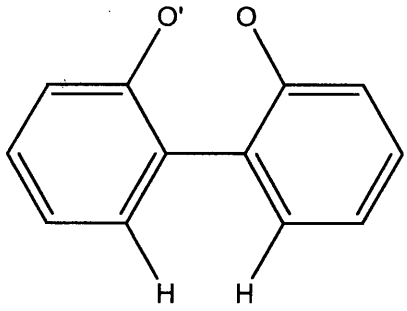

Figure 3.6 The *o,o'*-substituted biphenyl fragment

3.5.3 Non-*ortho* substituted biphenyls

Here the fragment drawn of biphenyl has hydrogen atoms at the *ortho* positions, 2, 2', 6, and 6', see Figure 3.7. Since there are no *ortho* substituents this means that there are fewer structures than the comparative studies in chapters 11 and 12.

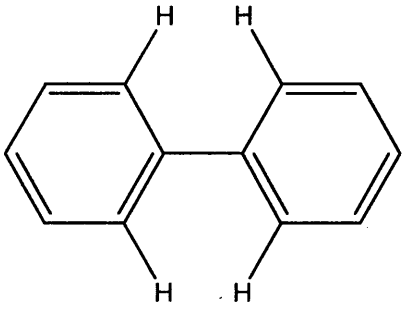

Figure 3.7 The non *ortho*-substituted biphenyl fragment

3.5.4 Heteroaromatic biphenyl type structures

Here the difference in the searches is to the fragment drawn in QUEST3D. Instead of specifying carbon atoms in the rings the search allows for any atoms to be present, with the added criterion that at least one atom present in the ring must be a non carbon atom, see Figure 3.8. In addition the structure is not allowed to be the biphenyl fragment, Figure 3.9.

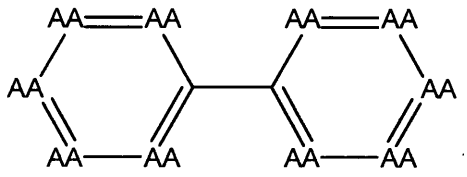

Figure 3.8 The Heteroaromatic fragment, where AA refers to any atom

3.5.5 Biphenyls

With searching for all biphenyl structures in the database a fragment of biphenyl is drawn, see Figure 3.9, there is no stipulation of groups on any of the carbon atoms, therefore all positions on the fragment may have any substituent present.

The search followed that described in the manner of 3.5.2, except all positions were allowed to be occupied

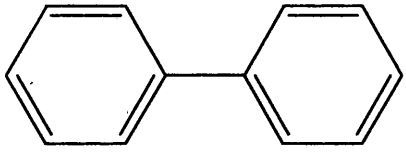

Figure 3.9 The biphenyl fragment

3.5.6 X-X Interaction

This database study was different from the others described here. This search was designed to find *o,o*-biphenyls with halogen atoms at the *ortho* positions, similar to section 3.5.2., the difference in this case is that any halogen is specified at the *ortho* positions and the distance between these substituents is measured.

3.5.7 Bond Distances

Here the bond distances rather than the dihedral angle was specified to be searched for. The relevant figures in Chapter 13 show the specific fragments with their *ortho*, *meta*, and *para* labels. In the searches themselves the *o*, *m* and *p* labels were searched for with the AA (any atom) group.

3.6 REFERENCES

1. Allen, F. H.; Davies, J. E.; Galloy, J. J.; Johnson, O.; Kennard, O.; Macrae, C. F.; Mitchell, E. M.; Mitchell, G. F., Smith, J. M., Watson, D. G., *J. Chem. Inf. Comput. Sci.*, **1991**, 31, 187.
2. Allen, F. H.; Gamer, S. E.; Howard, J. A. K., Pitchford, N. A., *Acta Crystallogr.*, **1994**, B50, 395.
3. Allen, F. H.; Howard, J. A. K., Pitchford, N. A., *Acta Crystallogr.*, **1993**, B49, 910.
4. Allen, F. H.; Howard, J. A. K.; Pitchford, N. A., Vinter, J. G., *Acta Crystallogr.*, **1994**, B50, 382.
5. Allen, F.; Brammer, L.; Kennard, O.; Taylor, R., Watson, D., *J. Chem. Soc., Perkin Trans 2.*, **1987**, S1.
6. Allen, F. H.; Doyle, M. J., Auf der Heyde, T. P. E., *Acta Crystallogr.*, **1991**, B47, 412.
7. Allen, F. H.; Doyle, M. J., Taylor, R., *Acta Crystallogr.*, **1991**, B47, 29.
8. Allen, F. H.; Doyle, M. J., Taylor, R., *Acta Crystallogr.*, **1991**, B47, 41.
9. Allen, F. H.; Doyle, M. J., Taylor, R., *Acta Crystallogr.* **1991**, B47, 50.
10. Ashida, T.; Tsunogae, Y.; Tanaka, I, Yamane, T., **1987**, *Acta Crystallogr.* B43, 212.
11. Brock, C. P., Dunitz, J. D., *Chem. Mater.*, **1994**, 6, 1118.
12. Brock, C. P., Minton, R. P., *J. Am. Chem. Soc.*, **1989**, 111, 4586.
13. Cambridge Structural Database System Users Manuals, *Getting Started with the CSD System*, **1994**, Cambridge Crystallographic Data Centre, 12 Union Road, Cambridge, U.K.
14. Cambridge Structural Database System Users Manuals, *Volume III*, Appendix 1, **1994**, Cambridge Crystallographic Data Centre, 12 Union Road, Cambridge, U.K.
15. Cambridge Structural Database System Users Manuals, *Volume III*, Appendix 15, **1994**, Cambridge Crystallographic Data Centre, 12 Union Road, Cambridge, U.K.
16. Cambridge Structural Database System Users Manuals *VISTA* 2.0 Users Guide, **1995**, Cambridge Crystallographic Data Centre, 12 Union Road, Cambridge, U.K.
17. Desiraju, G. R., *Angew., Chem. (Int. Ed. Engl.),* **1995**, 34, 2311.
18. Hoy, V. J., *PhD. Thesis*, University of Durham, **1997**
19. Kennard, O., Taylor, R., *Acta Crystallogr.*, **1986**, B42, 112.
20. Lommerse, J. P. M.; Stone, A. J.; Taylor, R., Allen, F. H., *J. Am. Chem. Soc.*, **1996**, 118, 3108.

21. Mighell, A. D.; Himes, V. L, Rodgers, J. D., *Acta Crystallogr.*, **1983**, A39, 737.
22. Murry-Rust, P., Motherwell, W. D. S., *Acta Crystallogr.*, **1978**, B34, 2518.
23. Murry-Rust P., Motherwell, W. D. S., *Acta Crystallogr.*, **1978**, B34, 2534.
24. Murry-Rust, P., Bland, R., *Acta Crytstallogr.*, **1978**, B34, 2527.
25. Orpen, A. G.; Brammer, L.; Allen, F. H.; Kennard, O.; Watson, D. G., Taylor, R., *J. Chem. Soc. Dalton Trans.*, **1989**, S83.
26. Pimentel, G. C., McClellan, A. L., *The Hydrogen Bond*, **1960**, Freeman Press, San Francisco.
27. Sayre, D., *Acta Crystallogr.*, **1952**, 5, 60.
28. Sutton, D. J., *J. Chem. Soc.*, **1963**, 1105.
29. Taylor, R., Kennard, O., *J. Am. Chem. Soc.*, **1982,** 104, 5061.
30. Wilson, A. J. C., *Acta Crystallogr.* **1988**, A44, 715.
31. Wilson, A. J. C., *Acta Crystallogr.* **1990**, A46, 742.
32. Wilson, A. J. C., *Z. Krystallogr.*, **1991**, 197, 85.
33. Wilson, A. J. C., *Acta Crystallogr.*, **1993**, A49, 795.

CHAPTER 4:

AN INTRODUCTION TO ASPECTS OF PHOTOCHEMISTRY

4.1 INTRODUCTION

This chapter gives a brief introduction to aspects of photochemistry, so they may be understood to a greater extent in the relevant chapters. This chapter is by no means a comprehensive guide to photochemistry but merely an introduction to terms and concepts that are referred to and used in this thesis. For a proper introduction to photochemistry, there are specialised texts, which should be referred to (Wayne and Wayne, 1996).

When a chemical reaction is being considering there are two paths by which the reaction can proceed, either *via* thermal excitation, or alternatively *via* photo excitation (*i.e.* the absorption of photons). When the reaction is thermal, it is the absorption of heat that increases the translational, rotational and vibrational energies of the reactant that initiates the reactions. It is the collisions between molecules at certain orientations with a thermal energy higher than the necessary activation energy that are able to distort the electronic structure of the molecules and lead to electronic reorganization, namely a chemical reaction, and create the product. This of course this can also be simulated by increasing the kinetic motion of the solution (i.e. by shaking the mixture). Photochemical reactions involve a completely different pathway and are initiated by the absorption of a photon by a molecule. This promotes an electron from the highest occupied molecular orbital (HOMO) to the lowest unoccupied molecular orbital (LUMO), and so the chemical reaction occurs *via* the direct disturbance of the electronic structure of the molecule.

Since both these types of reaction have different processes involved, the thermal and the photochemical reactivities for the same molecule are generally quite different. An example is seen with the 1,3-butadiene molecule, the heating of 1,3-butadiene in cyclohexane to 500 - 600 K the result gives predominately the Diels-Alder cycloaddition product. However, irradiation of the molecule with 254 nm ultraviolet (UV) light gives the intra-molecular ring-closure product efficiently. Thus a molecule in the excited state will behave as a different species from the same molecule under thermal conditions in the ground state. The fact that many compounds react differently in the excited state can be attributed to the difference in the electronic structure and the extremely high energy of the electronically excited state. Generally the same excitement of the structure cannot be obtained thermally. For example, 1,3-butadiene in the excited S_1 state has energy corresponding to 473 kJ/mol^{-1}, to achieve the same energy thermally, the molecules need to be heated to a temperature of approximately 104° C and in practice, this temperature

usually destroys the molecular structure. Another distinct difference between the two types of reaction is that reactions with $\Delta G > 0$ can sometimes be accomplished photochemically whereas their reactions are thermodynamically impossible.

An understanding of structure-reactivity relationships from mechanistic studies enables photochemists to deduce the electronic structures of excited states ((Calver and Pitts, 1966) and (Kagan, 1993)). The ground state electronic configuration of organic molecules consists of bonding molecular orbitals (MOs) each with a pair of electrons and unoccupied anti-bonding MOs. Electronically excited molecules are short lived and will dissipate the excess energy to go back to the ground state. This dissipation process can be either radiative, by the ejection of photons or non radiative or chemical reactions with either another molecule (excited or not excited) or with itself. In the following chapters on photochemistry it will be the excited state σ-bond cleavage reactions that will be the main theme and so here a brief introduction to their mechanistic possibilities will be detailed. Three of the most common types of the bond fragmentation process are;

1. Homolysis, where the bonding electron pair is equally apportioned between two departing fragments.
2. Heterolysis, where the bonding electron pair remains with one fragment.
3. Mesolytic cleavage, which involves the fragmentation of radical ions, formed from electron transfer.

The particular pathway of a reaction is determined by a number of factors including solvent, leaving group and the excited state in which the reaction takes place (singlet versus triplet). Since most intermediates of these reactions are short lived there are several time resolved techniques that have been utilised for study, these include laser flash photolysis (LFP) and pulse radiolysis (PR). Data from these techniques has given a great help in the elucidation of many photochemical reaction mechanisms

4.1.1 The Redistribution of Electron Density

The change in charge distribution of an aromatic molecule in the excited state can be to a first approximation understood using simple Hückel Molecular Orbital (HMO) theory. According to this theory, the s-electron density q_r on the r^{th} carbon is given by;

$$q_r = \Sigma_i \, n_i c_{ir}^2 \qquad \text{Equation 4.1}$$

where n_i is the number of electron(s) occupying the i^{th} orbital and C_{ir} is the orbital coefficient of the i^{th} orbital at the r^{th} carbon atom. Since $C_{HOMO,r}$ is normally different from $C_{LUMO,r}$ the excited state charge distribution is normally different from the ground state. It was noticed that the basicity of aromatic hydrocarbons in the singlet and triplet excited states is higher, by many orders of magnitude, than when it is in the ground state (S_0) (Kuz'min *et al*, 1967). It was shown by deuterium-hydrogen exchange experiments that the basicity of the *meta*-position of mono-substituted benzenes bearing electron donating groups (e.g. methoxy, hydroxy and methoxy) increases dramatically upon electronic excitation ((Spillane, 1975) and (Lodder and Havinga, 1972)). The charge distribution and the localization energy for electrophilic attack of a proton to phenol in the first excited singlet state (S_1) has been calculated. (Bie and Havinga, 1972). The result of this calculation indicated that the *meta* and *ortho*-positions of the molecule have higher electron density and lower localization energy than the *para*-position. Thus the prediction from these results is that the *meta* and *ortho*-positions should be more reactive than the *para*-position towards excited state protonation, which is consistent with the experimental observations.

It has been shown that poly-substituted benzenes are photochemically protonated at position(s) that are different from those expected under thermal conditions ((Smith, 1969) and (Zhang *et al*, 1994)). It has been found that simple HMO calculation can also be used to rationalize the regioselectivity for photoprotonation of these molecules (Wan and Wu, 1990). Generally, it is believed that these reactions occur in S_1, although it has been known for both triplet and singlet states to be involved in some cases. When the aromatic compound possesses a high intersystem crossing yield, the reaction proceeds primarily *via* the triplet state (George, 1971).

When some positions in a neutral molecule become electron rich in S_1 other positions become electron deficient (more electrophilic). This enhanced electrophilicity in the S_1 state can sometimes change the reactivity of the aromatic rings dramatically. This can be observed in many aromatic molecules such as naphthalene **(1)**, biphenyl **(2)**. and many of their derivatives, which are of great interest in this thesis, are immune to nucleophilic attack in the ground state. However they can undergo nucleophilic substitutions with normal nucleophiles in S_1 ((Letsinger and Steller, 1969), (Gunst and Havinga, 1973) and (Griffiths and Hawkins, 1973)). Another result of this charge redistribution is that the polarity of the molecule in the excited state is different from that of the ground state. It has been shown that naphthalene **(1)** is polarized along the long axis in S_1 ((Stevens and Strickler, 1973) and (Klevens and Platt, 1949)). Similarly, biphenyl **(2)** has also been shown to polarize longitudinally in S_1 (Berlman, 1970). More recently, it was shown (Shi and Wan, l995) that biphenyls **(3)** and **(4)** are also highly polarized in S_1 with most of the negative charge residing in the benzene ring not bearing the substituent, see Figure 4.1.

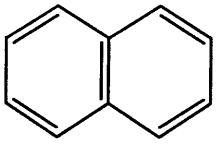

(1)

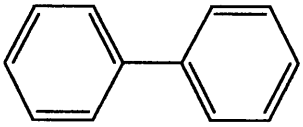

(2)

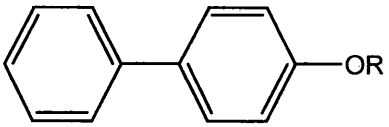

(3): R=H
(4):R=CH_3

Figure 4.1 Representation of structures (1), (2), (3) and (4)

4.1.2 Stokes Shift

Stokes Shift is the difference in wavelength between absorbed and emitted quanta, in wavelength shifters or scintillators. The emitted wavelength is always longer (if single photons are absorbed) or equal to the incident wavelength, due to energy conservation; the difference is absorbed as heat in the atomic lattice of the material. Generally if a molecule experiences large conformational and/or polarity changes upon electronic excitation, a large loss of energy will occur and vice versa. Stokes was the first person to realize this phenomenon.

4.1.3 The Förster Cycle

Förster related the acid-base dissociation of the ground state to that of the excited state for a general acid-base pair by a four-state cycle.

The Förster cycle is a thermodynamic determination of pK and thus provides no direct information about the kinetics of Excited State Proton Transfer (ESPT). However in conjunction with certain theoretical models of proton transfer (PT), such as the Marcus theory (Marcus, 1968 and 1975) and the Eigen model (Eigen, 1964), the thermodynamic property shows some correlation with the rate of proton transfer. Early studies made extensive use of Förster cycle and fluorescence titration methods.

Recent instrumental advances in time-resolved spectroscopy have made direct kinetic measurements of ESPT possible. By using pico- and femto-second laser systems, some ultra-fast rates can been measured directly and thus the dynamic determination of pK becomes possible.

4.1.4 The Franck-Condon Principle

The Franck-Condon principle states that a molecule preserves the nuclear conformation of its initial state during any electronic transition. So the initial state obtained directly after excitation of a molecule has the ground state geometry ((Franck, 1925) and (Condon, 1928)).

4.2 ACID BASE PROPERTIES

4.2.1 Change the Acid-Base Property

An effect brought about by excited state charge redistribution is the change of charge density on the substituents. It is well established that electronic excitation makes the ArOH protons more acidic and the carbonyl group conjugated to an aromatic ring more basic. For example, the pK_a of phenol is 10 in S_0 and 4 in S_1, while the pK_a of benzoic acid is ~ 4.2 in S_0 and 6 - 10 in S_1 (Wehry and Rogers, 1966). The stronger acidity observed for phenols and naphthols in S_1 is due to the greater electron-donating effect of the oxygen atom making the proton more acidic. Carbonyl groups become more electron withdrawing upon excitation and as a result, carbonyl groups are generally more basic in S_1 (Martynov *et al*, 1977). The same type of acid-base property change is also observed for other non-oxygen acids and bases such as the sulphur and nitrogen substituted analogs. It has been reported that the acidity of some carbon acids had a dramatic increase upon excitation, enough to allow the benzylic C-H protons to be deprotonated by H_2O. It was found that the rate of protonation of some functional groups could be increased by 11 - 14 orders of magnitude in S_1 (Wan *et al*, 1982). And when irradiated in a solvent these molecules can undergo excited state proton transfer (ESPT).

4.2.2 Excited State Acid-Base Property

The acid-base property of a molecule is used to measure the dissociation constant K_a. The determination of these constants can be easily determined for the ground state by a variety of readily available techniques. In the excited state, the traditional methods used for ground state measurement are not valid. The difficulties in measuring excited state dissociation constants come from the fact that the concentration of the excited state is much lower than the ground state and the lifetime of the excited state is usually extremely short. Thus the direct determination of the acid-base property of S_1 requires both an ultra-fast experimental technique and a highly sensitive detection technology to work on the same time scale and so the most modern equipment is desired. Due to these technical problems, the excited state dissociation constants (K_a^*) reported in the early days were all determined *via* direct methods. These direct methods are extremely powerful tools and even with the modern equipment available for direct determination of the excited state proton transfer rates, these traditional methods are still often used. One well-known method is the Förster cycle, see section 4.1.3.

4.3 PROTON TRANSFERS

4.3.1 Excited State Proton Transfer (ESPT)

The first example of ESPT was discovered in 1931 (Weber, 1931). It was observed that both the absorption and fluorescence spectra of l-naphthylamine-4-sulphonate were dependent on the pH, *viz.*, the spectra shift considerably at certain pHs. It took twenty years to realize that this phenomenon is the result of an excited state intermolecular proton transfer (ESIerPT). The first example of excited state intra-molecular proton transfer (ESIraPT) was reported in 1995 (Weller, 1955), and it was found that the fluorescence emission of methyl salicylate showed a large Stokes shift. When the acidic phenolic proton was substituted by a methyl group, this unusually large Stokes shift disappeared and the fluorescence emission showed the expected mirror image relationship with the absorption spectrum. This suggested that the fluorescence emission observed for methyl salicylate is due to an excited state isomer formed *via* ESIraPT. Since then extensive studies have been carried out in the field of excited state proton transfer, especially for intra-molecular types, due to the important potential application for this class of photoreaction.

4.3.2 Intra-molecular Proton Transfer (ESIraPT)

The term ESIraPT applies when both the proton donor and proton acceptor reside at the same molecule. Such reactions typically involve transferring an acidic proton from an oxygen atom to a more basic oxygen or nitrogen acceptor, to give the tautomer of the substrate. In this respect ESIraPT is a tautomerization reaction in the S_1 state. ESIraPT reactions have been classified into four distinct classes according to the mechanism of reaction;

1. the intrinsic intra-molecular transfer
2. concerted biprotonic transfer
3. static and dynamic catalysis of proton transfer
4. proton-relay tautomerization.

Details of the specifics of these reactions will not be further elucidated here, however they are detailed within the relevant texts such as Kasha (Kasha, 1986).

4.3.3 Inter-molecular Proton Transfer (ESIerPT)

ESIerPT usually involves transferring a proton from the substrate to a proton acceptor, in the excited state this is generally the solvent molecule. Therefore the rate of proton transfer depends both on the acidity of the substrate and the basicity of the acceptor. The more basic the acceptor and the more acidic the proton of the substrate, the faster is the observed proton transfer rate. ESIerPT in polar solvents is slightly different and proceeds *via* the charge transfer type of transition state, the products found are solvated ions. Therefore the ESIerPT rate may also affect the rearrangement of the solvent molecules in the solvent shell. In slower reactions the rate can be as low as 10^7 s^{-1}, and it is limited by the reorientation time of the polar solvent molecules. Faster reactions, however, can have a rate constant as large as $10^{11}s^{-1}$, which is limited by diffusion. The general observation is that most ESIerPT proceeds adiabatically in the relaxed excited singlet state.

4.4 MOLECULAR GEOMETRY, FLUORESCENCE EMISSION SPECTRA AND SPECTROSCOPIC BEHAVIOUR

Fluorescence emission concerns a transition from S_1 to S_0. According to the Franck-Condon principle the emitting species should also conserve its excited state nuclear conformation immediately after emitting a photon. So the emission spectra should reflect some conformation information regarding the S_1 state. In biphenyl type structures the fluorescence emission spectrum is affected by the S_1 twist angle τ, which is the dihedral angle between the two rings. The twist angle in the ground state also influences the absorption spectrum. The smaller the S_1 twist angle the more red shifted the emission spectrum and vice versa. For many biphenyl type molecules the spectroscopic properties have been summarised into five distinctive categories;

1. Planar in both S_1 and S_0. These molecules have rigid and planar geometry. Simple aromatic and *o, o'*-bridged biphenyl systems are examples of this. These molecules will show a small Stokes shift as well as narrow, highly structured and red shifted absorption and fluorescence spectra.
2. Nonplanar in both S_1 and S_0. This occurs when the energy barrier for rotation is restricted such that S_1 planarization is seriously inhibited. An example of this type is 9,10-diphenyl anthracene. The absorption and fluorescence spectra are narrow and slightly structured, blue and red shifted respectively.
3. Nonplanar in S_0, planar in S_1, These molecules have large geometry changes upon excitation and have a relatively rigid S_1. Examples of these are non solid state biphenyl and many derivative compounds. The absorption spectra are usually blue shifted and diffuse with the fluorescence spectra red shifted, structured and narrow.
4. Nonplanar in S_0, more nonplanar in S_1. These molecules become more twisted upon excitation. An example is 1,1-diphenylethylene. The absorption spectra are slightly structured and blue shifted with the fluorescence spectra diffuse and red shifted.
5. Planar in S_0, non-planar in S_1. These twist to non planarity upon excitation. An example is *trans*-stilbene (Saltiel, 1967). Absorption spectra are narrow with fluorescence spectra broad both are red shifted.

4.5 ALTERING MOLECULAR GEOMETRY OF BIPHENYLS

A family of molecules that undergo significant geometry change in the excited state are biphenyls. It is well known and assumed that these molecules are generally twisted in the ground state but planar (or more planar) in the excited state. This is a sweeping generalization and chapters 10-12 give a more comprehensive picture. There are many cases where biphenyls in the ground state have a planar (or near planar) geometry, but photo excitation is known to increase the planarity of the twisted biphenyls. The effect of photo excitation on biphenyls with planar geometry has not been thoroughly examined: it is assumed that there will be very little change to the dihedral angle but this assumption may prove erroneous. In all cases encountered in the work conducted for this thesis, the starting materials have been twisted and the molecules tend towards planarity upon photo excitation. Generally, data related to the ground state molecular conformation may be obtained from X-ray analysis, UV-Vis spectrophotometry and NMR spectroscopy and molecular mechanics calculations. Crystallographic analysis is limited to the solid crystalline state with reasonable size crystals needed to be grown, but in terms of quantitative results it is the best and most definitive way to obtain structural information. However, methods to determine the geometry of S_1 are limited due to the difficulty of probing very short-lived species. A method of observing the excited state using X-ray diffraction is to "hold" the excited state by creating a reaction that proceeds in the excited state. If this reaction holds the structure in a particular orientation then the structure must stay in the excited state geometry because of the stereochemistry, an example of this being the closed ring product (see chapter 6). These reactions can be made to happen in solid, liquid or gas phases, but of course the gases and liquids have to be crystallized to analyze the results by X-ray diffraction analysis. Stokes shift data provide a qualitative measurement of the molecular geometry change between S_0 and S_1. It is a simple but powerful tool to probe for geometry changes upon electronic excitation.

4.6 REFERENCES

1. Berlman, I. *J. Chem. Phys.*, **1970**, 52, 5616.
2. Bie, D.; Havinga, E. *Tetrahedron*, **1965**, 21, 2359.
3. Calver, J. G.; Pitts, Jr., J. N. *Photochemistry*; John Wiley and Sons Inc.: New York; **1966**, 22.
4. Condon, E. *J. Phys. Rev.*, **1928**, 32, 858.
5. De Gunst, G.; Havinga, E. *Tetrahedron*, **1973**, 29, 2167.
6. Förster, T. *Naturwiss.*, **1949**, 36, 186.
7. Franck, J. *Trans. Faraday Soc.*, **1925**, 21, 536.
8. George, F. J. *Phys. Chem.*, **1971**, 75, 12.
9. Griffiths, J.; Hawkins, C. *Chem. Comm.*, **1973**, 111.
10. Kagan, J. *Organic Photochemistry: Principles and Applications*; Academic Press: San Diego; **1993**.
11. Kasha, M. *J. Chem. Soc., Faraday Trans. 2*, **1986**, 82, 2379.
12. Klevens, H.; Platt, J. *J. Chem. Phys.*, **1949**, 17, 470/481.
13. Kuz'min, M.; Uzihov, B.; Berezin, I. *Zhur. Fiz. Khim.*, **1967**, 41, 446.
14. Letsinger, R.; Steller, K. *Tetrahedron Lett.*, **1969**, 1401.
15. Lodder, G.; Havinga, E. *Tetrahedron*, **1972**, 28, 5583.
16. Martynov, I.; Demyashkevich, A.; Uzhinov, B.; Kuz`min, M. Russ. *Chem. Rev.*, **1977**, 46, 1.
17. Saltiel, J. *J. Am. Chem. Soc*, **1967**, 89, 1036.
18. Shi, Y.; Wan, P. *J. Chem. Soc. Chem. Commun.*, **1995**, 1217.
19. Smith, B. *J. Chem. Soc.*(A), **1969**, 2673.
20. Spillane, W. *Tetrahedron*, **1975**, 31, 495.
21. Stevens, C.; Strickler, S. *J. Am. Chem. Soc.*, **1973**, 12, 3922.
22. Wan, P.; Culshaw, S.; Yates, K. *J. Am. Chem. Soc.*, **1982**, 104, 2504.
23. Wan, P.; Wu, P. *Can. J. Chem.*, **1990**, 822.
24. Wayne, C. E.; Wayne, R. P. *Photochemistry*, **1996**, Oxford University Press.
25. Weber, K. *Z. Phys. Chem.* B, **1931**, 15, 18.
26. Wehry, E.; Rogers, L. *J. Am. Chem. Soc.*, **1966**, 88, 351.
27. Weller, A., *Naturwiss.*, **1955**, 42, 175.
28. Zhang, G.; Shi, Y.; Mosi, R.; Ho, T.; Wan, P. *Can. J. Chem.*, **1994**, 72, 2388.

CHAPTER 5:

BIPHENYL AND DERIVATIVE COMPOUNDS

5.1 INTRODUCTION

In forthcoming chapters in this thesis biphenyl compounds and derivatives are examined either by photochemical means, X-ray and neutron diffraction analysis or using a database (which mainly contain X-ray diffraction data). In this chapter an overview is given of these structures, which shows their history, properties and applications, before examining more specialized aspects and examining biphenyl itself and several derivative compounds.

Biphenyl is a simple aromatic organic compound, the structure consisting of two phenyl (benzene) rings joined together by a single bond between two of the carbon atoms in either ring, (see Figure 5.1). Although it is reasonably unreactive and as a solid is stable in air and to moisture under standard temperature and pressure, biphenyl is reactive enough that it will undergo reactions under appropriate conditions and it is commonly used as a reagent. Biphenyl is a white crystalline solid, insoluble in water, has a flash point of 113° C, an auto-ignition temperature of 540°C, a boiling point of 254°C and melts at 69°C. Biphenyl is also classed as a mild irritant.

The compound biphenyl itself was first synthesized by Rudolph Fittig in 1862 (Fittig, 1862), and since then it has become of interest to scientists in several ways. In chemistry biphenyl is used as a reagent by organic and inorganic chemists. Studies involving biphenyl include those utilizing the biological properties and many papers are published each year involving biphenyl derivatives (*e.g.* Puente *et al*, 1998). Biphenyl also has applications in the polymer field (Madheswari, 1992). It became of more interest in the second half of the 20th century with the development of modern analytical techniques (crystallographic, IR, photolysis techniques, etc), that can measure the biological, chemical and structural properties of this compound in various states ((Bastiansen, 1950) and (Roberts, 1985)). In 1960 biphenyl was structurally determined using X-ray diffraction analysis for the first time (Trotter, 1960) and again in 1962 (Hargreaves & Rizvi, 1962). Due to the absence of heavy atoms in the structure, biphenyl itself was much more difficult to solve than heavy atom derivatives, many of which had already been reported by that time ((Fowweather & Hargreaves, 1949) and (Merrit & Schroeder, 1956)). These commonly had bromine, chlorine and iodine atoms present and were solved using the Patterson method (Fowweather & Hargreaves, 1949).

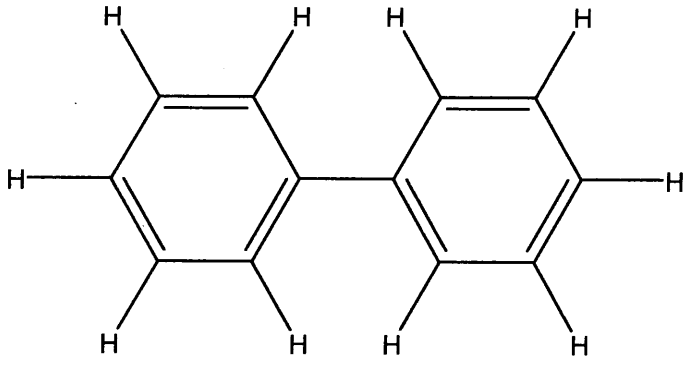

Figure 5.1. The chemical structure of the biphenyl molecule

The X-ray diffraction analyses in the early 1960's showed that there was no structural twisting about the C-C linkage bond away from the planar structure. This was in stark contrast to other analysis previously carried out that used electron diffraction with gaseous biphenyl which found a twisted geometry with a dihedral angle of 45°(Bastiansen, 1950). Later optical studies showed a twist of 15-30°, whilst in solution the angle has been found to be 25° (Takei *et al*, 1988). Studies on substituted biphenyls by both X-ray diffraction analysis ((Rømming *et al*, 1974), (Reboul *et al*, 1993) and (Lesser *et al*, 1975)) and in the gas phase (Bastiansen, 1950) have found the rings to be twisted about the C-C bond. The only structural study that produced a planar structure was the X-ray diffraction analysis of unsubstituted biphenyl. Recently however several substituted biphenyls have also had planar or near planar structures ((Yakushi *et al*, 1974), (Brock and Haller, 1984), (M^{c}Kinney and Singh, 1988) and (Maguire *et al*, 1996)). The early X-ray diffraction structural findings on biphenyl were superseded in 1976 and 1977 using superior equipment and analytical procedures (Charbonneau & Delugeard, 1976 & 1977): X-ray diffraction studies at 110 K and 293 K indicated that the structure of biphenyl is not truly planar, with the rings slightly deviating from the plane. Although not planar the twist is small (<1°) and the structure is still considered to have a near planar geometry. Later findings suggested that an X-ray diffraction study conducted on biphenyl somewhere below 75 K would show the two individual enantiomers. The structure was analyzed using neutron diffraction and a phase change, to an incommensurate phase, was discovered (Cailleau & Badour, 1979). In this incommensurate

phase biphenyl exists as a super cell with the separate conformations of biphenyls existing within this super cell. Upon investigation by typical X-ray diffraction analysis as conducted in this thesis (see chapter 2), the structure given will be an average of the structure in the super cell, creating a smaller cell with more diffuse electron density.

Probably the most commercially important aspect of biphenyl derivative compounds are the biological applications (Puente *et al*, 1998). An important factor in terms of its chemical reactions, and thus all subsequent applications, are the properties of and surrounding, the C-C bond between the two rings. This twisting about this bond affects the chemical reactivity of the structure, inter- and intra-molecular interactions and the overall macromolecular structure. For these types of compound the C-C bond has a tendency to be partially conjugated due to the aromatic phenyl rings on either side pushing electrons through the C-C bond and creating a fully conjugated/aromatic system. This leads to a slight shortening of the ring separation, although not as short as a truly aromatic system. Theoretically the conjugation will be at a maximum when the system is flat or very near planar allowing maximum electron movement in the system. Although the system is less aromatic than benzene, it does have the obvious similarities in the two phenyl rings. However, the flat conformation results in the *ortho* substituents on substituted biphenyl derivatives becoming sterically congested (Figure 5.2). This occurs particularly when the *ortho* substituents are non hydrogen atoms, leading to a tendency to twist from the plane to avoid the steric repulsion. Since twisting from the plane lessens the amount of conjugation, there is a trade off between the amount of conjugation about the C-C bond and twisting due to *ortho* substitution. When there are large *ortho* substituent groups the C-C bond is often twisted to greater than 60°, this greatly limits the amount of conjugation. When the positions *meta* and *para* are substituted then there is very little steric interaction between these substituents. It has been noted (Brock & Minton, 1989) that the twisting of the biphenyl and the bond length of the ring joining bond (which is directly related to conjugation, i.e. shorter bond length = greater conjugation) are not linked and one has no discernable effect on the other. See chapter 11 for more details.

In 1950 Otto Bastiansen published a paper called "The molecular structure of Biphenyl and some of its derivatives"(Bastiansen, 1950) which used electron diffraction techniques to analyze both non-*ortho* and *ortho* substituted biphenyls in the gas phase. His findings showed that for three *o,o'*-biphenyls (dichloro, dibromo and diiodo), the twisting of the rings was closer to that of the *cis* conformation than that of the *trans*. This agreed with the earlier findings (Fowweather & Hargreaves, 1950), which studied several similar structures in the

solid state using X-ray diffraction techniques. These findings initiated the speculation that there may be a possible halogen-halogen attractive interaction involved for halo *o,o'*-substituted biphenyls. This results in the preference for the *cis* conformation for these types of systems (Bastiansen *et al.*, 1979) and to what has been termed an *ortho* effect. This *ortho* effect is a general occurrence that happens for all *o,o'*-substituted biphenyls and is not exclusive to the halo substituted biphenyls. The effect and consequences are more fully examined in chapters 10, 11 and 12 and these will be further explained therein.

Biphenyl compounds have been found to be of much interest photochemically (Shi *et al.*, 1998) and it has been on this topic that interest in biphenyls in this thesis was initiated. As previous studies have shown ((Brock & Minton, 1989), (Wright *et al*, 1982), (Bowen Jones & Brown, 1982), (Leser & Rabinovitch, 1978) and (Chen *et al*, 1996)) the *o-o'*-biphenyl has the tendency to be twisted. The extent of this twisting is due to the particular *o-o'*-substituents and how they interact with one another and the rings, *via* inter-/intra-molecular interactions or on the basic stereochemistry. Not surprisingly, large bulky groups give larger dihedral angles, although this can be greatly affected by the inter-/intra-molecular interactions present. When the biphenyl becomes photoexcited it tends towards planarity ((Huang *et al*, 1991) and (Shi & Wan, 1995)), and this can be very interesting, especially when *ortho* substituents are present. It is possible for the *ortho* substituents to use the twist to become involved in an interaction. Ring closure reactions are one specific type of chemical reaction that can utilize the inherent twisting motion generated when biphenyl compounds are photoexcited (Shi *et al*, 1998). The degree of twisting also has notable effects on the electronic spectra of biphenyls, with large dihedral angles along the C-C linkage bond eliminating conjugation transmission of electron density so that the resulting UV spectra is similar to an isolated ring structure (Roberts, 1985).

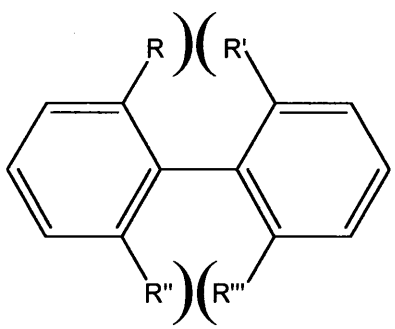

Figure 5.2 Showing the steric crowding of the *ortho* substituents on planar biphenyls

5.2 THE ULTRA VIOLET SPECTRA OF BIPHENYL TYPE COMPOUNDS

The UV spectra of such a systems have been shown to resemble that of an isolated ring structure (Roberts, 1985). The conformation and twisting of biphenyls can be studied in this way. ^{13}C NMR can also be used to study the twist, with ^{13}C shifts being used to estimate inter-planar angles (Roberts, 1985).

There are two energy types that determine the conformation of biphenyls: these are the repulsion energy, E_s, due to the steric interference, and the delocalization energy, E_π, due to the π-electron delocalization from conjugation. The repulsive energy is positive and the π-electron delocalization energy is negative. For calculations the total potential energy, E_T, is taken as the sum of these two contributions;

$$E_T = E_s + E_\pi \qquad \text{Equation 5.1}$$

The equilibrium twist is taken to be when E_T is at a minimum and thus the geometry of the structure is determined by the relative magnitudes of E_s and E_π.

In all phases but the low temperature solid, biphenyl shows structureless electronic spectra due to vibrational and rotational congestion, which gives no precise information on the structure of the molecule. It has been suggested that biphenyl may have a coplanar conformation in the excited electronic state (Takei *et al.*, 1988).

Biphenyls tend to be relatively unreactive because of the aromatic properties they possess and there are no electron donating or withdrawing groups present in the system. When there is a substituent present (obviously this may have resulted from a reaction of unsubstituted biphenyl) then the substituent will tend to have an effect on the reactivity of the system. The manner in which the substituent effects the system is dependent on the type of substituent involved and to which position it is attached. In this respect the biphenyl type molecule is similar to other aromatic systems and each ring can be viewed in the same way as a phenyl ring with a phenyl group attached (substituted benzene), a phenyl benzene.

5.3 PHOTOCHEMICAL ASPECTS OF BIPHENYL AND DERIVATIVES

Biphenyl has a very intense and structureless conjugation band, called the A band, with λ_{max} = 253nm in the crystalline state. In the gas phase this is at 238nm and solution it is 247nm (Suzuki, 1967). This band is so strong and broad for biphenyl that any weaker band in this region is hidden (Pickett *et al.*, 1963). The broad and structureless features of this band indicate that the conformation of biphenyl is not rigid and the dihedral angle only reflects the most probable equilibrium conformation this agrees with the studies described in 5.1.

The introduction of substituents into the 2,2',6, and 6' positions is expected to increase the steric interference between the two benzene rings and thus increases the dihedral angle.

If one can force the two benzene rings to a planar conformation, the molecule will have maximal conjugation. This was observed experimentally in *o,o'*-bridged biphenyls when the ultra violet spectra of 9,10-dihydrophenanthrene and 4,5-methylene-9,10-dihydrophenanthrene were compared to biphenyl. It was found that the spectra of these compounds have similar intensity as biphenyl but are red-shifted due to a more planar geometry and better conjugation. It is well known that introduction of methyl groups onto benzene will also lead to a spectral red shift, however the methylene groups in these molecules alone cannot account for such a large shift. Therefore, geometric changes must be involved (Jones, 1941).

The spectra of a series of *o,o'*-bridged biphenyls have been compared (Suzuki, 1967). It was found that as the number of the bridging carbon atoms increases, the geometry of the biphenyl moiety is gradually forced away from the planar geometry, which results in a progressive blue spectral shift.

5.4 THE X-RAY DIFFRACTION STRUCTURE OF BIPHENYL AND DERIVATIVE COMPOUNDS

5.4.1 The Low temperature X-ray diffraction structure of Biphenyl (1)

As mentioned earlier in this chapter, the X-ray and neutron structure of biphenyl has been investigated several times, and the structure is known in reasonably fine detail. But as laboratory apparatus has improved it is possible to study the structure of biphenyl in a new way. Here the crystals are examined with X-radiation at extremely low temperature and since a phase transition has been discovered to occur at 37 K (Charbonoaues, 1983) it was decided to examine the structure of biphenyl with a temperature as low as possible yet above the phase transition temperature. This examined the bond lengths and angles of the system to more accurately image the true structure. The temperature was set to 40 ± 2 K and using an ultra low temperature cooling system mounted on the SMART CCD and the relevant procedure carried out, as described in chapter 2.

The space group used in the original solution, $P2_1/a$, was found to be inadequate for this low temperature structure and it had to be solved and refined in *Pc*. The structure has pseudo symmetry and initially appears to be in the space group $P2_1/a$ but even once the solution was found using a full sphere and the structure refined the structure would not convert to the $P2_1/a$ space group. So the space group at 40(2) K is *Pc*. This pseudo symmetry is interesting and can only be found at the extremely low temperature. A space group determination was conducted on the same crystal at 80(2) K and the $P2_1/a$ cell was easily determined.

This structure showed a small dihedral angle but as seen in the previous study (Charbonoaues, 1977), there is some residual twisting in the structure. In this examination the dihedral angle is 0.55(25)°. The structure itself refines well in the Pc space group and all parameters are within acceptable values (see Table 5.2 for full details). In the ellipsoid plot at 50% probability the atoms are small, as to be expected at this very low temperature. The bond lengths examined with this study have a reasonably large variance with the C-C linkage bond 1.499(2) Å and the ring distances ranging from 1.379(6) to 1.428(6) Å. This is large and is presumably due to packing effects or an effect of the structure being close to the phase transition. Given the study of the bond lengths of biphenyl later in this thesis (Chapter 13), these values are useful for comparison, see Table 5.1.

In the refinement the hydrogen atoms were easily determined from a residual electron density map and the refinement remained stable with all the hydrogen atoms freely refining. However,

since the magnitude of the electron density of the hydrogen atoms is low and therefore their positions cannot be determined with a great deal of accuracy the atoms are fixed to the carbons for the final model described here.

The dihedral angle of biphenyl is near planar, although with a slight deviance from the plane with an average dihedral angle of 0.55(25)°. The bond lengths of biphenyl are of the approximately expected values, with the lengths approximately uniform throughout the system for the bond lengths other than C(1)-C(1'), which is not a fully aromatic bond. This demonstrates that the rings themselves are fully aromatic and that the attachment of the other ring does not have any noticeable effect on the bond lengths. The packing diagram of biphenyl (see Figures 5.5a, 5.5b and 5.5c) shows that there are no inter-molecular interactions and this includes an absence of any π interaction in the form of π-stacking. The inter-planar distance is approximately 5.58 Å.

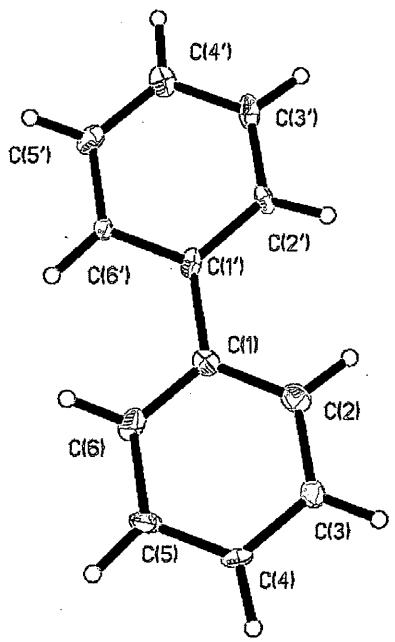

Figure 5.3 Thermal ellipsoid plot of biphenyl at 40 K, showing 50% probability

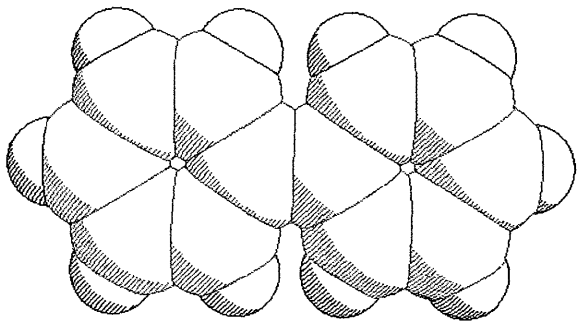

Figure 5.4 The space filled view of the X-ray diffraction structure of biphenyl (1)

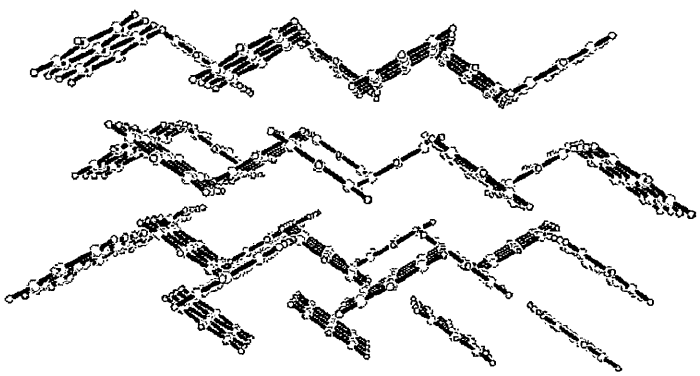

Figure 5.5a The packing structure of biphenyl (1), showing the layered structure.

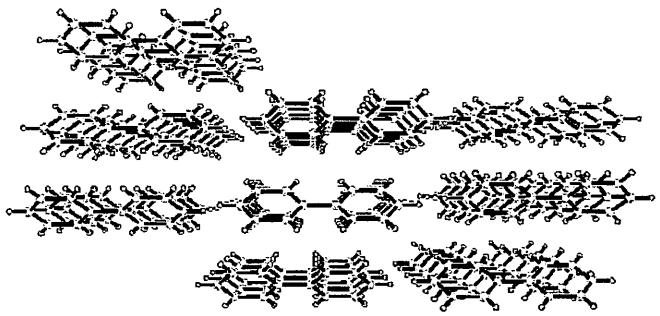

Figure 5.5b Packing structure of biphenyl (1), viewed perpendicular to the plane of the rings

Figure 5.5c Packing of biphenyl (1), showing the relative orientation of the ring planes.

Bond	Distance (Å)	Bond	Distance (Å)
C(1)-C(1')	1.499(2)	C(1')-C(2')	1.428(6)
C(1)-C(2)	1.401(7)	C(2')-C(3')	1.372(6)
C(2)-C(3)	1.379(6)	C(3')-C(4')	1.404(7)
C(3)-C(4)	1.394(7)	C(4')-C(5')	1.392(7)
C(4)-C(5)	1.390(7)	C(5')-C(6')	1.403(6)
C(5)-C(6)	1.411(6)	C(6')-C(1')	1.413(6)
C(6)-C(1)	1.386(7)		

Table 5.1 The bond distances of biphenyl at 40 ± 2 K

5.4.2 The structure and bonding of 4, 4'-bipyridyl (2)

In an effort to study the effects of inter-molecular interaction of the *para* groups in biphenyls, it was decided to study common hydrogen bonding motifs and their effect.

This structure is an analogue of biphenyl and it would be expected to be similar in conformation. For this analysis the crystals generated have water included. This is not surprising since the nitrogen atoms on the rings are susceptible to forming interactions with hydrogen bonding donors and H_2O interacts well. The H_2O forms hydrogen bonds with the nitrogen atoms and the structure forms a series of hydrogen bonded layers, see Figure 5.7. In this case there is possible weak π-stacking present and the crystallized state adopts this layered structure with the inter-planar distance of approximately 3.73 Å. This distance is larger than that for graphite (3.4 Å) and generally anything larger than 3.4 Å is not considered significant. Over all the presence of the H_2O is undesired and a bipyridyl structure without solvent present would have been preferred, unfortunately suitable crystals without the water could not be obtained. There is no ring distortion caused by the nitrogen atoms in the ring. The torsion angles are greater than biphenyl **(1)**, being 41.5(3)° and 40.8(4)° with the C-C bond lengths 1.528(8) Å and 1.465(8) Å respectively. It is interesting that this structure has a smaller inter planar distance than biphenyl yet with no significant π-stacking present. This is probably due to the packing allowing closer inter-planar distance with the twisted structure, however there may be a weak interaction present.

Since this study was conducted a 4, 4'-bipyridyl with no solvent within the unit cell has been determined (Boag *et al,.*1999). This reported structure has smaller dihedral angles (approximately 34° and 19°) and packs in an hydrogen bonded sheet structure. Although not as twisted as the structure reported in this thesis, it still has a relatively large twist away from the plane.

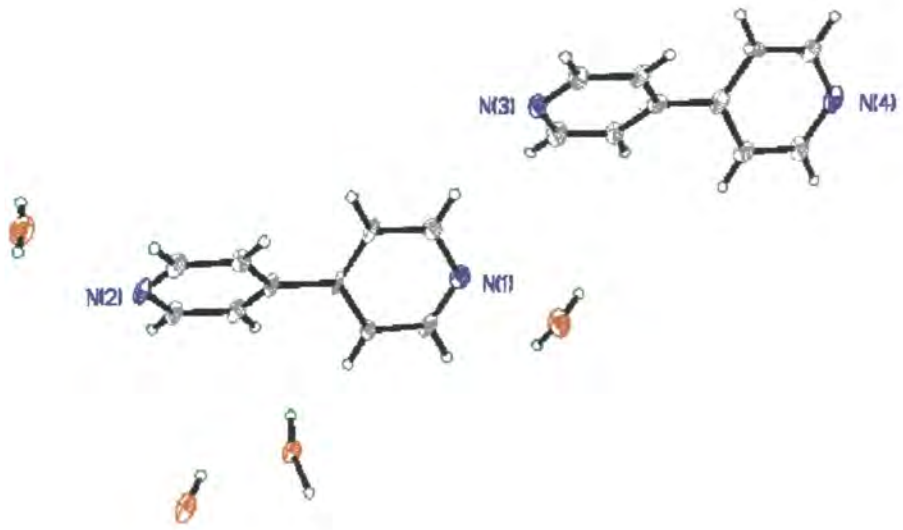

Figure 5.6 The structure of 4, 4'-bipyridyl (2), with disordered H_2O present.

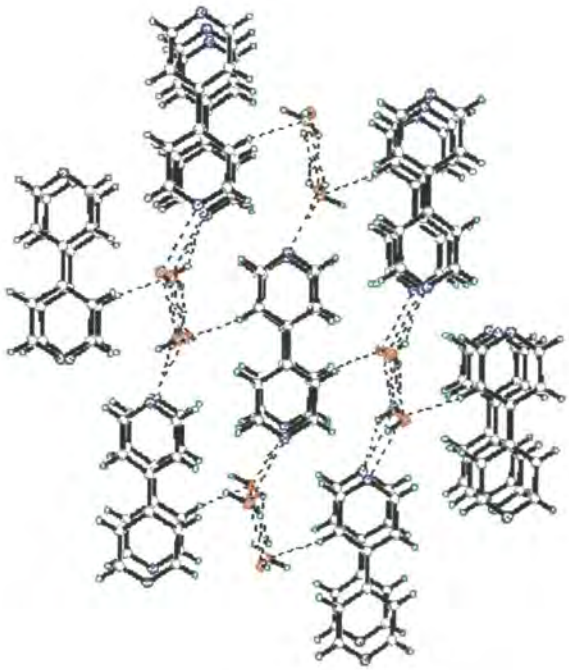

Figure 5.7 The packing of 4, 4'-bipyridyl/H_2O, showing the inter-molecular interaction between the water and bipyridyl nitrogens.

5.4.3 The structure and bonding of 4-Biphenylcarboxylic acid (3)

In this case a single carboxylic acid group was chosen on the *para* position with no other substituents present on the ring, see Figure 5.8. Initially it was expected that this structure would have been studied and the results deposited in the Cambridge Structural Database. However, even though the compound is readily available from manufacturers upon inspection was not found in the CSD. As a consequence of this the structure was deemed interesting enough to do a diffraction analysis on and thus the crude compound was obtained and crystallized. The crystallization was achieved using evaporation of the solvent, acetone. The crystals formed readily although did not grow to be very large from acetone, and did not form readily in toluene, methanol or ethanol. The crystals formed were colourless and needle like.

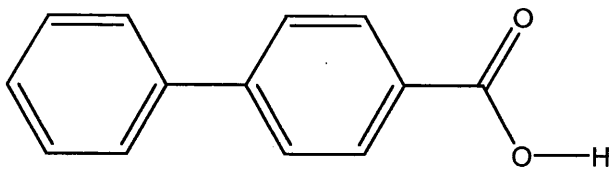

Figure 5.8 The represented structure of 4-biphenylcarboxylic acid (3)

A diffraction experiment was conducted using the SMART CCD area detector, at 150(2) K. The crystals diffracted well (considering their size and molecular structure) and the diffraction experiment proceeded without problems.

The subsequent analysis of **(3)** found the unusually high 12 cell formula units, 4 sets of 3 molecules in the asymmetric unit, see Figure 5.9.

As expected the carboxylic acid groups form hydrogen bonds in a relatively simple motif, with both the COH and CO parts involved in hydrogen bonding to the same acid group on another structure. Two of the structures in the asymmetric unit are inter-molecularly hydrogen bonded to each other while the other is hydrogen bonded to an equivalent structure in another asymmetric unit in all three molecules in the asymmetric unit have different amounts of twisting, and each molecule is truly an independent species. It is interesting that there is such variation in the torsion angles, since all the molecules have crystallized in the one asymmetric unit under the same conditions. Although the variance in the amount of twisting is not large there is a definite difference in the dihedral angles. A major distinction in

the separate molecules is the difference in the carbon-oxygen distances. For the structure not bonded to the other two in the unit cell then the C-O distances are 1.264(2) Å and 1.286(2) Å (Figure 5.10). These lengths are similar, although different enough to distinguish between the separate C=O and C-O-H parts of the acid group. When examining the C=O distances in the two structures linked together in the asymmetric unit the distances are similar to each other, with C15-O6 and C15-O8 at 1.277(2) Å and 1.269(2) Å respectively (see Figure 5.9 and 5.10) and C27 to O2 and O3 at 1.274(2) Å for both distances. The reason for this similarity is probably due to an averaging of the two sites in the crystal, with the C-O and C=O positions of the acid group swapping positions on independent structures within the crystal structure. The event of independent molecules in the crystal flipping between the two sites seems extremely unlikely given the spherical shape of the thermal ellipsoids. Another possible explanation is the occurrence of proton transfer between the two molecules and thus the averaging of the two CO distances within the acid group. The similarity of the C-O/C=O bond distances is an interesting feature of this structures, the exact nature of the C-C bond and consequently the nature of the hydrogen bonding in the structure would be better determined by an analysis of ultra low temperature diffraction. Figure 5.10 shows the expanded hydrogen bonding with the symmetry equivalent structures, with a O-H···O bond distance of 1.604(3) Å. There is no π-bonding present, see Figure 5.11. The inter-planar distance is approximately 7.4 Å. Since there are three independent molecules there are three dihedral angles, these are 27.9(6)°, 34.3(4)° and 32.2(5)°. Since there is no π-stacking and/or *ortho* or *meta* intra/inter-molecular interactions, the rings should be free to adopt any conformation. A twist is observed which indicates that this may be a preferred biphenyl ring conformation of a biphenyl derivative without the influence of the π-stacking.

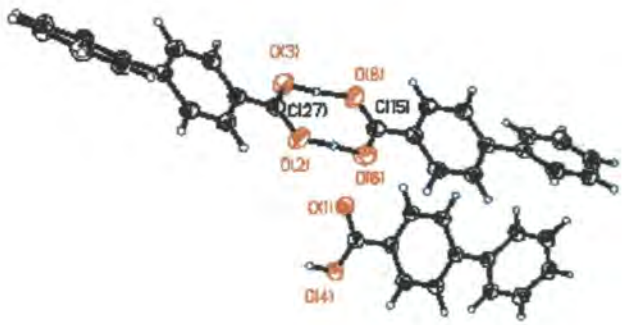

Figure 5.9 The thermal ellipsoid plot at 50% probability of the independent units of 4-biphenylcarboxylic acid (3)

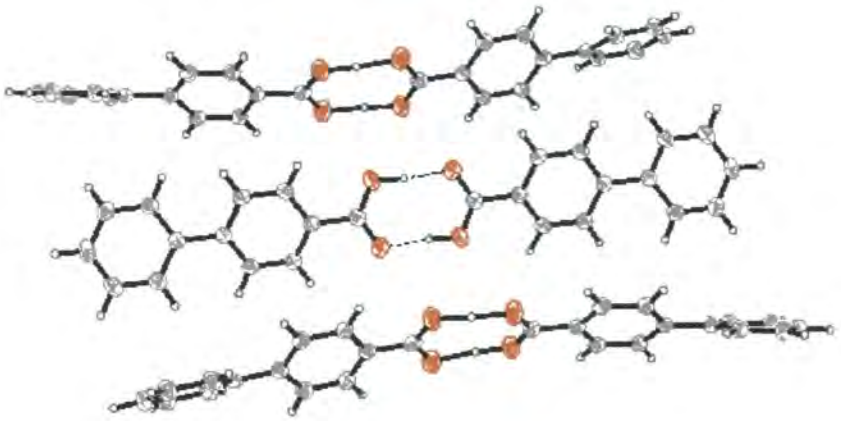

Figure 5.10 The expanded structure of 4-biphenylcarboxylic acid (3) showing all the hydrogen bonding present in the structure

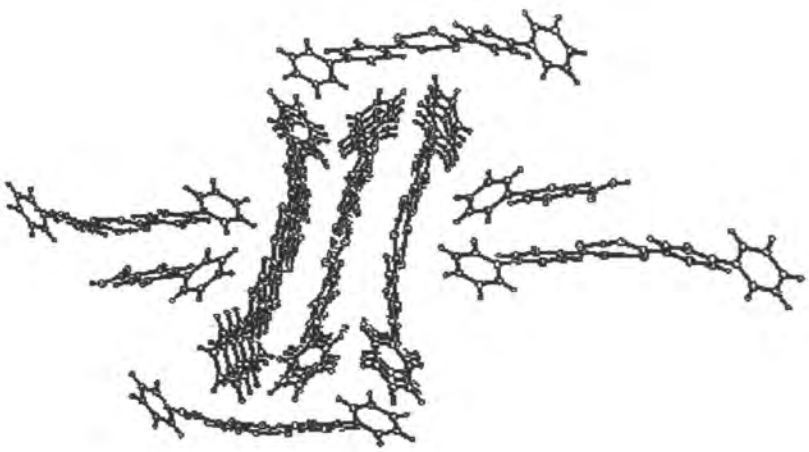

5.11 The packing structure of 4-biphenylcarboxylic acid (3)

5.4.4 The structure of 4,4'-dihydroxybiphenyl (4)

Similar to 4,4'-bipyridyl **(2)** and to 4-biphenyl carboxylic acid **(3)**, this structure has obvious hydrogen bonding groups attached at the *para* position and as with the previous cases the structure utilises these for hydrogen bonding. The structure itself is more similar to that of 4,4'-bypyridyl in that there is a near planar dihedral angle of 0.15 °. The inter planar distance of 5.34 Å is similar to that of biphenyl **(1)** (5.58 Å).

There is hydrogen bonding present in the form of O-H···O bonds. This bonding is singular and create chains in the structure. These hydrogen bonds have a length of 1.956(5) Å. The structure itself is completely symmetrical with an inversion point at the mid point between C5 and C5A, with respect to the inter/intra-molecular interactions. This structure is that which would be expected, as the hydrogen bonding is from the sole hydrogen bond donor/acceptor OH group present. It is interesting that the structure with a small dihedral angle, akin to biphenyl has an inter planar distance similar although not identical to biphenyl.

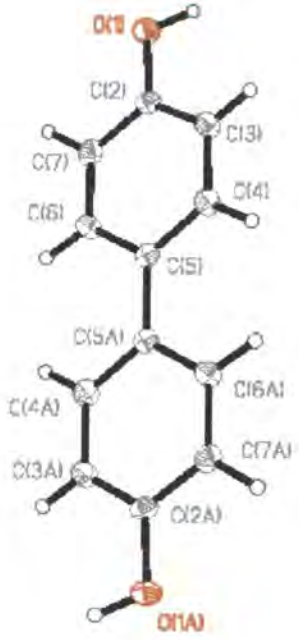

Figure 5.12 The structure of 4,4'-dihydroxybiphenyl (4), with 50% thermal ellipsoids.

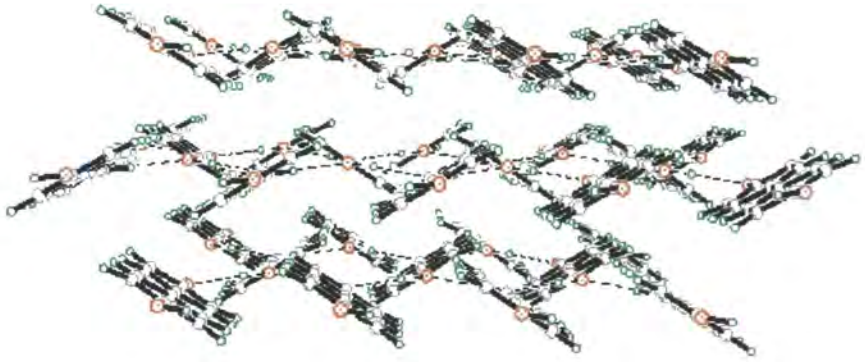

5.13 The packing of 4,4'-dihydroxybiphenyl, showing the layered structure.

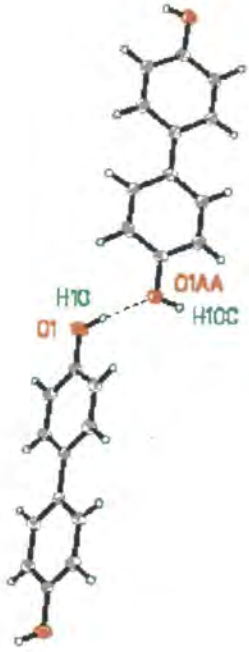

5.14 The Hydrogen bonding structure of 4,4'-dihydroxybiphenyl (4)

5.4.5 The structure of 2-hydroxymethyl-3'-hydroxybiphenyl (5)

The crystal of the compound **(5)** was mounted on a glass fiber and was cooled to 150(2) K with a stream of dry N_2. The data were collected on a Siemens SMART CCD diffractometer employing graphite monochromated Mo-Kα radiation λ= 0.71073 Å.

The structure of **(5)** in the solid state is connected through a series of hydrogen bonds. The OH groups are good both donor and acceptor groups for hydrogen bonding. The hydrogen bonds in the structure are positioned to form a 3-dimensional network of such bonds. The structure has a somewhat layered structure with an inter-planar distance of approximately 3.56 Å. This is longer than generally accepted as an interaction (*c.f.* graphite at 3.4 Å) and although a weak interaction is possible it is not be considered to be an interaction but simply the way phenyl groups have orientated in the lattice.

The structure is moderately twisted with a dihedral angle of 58.8(7)°, as anticipated with the *ortho* substituents present. The conformation of the structure is the *trans* conformation, which is the less common isomer (see chapter 10), crystallographic data is detailed in Table 5.2.

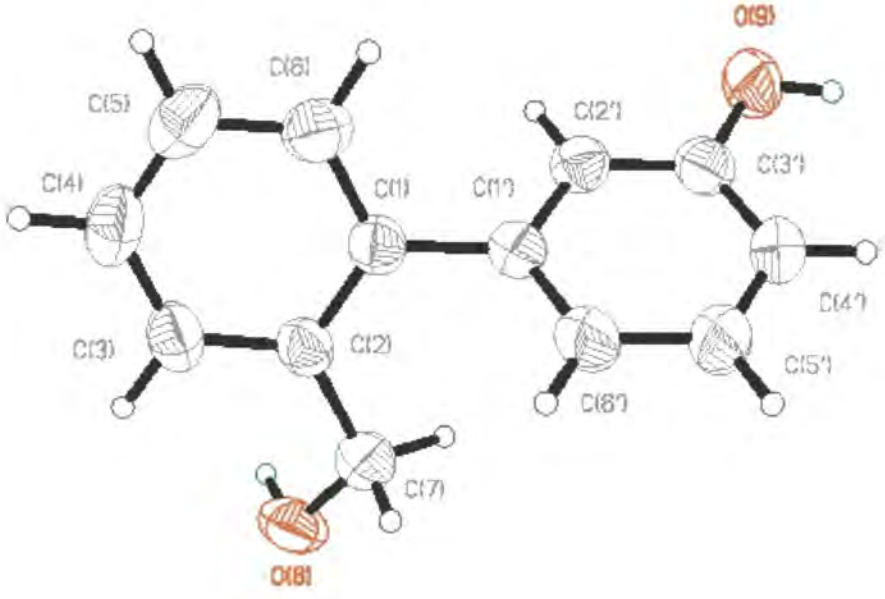

Figure 5.15 The Thermal Ellipsoid plot of 2-methoxy-3'-hydroxybiphenyl (5), with 50% probability

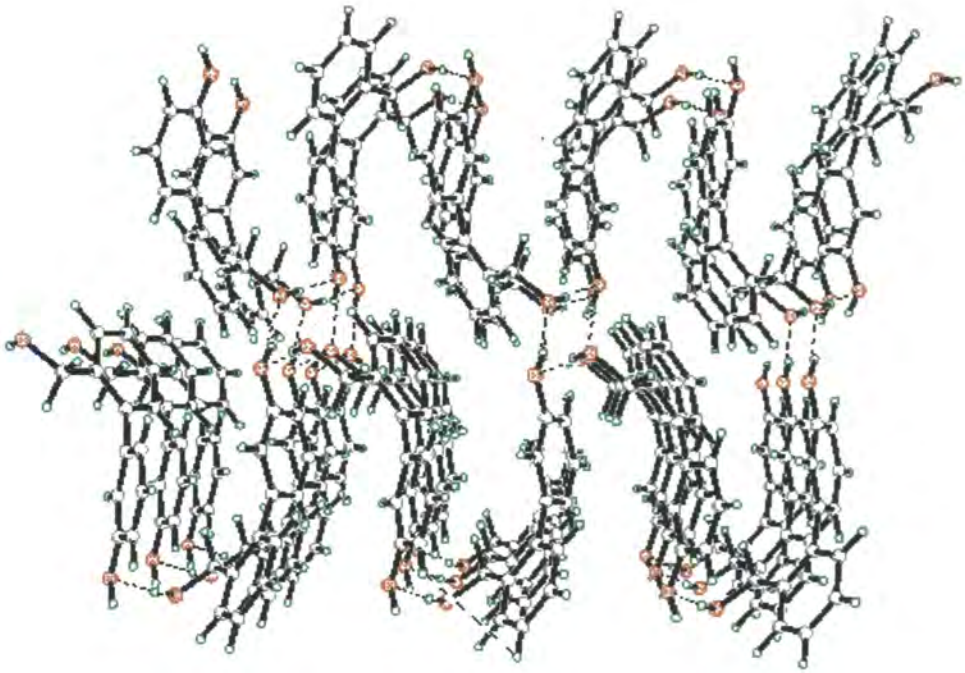

Figure 5.16 The packing of structure of (5), looking down through on the layered structure

	Biphenyl (1)	(2)*	(3)	(4)	(5)
Formula	$C_{12}H_{10}$	$C_{10}N_2H_8$	$C_{13}H_{12}O_2$	$C_{12}H_{12}O_2$	$C_{13}H_{12}O_2$
Formula Weight	154.20	156.2	200.23	188.22	200.23
Crystal Colour	Colourless	Colourless	Colourless	Colourless	Colourless
Temperature (K)	150	150	150	150	150
Wavelength (Å)	0.71073	0.71073	0.71073	0.71073	0.71073
Crystal System	Pc	P2(1)/c	P2(1)/c	P2(1)/c	$P2_12_12_1$
Space group	Monoclinic	Monoclinic	Monoclinic	Monoclinic	*Ortho*rhombic
a= (Å)	9.47170(10)	9.170(2)	7.4031(15)	10.560(2)	7.379(2)
b= (Å)	5.5768(2)	7.450(2)	26.744(5)	5.3400(11)	8.039(2)
c= (Å)	7.8156(2)	14.740(3)	15.685(3)	7.8900(16)	17.762(4)
α= (°)	90	90.000	90	90	90
β= (°)	93.901(2)	100.96(3)	103.24(3)	95.25(3)	90
γ= (°)	90	90.000	90	90	90
Volume ($Å^3$)	411.877(19)	988.6(3)	1053.6(4)	443.06(16)	1053.6(4)
Z	2	4	12	2	4
Calculated Density (Mg/m^3)	1.243	1.288	1.320	1.411	1.262
Absorption Coefficient (mm^{-1})	0.070	0.092	0.088	0.095	0.084
F (000)	164	406	1272	200	424
θ Range for Collection (°)	4.24 to 27.36	1.41 to 27.52	1.52 to 27.44	1.94 to 27.48	2.29 to 27.49
Index Ranges	-11<=*h*<=10, -6<=*k*<=5, -9<=*l*<=9	-11<=*h*<=7 -9<=*k*<=9 -16<=*l*<=19	-9<=*h*<=9, -33<=*k*<=34, -19<=*l*<=20	-12<=*h*<=13, -6<=*k*<=6, -10<=*l*<=9	-9<=h<=5, -9<=k<=10, -21<=l<=19
Reflections collected	2188	6574	21353	2822	4382
Independent reflections	1286	4307	6896	1018	2083
Data/restraints/ parameters	1286 / 2 / 110	4307 / 1 / 254	6887 / 0 / 497	1018 / 0 / 80	2083 / 0 / 164
Goodness-of-fit on F^2	1.180	0.997	1.064	2.131	1.044
Final R indices [I>2sigma(I)]	0.0475	0.0831	0.0465	0.0850	0.0369
R indices (all data)	0.1420	0.2509	0.1165	0.3165	0.1005
Extinction coefficient	0.052(18)	0.015(4)	0.0022(4)	0.00(2)	.030(5)
Largest diff. Peak and hole. ($e.Å^3$)	0.204 and -0.258	0.487 and -0.339	0.243 and -0.424	0.437 and -0.295	0.115 and -.122

Table 5.2 The Crystallographic data for structures (1)-(5) :* is without the disordered solvent

5.4.6 Summary of Diffraction of biphenyl and derivatives

Biphenyl **(1)** itself is almost planar and there is no discernable π-stacking present this is similar to that of **(4)** and in terms of geometry these two structures are similar, however, **(4)** has hydrogen bonding that is not present in **(1)**. The structures **(2)**, **(3)** and **(5)** are all twisted and have greater inter-planar spacing and in these respects have similar structures. Structure **(4)** has *para* groups present and these groups on the structure do not result in a twisted geometry, which is the case of **(2)**, **(3)** and **(5)**. The reasons behind this are dealt with in more detail in chapter 13. Structure **(2)** although having different groups at the *para* position still has the twisted geometry, it appears that biphenyl is stereochemically different from most of the substituted analogues as illustrated in chapters 10-13.

It is interesting to note that in all these structures there is a lack of π-stacking, since the inter-planar distances are too long. This is slightly surprising given the obvious availability of the phenyl rings to be involved in such interactions, especially in the case of biphenyl **(1)** which has no other inter-/intra-molecular interactions.

5.5 REFERENCES

1. Bastiansen, O. *Acta Chem. Scand.* **1950**, *4*, 926.
2. Bastiansen, O.; Kveseth, K.; Møllendal, H. *Topics in current Chemistry.* **1979**, 101.
3. Bowen Jones, J.; Brown, D. S. *Acta Cryst.*, **1982**, B38, 317.
4. Brock, C. P.; Minton, R. P. *J. Am. Chem. Soc.* **1989**, *111*, 4586.
5. Cailleau, H.; Baudour, J. L.; Zeyen, C. M. E. *Acta Cryst*, **1979**, B35, 426.
6. Charbonneau, G. P.; Delugeard, Y. *Acta Cryst.*, **1976**, B32, 1420.
7. Charbonneau, G. P.; Delugeard, Y. *Acta Cryst.*, **1977**, B33, 1586.
8. Chen, X-M.; Luo, G-B.; Tong, M-L.; Zhou, Z-Y. *Acta Cryst.*, **1996**, C52, 1727.
9. Fittig, R Justus *Liebigs Annalen Chemie*, **1862**, *121*, 361.
10. Jones, R., **1943**, *J. Am. Chem. Soc.*, 63, 1658.
11. Fowweather, F.; Hargreaves, A.; *Acta Cryst.*, **1950**, 3, 81.
12. Jones, R., *J. Am. Chem. Soc.*, **1943**, 63, 1658.
13. Hargreaves, A.; Rizvi, S. H. *Acta Cryst.*, **1962**, 15, 365.
14. Howard J. A. K., unpublished results.
15. Huang, C. G.; Beveridge, K. A.; Wan, P. *J. Am. Chem. Soc.* **1991**, *113*, 7676.
16. Lesser, D. P.; De Vries, A.; Reed, J. W.; Brown, G. H. *Acta Cryst.* **1975**, B31, 653.
17. Madheswari, D., Nanzundan, S., Reddy, A. V. R, *Eur. Polym. J.*, **1992**, 28, Nó. 9, 1123.
18. Maguire, J. M.; Multzer, J.; Bats, J.W., *J. Org. Chem.*, **1996**, 61, 6936.
19. Merritt, L. L. Jr.; Schroeder, E. D. *Acta Cryst*, **1956**, 9, 801.
20. Pendás, A. M., López-Otín, C., **1998**, *Genomics*, 51, 459-462.Suzuki, H., **1967**, Electronic Absorption Spectra and Geometry of Organic Molecules, Academic Press, New York Press, New York London.
21. Pickett, L.; Walter, G.; France, H.; *J. Am. Chem. Soc.*, **1963**, 58, 2296.
22. Puente, X. P., Pendás, A. M., López-Otin, C., *Geonomics*, **1998**, 51, 459.
23. Reboul, J. P.; Pèpe. G.; Siri, D.; Oddon, Y.; Caranoni, C.; Rahal, H.; Soyfer. J. C.; Barbe, J. *Acta Cryst*, **1993**, C49, 735.
24. Roberts, R. M. G. *Magn. Res. Chem.*, **1985**, 23 52.
25. Rømming, C. Seip, H. M.; Øymo, I.-M. A. *Acta Chem. Scand.* **1974**, A28, Nõ. 5, 507.
26. Shi, Y.; Wan, P. *J. Chem. Soc., Chem. Commun.*, **1995**, 1217.
27. Shi, Y.; MacKinnon, A.; Howard, J. A. K.; Wan, P. *J. Photochemistry and Photobiology A:Chemistry*, **1998**, 113, 271.

28. Suzuki, H., *Electronic Absorbtion Spectra and Geometry of Organic Molecules*, **1967**, Academic Press, New York Press, New York London.
29. Takei, Y.; Yamaguchi, T.; Osamura, Y.; Fuke, K.; Kaya, K. *J. Phys. Chem.*, **1988**, 92, 577.
30. Trotter, T.; *Acta Cryst.*, **1961**, 14, 1135.
31. Wright, J. J.; Cooper, A. B.; M^{c}Phail, A. T.; Merrill, Y.; Nagabhushan, T. L.; Puar, M. S. *J. Chem. Soc., Chem. Commun.*, **1982**, 1188.

CHAPTER 6:

SOLID STATE AND SOLUTION PHASE PHOTOCYCLIZATION OF α,α-DIPHENYL-2-(2'-HYDROXYPHENYL) BENZYL ALCOHOL

6.1 INTRODUCTION

X-ray diffraction analysis has shown the structure of α,α-diphenyl-2-(2'-hydroxphenyl)benzyl alcohol **(5)** (see Figure 6.1,) and that it is highly twisted (dihedral angle between of the biphenyl ring system is approximately 80°). It photocyclizes efficiently in CH_3CN solution as well as in the crystalline state, to give the much more planar α,α-diphenyldibenzo[b,f]pyran **(7)**. The analogue of α,α-diphenyldibenzo[b,f]pyran, **(1)** (Figure 6.2), has also been characterized by X-ray analysis. The mechanism of reaction in CH_3CN solution is believed to involve initial excited state intramolecular proton transfer from the phenol OH to the benzylic CPh_2OH. The reaction in the solid crystalline state is proposed to involve an excited state inter-molecular proton transfer. The compound crystallizes as hydrogen bonded dimers in a unit cell consisting of eight molecules in which the phenol OH is hydrogen bonded to the oxygen atom of the benzylic CPh_2OH group.

In this chapter the compounds will be referred to by their corresponding numbers as shown in Figures 6.1 and 6.2.

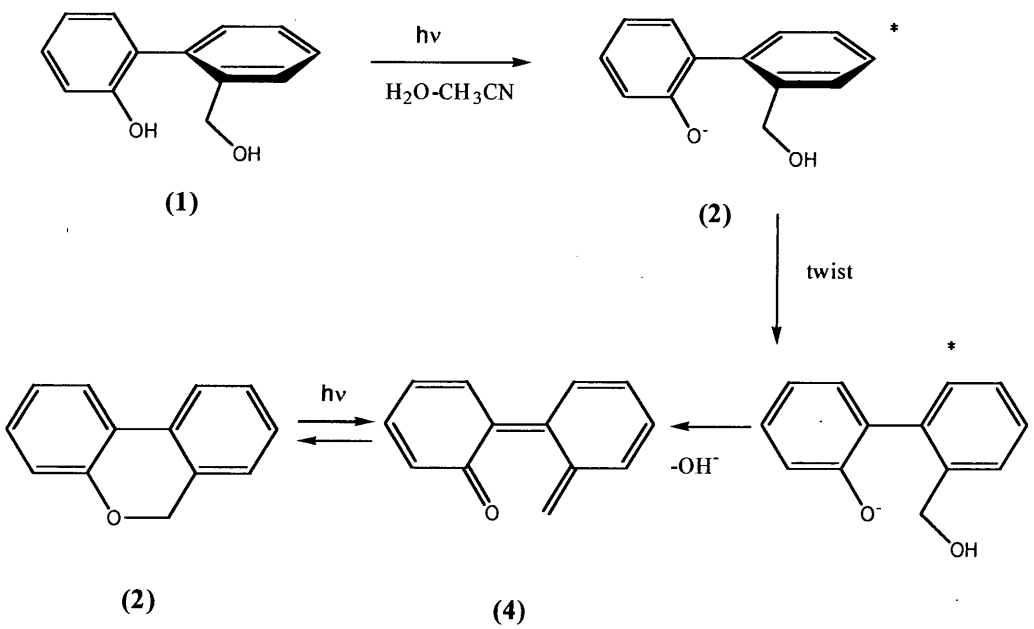

(1) (2) (2) (4)

Figure 6.1 Scheme 1 representing the photoreaction of (1) to (4)

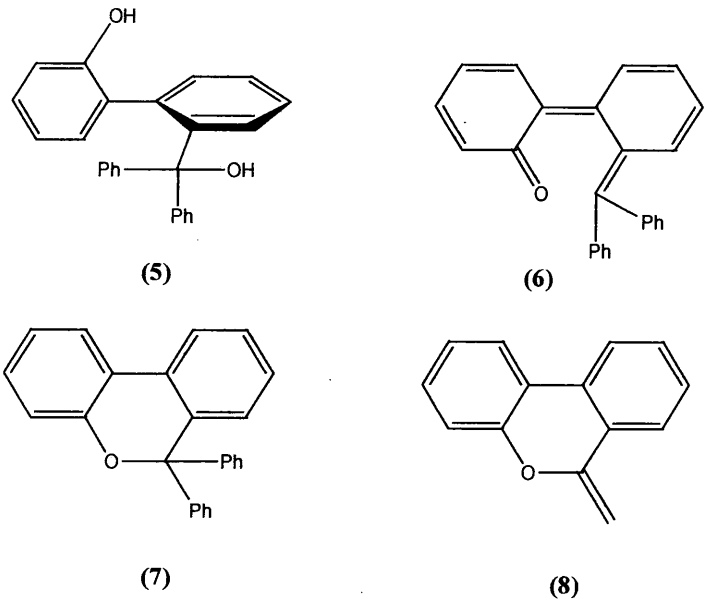

Figure 6.2 Structural representation of (5), (6), (7) and (8)

The starting material **(5)** has been fully characterized by both X-ray and neutron diffraction, determining the hydrogen bonding character. The product **(7)** has also been characterized as well as the analogue **(1)**.

The study of photochemical reactions in the solid state has been of intense interest now for many years (Hollingsworth, 1990). Recently, organic photochemists have utilized such reactions for controlling stereoselectivity (Ramamurthy, 1987) and regioselectivity (Scheffer, 1991) with promising results, as well as exploring the mechanism of solid state photoreactions requiring large torsional motions (Leibovitch, 1997) and photosolvolysis in the solid state (with co-crystallized solvent molecules) (Sakamoto, 1996). Here it has been chosen to study the solid state photocyclization of the α,α-diphenyl-substituted biphenyl derivative **(5)** (α,α-diphenyl-2-(2'-hydroxyphenyl)benzyl alcohol) due to the ease in which crystals suitable for X-ray crystallography can be grown, it was also chosen to study the expected large dihedral angle of the biphenyl ring system, and the potential of using laser flash photolysis (in solution) to monitor for the formation of the corresponding *o*-biphenyl quinone methide **(6)**, which might be sufficiently long-lived for its detection due to the greater conjugation expected in the additional benzene rings at the α-position. It can be seen that **(5)** photocyclizes efficiently in solution as well as in the solid state, to give the expected pyran **(7)**. The X-ray crystallographic analysis shows the structure and an absence of any included water in the unit cell of the crystal, with the O-H protons exhibiting both intra and inter-molecular hydrogen-bonding. Photocyclization

mechanisms involving initial excited state intra and inter-molecular proton transfer are presented and discussed.

6.2 BACKGROUND

In 1991 a new type of photocyclization reaction involving *o,o'*disubstituted biphenyls was reported by Wan and coworkers (Huang, *et al.* 1991), the parent reaction of which converted 2-(2'-hydroxyphenyl)benzyl alcohol **(1),** see Figure 6.2, to 6H-dibenzo[b,d]pyran **(2)** in high chemical yield, with quantum yields as large as 0.5 in basic aqueous CH_3CN solution. The reaction was also observed in neat CH_3CN, but with lower quantum efficiency ($\Phi = 0.12$). The X-ray diffraction analysis of the structure of **(1)** (Huang, *et al.* 1991) shows a highly twisted biphenyl ring system (dihedral angle of 68 °) where the two *ortho* benzene ring substituents (OH and CH_2OH) are in a *cis*-arrangement. This is most likely due to intra-molecular hydrogen bonding between the two *ortho* hydroxyl groups, but as seen in chapters 10-13 the reason for biphenyl twistings are often much more complex. Since product **(2)** has a much smaller dihedral angle of 24° from a molecular mechanics (Alchemy III (Tripos Associates, 1995)) calculation, the overall photoreaction requires a significant twisting motion to planarity along with substantial charge redistribution in the excited singlet state to effect the cyclization, with an overall loss of H_2O.

A mechanism of the reaction was proposed (Scheme 1, Figure 6.2) in aqueous CH_3CN solution which requires the phenol moiety to ionize, in solvent, to give the electronically excited phenolate ion **(3)**. Twisting motion at this stage allows conjugation of the two benzene rings which, due to the enhanced electron donating effect of the phenolate ion in the excited state, causes the hydroxide ion from the benzylic position to be ejected. This gives rise to a relatively planar *o*-biphenyl quinone methide **(4)** which undergoes electrocyclic ring closure to give the observed product **(2)**. The observation that the photocyclization also proceeds in neat CH_3CN suggests the mechanisms involve intra-molecular proton transfer. More recently, it has been found that exploratory photolysis of crystalline samples of **(1)** also gave **(2)** (Scheffer, 1987). This implies that a polar solvent is not required for the reaction although the efficiency may be enhanced when a polar solvent is used, probably *via* a change in reaction mechanism. These results led to in more detailed exploration of the photocyclization of these compound types in the solid state, which is reported herein.

6.3 EXPERIMENTAL DETAILS

6.3.1 Experimentation and Equipment

The ^1H NMR spectra were taken on Bruker AC300 or AM360 spectrometers in $CDCl_3$ or acetone-d_6. Mass spectra were obtained on a Kratos Concept H (EI) instrument. UV-Vis spectra were measured on a Cary 5 instrument. Preparative photolyses were carried out using a Rayonet RPR 100 photochemical reactor using 254 or 300 nm lamps. Reaction mixtures for these photolyses were contained in 100 or 200 ml quartz tubes, which were cooled to 15° C using a cold finger (tap water) and purged continuously during photolysis using a stream of argon *via* a stainless steel syringe needle. The X-ray and neutron diffraction experimental details are given in the relevant sections of this chapter, see chapter 2.

6.3.2 Materials

Anhydrous CH_3CN used for fluorescence studies was distilled over CaH_2 and used immediately. Preparative thin layer chromatography (TLC) was carried out on 20 cm^2 silica gel Uniplates (Analtech). 2'-Hydroxybiphenyl-2-carboxylic acid lactone **(8)** required for the synthesis of **(5)** was prepared using a previously described method (Shi and Wan, 1995 and 1997).
Lactone **(8),** 5.0 g (25 mmol), was dissolved in 250 ml of dry THF, and 160 mL of 1.8 M phenyl lithium was added with stirring over 2 hours. The mixture was then refluxed for 4 hours. After reaction, the solution was quenched with a mixture of ice and saturated NH_4OAc and extracted three times with CH_2Cl_2. A colourless oil was obtained after the solvent was abstracted. This crude oil was washed several times with hexanes after which it solidified on standing for several days. This solid was first recrystallized from toluene-hexanes and then from a mixture of hexanes, CH_2Cl_2, and CH_3COCH_3, to give good quality crystals (suitable for X-ray diffraction experimentation) of pure **(5)** (1.75 g, 20%), m.p. 103°C, 5.72% H; found 85.16 C, 5.71% H. Due to the efficient loss of water in the mass spectrometer, no attempts were made to obtain an exact mass, since the X-ray crystal structure provided complete characterization of the structure.

6.3.3 Product studies

6.3.3.a Photolysis of (5) in 100% CH_3CN and 1:1 H_2O-CH_3CN

A solution of **(5)** (147 mg) in CH_3CN (200 mL) was photolyzed (254 nm) in a quartz tube for 30 minutes using the general procedure. The solvent was then removed by rotary evaporation. The residue (60% conversion to pyran **(7)** by ^1H NMR) was chromatographed on preparative thin layer chromatography (silica; 2:1 hexanes-CH_2Cl_2). The first band was collected to give a white solid, which was recrystallized from CH_3CN to give pure **(7)**, m.p. 137-139 ° C.
When photolyzed in 1:1 H_2O-CH_3CN, the conversion to **(7)** was about 50% higher (by UV-Vis and ^1H NMR) indicating a more efficient reaction when water is present. In addition, at very high conversions, minor side products were observable in runs in 100% CH_3CN whereas they were absent in 1:1 H_2O-CH_3CN.

6.3.3.b Photolysis of (7) in 1:1 H_2O-CH_3CN and 1:1 CH_3OH-CH_3CN

A solution of **(7)** (1.4×10^{-4} M, in 1:1 H_2O-CH_3CN or 1:1 CH_3OH-CH_3CN) was placed in a curette (3.0 mL) and irradiated at 254 or 300 nm. No changes were detected by UV-Vis spectrophotometry even on prolonged irradiation indicating the lack of any conversion to the ring-opened product ((**5**) in 1:1 H_2O-CH_3CN, and the corresponding methyl ether in 1:1 CH_3OH-CH_3CN). This was confirmed by ^1H NMR spectra of preparatory runs (more concentrated solutions; 60 minute photolysis), which showed only **(7)**.

6.3.3.c Photolysis of crystalline samples of (5)

A small amount of **(5)** (4 mg) was crushed into a fine powder in a mortar and then irradiated (in the mortar, opened to air) at 254 nm for 150 min. The sample was then dissolved in $(CD_3)_2CO$ and ^1H NMR showed 25% conversion to pyran **(7)**. No detectable side products were observed with NMR analysis. The cell was then irradiated at 300 nm for five hours. Analysis of the sample (^1H NMR) showed 10% conversion to **(7)**.
As an alternate method for studying the solid state photolysis, a solid film of **(5)** (4 mg) was cast between two quartz plates using CH_2Cl_2 and the solvent removed on a vacuum pump (residual 5-8% CH_2Cl_2 by NMR). This method allowed the progress of the photoreaction to be directly monitored by UV-Vis spectrophotometry, which showed clean conversion to **(7)** on photolysis, similar to that observed in runs in 1:1 H_2O-CH_3CN. With prolonged photolysis the highest conversion achievable was 50% and there was an absence of detectable side products.

6.3.3d Photolysis of (1)

Photolysis of **(1)** in aqueous CH_3CN gave a strong and broad transient absorption spectrum with the major band at ~ 600 nm. The transient spectrum was broad (450-800 nm) with the identical decay rates at all wavelengths. This suggests that the spectrum is due to the same species. The λ_{max} is red shifted as the solvent polarity increases which suggests that the species is highly polar. The photolysis of **(1)** is independent of pH although the decay rate showed high dependence on pH and solvent, but is not affected by O_2. Photolysis of **(1)** in 1:1 H_2O-CH_3OH resulted in a clean conversion to the corresponding methyl ether **(10)** (Figure 6.3).

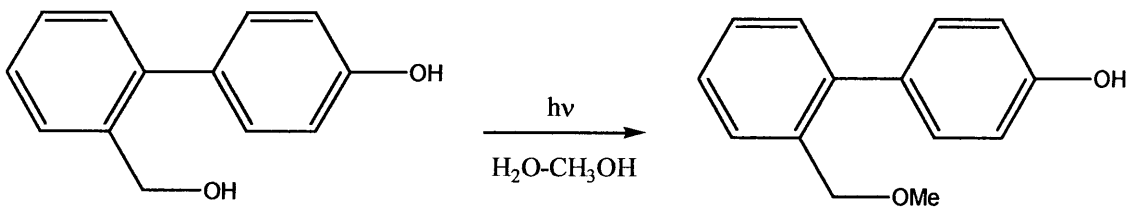

(1) **(10)**

Figure 6.3 The scheme for the photolysis of (1) to (10).

6.3.4 Laser flash photolysis

Laser flash photolysis (LFP) experiments were carried out by Professor Peter Wan at the University of Victoria LFP Facility. A Spectra-Physics GCR 12 YAG laser at 266 nm (< 30 mJ) was used for excitation and signals were digitized with a Tektronix TDS 520 recorder. Samples were prepared in quartz cells in a flow system to avoid photolysis of the photoproduct, which is formed efficiently. Purging was carried out using N_2 or O_2 prior to photolysis.

6.3.5 Quantum yields

Quantum yields for photocyclization of **(5)** to **(7)** were measured using UV-Vis spectrophotometry to follow the progress of the reaction. Experiments were carried out on an optical bench equipped with an Oriel 200 W Hg arc lamp and a monochromator set at 280 nm (slits = 10 nm). Generally, a quartz cuvette containing a 3.00 mL solution of the substrate was purged with argon for 5 min. and then irradiated for a set time period on the optical bench. The

extent of conversion to **(7)** was followed at λ_{max} = 308 nm (of the second absorption band of **(7)**), with ε = 6384 mol^{-1} L cm^{-1}. The light intensity was measured by potassium ferrioxalate actinometry (Shin, 1996). The initial concentration of the substrate was adjusted such the absorbance at 280 nm was > 2. The following quantum yields for photocyclization of **(5)** to **(7)** were measured: Φ = 0.18 ± 0.02 (100% CH_3CN); 0.26 ± 0.03 (1:9 H_2O-CH_3CN); 0.27 ± 0.03 (1:1 H_2O-CH_3CN); 0.15 ± 0.02 (100% CH_3OH); 0.19 ± 0.02 (100% THF). No attempts were made to measure Φ for the solid state photolyses although qualitatively, the conversions were equally as efficient when compared to similar runs carried out in solution.

6.4. RESULTS AND DISCUSSION

6.4.1 Product studies in solution

UV-Vis traces of a sample of **(5)** in 1:1 H_2O-CH_3CN photolyzed at 254 nm shows large changes consistent with transformation to the ring-closed product **(7)**, which is more intensely absorbing due to the improved conjugation of the more planar biphenyl ring system. Conversions can be taken to be essentially 100% since the final spectrum obtained is that of pure **(7)**. A similar trace taken in 100% CH_3CN is less clean as absorption > 340 nm increases significantly at higher conversion. These results are confirmed by preparatory photolyses in which the yield of **(7)** is essentially quantitative when photolyzed in 1:1 H_2O-CH_3CN whereas in 100% CH_3CN, yields of 80-90% were observed.

In product studies of the parent system 1, photolysis in 1:1 H_2O-CH_3CN gave a photostationary ratio of *circa.* 98% of **(2)** and a residual 2% of **(1)** on exhaustive photolysis, implying that the photochemical reaction is reversible. This was confirmed by photolysis of **(2)** in 1:1 H_2O-CH_3CN, which gave a 2% yield of **(1)** on extended irradiation. That is, *o*-biphenyl quinone methide **(4)** undergoes electrocyclic ring closure to form **(2)** much faster than it is attacked by H_2O to form **(1)**. In the present case of **(5)**, it would appear that the corresponding *o*-quinone methide **(6)** is not attacked by H_2O but reacts only *via* electrocyclic ring closure. This is confirmed by photolysis of **(7)** in 1:1 H_2O-CH_3CN or 1:1 CH_3OH-CH_3CN, which resulted in no observable reaction (to give **(5)** or the corresponding methyl ether) even on extended photolysis. A reasonable explanation for the lack of any nucleophilic trapping products of **(6)** is the increased steric hindrance of the α-benzylic position (with two phenyl groups) which should retard nucleophilic attack at this site.

In the study of the mechanism of photocyclization of **(1)**, it was found that the photocyclization quantum yield was about twice as high in aqueous CH_3CN than in neat CH_3CN. This was rationalized as being due to the greater ability of water to solvate the phenolic proton, which is liberated on photoexcitation. A plot of quantum yield against pH (in aqueous solution) showed a titration curves at approximately pH 1 and 10, corresponding to the singlet excited state and ground state of the phenol moiety, respectively. These results support a mechanism in which the excited state phenolate ion is on the reaction pathway in the photocyclization mechanism in solution. Quantum yield measurements for photocyclization of **(5)** in a variety of solvents (*vide supra*) are consistent with this mechanism. Indeed, the quantum yields measured for **(5)** are very similar to those observed for **(1)** indicating that the presence of the two phenyl groups has very little effect on the photocyclization quantum yield. The photocyclization quantum yields for **(5)** are marginally higher, 0.27 compared to 0.21 for **(1)** in 1:1 H_2O-CH_3CN and 0.18 compared to

0.12 for **(1)** in 100% CH_3CN. This may be a reflection of the lack of nucleophilic trapping of **(5)** by H_2O generated *in situ* or from the solvent (which leads back to starting material and hence reduce the observed > quantum yield for photocyclization).

6.4.2 X-ray Crystallography and Product Studies in the Solid State

6.4.2.a The structure of α,α-diphenyl-2-(2'-hydroxyphenyl)benzyl alcohol (5)

The crystal of the compound **(5)** was mounted on a glass fibre and was cooled to 150(2) K with a stream of dry N_2. The data were collected on a Siemens SMART CCD diffractometer employing graphite monochromated Mo-Kα radiation λ= 0.71073 Å. The data were then integrated with the Seimens SAINT program. There was no absorption correction applied. The crystal structure data for **(5)** is given in Table 6.1.

In the X-ray diffraction analysis it was found that **(5)** crystallizes in space group *C2/c* with eight molecules in the unit cell, water molecules were also found in the crystal. The eight molecules are arranged into four inter-molecularly hydrogen bonded dimers (see Figures 6.4 and 6.5), (phenol OH hydrogen bonded with the benzylic O; O1-H2A/OlA-H2) distance is 1.86(3) Å, where atom X(A) is related to atom X by an inversion operation, these dimers are held together by both inter and intra molecular hydrogen bonding. The inter/intra molecular bonding forms an eight membered ring involving four hydrogen and four oxygen atoms, with two inter and two intra molecular hydrogen bonds.

The hydrogens in the structure were fixed except those hydrogen atoms that were attached to the oxygen atoms (the hydrogen atoms likely to be involved in hydrogen bonding), these particular atoms were found freely in the structure solution and freely refined. The fact that these hydrogen atoms were found in the structure solution and the lack of disorder present for these atoms indicates that the hydrogen atoms are strongly located in the one area of the asymmetric unit and so gives greater credit to their involvement in some form of inter/intra molecular interaction. Each dimer is also intra-molecularly hydrogen bonded (benzylic OH hydrogen bonded with phenol O; O2-H1/O2A-HlA) with a distance of 1.88(3) Å. The dimer units are separated by distances within the normal van der Waals distances and the geometry of the monomer shows no exceptional or unusual features.

This conformation of this structure is showing the *cis* arrangement of the two substituents on the biphenyl (the phenol OH and benzylic moiety), which is the optimal arrangement for photocyclization. This arrangement (*cis*) is in contrast to that of **(1)**, which was of the *trans* configuration.

	α,α-diphenyl-2-(2'-hydroxy-phenyl)benzyl alcohol (5)	**The pyran product (7)**
Formula	$C_{25}H_{20}O_2$	$C_{25}H_{18}O$
Formula Weight (g/mol)	352.41	334.39
Crystal Colour	Colourless	Colourless
Crystal Description	Block	Plates
a= (Å) b= (Å) c= (Å) α= (°) β= (°) γ= (°)	22.929(4) 13.038(2) 12.446(3) 90 93.3780(10) 90	9.520(2) 14.990(3) 36.810(7) 90 91.74(3) 90
Temperature (K)	150°(2)	150°(2)
Wavelength (Å)	0.71073	0.71073
Crystal System	Monoclinic	Monoclinic
Space group	C2/c	P2(1)/c
Volume	3698(1)	5250.5(18)
Z	8	12
Number of Reflections Used	1488	2349
Calculated Density	1.266	1.269
Absorption Coefficient (mm^{-1})	0.79	0.076
F (000)	1488	2112
θ Range for Collection (°)	1.79 to 25.53	1.11 to 17.53
Index Ranges	–13<=h<=27, -13<=k<=14, -14<=l<=14	-8<=h<=8, -12<=k<=12, -31<=l<=31
Reflections collected	7728	13408
Independent reflections	3039	3337
Data/restraints/parameters	2999 / 0 / 305	3331 / 0 / 704
Goodness-of-fit on F^2	1.207	1.080
Final R_1 indices [I>2sigma(I)]	0.0491	0.0365
wR_2 indices (all data)	0.1455	0.0680
Extinction coefficient	0.0030(2)	0.0015(2)
Largest diff. Peak and hole.	0.185 and -0.201 e.$Å^{-3}$	0.139 and -0.155 e.$Å^{-3}$

Table 6.1 X-ray crystal data for structures (5) and (7)

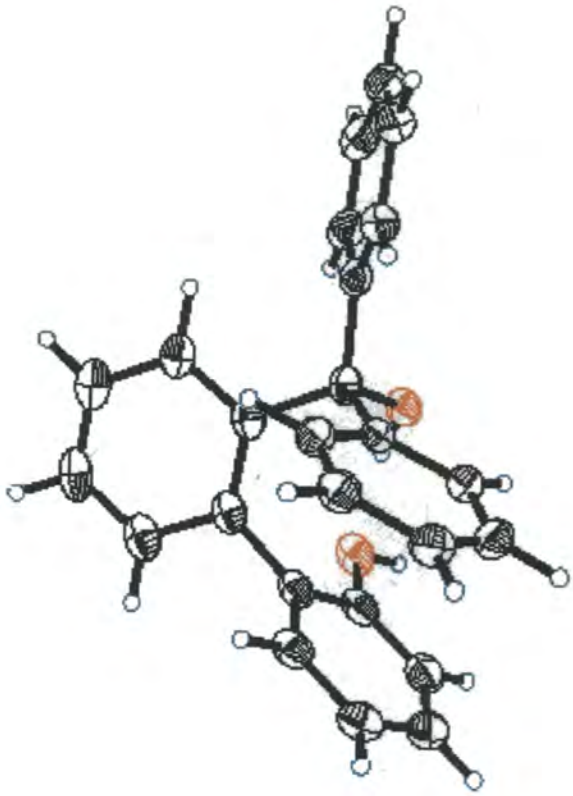

Figure 6.4 The thermal ellipsoid plot of (5), with 50% probability

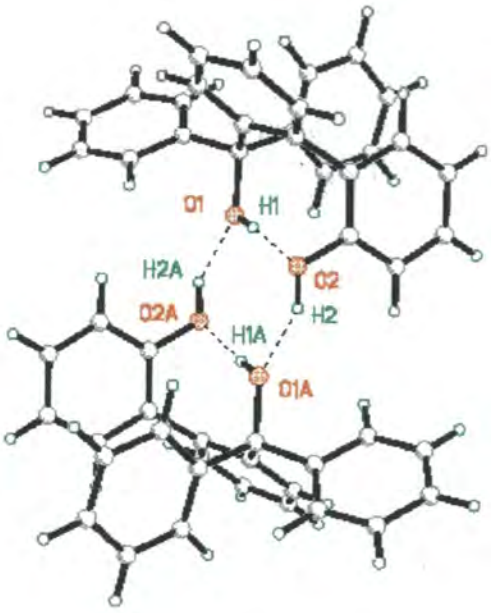

Figure 6.5 The hydrogen bonded structure of (5)

6.4.2.b The structure of the pyran product (7)

Suitable crystals of **(7)** for X-ray analysis were not available directly from the solid state reaction but upon recrystallisation from toluene, which took several months to obtain, decent crystals were produced. Thus Alchemy III (Tripos, 1995) was first used to generate an optimized geometry for **(7)**, the result giving a much less twisted biphenyl ring structure than for **(5)**, with a dihedral angle of 26°, which is only slightly more twisted than the parent pyran **(2)** (24° by Alchemy III). However, it is clear that a substantial twisting to planarity is required for **(5)** to give rise to **(7)** on photolysis. The X-ray analysis of **(7)** showed that the structure obtained in the solid state was close to that predicted by the Alchemy III program but there were distinct differences within the structure, see Figure 6.6. In the structure there are three molecules of **(7)** in the asymmetric unit. All three of these molecules have different dihedral angles thus partially explains why the crystals that were obtained directly from the solid state reaction were not suitable for complex X-ray analysis. The large amount of twisting and the nature of the interaction between the separate molecules that was involved in the solid state reaction (in order to generate the three structures in the asymmetric unit) almost certainly destroys much of the crystalline nature of the solid. The solid produced was probably a conglomerate of separate repeating units, making the solution of the structure of this solid directly from the photochemical reaction of **(5)** to **(7)** impossible with single crystal X-ray diffraction analysis. The crystal in this case would behave very much like a twinned crystal. Needless to say, the photoreaction does indeed produce the product, **(7)**, in the solid state but the complexity and dynamics of this reaction also create enough disturbance at the molecular level to destroy the measurable crystallinity.

Product studies of crystalline samples of **(5)** as well as samples cast as a solid film show an efficient and clean photoconversion to **(7)**. The crystal environment does not impart any substantial impediment to this photocyclization requiring substantial torsional motion. Since water is not included in the crystal lattice, the mechanism of photocyclization cannot involve water-assisted ionization of the phenol moiety, as proposed in aqueous solution.

The manner in which **(5)** crystallizes (as dimers) offers an intriguing mechanism for photocyclization in the solid state. It is proposed that the mechanism for photocyclization of **(13)** involves initial inter-molecular proton transfer from the phenol OH to the oxygen of the benzyl moiety of the hydrogen bonded partner **(2)**, to generate a "zwitterionic dimer" **(9)**. Loss of hydroxide ion from **(9)** gives rise to **(6)** and presumably a molecule of **(5)** still hydrogen bonded to a hydroxide ion and a proton, which on proton reshuffling regenerates **(5)** and a water molecule. Electrocyclic ring closure of **(6)** gives the expected **(7)**, see Figure 6.7. This mechanism implies that the maximum conversion of **(7)** is 50%, and this is consistent with

experimental observations. The overall mechanism involves the hydrogen bonded partner mediating the proton transfer and stabilizing the incipient charge separation. This apparently cannot be accomplished with a single water molecule, as **(5)** (monomeric form) does not react further. Figure 6.7 gives a proposed possible mechanism, which results in the loss of H_2O. However, loss of OH^- and H^+ is also possible.

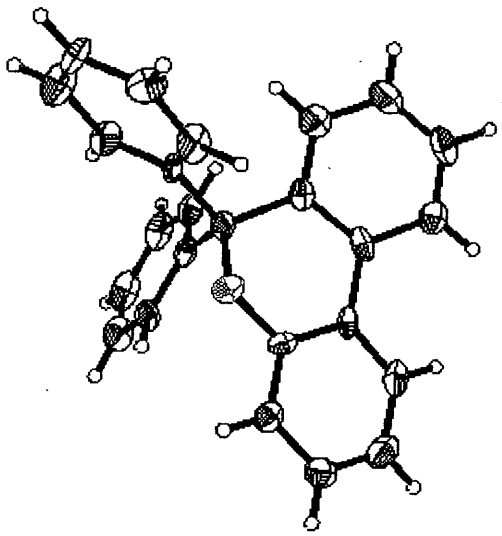

Figure 6.6 The thermal ellipsoid plot of (7), with 50% probability

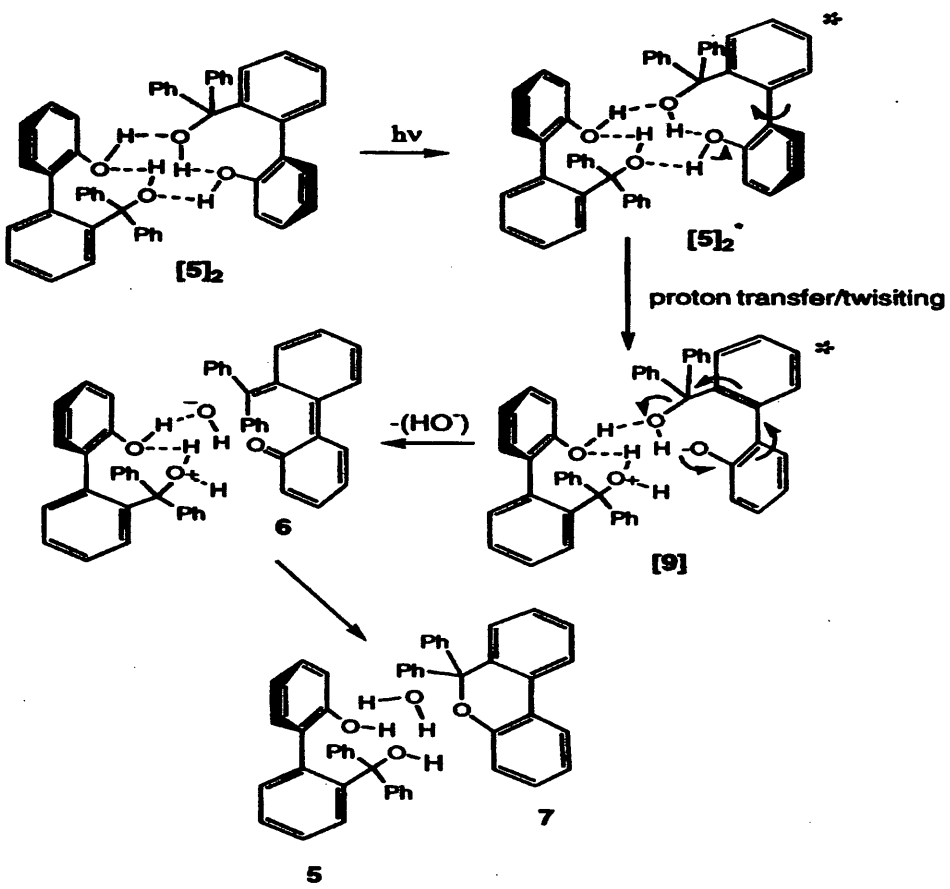

Figure 6.7 Scheme 2, possible mechanism representing (5) to (7)

6.4.3 Laser Flash Photolysis (LFP)

LFP studies of **(5)** were carried out as an attempt to directly show the involvement of *o*-biphenyl quinone methide **(6)** in the reaction mechanism in solution. It has been shown that photogenerated biphenyl quinone methides that cannot undergo electrocyclic ring closure are readily observable by LFP, with lifetimes in the 0.4-70 μs range in aqueous solution with long-wavelength maxima (500-575 nm) (Shi *et al.*, 1995). Although **(6)** does undergo electrocyclic ring closure, it was anticipated that the added phenyl groups might provide sufficient additional conjugation to decrease its reactivity. Previous nanosecond LFP studies of **(1)** gave no observable transients assignable to **(4)** supporting the notion that *o*-biphenyl quinone methides of the type **(4)** are very short lived.

Laser flash photolysis of **(5)** in 1:1 CH_3CN-H_2O gave only a weak transient in the 340-500 nm region (λ_{max} = 420 nm). This transient was not affected by added ethanolamine and O_2. This transient decays with a fast rate (6.7 x 10^5 s^{-1}) which suggests there is more than one species

involved. Since known biphenyl quinone methides absorb at much longer wavelength (500-575 nm) and are efficiently quenched by added ethanolamine, the transient observed for **(5)** is most likely due to a side reaction of **(5)**. Thus it is clear that even **(6)** is too short lived for detection by nanosecond LFP. The possibility that **(6)** might be longer lived in the solid state and hence detectable using the present apparatus is a subject for further investigation.

6.5 NEUTRON DIFFRACTION STUDY

6.5.1 Introduction

The X-ray study of the compound shows that the conformation was of the near *cis* type, which fits with the general trend for *o-o'*-biphenyls ((Brock & Minton, 1989) and (Roberts, 1985)). It is believed that this can be attributed to an O-H···O interaction, rather than preference for the *cis* conformation. Unfortunately, since the electron density hydrogen is so small, often peaks that appear as bond deformations are simply spurious peaks. So X-ray diffraction studies cannot give an accurate picture of any deformation present in the hydrogen bonding. Both the inter- and intra-molecular hydrogen bonds (determined by X-ray analysis) are within the approximately average range of the main body of hydrogen bond lengths, at 1.86(3) and 1.88(3) Å respectively, (see Figure 6.5). The range of hydrogen bonds, for CO-H···O-C type systems, can be taken as 1.4 Å to 2.75 Å (the length of the 2 van der Waals radii), with a large proportion of these at 1.4 Å to 2.2 Å (see Figure 6.5). With both the inter and intra distances approximately equal, this indicates that the intra-molecular interaction is of an optimum length. To determine the positions of protons in this compound accurately, the thermal motion of the hydrogen atoms involved in the hydrogen bonding and the twisting of the rings relative to each other, and hence to establish the role of the hydrogen bonding and inherent twisting of the C-C bond between the rings in the structure, the neutron diffraction study was conducted. Since neutrons are scattered by the atom nucleus rather than the electron density, the atomic position of the hydrogen can be determined with the same degree of accuracy as for carbon and oxygen atoms in the structure and so the length of the hydrogen bond determined extremely accurately.

6.5.2 Results and discussion

Structure refinement was carried out on F^2 using the previously determined X-ray parameters as a starting model. In the final refinement, position and anisotropic thermal parameters were refined for all atoms, including hydrogen atoms. The refinement converged satisfactorily to R1 = 0.0824, wR2 = 0.1248 using this model. The resulting model is shown in Figure 6.8, with the refinement parameters summarized in Table 6.2.

As already determined by the X-ray analysis in this chapter, the conformation of α,α-diphenyl-2-(2'-hydroxyphenyl) benzyl alcohol is nearer the *cis* geometry than the *trans*, this is in agreement with the general trend of these compounds, although there are some notable exceptions to this ((Singh and McKinney, 1987), (Itoh *et al*, 1989) and (Howard *et al*, 1976)). The dihedral angle in *o-o'*-biphenyls is usually between 50 and 80° (Brock and Minton, 1989),

and in this compound it is relatively large at 80° but this is as expected with the large sterically demanding [$C(Ph)_2OH$] group present (see Figure 6.8). The compound crystallizes as hydrogen bonded dimers in the solid state, with both inter and intra molecular hydrogen bonding present enabling a direct comparison within the eight-membered ring which binds the two molecules together. The unit cell consists of four dimers (see Figure 6.9). Since O-H groups in general readily form hydrogen bonds and so have a relatively strong attraction to each other, then there is a reasonable probability that hydrogen bonding would be favoured here and thus be the reason this compound prefers to adopt the near *cis* arrangement. If there is intra-molecular hydrogen bonding then the rings will have to be positioned so as to align in the near *cis* conformation to allow for interaction. A conformational preference that is strong for a specific dihedral angle may show up with this hydrogen bond either shortened or lengthened. This case is interesting and useful since there is inter as well as intra-molecular hydrogen bonding allowing us to characterize both types of hydrogen bond lengths in one structure. It also allows us to ascertain whether the intra-molecular hydrogen bonding is significantly shorter, longer or more distorted than the inter, as to be a consequence of the twisting of the phenyl rings or whether the hydrogen bonding is the main factor in the twisting. There is some flexibility in the $C(Ph)_2OH$ group in the monomeric state, but the phenyl groups are sterically hindering enough, so as to keep the oxygen position fixed relative to the twist when in the dimer.

Intra-molecular hydrogen bonding is the major influence for this preference. The two H···O distances in the O-H···O interactions are 1.788(8) Å and 1.820(7) Å for the intra- (O2-H1/O2A-H1A) and inter-molecular bonds (O1A-H2/O1-H2A) respectively, see Figure 6.8. This is close to the average length in the main peak of 1.821 Å for these structures in the Cambridge Structural Database (CSD). Although the magnitude of the intra-molecular bond is slightly smaller than for inter, it is not significantly so and it is not suggested that the difference arises from the twisting of the rings, and the twist definitely does not give rise to exceptionally short or long hydrogen bonds. This structure seems to fit into the mostly *cis* conformational trend of *o-o*'-biphenyl compounds and the reason is that, it is the hydrogen bonding in the dimer which determines the conformation in the solid state. Certainly the eight-atom hydrogen bonded ring only exists in the *cis* arrangement but this dimeric form seems to be stable enough to be the controlling factor in the conformation of the structure. The observation here is that the intra-molecular hydrogen bonds determine the conformational configuration of this compound and it is not a consequence of the *cis* conformational preference that prevails in these types of compounds.

There are a number of OH *o-o*'-substituted biphenyls in the CSD, and given the identification of intra-molecular hydrogen bonding in this compound that determines the stereochemistry, it is possible that the *cis* conformation of many of these structures is due to intra-molecular hydrogen

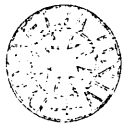

bonding. Obviously a detailed neutron structure cannot be possible for all similar type compounds, but it is felt that this study is representative and informative.

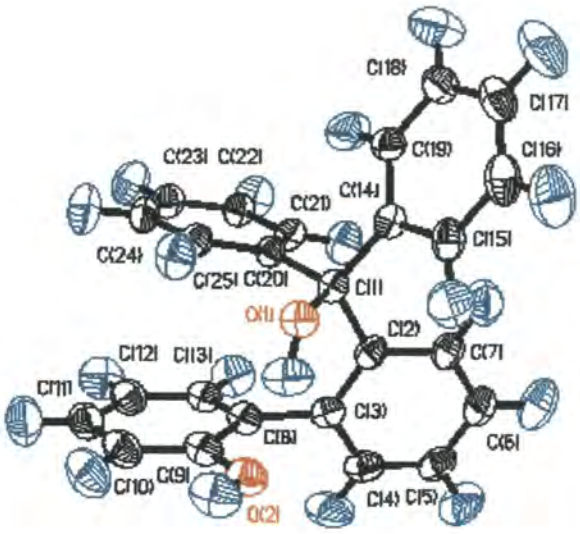

Figure 6.8 The thermal ellipsoid plot of (5), with neutron data, 50% probability

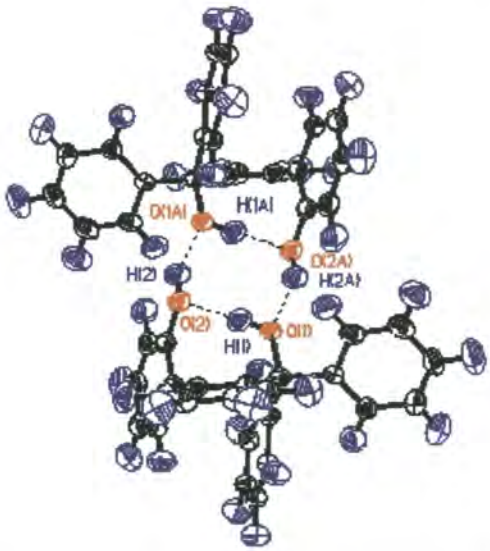

Figure 6.9 The dimers of (5) plotted with neutron diffraction data

6.5.3 Experimental

The crystal was fixed to an aluminium pin using thin strips of aluminium tape and mounted in a Displex cryostat on a two-circle chi, phi goniometer. The sample was cooled to 150 K for the data collection, the same temperature as for the X-ray analysis. Data were collected on the SXD instrument at the ISIS spallation neutron source, using the time-of-flight Laue diffraction method (Wilson, 1997). Basically this method uses a wavelength-sorted white neutron beam, together with large area position-sensitive detectors, to allow a large volume of reciprocal space to be measured in a single crystal setting (a "frame"). The full data collection comprises a series of such frames, each collected with a stationary crystal-detector arrangement.
The data collection parameters are summarized in Table 6.2. A total of 42 frames, each containing information from two detectors, was collected, with an exposure time for each frame of around six hours. The precise exposure time depended on the neutron flux/hr, with the crystal exposed to the same total neutron flux in each frame.

The distance from sample to detector, L_2, is 204 mm and 143 mm for the low and high angles to the centre of the detector, 2θc, respectively. The intensities were extracted and reduced to structure factors using standard SXD procedures. A total of 14963 intensities were integrated, reducing to a unique set of 3129 observed structure factors [I>2sigma(I)] on merging (Rint=0.07).

Table 6.2 The Neutron diffraction data for (5)

Formula	$C_{25}H_{20}O_2$	Volume	3697.6(13) $Å^3$
F (000)	1016	Z	8
Crystal Colour	Colourless	Temperature (K)	150(2)
Crystal Description	Wedge	Calculated Density	1.265 Mg/m^3
Independent reflections	3129	Absorption Coefficient	0
Crystal Dimensions (mm)	1.6 x 1.2 x 0.8	Formula Weight (g/mol)	352.41
Space group	C2/c	Crystal System	Monoclinic
θ Range for Collection (°)	4.59 to 42.71	Index Ranges	0<=h<=42, 0<=k<=23, -22<=l<=22
a= (Å) b= (Å) c= (Å)	22.929(4) 13.038(2) 12.446(3)	α= (°) β= (°) γ= (°)	90 96.3780(10) 90
Data/restraints/parameters	3129 / 0 / 425	Final R^1 index [I>2sigma(I)]	0.0816
Reflections collected	3131	WR_2 index (all data)	0.1248
Extinction coefficient	0.0036(4)		

6.6 SUMMARY

This study has shown that the photocyclization of α,α-diphenyl-2-(2'hydroxphenyl)benzyl alcohol **(5)** to the corresponding pyran **(7)** is not inhibited in the solid state although the reaction requires significant torsional motion. It is believed the dimeric structure of **(5)** observed in the solid state offers a unique mechanism for the reaction involving both inter and intra-molecular proton transfers and explains why the maximal yield in the solid state is 50%.

The conformation of **(5)** is governed by the hydrogen bonding present, which gives the *cis* conformation. This *cis* orientation facilitates the solid state ring closure reaction to form **(7)**. There is a tendency for biphenyl compounds to adopt this *cis* conformation but not all biphenyls adopt this geometry. So a factor in choosing a structure with suitable geometry is important for such chemistry, chapters 10-13 deal with these geometric factors for biphenyls and give factors for the *cis versus trans* conformation.

6.7 REFERENCES

1. Bastiansen, O., *Acta. Chem. Scand.*, **1950**, 4, 926.
2. Bastiansen, O.; Kveseth, K.; Mölendal, H., *Topics in Current Chem.*,**1979**, 81.
3. Brock, C. P.; Minton, R. P., *J. Am. Chem. Soc*, **1989**, 111, 4586.
4. Fittig, R., *Justus Liebigs Ann. Chem.*, **1862**, 121, 363.
5. Fowweather, F.; Hargreaves, A., *Acta Crystallogr.*, **1950**, 3, 81.
6. Geise, H. J.; Lenstra, A. T. H.; De Borst, C, Moes, G. W., *Acta Crystallogr.*, **1986**, C42, 1176.
7. Hayashi, N.; Mazaki Y.; Kobayashi, K. ,*Tetrahedron Lett.*, **1994**, 35, 5883.
8. Hollingsworth , M. D.; McBride, J. M. *Adv. Photochem.*, **1990**, 15, 279;
9. Howard, C. C.; Johnstone, R. A. W.; King, T. J.; Lessinger, L., *J. Chem. Soc., Perkin Trans I*, **1976**, 1820.
10. Huang, C.-G.; Beveridge, K. A.; Wan, P., *J. Am. Chem. Soc.*, **1991**, 113, 7676.
11. Huang, C.G. Shi Y., Wan P., unpublished results.
12. Itoh, Y.; Brossi, A.; Hamel, E.; Flippen-Andersen, J. C.; George, C., *Helv. Chim Acta*, **1989**, 72, 196.
13. Kaupp G.; Haak M., *Angew. Chem. Int. Ed. Engl.*, 35 , **1996**, 2774.
14. MacKinnon, A.; Howard, J. A. K., 1997, unpublished results.
15. Murov, S. L; Carmichael I.; Hug G. L., *Handbook of Photochemistry, 2nd edition*, M. Dekker, New York, **1993**.
16. Ramamurthy, V.; Venkatesan, K., *Chem. Rev.*, 87, **1987**, 433; Pokkuluri P.R., in V. Ramamurthy (Ed.),
17. Photochemistry in Organized and Constrained Media, VCH, New York Press, **1991**.
18. Roberts, R. M. G., *Magn. Res. Chem*, **1985**, 23, 52
19. SAINT Version 4.050, Siemens Analytical X-ray Instruments, Madison, USA, **1995**.
20. Scheffer, J. R.; Garcia-Garibay M.; Nalamasu O., *Org. Photochem.*, 8, **1987**, 249.
21. Sekine, A.; Ohashi, Y.; Yoshimura, K.; Yagi, M.Higuchi, *J.Acta Crystallogr.*, **1994**, C50, 1101.
22. Sheldrick, G. M., SHELXL-93, Program for Refinement of Crystal Structures, University of Göttingen, Germany, **1993**
23. Sheldrick, G. M., SHELXTL-Plus, Release 4.1, **1991**, Siemens Analytical X-ray Instruments, Madison, USA.
24. Shi, Y.; Wan, P. *J. Chem. Soc.*, Chem. Commun., **1995**, 1217.
25. Shi, Y.; MacKinnon, A.; Howard, J. A. K.; Wan, P., *J. Photochem. Photobiol, A. Chem.*, **1998**, 113,3, 271.

26. Shin S. H.; Keating A. E.; Garcia-Garibay M. A., *J. Am. Chem. Soc.*, 118, **1996**, 7626.
27. Singh, P.; Pederson, L. G.; McKinney, *Acta Crystallogr*, **1986**, C42, 1172.
28. Smare, D. L., *Acta Crystallogr.*, **1950** 1, 150.
29. SMART Version 4.050, Siemens Analytical X-ray Instruments, Madison, USA, **1995**.
30. Tripos Associates, Inc., St. Louis, Missouri, USA. *Alchemy III,* **1995**.
31. Wilson, C. C., *Journal of Molecular Structure*, **1997**, 405, 207.
32. Zhang, G.; Shi, Y.; Mosi, R.; Ho, T.; Wan, P., *Can. J. Chem.*, **1994**, 72, 2388.

CHAPTER 7:

A STUDY OF PHOTOREACTIVE BIARYL MOLECULES

7.1 AN INTRODUCTION TO BIARYL METHANOLS WITH NAPHTHALENE RING

This chapter focuses on the biaryl systems, with specific reference to their photochemistry and how X-ray diffraction analysis can be used to study such reactions. This chapter will give details on the synthesis, the photochemistry and some relevant chemistry as well as the diffraction data analysis of the photoactive compounds **(1)**, **(2)** and **(3)**, see Figure 7.1.

Biaryl methanols **(1)-(3)** were synthesized from the corresponding lactones by reduction with $LiAlH_4$, Figure 7.2 shows the synthesis of **(1)**. These lactones were synthesized using palladium-catalyzed intra-molecular aryl coupling reactions in the manner of a previously described method (Bringmann *et al.*, 1992 & 1993).

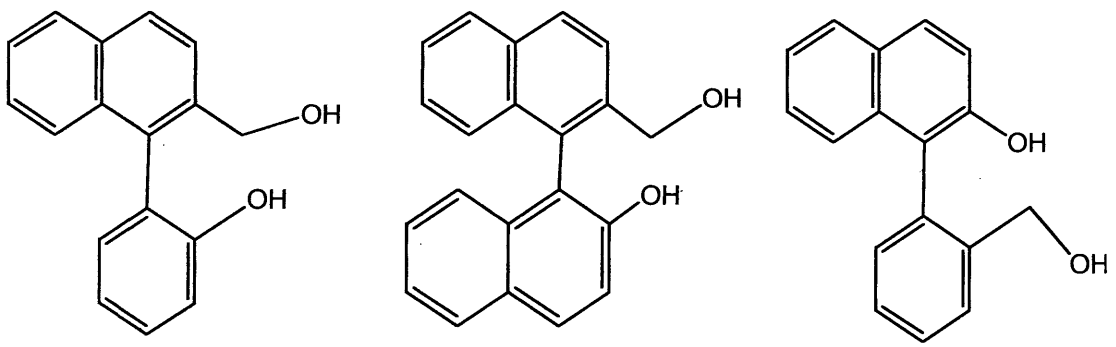

(1) **(2)** **(3)**

Figure 7.1 The Biaryl molecules
(1) 2-[2'-(Hydroxymethyl)-1'-Naphthal]phenol,
(2) 2-Hydroxy-2'-hydroxymethyl-1,1'-Binaphthyl and
(3) 1-[2'(Hydroxymethyl)phenyl]-2-naphthol

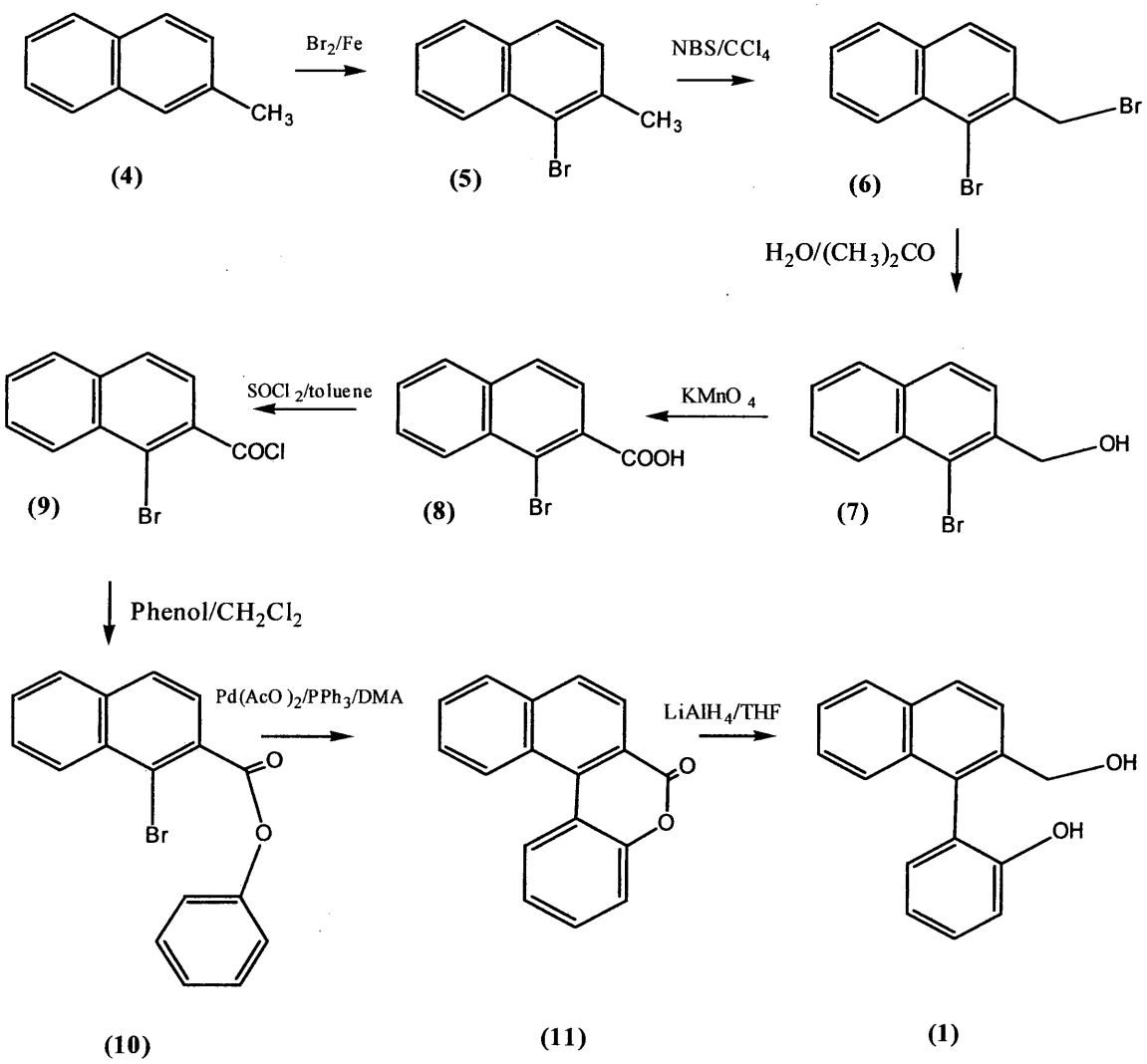

Figure 7.2 The reaction scheme to produce compound (1)

7.2 PHOTOCYCLIZATION IN THE SOLID STATE.

Since molecular motion in solids is highly restricted, these reactions have been extremely useful in the control of both stereoselectivity (Shin *et al.*, 1996) and regioselectivity (Robinson and Robinson, 1986). As demonstrated in chapter 6 with the structure α,α-diphenyl-2-(2'-hydroxyphenyl)benzyl alcohol, biphenyls can photocyclize quite efficiently in the solid state. Similarly the binaphthyl compound **(2)** can also undergo photocyclization in the solid state although due to steric restrictions the efficiency of the reaction is much lower (Figure 7.3). In the solid state samples of **(1)** do not show any reactivity when subjected to the same conditions as the biphenyl molecules. However, since the solid state reaction requires large torsional motion (to reach the planar form), it is expected that the density of the solid state will also effect this torsional motion and thus the efficiency of cyclization.

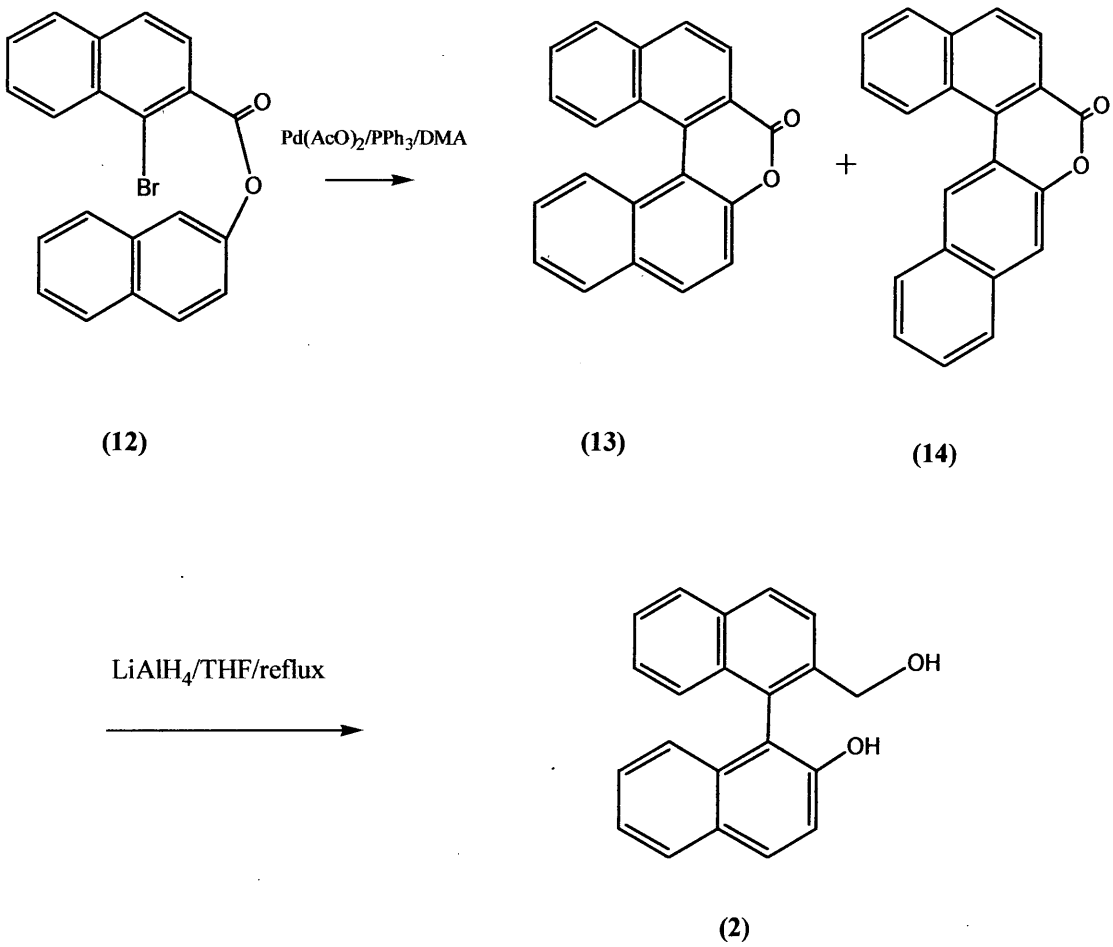

Figure 7.3 The reaction scheme to produce compound (2)

7.3 2-[2'-(HYDROXYMETHYL)-1'-NAPHTHYL]PHENOL (1)

7.3.1 Synthesis and analysis of 2-[2'-(Hydroxymethyl)-1'-Naphthyl]phenol (1)

A sample of 2-methylnaphthalene (**4**) was brominated at the 1-position to give 1-bromo-2-methylnaphthalene (**5**) with 90% yield. A second bromine was then introduced by bromination at the methyl group, following a known procedure, (Newman and Kosak, 1949) this gave structure (**6**) in 90% yield. This dibromide (**6**) was converted to (l-bromo-2-naphthyl)methanol (**7**) almost quantitatively by reflux in 1:1 $(CH_3)_2CO$-H_2O overnight. The l-bromo-2-naphthoic acid (**8**) was obtained in ~80% yield from oxidation of (**7**) with $KMnO_4$. Acid (**8**) was then converted to the acid chloride (**9**) by reflux with $SOCl_2$. Treatment of (**9**) with phenol gave ester (**10**) in 90% yield. Intra-molecular aryl-aryl coupling with $Pd(OAc)_2$ gave (**11**) in 70% yield (Bringman *et al*, 1992). Reduction of (**11**) with $LiAlH_4$ gave (**1**) in essentially quantitative yield. The overall yield of (**1**) is 20 - 30%.

Compounds (**5**)-(**8**), (**10**) and (**11**) were identified using ^1H NMR (90 MHz, $CDCl_3$), with (**7**), (**8**), (**10**) and (**11**) additionally using Mass Spectroscopic analysis.

7.3.2 X-ray analysis of 2-[2'-(Hydroxymethyl)-l'-Naphthyl]phenol (1)

X-ray diffraction analysis shows that (**1**) is in the *cis* conformation in the crystalline state, but the dihedral angle is much larger, 87.7(7)°, nearly perpendicular, see Figure 7.4 than the parent compound (approximately 68.4°). There are inter-molecular hydrogen bonds (between O1 of one molecule and H2 of another), see Figure 7.4. The length of this hydrogen bond is short (1.72 (4) Å). The hydrogen bonds in this structure probably account for the *cis* orientation. However, it is possible that it is this *cis* conformational preference results in the short hydrogen bonds.

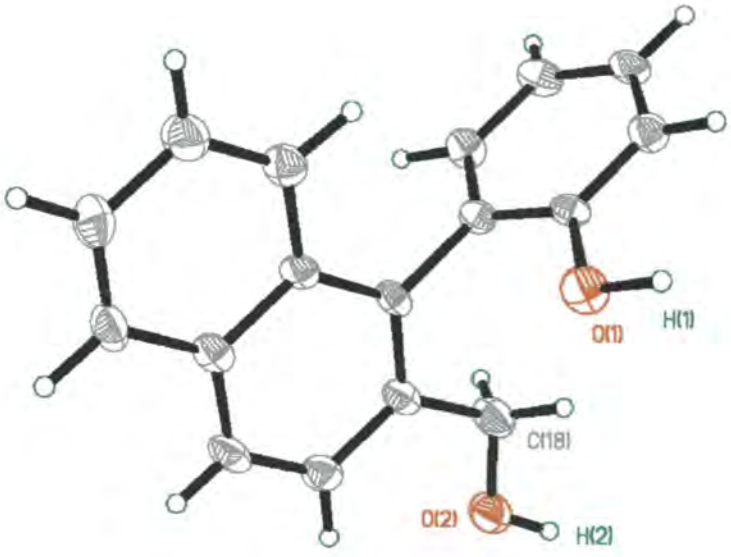

Figure 7.4 The structure of 2-[2'-(hydroxymethyl)-l'-naphthyl]phenol (1), with 50% thermal ellipsoid plot

7.3.3 Analysis of (1)

There is a decrease in quantum yield of cyclization for **(1)** on addition of H_2O. A possible explanation for the decrease in quantum yield of cyclization observed is that QM **(16)** isomer can be trapped by H_2O more efficiently (to reproduce **(1)**), than electrocyclic ring closure to give **(15)**. The fact that the photostationary state contains 40% of **(1)** is consistent with this explanation. Prolonged photolysis, gives rise to a small amount (~10 %) of unidentified side products which were probably the secondary photodecomposition of methyl ether **(17)** (see Figure 7.5). Photolysis of chromene **(15)** (see Figure 7.6) in neat CH_3OH gave a photostationary state ratio of 21:79 (**15**:**17**) and this indicates a reversibility of the reaction. In the UV absorption spectrum of chromene **(15)** shows a red-shifted strong absorption band in the region 320 - 340 nm, where the starting material **(1)** does not absorb. The ^1H NMR of **(15)** showed a sharp singlet, which was assigned to the two methylene protons. The sharp singlet indicates that the two methylene protons are chemically equivalent (or rapidly exchangeable) which suggests that **(15)** has an essentially planar conformation. It has been shown that **(15)** is achiral in the NMR time scale (Bringmann *et al.*, 1992).

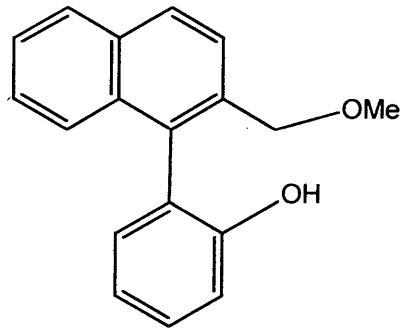

(17)

Figure 7.5 The probable side product (17)

Since **(15)** is almost planar it therefore attains better conjugation of the aromatic rings. By monitoring the growth of this band at λ_{max}= 337 nm this reaction can be more conveniently followed by UV spectrophotometry. Photolysis of a sample (8.8 x 10^5 M) of **(1)** in CH_3CN results in the progressive growth of this band at λ_{max}= 337 nm which is due to formation of chromene **(15)**. After a photolysis time of two minutes, the UV spectrum recorded was the same as that of a known sample of **(15)**. Therefore **(1)** can be quantitatively converted to **(15)**. The ^1H NMR shows a closely spaced AB quartet, which suggests that the rotation of the methylene group is restricted at room temperature, this is probably due to steric reasons and/or inter-molecular hydrogen bonds. An absence of OH peaks in neat CD_3CN suggests that the alcoholic and phenolic OH protons are exchanging fast thus broadening the peaks. As the NMR solvent used was reasonably dry and the substrate concentration was higher than any possible protic impurity in the solvent, this is most likely due to proton exchange *via* the intra-molecular hydrogen bonds.

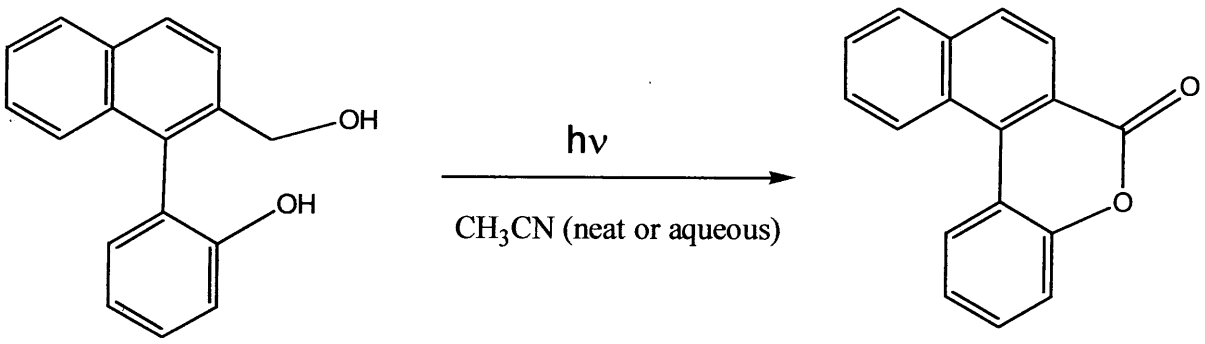

(1) **(15)**

7.6 The photocyclization reaction of (1) to (15)

7.3.4 Photolysis of 2-[2'-hydroxymethyl)-l'-naphthyl]phenol (1)

Photolysis (254 nm) of a 2.2 x 10^3 M solution of 2-[2'-(hydroxymethyl)-1-naphthyl]phenol **(1)** in CH_3CN led to formation of the cyclization product **(15)**. The ^1H NMR of **(15)** showed a sharp singlet at δ 5.14 ppm, which was assigned, to the two methylene protons. The chemical shift for the methylene protons of the product is shifted downfield by 0.58 ppm, compared to the starting material **(1)**, this is consistent with the structural transformation. This sharp singlet also indicates that the two methylene protons of **(15)** are chemically equivalent or rapidly exchangeable. This suggests that chromene **(15)** has an essentially planar conformation. It has also indicated that **(15)** is achiral in the NMR time scale (Bringmann *et al.*, 1992). The aromatic protons of **(15)** are also shifted significantly downfield. On prolonged photolysis **(1)** can be quantitatively converted to **(15)** in this solvent. No side products were detectable by GC or ^1H NMR. This was further confirmed by photolysis of an authentic sample of **(15)** under the same conditions where no product was detectable and an excellent material balance was observed by GC after photolysis for 30 min, indicating the absence of a photoreaction. Prolonged photolysis did not change this product/starting material ratio.

7.4 2-HYDROXY-2'-HYDROXYMETHYL-1,1'-BINAPHTHYL (2)

7.4.1 Synthesis of 2-Hydroxy-2'-Hydroxymethyl-1,1'-Binaphthyl (2)

Binaphthyl methanol **(2)** can be made using the same procedure outlined in Figure 7.2, resulting in two isomers 4H-benzo[f]naphtho[2,1-c]chromen-4-one **(13)** and 7H-benzo[g]naphtho[2,1-c]chromen-7-one **(14)**. It has previously been reported that these two isomers were formed in approximately 2:1 (**13**:**14**) ratio (total yield of the two isomers = 60%) under the same conditions as previously used for synthesis of **(11)** (Bringmann *et al.*, 1992). This reported that the reaction conditions were modified to successfully raise this ratio to 9:1 without a decrease in the total yield of the two isomers. Pure **(13)** was obtained after simple recrystallization from a mixed solvent consisting of CH_2Cl_2, toluene, and hexanes. Reduction with $LiAlH_4$ in THF converted **(13)** to alcohol **(2)** quantitatively.

7.4.2 Structural characterization of 2-Hydroxy-2'-Hydroxymethyl-l,l'-Binaphth (2)

The ^1H NMR gave a highly resolved AB quartet corresponding to the two methylene protons, and therefore suggesting the rotation of the methylene group is restricted. This is expected due to the greater steric hindrance for rotation in this molecule. Similar to **(1)** and **(3)**, OH peaks are absent in CD_3CN.

7.4.3 X-ray diffraction analysis of 2-Hydroxy-2'-Hydroxymethyl-l,l'-Binaphthyl (2)

The crystalline state of the molecule has inter-molecular hydrogen bonds (between O12/O12B and HO1B, bond length at approximately 1.9 Å) (see Figure. 7.7). As expected, the molecule is highly twisted, dihedral angle = 80°, and has the *cis* conformation, with respect to OH and CH_2OH groups. However, the methylene oxygen is disordered in a way that 75% is O12, and the other 25% is O12B. The disorder may be symptomatic of the lack of inter-/intra- molecular interactions for this group.

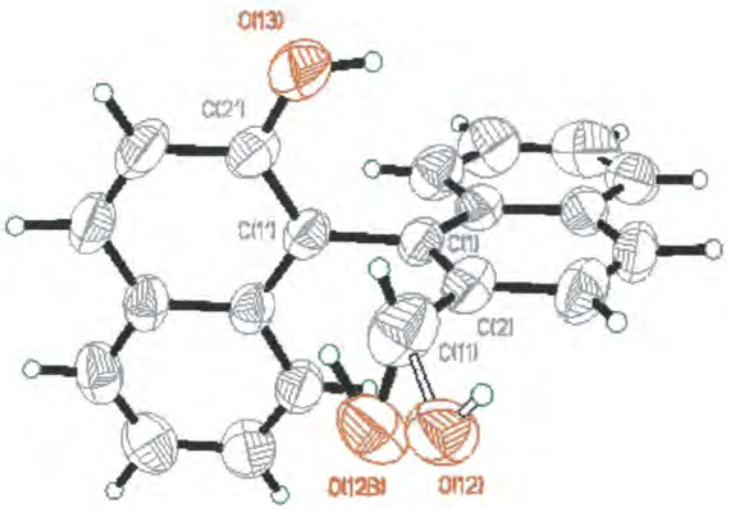

Figure 7.7 The structure of 2-hydroxy-2'-hydroxymethyl-1,1'-binaphthyl (2), with 50% thermal ellipsoids, showing the disordered O12 and O12B

7.4.4 Photolysis of 2-Hydroxy-2'-Hydroxymethyl-1,1'-Binaphthyl (2)

The binaphthyl compound **(2)** is the most sterically hindered of all compounds studied. Surprisingly, it also photocyclizes to produce 4H-benzo[f] naphtho [2,1 - c]chromene **(24)** almost quantitatively, see Figure 7.8. As expected, the UV spectrum of **(24)** is red shifted (by 20 nm) compared to the starting material **(2)** due to the much less twisted geometry of **(24)**. The chemical shifts of the methylene protons are shifted downfield and appear as two suggesting that the compound is highly twisted out of planarity. Although **(2)** is much more sterically congested than **(3)**, the quantum efficiency for cyclization is higher. No side product was detectable by ^{1}H NMR.

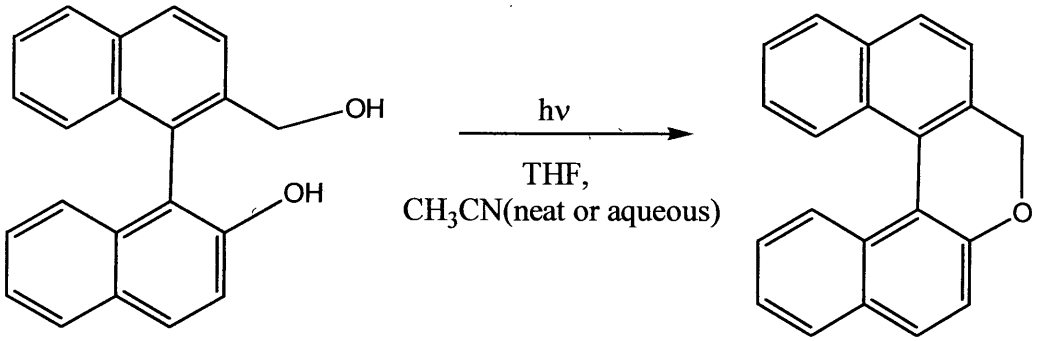

(2)

(24)

Figure 7.8 The photocyclization reaction from (2) to (24)

7.5 1-[2'-(HYDROXYMETHYL)PHENYL]-2-NAPHTHOL (3)

7.5.1 Synthesis of l-[2'-(Hydroxymethyl)phenyl]-2-naphthol (3)

The synthesis started with the commercially available 2-bromobenzoic acid **(18)**. After converting **(18)** to acid chloride **(19)** using the above method followed by reacting with 2-naphthol **(7)**, ester **(20)** was obtained in high yield (90%). Ester **(20)** was subjected to a palladium-catalyzed intra-molecular aryl coupling to give two isomers, 5H-dibenzo[c,f]chromen-5-one **(21)** and 5H-dibenzo[c,g]chromen-5-one **(22)**, in an approximately 3:1 ratio (**21** : **22**) corresponding to the coupling of the bromide to the α and the β positions of the naphthalene moiety, respectively. The final yield of **(21)** was quite low at 20-30%. 1-[2'-(hydroxymethyl)phenyl]-2-naphthol **(3)** was obtained by reduction of **(21)** with $LiAlH_4$. The ^1H NMR (360 MHz $(CD_3)_2CO$, D_2O exchanged) of **(3)** also shows an AB which suggested that methylene rotation is hindered. It was found that lactone **(21)** can also be synthesized photochemically in one step. Irradiation of a mixture of 2-bromobenzoic acid **(18)** and 2-naphthol **(7)** in CH_3CN gave **(21)** in 10 - 20% yield. The shorter synthetic route and high regioselectivity are the major advantages of this photochemical method. The byproduct of this reaction, benzoic acid, can be easily removed by flash chromatography. However, scaling-up photochemical reactions is an intrinsic problem which prevented this route to be useful for preparing large scale and amounts of **(21)**, see Figure 7.9.

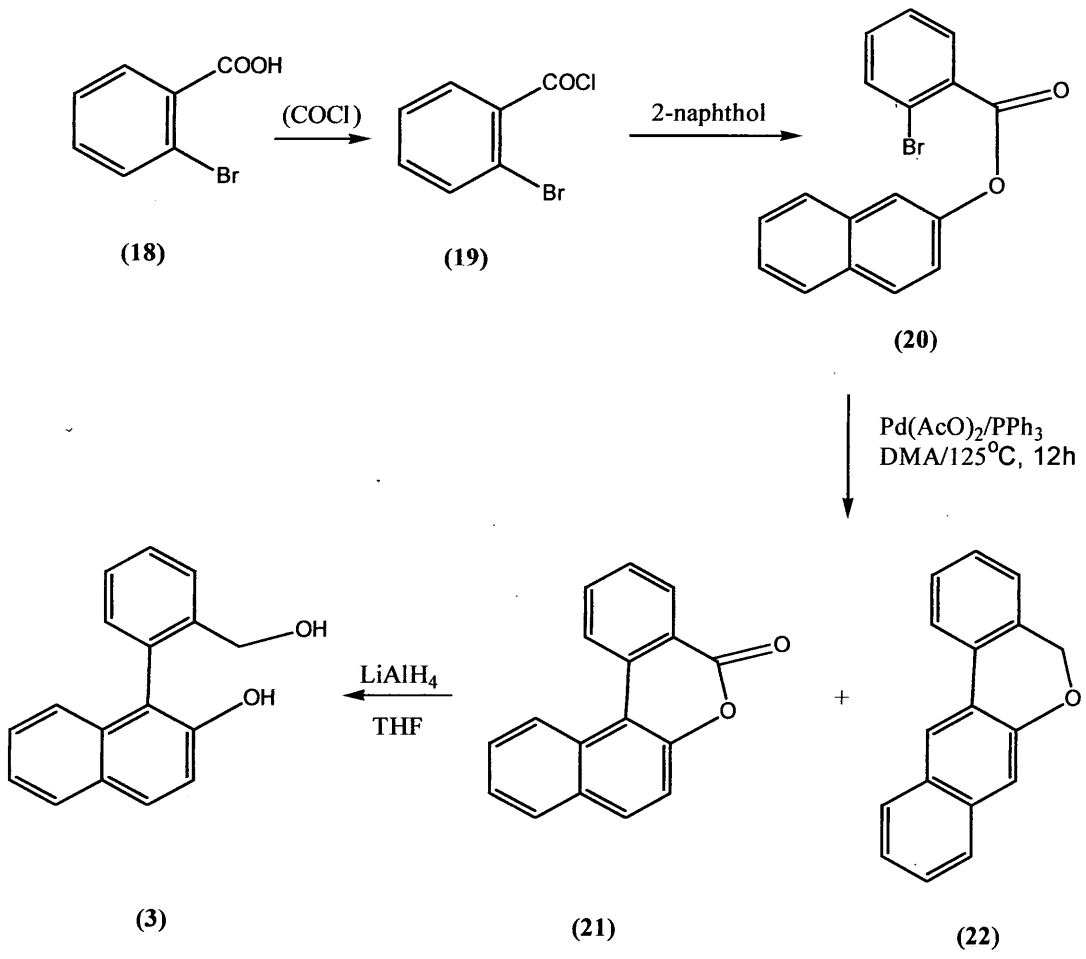

Figure 7.9 The reaction scheme to product (3)

7.5.2 X-ray diffraction analysis of l-[2'-(Hydroxymethyl)phenyl]-2-naphthol (3)

This structure has two independent molecules in the asymmetric unit, see Figure 7.10. There is twinning within the crystal and the diffraction analysis was unable to give an accurate model for this compound, despite several attempts. It exists in the extremely common (for organics) space group $P2_1/c$. There is no evidence of any inter-molecular interaction (i.e. hydrogen bonding or π-stacking). There is also no evidence for intra-molecular interaction as might have been conjectured as existing with the *ortho* groups present. Unlike many of the *o,o'*-biphenyl compounds (see chapters 10-12) the structure is of the *trans* configuration with respect to the hydroxy and methoxy groups with a high degree of twisting (dihedral angles of 99.1(5)° and 101.4(4)° for the two independent species) (see Figure 7.10). This of course makes the intra-molecular interaction between the oxygen containing groups extremely unlikely, although with the inherent errors resulting from the twinning this cannot be determined accurately.

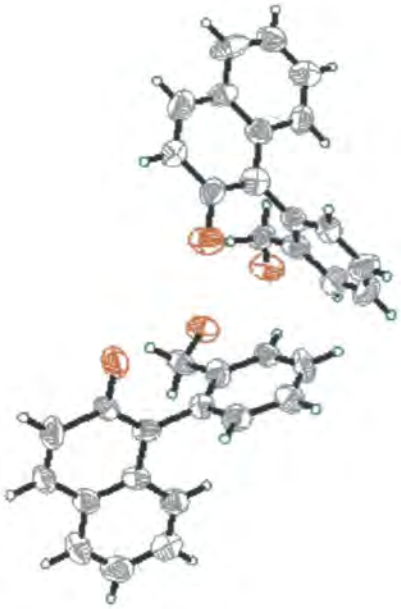

Figure 7.10 The two independent molecules of l-[2'-(hydroxymethyl)phenyl]-2-naphthol (3), with 50% thermal ellipsoids

7.5.3 Photolysis of l-[2'-(Hydroxymethyl)phenyl]-2-Naphthol (3)

Irradiation of alcohol **(3)** in a variety of solvents (THF, CH_3CN or aqueous CH_3CN) gave the expected product **(23)** as the only product. The ^1H NMR of **(3)** showed an AB, which progressively decayed upon photolysis. With exhaustive photolysis, the 'H NMR spectrum of the residue was identical to that of a sample **(23)**. When compared to the photolysis of its isomer **(1)** under identical conditions, the reaction proceeded slower (smaller quantum yield). For example, photolysis of $2x10^{-3}$ M of **(3)** in 1:1 CH_3CN-H_2O under the conditions took more than ten hours to reach the photostationary state ratio of 95:5 (**23**:**3**), see Figure 7.11.

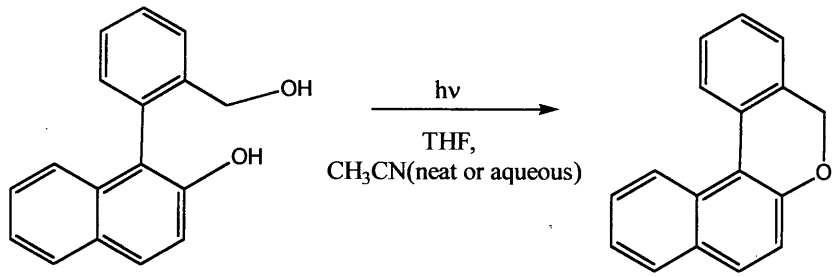

(3) (23)

Figure 7.11 The photocyclization reaction of (3) to (23)

7.6 SUMMARY AND DISCUSSION

The excited state planarization is the crucial step for this photocyclization reaction, since the elimination of OH^- requires the charge transfer (from the ArOH moiety), whereas this excited state charge transfer requires a more planar S_1. The reactions can proceed *via* initial twisting followed by adiabatic deprotonation from the planar S_1, depending on the relative rates of ESPT (k_{-H}) and twisting (k_t). When the steric hindrance for the twisting is small enough $k_{-H} << k_t$, then initial twisting followed by deprotonation dominates (Shi, 1997).

Biaryl methanols (**(1) – (3)**) are intra-molecularly hydrogen bonded in aprotic solvent (such as neat CH_3CN) in the ground state, and CH_3CN is not capable of deprotonating the ArOH protons, it is concluded that the photocyclization in this solvent proceeds *via* the ESLraPT mechanism, the ArOH proton is initially transferred to the $ArCH_2OH$ oxygen *via* an intra-molecular hydrogen bond followed by elimination of a molecule of H_2O to give the corresponding QM intermediate. The efficiency of the reaction will depend on, to a significant extent, the ESIraPT rate (k_{-H}), or the acidity of the phenolic proton in S_1. This can be seen from a comparison between **(1)**, **(2)**, and **(3)**, in which **(1)** has the highest k_{-H} and the highest quantum yield. Structures **(1)-(3)** do not show a large Stokes shift because of the presence of the naphthalene rings.

7.6.1 Naphthyl compounds (1) and (2)

The fluorescence study suggests that the excited S_1 state of the neutral molecule is twisted while the deprotonated form is more planar. In other words, these molecules twisted to the planar forms only after the adiabatic deprotonation in S_1 . The mechanism for cyclization involves adiabatic deprotonation of the twisted S_1 followed by twisting to the planar form which then eliminates the hydroxide ion from the arylmethyl position to give the required QM intermediates.

7.6.2 Naphthyl Compound (3)

Unlike **(1)** and **(2)**, both the neutral and deprotonated forms of **(3)** stay twisted upon excitation. The Stokes shift and the spectral width of this molecule are essentially the same as those of 2-naphthol, which suggests the lack of enough driving force for the S_1 planarization and of strong electronic interaction between the two chromophores. In other words, the two chromophores

within the molecule are essentially independent in both S_0 and S_1. As an approximation, the two chromophores of the molecule can be treated independently without introducing substantial error. Based on this approximation, absorption of a photon by the molecule can initially lead to two different excited states. **(3a)** where the photon was absorbed by the naphthol moiety and **(3b)** where the photon enters the benzyl alcohol moiety. The cyclization reaction requires the electronic interaction of the excited chromophore and the unexcited chromophore to give a more planar (thus more conjugated) S_1. It is expected that **(3a)** can also give **(3b)** efficiently *via* energy transfer. Furthermore, the naphthol moiety has much larger extinction coefficient than the benzyl alcohol moiety at the excitation wavelength (280 nm). The mechanism requires the transfer of enough negative charge on the naphtholate ion moiety to the benzyl alcohol moiety in order to activate the elimination of the OH group.

	(1)	(2)	(3)
Formula	$C_{17}H_{14}O_2$	$C_{21}H_{15}O_2$	$C_{17}H_{14}O_2$
Formula Weight	250.28	299.33	250.28
Temperature (K)	150(2)	150(2)	293(2)
Crystal System	Orthorhombic	Monoclinic	Monoclinic
Space group	*P*2(1)2(1)2(1)	*P*2(1)/*c*	*P*2(1)/*c*
a= (Å) b= (Å) c= (Å) α= (°) β= (°) γ= (°)	7.219(3) 12.322(2) 14.209(2) 90 90 90	12.44 (2) 9.28 (3) 14.80 (1) 90.000 112.40(3) 90.000	22.73 (5) 7.51 (10) 15.24 (11) 90.000 90.026(10) 90.000
Volume (A^3)	1264.0(3)	1579.6(6)	2602.39(3)
Calculated Density (Mg/m^3)	1.315	1.259	1.426
Absorption Coefficient (mm^{-1})	0.09	0.080 mm^{-1}	0.13 mm^{-1}
F (000)	528	628	1155.0
Index Ranges	-9=<h=< 8, -13=<k=<15, -18=<l=<17	-7<=h<=16, -11<=k<=12, -19<=l<=18	-29=<h=<28, -9=<k=<8, -19=<l=<19,
Reflections collected	9219	10071	19162
Data/restraints/ Parameters	2903/0/214	3579/0/251	5918/0/368
Goodness-of-fit on F^2	1.208	1.188	4.579
Final R indices [I>2sigma(I)]	0.0801	0.0707	0.2611
R indices (all data)	0.2175	0.1981	0.6265
Extinction coefficient	None	0.006(2)	0.254 (2)
Largest diff. Peak and hole ($e.A^{-3}$)	0.31 and -0.35	0.200 and -.153	1.01 and -0.98

Table 7.1 X-ray Diffraction data for (1), (2) and (3)

7.7 REFERENCES

1. Bringmann, G.; Hartung, T.; Göbel, L.; Schupp, O.; Ewers, C.; Schöner, B.; Zagst, R.; Peters, K.; Schnering, H.; Burschka, C., *Leibigs Ann. Chem.*, **1992**, 225.
2. Bringmann, G.; Hartung, T, *Tetrehedron*, **1993**, 49, 7891.
3. Newman, M.; Kosak, A., *J. Org. Chem.*, **1949**, 14, 375.
4. Robinson, G.; Thistlethwaite, P., *J. Phys. Chem.*, **1986**, 90, 4224.
5. Shi, Y., *PhD. Thesis*, University of Victoria, B.C., Canada, **1997**.
6. Shin, S.; Keating, A.; Garcia-Garibay, M., J. *Am. Chem. Soc.*, **1996**, 118, 7626.

CHAPTER 8:

QUINONE METHIDES

8.1 INTRODUCTION

It has been suggested that there is an efficient formation of an *ortho*-quinone methide (*o*-QM) from the photolysis of *ortho*-hydroxybenzyl alcohol **(3)** in aqueous solution which explains the facile photolysis of this compound observed in 1:1 MeOH-H_2O (formation of the corresponding methyl ether) (Wan *et al.*, 1986, 1987 and 1989). A further investigation of the possibility of *o*-QM formation from various hydroxybenzyl alcohols as a general photochemical process examined the photochemistry of a number of hydroxybenzyl alcohols including **(1)** and **(3)** (Yang, 1994). This research found strong evidence for the efficient generation of *o*-QMs from photolysis of **(1), (2)** and **(3)**, see Figure 8.1.

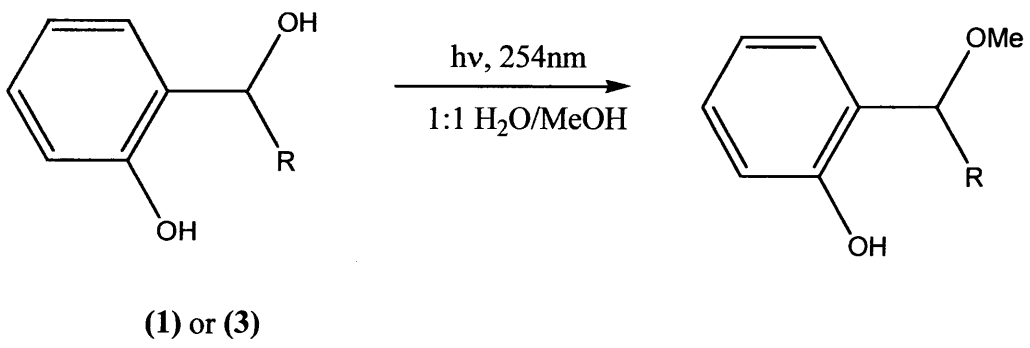

(1) or **(3)**

Figure 8.1 Photolysis reaction of (1) R=Ph and (3) R=H.

This chapter focuses on the investigation of the photochemistry of a variety of hydroxybenzyl alcohols in aqueous solution with the view to examine the possibility that there is a general way for quinone methides to be prepared from simple hydroxybenzyl alcohols. The detection of these and other QM intermediates by transient spectroscopy will prove their existence. This chapter focuses on the photochemistry and structure of structure **(1),(2),(3)** and **(4)**, see Figures 8.1 and 8.2.

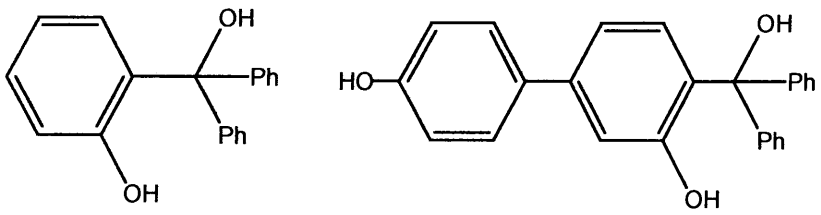

(2) (4)

Figure 8.2 The structures of (2) and (4)

8.2 PHOTOGENERATION OF QUINONE METHIDES FROM HYDROXYBENZYL ALCOHOLS

Studies on the parent *o*-hydroxybenzyl alcohol **(3)** and the α-phenyl substituted analogue **(1)** have shown evidence for the photogenerated intermediate (Yang, 1994). Both of these structures reacted *via* efficient photolysis in aqueous methanol resulting in the formation of the corresponding methyl ether in high yields (e.g. 65-70% for 10 minutes photolysis at 254 nm), see Figure 8.1. Photolysis of these two compounds in the presence of electron-rich dienophiles such as ethyl vinyl ether gave the regioselective [4+2] Diels-Alder adducts, see Figure 8.3.

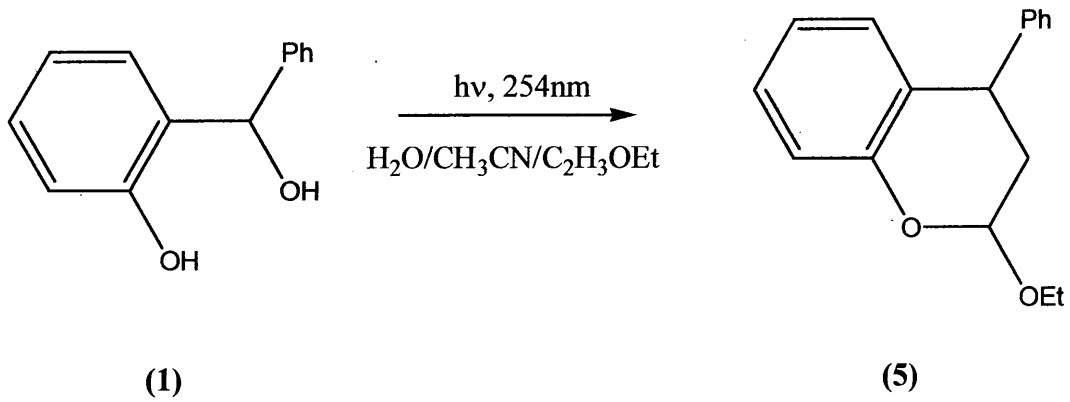

(1) **(5)**

Figure 8.3 [4+2] Diels-Alder photoreaction of (1) to (5)

8.3 HYDROXYBENZYL DIPHENYL ALCOHOL (2)

Laser Flash Photolysis of **(2)** produced a strongly absorbing transient in either acetonitrile or 1:1 H_2O-CH_3CN with no appreciable decay within 2 ms. The transient spectrum for **(2)** is almost identical to that of **(1)**. This indicated that for both have a similar transient being generated and the additional phenyl substitution on benzylic carbon has little effect on absorption characteristics. The relative quantum yield for the formation of transient **(2)** was shown, at 360 nm as a function of water content (in CH_3CN). It has been reported that the (*p*-methoxyphenyl)diphenylmethyl cation has a lifetime of 0.71 ms in 2:1 1 H_2O-CH_3CN and this is much shorter than the transient observed for **(2)** (McClelland *et al*, 1989).

8.4 SYNTHESIS AND ANALYSIS OF THE STRUCTURES OF (1), (2), (3) AND (4)

The *o*-hydroxybenzhydrol **(1)** was made by the addition of phenylmagnesium bromide or phenyllithium to salicylaldehyde and *o*-hydroxybenzhydrol. Structure **(2)** was made by the addition of phenylmagnesium bromide or phenyllithium to methyl salicylate. Hydroxybenzyl alcohol **(3)** is a commercially available product.

Alcohol **(4)** was synthesized from the commercially available 4'-hydroxy-4-biphenylcarboxylic acid **(6)** *via* the standard route with Grignard reagents shown in Figure 8.4

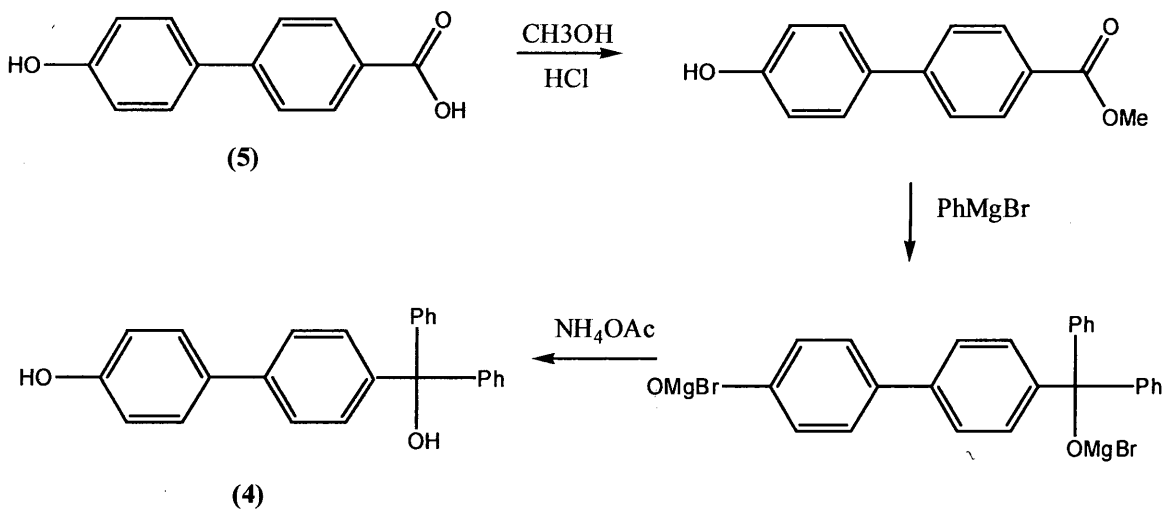

Figure 8.4 The synthesis of (4)

The ^{1}H NMR spectra of **(1)** and **(3)** showed no readily assignable peak(s) for either hydroxyl proton. In the expanded spectra, hidden under other peaks, were one or two very broad bands, which were D_2O exchangeable. The ^{1}H NMR spectra of **(2)** showed two broad peaks, which were assignable to the two hydroxyl protons. Photolysis was studied using UV-Vis specrophotometry in aqueous CH_3CN to gain initial insight into whether the corresponding proposed quinone methides were observable without the need for laser flash photolysis. Photolysis of **(1)** in acetonitrile resulted in the formation of a yellow solution, which turned to orange red and then deep red brown in colour. UV-Vis spectra was recorded before and after the photolysis, before photolysis the material absorbed at < 300nm where upon photolysis there was new absorption bands at 222 and 423 nm, which indicated a new species. The transient decayed slowly in neat CH_3CN, although the yellow colour remained. The red shift of λ_{max} on changing to more polar solvents indicate that these transitions are π, π^* in character. The UV-Vis analysis

shows that the transients are photogenerated from benzhydrol **(1)**. Laser flash photolysis gave strong signals with no observable decay within the millisecond range. A significant amount of transient was also formed on photolysis in neat CH_3CN (under N_2 or O_2), although the absorption bands were significantly blue shifted with the bands 455 and 345 nm shifted to 410 and 330 nm respectively. The transient spectra from **(1)** was also taken with different pH (1-2 and 11-12) and the results consistent with a mechanism for formation of the QM *via* an excited phenolate state.

8.5 STRUCTURAL X-RAY DIFFRACTION ANALYSIS

8.5.1 X-ray diffraction analysis of α-phenyl-*o*-hydroxybenzyl alcohol

The X-ray structure analysis of α-phenyl-*o*-hydroxybenzyl alcohol **(1)** shows that there is extensive inter-molecular hydrogen bonds. The two benzene rings are almost perpendicular to each other. Each phenol proton is pointed away from the benzylic carbon and hydrogen bonded with the benzylic oxygen atom in a second molecule, which is hydrogen bonded similarly to a third one, see Figure 8.5. There are two independent structures in the asymmetric unit. The C2-O1 and C2'-O1' bonds are 1.355(10) Å and 1.366(10)Å respectively with the phenyl-oxygen bond lengths 1.409(10) Å and 1.437(11) Å. There is a lot of thermal motion in the crystal as can be seen in the relatively large thermal ellipsoids. There is no evidence of any inter- or intra-molecular interactions within the crystal structure.

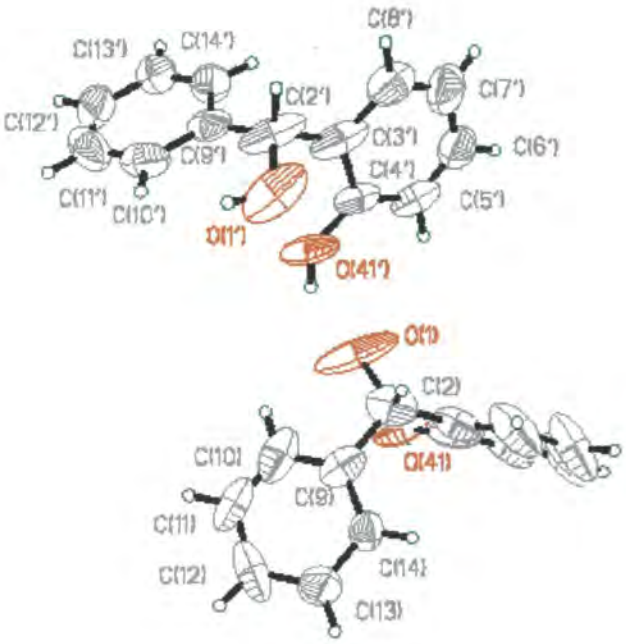

Figure 8.5 The structure of α-phenyl-*o*-hydroxybenzyl alcohol (1), with 50% thermal ellipsoids.

8.5.2 X-ray diffraction analysis of (2)

There is intra-molecular hydrogen bonding in the structure. The three adjacent benzene rings are positioned in a propeller type orientation, see Figure 8.6. The X-ray structure analysis shows that the molecule exists as an inter- and intra-molecularly hydrogen bonded dimer. There is intra-molecular hydrogen bonding, the O···H-O hydrogen bonds are short at 1.747(8) Å, (see Figure 8.6). The structure exists in the solid state as dimers, (see Figure 8.7), with the inter-molecular bonds a distance of 1.950(7)Å.

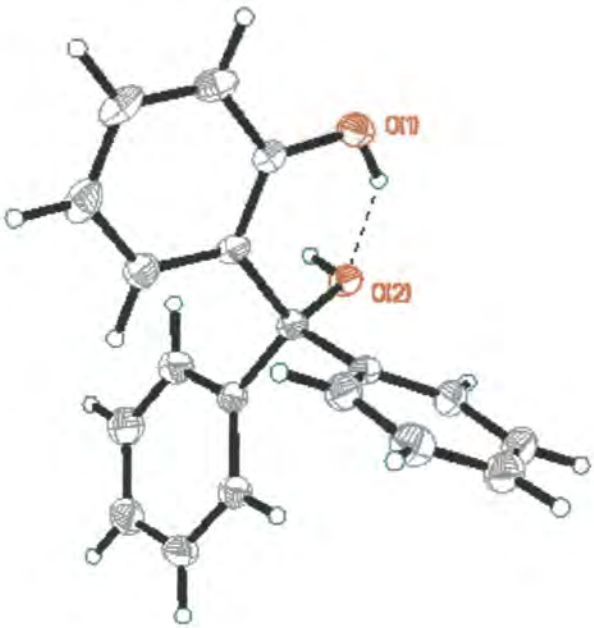

Figure 8.6 The structure of (2), showing the intra-molecular interaction, with 50% thermal ellipsoids

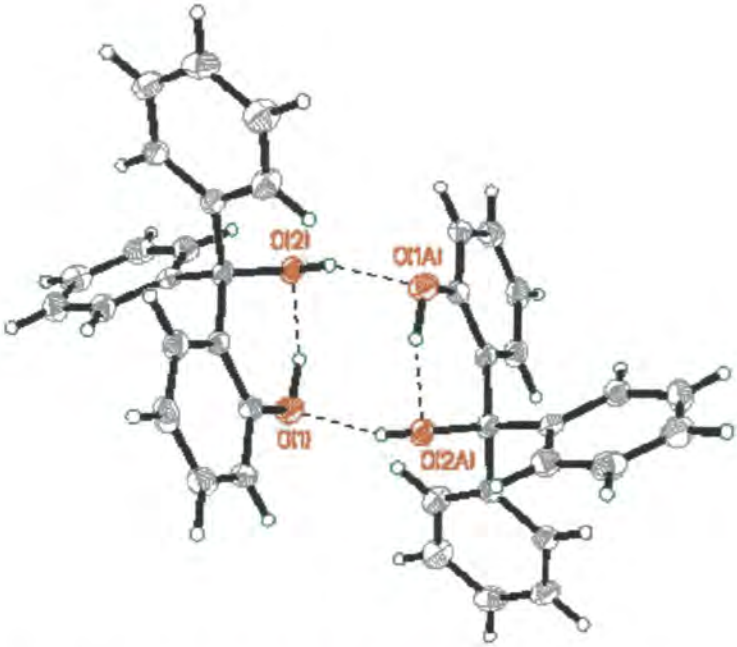

Figure 8.7 The dimeric structure of (2)

8.5.3 X-ray diffraction analysis of (4)

The synthesis of **(4)** produced yellow crystals. The X-ray diffraction structure shows that three phenyl rings attached to the carbon in a propeller geometry similar to that of **(2)** (see Figure 8.8). There is intra-molecular hydrogen bonding the proton on O2 with the O1 of another molecule, the O···H-O hydrogen bonds are short at 1.863(4) Å (see Figure 8.8). The biphenyl molecule has a dihedral angle of 31.8(7)°, which is relatively large considering the there are no *ortho* substituents present, although it fits the pattern of many of these types of structures (see chapter 5). There is no intra-molecularly hydrogen bonding in the structure. The main difference between this structure and **(2)** is the difference in intra-and inter-molecular hydrogen bonding. Whereas in **(2)** there is a dimer formed, in **(4)** this does not occur and the result is chains. This is presumably due to the length of this structure packing better with this inter-molecular hydrogen bonding.

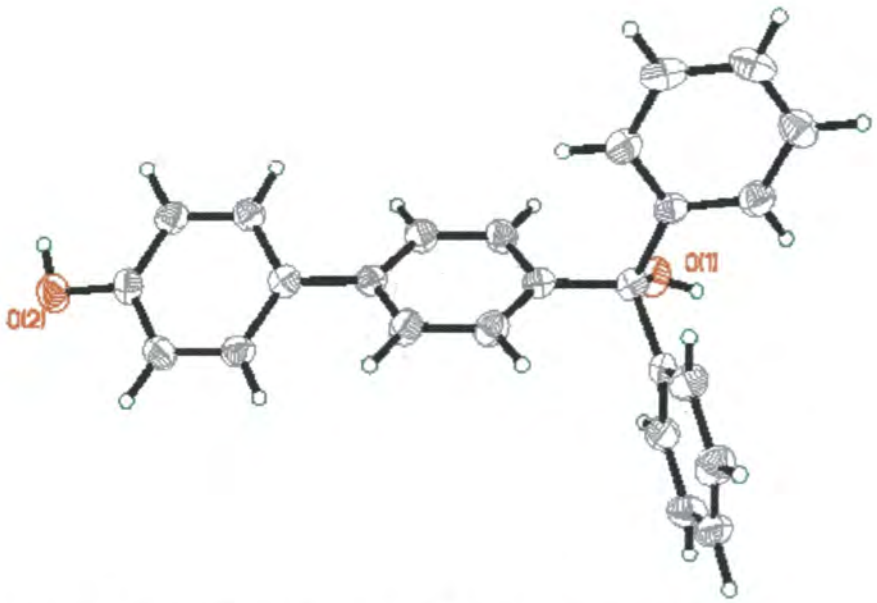

Figure 8.8 The structure of (4), with 50% thermal ellipsoid plots

8.6 PHOTOLYSIS IN AQUEOUS METHANOL

Photolysis of *o*-hydroxybenzhydrol **(1)** in 1:1 H_2O/MeOH gave the corresponding methyl ether (7%). The ^1H NMR of the reaction mixture showed the characteristic methoxy singlet of the methyl ether product. Prolonged photolysis of **(1)** (> 20 minutes) in 1:1 H_2O/MeOH gave increasing yields of the methyl ether and also a secondary photoproduct, *o*-benzylphenol. Studies of the similar **(3)** showed that the secondary product involved was produced exclusively from the secondary photolysis of the primary methyl ether product (Yang, 1994). Photolysis (254 nm) of a solution of **(4)** in MeOH-H_2O for 2.5 minutes led to the clean conversion (16%) to the corresponding methyl ether **(8)**. The same QM mechanism for **(1)** also applies to **(4)**. ^1H NMR and high resolution MS analysis of the product **(8)** was consistent with the formation of the methyl ether product **(8)** of the reaction.

8.7 PROPOSED MECHANISM FOR (1) TO (6)

UV-Vis studies have shown the formation of *o*-QM **(6)** from **(1)** in neat organic solvents. The yield of **(6)** decreases with the addition of water but the fluorescence lifetime (τ) shortens with increasing water content. This indicates that **(1)** remains extensively inter-molecular hydrogen bonded in the neat organic solvents, this hydrogen bonding would weaken the O-H strength and facilitate deprotonation on excitation. The resulting excited phenolate ion has the benzylic oxygen hydrogen bonded to a phenol proton which allows it to react with the loss of H_2O to form *o*-QM **(6)**, see Figure 8.9, however an alternative is an inter-molecular proton transfer mechanism.

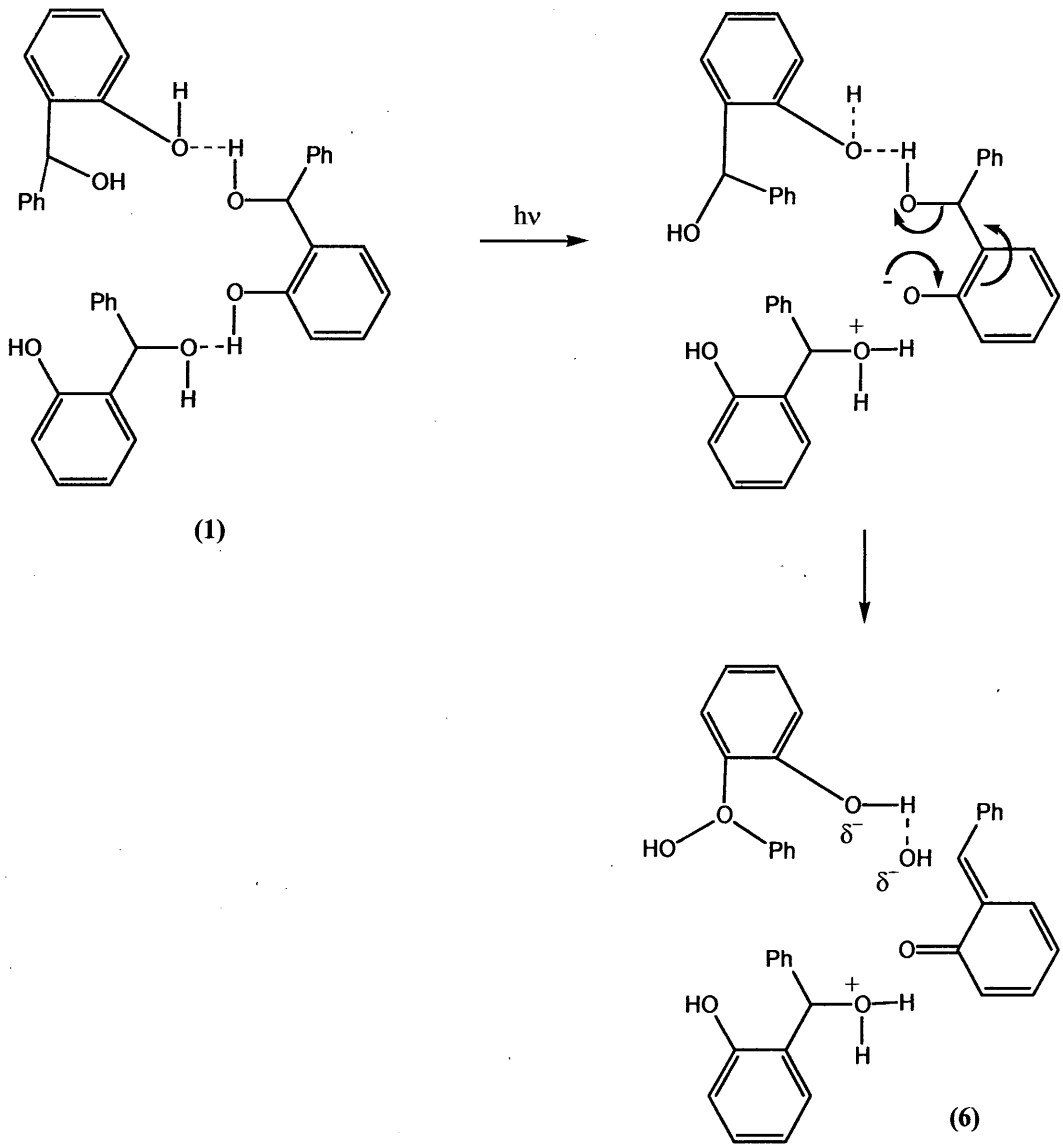

Figure 8.9 The reaction of (1) to (6)

8.8 PROPOSED MECHANISM FOR (4) TO (8)

When irradiated, the excited biphenyl alcohol **(4)** twists into a more planar geometry. A deprotonation proceeds due to the enhanced acidity of the phenol in excited state to give an excited phenolate ion, this ion undergoes an intra-molecular charge transfer reaction followed by a nucleophilic attack to give the photoproduct. If H_2O is introduced then the QM reacts in a way that generates the starting material **(4)** see Figure 8.10

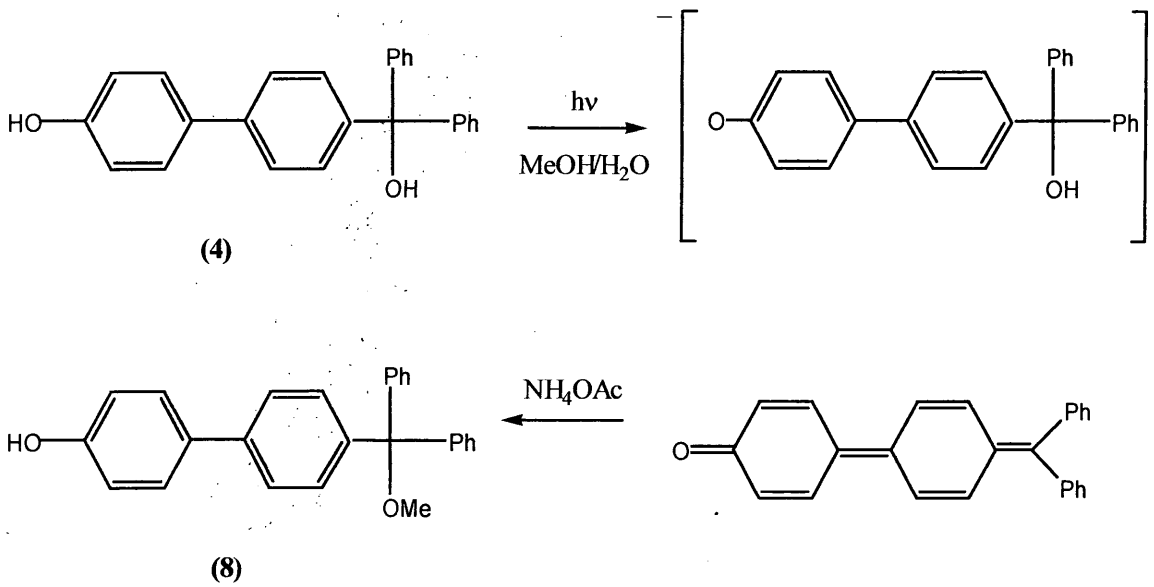

Figure 8.10 The mechanism for (4) to (8)

8.9 PROPOSED MECHANISM FOR (2) TO (7)

The photolysis of triphenyl alcohol **(2)** also generates the *o*-QM **(7)** in neat organic solvents. X-ray diffraction analysis shows that there is intra-molecular and inter-molecular hydrogen bonding present. Upon photolysis there is an intra-molecular proton transfer, with adiabatic deprotonation of singlet **(2)** generates an excited state phenolate ion, which then loses water to form the *o*-QM **(7)** and **(2)** hydrogen bonded to a water molecule. The fluorescence quantum yield of **(2)** increases slightly at low water content, this indicates that addition of water introduces a "water-assisted" mechanism for generation of **(7)**, this competes effectively with the intra-molecular proton transfer mechanism.

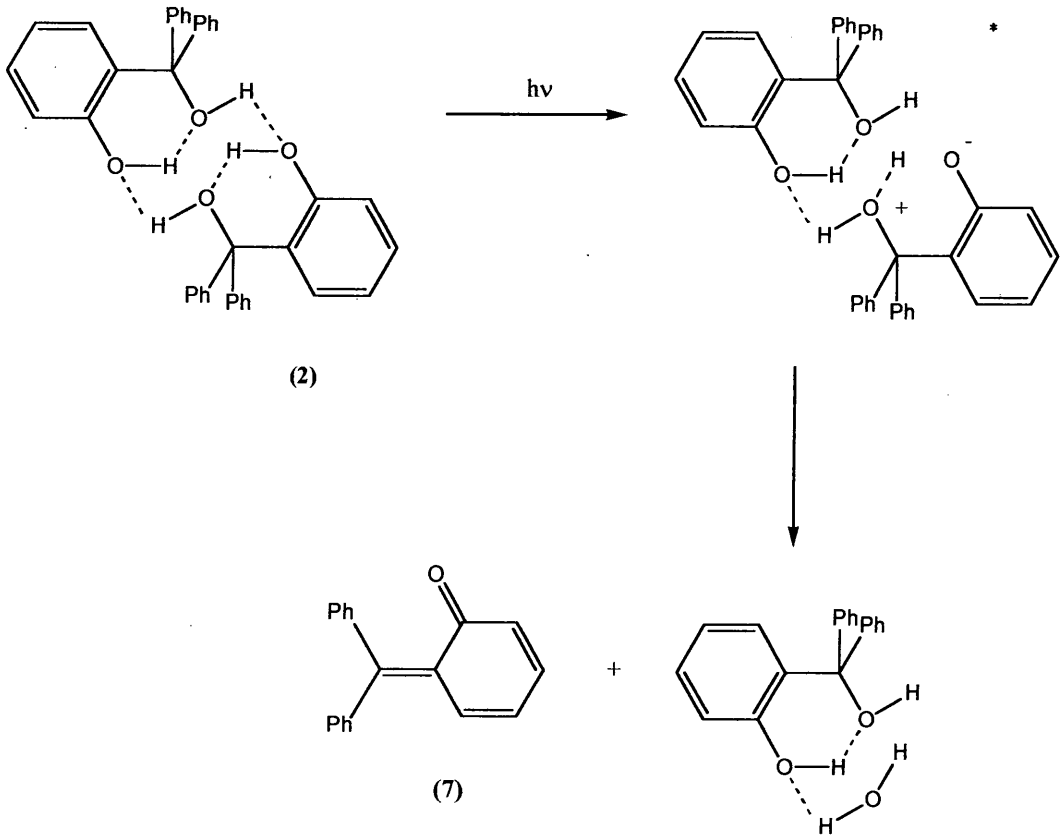

Figure 8.11 The proposed mechanism of (2) to (7)

8.10 REFERENCES

1. McClelland, R. A.; Kanagasabapathy, V. M.; Baniat, N. S.; Steenken, S. *J. Am. Chem. Soc.*. **1998**, 110, 6913.
2. Wan, P.; Chak, B., *J. Chem. Soc.,Perkin Trans. 2*, **1986**, 1751.
3. Wan, P.; Hennig, D., *J. Chem. Soc., Chem. Commun.*, **1987**, 939.
4. Wan, P.; Chak, B., Krogh, E., *J. Photochem Photobiol. A:*, **1989**, 46, 49.
5. Yang, C. *MSc. Thesis*, **1994**, University of Victoria, Victoria, British Columbia, Canada.

CHAPTER 9:

A REINVESTIGATION OF THE PHOTOCHEMISTRY OF α-AZIDOCINNAMATES

9.1 INTRODUCTION

Previously studies conducted on α-azidocinnamates reported that it gave rise to one diastereomer of a trimer in a stepwise and efficient manner by photolysis with the use of quartz equipment. Crystallographic and spectral methods were used to characterize both dimers, and they oxidized to give imidazoledicarboxylic esters, while the action of base on both dimer diastereomers leads to one rearranged dimer, a 1,2-dihydropyrimidine. It was slightly surprising that only a mixture of both diastereomeric dimers will give the trimer on further photolysis.

The photolysis of α-azidoalkenes (e.g. **(1)**, see Figure 9.1) were thoroughly examined and they have been shown to yield azirines **(2)**. In the case of α-azidocinnamates **(1)**, the reaction has been studied and this has shown that the reaction efficiently leads by way of dimers **(3)** to one diastereomer of the trimers **(4)** (Hickey *et al*, 1986).

The photolysis was conducted in quartz equipment in a four-bulb Rayonet apparatus and the process was corroborated (although not the yields) in several cases. The key steps are:

(1) Azide **(1)** conversion into azirine **(2)**, a well documented reaction (Hickey *et al.*, 1986);

(2) photo-activated azirine ring-opening by C-C bond cleavage to give an azomethine ylide, also well documented;

(3) **[4+2]** cycloaddition of this 1,3-dipole to another molecule of azirine to give the non-isolated dimers **(3)**;

(4) photo-ring-opening of the aziridine ring of the dimer to give another 1,3-dipole.

(5) cycloaddition of a second molecule of azirine to this new dipole to yield the trimer **(4)**.

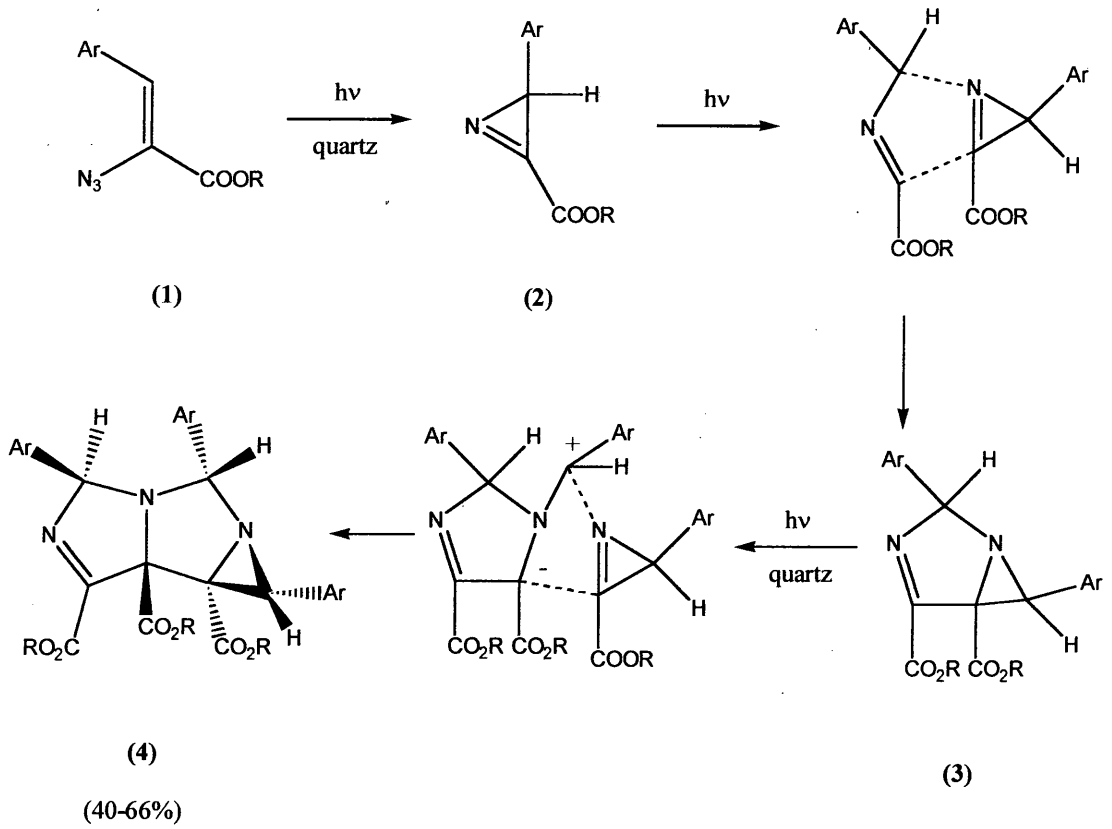

	R	Ar
a	Me	Ph
b	Et	Ph
c	Et	2-MeC_6H_4
d	Et	4-ClC_6H_4
e	Me	2, 6-$Cl_2C_6H_3$
f	Me	3,4,5-$MeO_3C_6H_2$

Figure 9.1 Scheme 1, representing the photoreaction mechanism from (1) to (4)

9.2 RESULTS AND DISCUSSION

In reviewing the previous results, it was decided to conduct a re-examination of photolysis of various α-azidocinnamates in acetone solution with a view to observing alternative chemistry, mediated by radical pathways. The observation that thermolysis of *o*-tolyl azidocinnamates in the presence of iodine (a 'heavy-atom' singlet-to-triplet nitrene converter) gave isoquinolines, presumably by triplet nitrene 'insertion' into the tolyl methyl group (Hickey *et al.*, 1986), see Figure 9.6 and later text.

Surprisingly the result was rapid and clean, giving a mixture of two isomeric dimers, and generally a good yield. The dimers shown in this chapter were shown conclusively to be the intermediates **(3)** that were predicted by the previous study (Casey *et al.*, 1985). More surprisingly, the same products formed when a non-sensitised photolysis was conducted in Pyrex equipment, either using the Rayonet reactor or more effectively using our novel simple, cheap and efficient reactors. Indeed even in quartz apparatus, the dimers **(3)** were easily isolated and only slowly transformed into the trimers **(4)** (see Table 9.1).

The dimers were always isolated as a pair of separable diastereomers **(3A)** and **(3B)**, usually formed in similar amounts, the structures of which were easily assigned by n.o.e., showing the two aliphatic C-H's interacting in **(3A)** but not in **(3B)**. Furthermore, their classification was easily recognized since the lower field CH-resonance in **(3A)** was always in the range of 6.1-6.3 ppm while that of 3B was at 6.8-7.1 ppm.

Entry	Cpd	Solvent	Filter	Time (h)	Temp (°C)	**(3A)**	**(3B)**	**(4)**	**(7)**	**(2)**
1	1a	P	Py	1	13	30	35	5	-	-
2	1a	A	Py	1	21	34	28	-	-	-
3	1a	P	Py	5.5	28	28	42	5	-	-
4	1a	P	Q	1	29	20	27	27	-	-
5	1a	A	Q	0.5	28	43	26	11	6	-
6	1a	P/A-12:1	Q	1	30	34	41	19	-	-
7	1a	P/A-12:1	Q	2	30	30	30	30	-	-
8	1a	P/A-12:1	Q	3	30	25	13	50	-	-
9	1a	P/A-12:1	Q	4	30	20	0	60	-	-

10	1b	P	Py	1.25	20	32	54	5	-	-
11	1b	A	Py	.125	20	51	36	-	-	-
12	1b	P	Q	0.6	45	21	42	21	-	-
13	1b	P/A-12:1	Q	1	30	25	38	36	-	-
14	1b	P/A-12:1	Q	2	30	11	21	62	-	-
15	1b	P/A-12:1	Q	3	30	-	1	87	-	-
16	1b	P/A-12:1	Q	4	30	-	87	-	-	-
17	1c	A	Py	0.5	20	24	48	4	-	-
18	1d	P	Py	1.5	20	25	14	-	-	-
19	1d	A	Py	5.6	20	38	19	-	-	-
20	1e	P	Py	1.5	20	-	37	-	-	42
21	1f	A	Py	1	27	-	-	-	-	99

Table 9.1 Products from the photolysis of azidocinnamates, P =Light petroleum, A = Acetone, Py = Pyrex and Q = Quartz .

In one case **(3Aa)** X-ray diffraction analysis (see Figure 9.2) gave a quantum structural assignment.

This led to several questions,

(1) What is the role of the solvent and the quartz/Pyrex glassware?

(2) Can we learn anything from the subsequent chemistry of the dimers?

(3) Why is only one stereomer of the trimer isolated, often in good yield, on quartz mediated photolysis, despite two dimers being precursors?

(4) How and why do both dimers give the one trimer?

The answer to the first question is relatively simple. It is evident that ring opening of an azirine occurs with lower energy (longer wavelength) light than that required for aziridine ring opening. This latter process therefore does not occur when acetone or Pyrex filters are used in the photolysis. The fact that the azirine ring-opening may involve radical species in the sensitised cases does not alter the reaction pathway of subsequent cycloadditions .

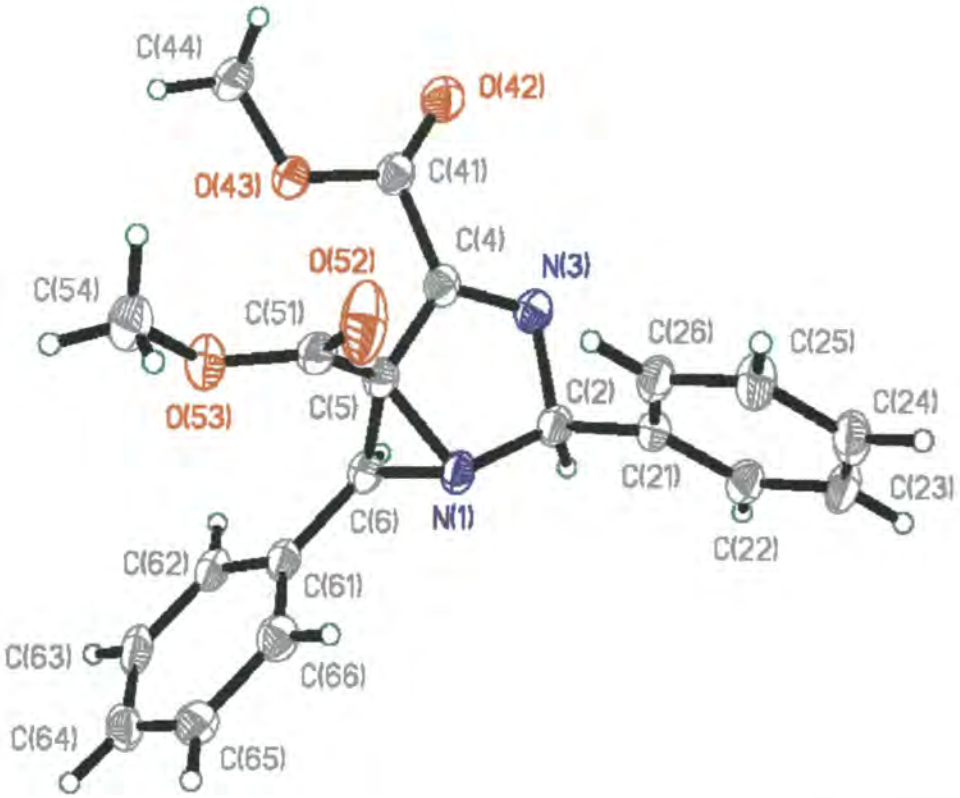

Figure 9.2 X-ray Structure of compound (3Aa), with thermal ellipsoid probability 50%

The dimers show several novel aspects of further chemistry. They are not indefinitely stable but slowly change in solution even in the dark, the methyl esters reacting faster than the ethyl. The rate of this process is dramatically increased by added base, but not by acid, this suggests that the basicity of the dimers cause autocatalytic rearrangement. Although the mixture of diastereomers gave one rearranged isomer from this action, which proved to be the dihydropyrimidine **(5)**, see Figure 9.5. The rearrangement mechanism of **(3)** to **(5)** is shown in Figure 9.3, Scheme 2.

This is a new type of rearrangement of such bicyclic systems and the structure of the rearranged dimer **(5)** produced crystals that were easily studied by X-ray crystallography. The oxidative treatment of the isolated dimers **(3A)** and **(3B)** or the mixture of both diastereomers were also studied. With DDQ, conversion to a mixture of an aryl aldehyde and the imidazole **(6)** was observed. The structure of the imidazoles was confirmed by an alternative literature-based synthesis from tartaric acid, see Figure 9.4, Scheme 3.

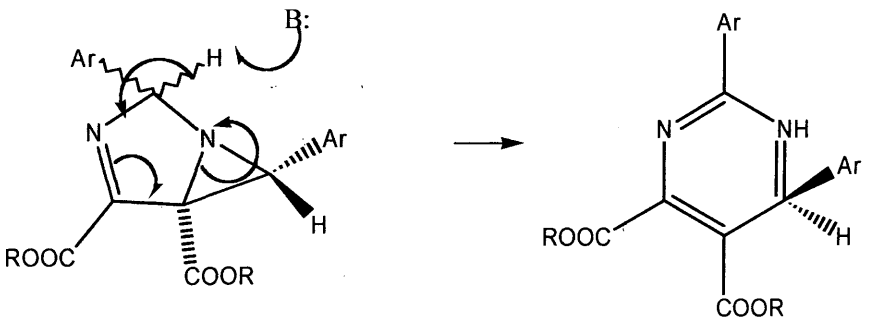

(3) (5)

Figure 9.3 Scheme 2, the mechanism for (3) to (5)

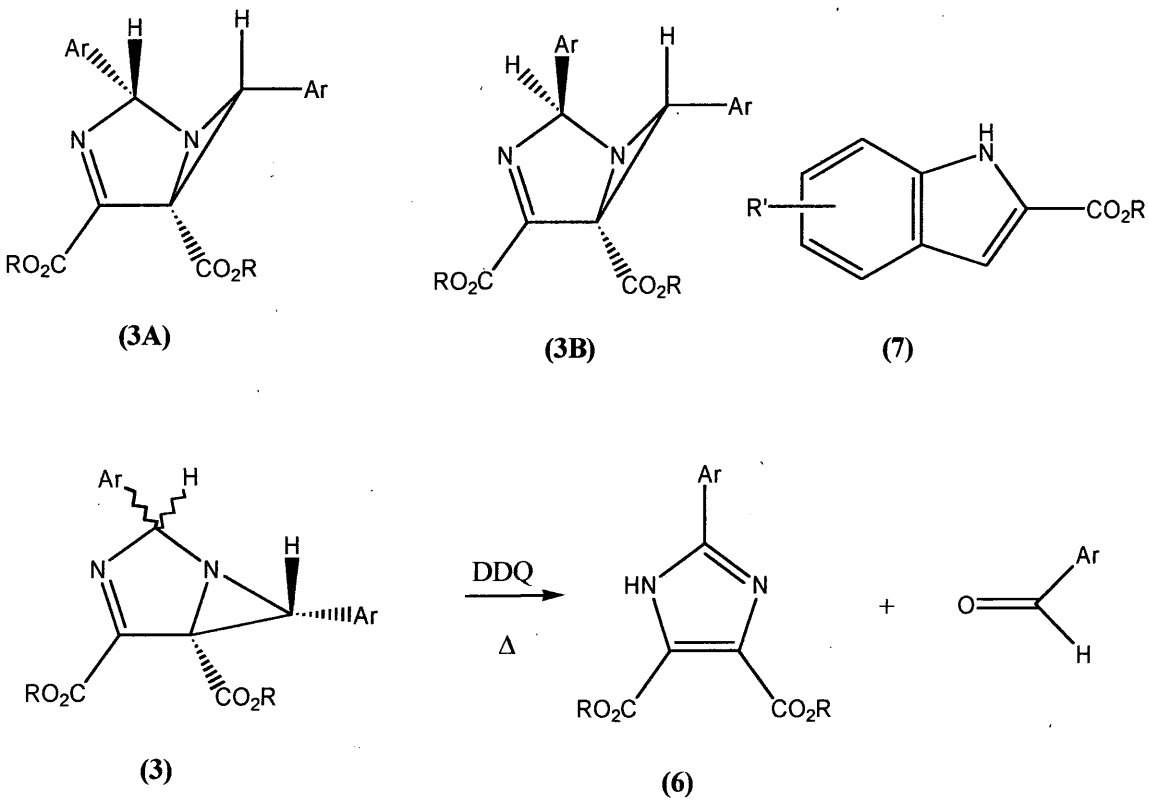

Figure 9.4 Scheme 3

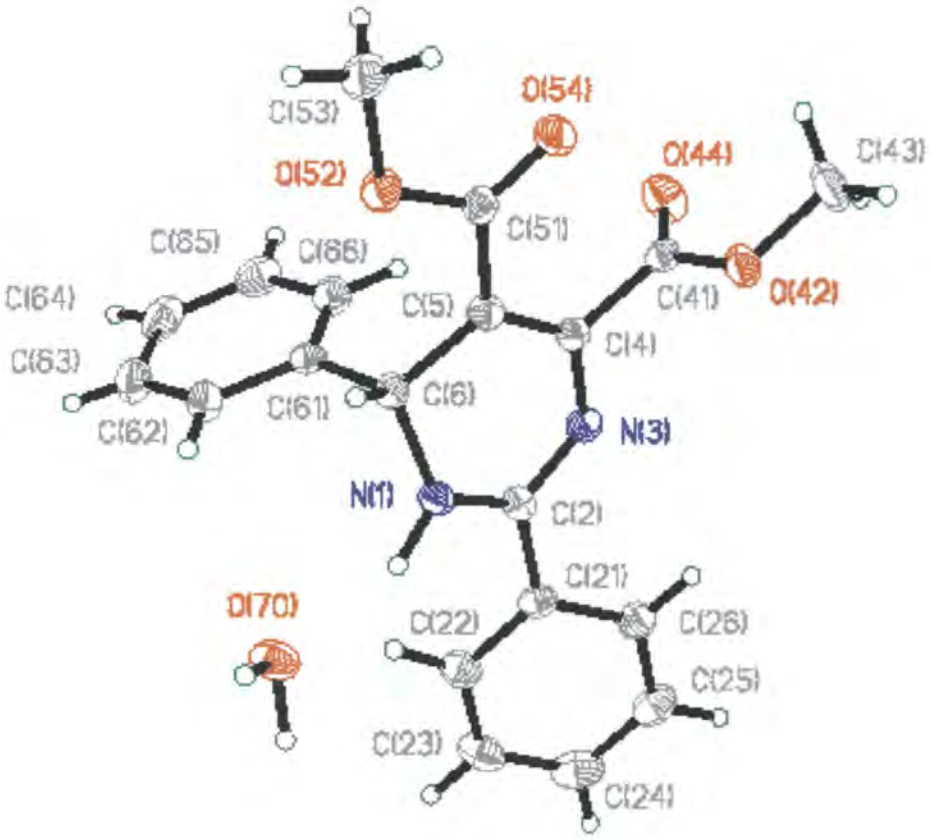

Figure 9.5 X-ray structure of compound (5), with thermal ellipsoid probability of 50%

In order to clarify further the mechanism of the photoreactions several experiments were conducted. Photolysis of various substituted α-azidocinnamates, **(1)**, proved instructive. Substituents in the phenyl ring which cause a bathochromic shift of the aryl UV absorption tend to allow the photolysis of the azide to be intercepted at the azirine stage. Thus the 3,4,5-trimethoxy derivative **(1f)** gave solely the postulated intermediary azirine **(2f)** (Table 9.1, entry 21). Furthermore the 2,6-dichloro-derivative **(1e)** could be taken through the whole process in a stepwise manner. Short photolysis in Pyrex gave the azirine **(2e)** while longer reaction time gave just one of the corresponding dimers **(3Be)**. Clearly, in cases where the aryl chromophore absorbs most of the irradiation, chemistry at the azirine centre slows or stops. As stated previously, when an ethyl or methyl azidocinnamate is photolysed in quartz equipment and monitored continually by NMR spectroscopy, firstly both dimers **(3)** are formed, to be slowly and totally replaced by the one trimer, **(4)**. When the mixture of dimers **(3A)** is further

photolysed using quartz equipment a slow conversion into the trimer **(4a)** is observed. The ratio of the two dimers and trimer [**3Aa:3Ba:4a**] after 1, 2, 3 and 4 hours changes from 34:41:19 to 30:30:30, 25:13:50 and finally to 20:0:60 (Table 9.1, entries 6-9). Again, only one stereomer of the trimer forms. Indeed, irradiation of either pure dimer gives no trimer, but slowly leads to decomposition of the dimer. Only a mixture of both dimers gives the trimer. A similar process is observed with the ethyl ester **(1b)**, which after 3 hours of irradiation is essentially completely converted to trimer **(4b)** in 87% yield (Table 9.1, entries 13-16). While both dimers will be in photoequilibrium with the parent azirine **(2)** it appears that one of the dimers ring-opens considerably more readily than the other, and that the other (or both) are a source of the azirine **(2)** (Scheme 4, see Figure 9.6). The stereochemistry of the resulting trimer indicates that the least congested dimer **(3A)** ring opens to give the new 1,3-dipole that is trapped by the regenerated azirine **(2)**.

The 2-methylphenyl-derivative **(1c)** gave solely the expected dimers **(3c)** with no sign of triplet nitrene attack of the methyl group which would give an isoquinoline, a reaction observed during the thermolysis of the same azide in the presence of iodine, a 'heavy-atom-triplet' forming system. This suggests that the acetone used as the solvent in our photolyses is acting more as a filter of short wavelength light than as a triplet sensistiser/radical mediator and that an ionic pathway is followed in the subsequent cycloaddition chemistry.

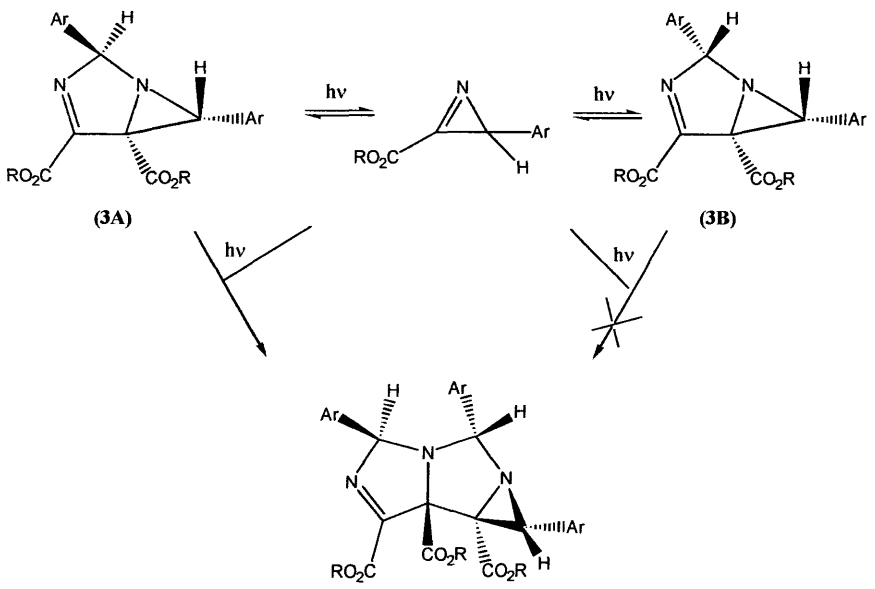

Figure 9.6 Scheme 4, the reaction of (3A) to (3B) and to (4)

In conclusion it is observed that a wavelength dependent photolysis of α-azidocinnamates **(1)** is independent of the solvent. All wavelengths transform the azides into the azirines **(2)** which form dimers **(3)** at any wavelength of irradiation. These dimers are in photo-equilibrium with the precursor azirines **(2)** and when low wavelength light is utilized the aziridine ring of the dimers **(3)** ring opens by C-C bond breakage. One isomer, probably **(3A)**, ring opens faster than the other and the resultant 1,3-dipole cyclo-adds to the azirine **(2)** uniquely to give one trimer **(4)**, see Figure 9.7. An alternative and less satisfactory explanation suggests that of the various alternatives, the trimer **(4)** is formed such as to minimize steric interactions. This scenario would suggest that some minor amounts of other isomers should have been detected.

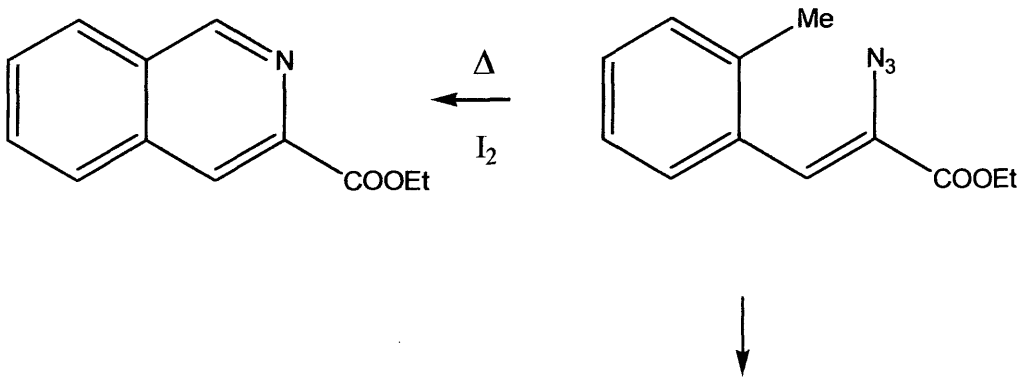

dimers of **(3)**, see Scheme 4, Figure 9.6

Figure 9.7 Scheme 5

9.3 EXPERIMENTAL

X-ray diffraction analysis was carried out on the SMART CCD diffractometer, see chapter 2. The solving and refinement of the structure was conducted using the SHELX programs as detailed in chapter 2.

The melting point were determined using a Reichert Kofler hot-stage apparatus. Infrared spectra were obtained on a Unicam Research Series 1 FTIR instrument as KBr discs or liquid films. NMR spectra were recorded in $CDCl_3$ as internal standard on a JEOL spectrometer. Chemical shifts are reported in ppm while the coupling constant J values are in Hz. Mass spectra were measured on a Kratos MS80RF mass spectrometer and microanalyses were carried out at Newcastle University. Thin layer chromatography (TLC) was performed with Merck silica $60F_{254}$ plates and Janssen silica (35-70 μm) was used for flash chromatography. Petrol refers to light petroleum of boiling point of 60-80 °C. Azidocinnamates were made according to literature methods (Hickey *et al.*, 1986). Photolyses were conducted under nitrogen using either the 'flathead' flask with water cooling or in a Rayonet apparatus as described by Rees and co-workers (Hickey *et al.*, 1986). In both cases TLC monitored the progress of the reaction.

9.4 GENERAL METHOD FOR THE PHOTOLYSES OF α-AZIDOCINNAMATES

The photolyses were performed under conditions of solvent, time, temperature and wavelength as shown in Table 9.1 and the solvent then removed on a rotary evaporator. The yellow oil remaining was examined by ^{1}H NMR spectroscopy and if necessary, purified by flash chromatography, to give the products.

Crystals of dimethyl 2-phenylimidazole-4,5-dicarboxylate **(6a)**, diethyl 2-phenylimidazole-4,5-dicarboxylate **(6b)**, diethyl 2-(4-chlorophenyl)imidazole-4,5-dicarboxylate **(6d)** were all obtained *via* solvent evaporation (Meth-Cohn, *et al.*, 1998).

9.4.1 The synthesis of dimethyl and diethyl 2-phenylimidazole-4,5-dicarboxylate (6a)

The literature method for the synthesis of 2-phenylimidazole-4,5-dicarboxylic acid from tartaric acid was followed (Anderson *et al*, 1989). A solution of this acid (0.5 g) in methanol or ethanol (20 cm^3) was treated with a few drops of sulphuric acid (98%) and heated under reflux for 4 hours. The bulk of the solvent was removed, water and dichloromethane added and the organic layer washed once with aqueous sodium bicarbonate and dried ($MgSO_4$). Evaporation gave the required ester which was recrystallised from aqueous ethanol, giving a product identical (m.p., mixed m.p. and infrared spectrum) to those described above.

	Compound 3Aa	Compound (5)
Formula	$C_{19}NO_2H_{11}$	$C_{19}NO_2H_{11}/H_2O$
Formula Weight	350.36	368.38
Crystal Colour	Colourless	Colourless
Crystal Description	Block	Block
Crystal Dimensions (mm)	0.3 x 0.3 x 0.25	0.4 x 0.4 x 0.3
Temperature (K)	150(2)	150(3)
Crystal System	Monoclinic	Monoclinic
Space group	*P*2(1)/*c*	*Cc*
a= (Å) b= (Å) c= (Å) α= (°) β= (°) γ= (°)	9.5450(19) 18.187(2) 10.449(4) 90.00 105.93(3) 90.00	13.892 (3) 17.649 (4) 8.2270 (16) 90 115.21(3) 90
Volume	1744.2(7)	1825.1(6)
Z	4	4
Calculated Density (Mg/m^3)	1.334	1.341
Absorption Coefficient (mm^{-1})	0.094	0.097
F (000)	736	776
θ Range for Collection (°)	2.22 to 28.32	1.99 to 25.36
Index Ranges	-12<=h<=12, -24<=k<=23, -13<=l<=13	-12<=h<=16, -21<=k<=21, -9<=l<=9
Reflections collected	13309	5564
Independent reflections	4323	2451
Data/restraints/ parameters	4323 / 0 / 243	2451 / 2 / 277
Goodness-of-fit on F^2	1.107	1.070
Final R_1 indices [I>2sigma(I)]	0.0712	0.0445
wR_2 indices (all data)	0.1902	0.1296
Extinction coefficient	0.0042(17)	0.0033(16)
Largest diff. Peak and hole. ($eÅ^{-3}$)	0.376 and -0.354	0.192 and -0.175

Table 9.2 Diffraction data for compounds (3A) and (5)

9.5 REFERENCES

1. Anderson, W. K.; Bhattacharjee, D.; Houston, D. M. *J. Med. Chem.*, **1989**, 32, 119.
2. Casey, M.; Moody, C. J.; Rees, C. W.; Young, R. J. *J. Chem. Soc. Perkin Trans. 1*, **1985**, 74.
3. Castle, R. N. *J. Heterocyclic Chem.*, **1964**, 1, 182.
4. Griffin, G. W.; Padwa, A, *Photochemistry of Heterocyclic Compounds*, editors O. Buchardt; Wiley, New York, **1976**, chapter 2, 41.
5. Hickey, D. M. B.; Moody, C. J.; Rees, C. W. *J. Chem. Soc. Perkin Trans. 1*, **1986**, 1119 and 1113.
6. Meth-Cohn, O.; Williams, N. J. R.; MacKinnon, A.; Howard, J. A. K., *Tetrahedron*, **1998**, 54, 9837
7. Padwa, A. *Acc. Chem. Res.*, **1976**, 9, 371.
8. Sheldrick, G. M., *Acta Crystallogr.*, **1990**, A46, 467.
9. Sheldrick, G. M., SHELXL-93, **1993**, Program for refinement of Crystal Structures, University of Göttingen, Germany.

CHAPTER 10:

THE TWISTING OF *ORTHO, ORTHO'*-BIPHENYL COMPOUNDS, AN ANALYSIS USING THE CSD

10.1 INTRODUCTION

Biphenyl was first synthesized in 1862 by Rudolph Fittig (Fittig, 1862). However, it was not until better analytical techniques were developed that the dihedral angle between the rings became measurable and since that time there has been considerable interest in the twist of the phenyl rings relative to each other. The dihedral angle and conformation of biphenyl derivatives and o-o'-substituted biphenyls, have attracted interest and caused confusion since several early X-ray diffraction studies were conducted in the solid state (Fowweather and Hargreaves, 1950 & Smare, 1948). Subsequently Otto Bastiansen carried out a series of studies into both the *ortho* and non *ortho*-substituted biphenyls in the gaseous phase (Bastiansen, 1950), where the rings were found to be twisted relative to each other. When the rings are free to rotate around the linking C-C bond then they will theoretically adopt the lowest energy conformation. Molecular mechanics (MM) calculations on these systems show that this energy minimum tends to be at 30-45° in the *trans* conformation (Shi *et al*,. 1998). The work carried out on biphenyl type structures has led to the discovery of what has been termed an "*ortho* effect" involving *o-o*'-biphenyls. However, the *ortho* effect has not been well defined and hence this phenomenon was considered to be worth investigating further.

When the only *ortho* substituents present are at the 2 and 2' positions (see Figure 10.1) there are three possible conformations that the *ortho* substituents on the rings can adopt relative to each other. When the torsion angle, τ, generatd by the twisting of the rings and between 2, 1, 1', 2' (See Figure 10.1) is from 0-90 ° then this is the *cis* (or *syn*) conformation and when τ is 90-180° then this is the *trans* (or anti) conformation.

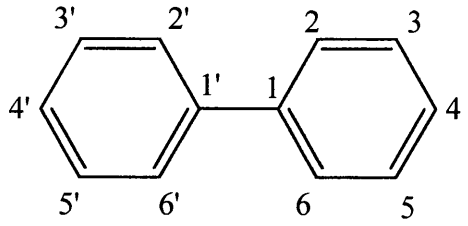

Figure 10.1 The positions of biphenyl, 1=*ipso*, 2=6=*ortho*, 3=5=*meta*, 4=*para*.

The τ angles 180-360 ° are a mirror of 0-180 °, reflected in 180 ° (180-270° *trans* and 270-360° *cis*). A third conformer where τ =90° is possible and although some structures have τ close to 90°, in practice exactly 90 ° never occurs, therefore the conformers can be categorized as either *cis/syn* or *trans/anti* (see Figure 10.2). Stereochemically speaking the *trans* conformer would be the more preferred, because the *o-o'* substituents will repel each other and this would be the driving force for this conformation. Bastiansen found that this was not the case and in the gas phase 2,2'-dichloro/dibromo/diiodo were in the *cis* conformation (Bastiansen, 1950). Subsequent studies in both the gas phase and the solid state, mainly using X-ray diffraction, have shown the generally preferred conformer is of the near *cis* type. The predominance of this conformation is a general trend for all *o,o*'-substituted biphenyls and occurs independently of substituent ((Brock and Minton, 1989), (Bastiansen, 1979) and (Roberts, 1985)). The magnitude of the dihedral angle of *o,o*'-substituted biphenyl is dependent largely on the size of the substituents attached at the *ortho* positions. In general if there is a bulky group at the *ortho* position then τ will be greater than when a smaller substituent is present. This is a simple steric factor: however it may prove to be more complicated if there are intra-molecular interactions between the *ortho* substituents or if there are packing forces preferring a smaller or larger τ in the solid state. Often the exact value of τ depends on the specific *ortho* substituent(s) and frequently the dihedral angle would seem to depend on a combination of these factors. This predominance of the *cis* conformation is not what would be expected initially. Since steric congestion would be thought to be a major factor the conformation would favour the *trans* conformer to minimize steric crowding. If there were a "*trans* effect" then the reason would simply be due to the steric congestion between the two *ortho* substituents. The fact that steric congestion appears to have little to no effect on the system is quite peculiar, and leads to conclusion that the "*ortho* effect" is indeed more influential to the system than the simple steric factors.

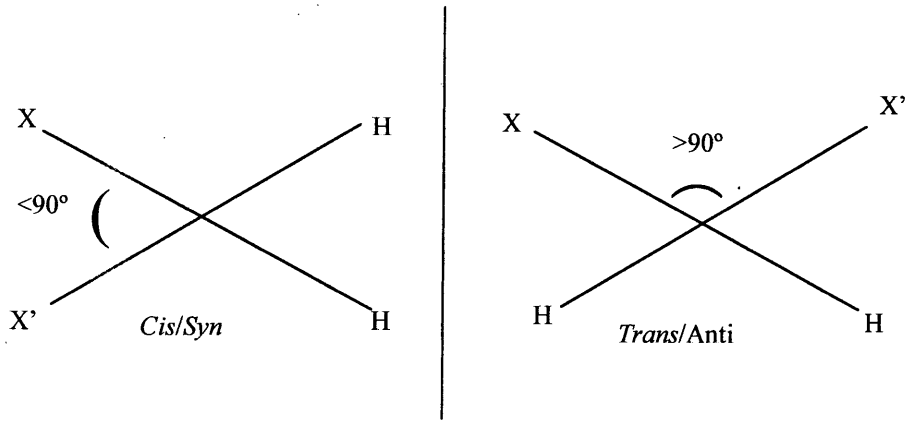

Figure 10.2 The *cis* and *trans* conformations of *o,o'*-substituted biphenyls, looking down the C-C bond linking the rings. X and H represent the substituted side and non-substituted sides respectively.

This *cis* conformational trend is not exclusive and indeed there are many structures that adopt a more nearly *trans* conformation, (e.g. 2,2',5,5'-tetrachlorobiphenyl (Chen *et al*,. 1996) and 2,2'-bis(acetamide)biphenyl (Reboul *et al*,. 1993). The trend appears to be independent of the type of *ortho* substituent present (Dyenes *et al*,. 1985). Evidence has been produced for there being an attraction between halogen atoms in halogen *o,o'*-substituted biphenyls in the gas phase ((Dyenes *et al*,. 1985) & (Bastiansen, 1985)). This factor may also play a part in the solid state but they must be part of a greater picture that includes all *o,o'*-substituted biphenyls preferring the *cis* conformer and not just *ortho* halogenated biphenyls.

An unusual degree of intra-molecular interaction may account for the conformational preference. However, this is unlikely since there is a wide range of *ortho* substituent types and this would not normally give a specifically high degree of preference for intra-molecular interaction even with specific groups that are prone to interaction. There is no reason that any specific compound would prefer intra-molecular interaction rather than inter- or *vice versa*. Although there are several factors that can influence and determine this, e.g. the bulk (if the group was large enough) of the substituted group at the *meta* as well as the *ortho* position. However, this would then influence the conformation towards the *trans* configuration. It is worth noting that the *para* active sites and interactions cannot have a steric effect on the dihedral angle since the *para* group faces

away from the rest of the structure. Unless there is interaction between it and *ortho* or *meta* substituents directly then the *para* substituent should not effect the dihedral angle. This conformational trend can be described and indeed from now on will be referred to as an "*ortho* effect". The reason for this effect has yet to be fully explained and to this end an extensive database search was carried out, using the Cambridge Structural Database (CSD). This is designed to investigate all *o,o*'-substituted-biphenyl compounds and to examine this "*ortho* effect" further, with a view to determining finally what factors are involved for this observed *cis* conformational preference, which substituents give the most pronounced "*ortho* effect" and hopefully to discover possible reasons and explanations into why this "*ortho* effect" occurs at all.

10.2 RESULTS AND DISCUSSION USING THE CSD

10.2.1 The *o,o'*-substituted biphenyls

Initially a search was conducted using the CSD on all *o-o'*-substituted-biphenyl compounds where the rings were unconnected to one another apart from the C-C linkage between them (see chapter 5). This set is designed to be separated into discrete subsets, and examined further. What was expected in this set was a possible tendency towards the *cis* conformer, because the intra-molecular interaction will be a factor that will be notable and of course it is known that there is an "*ortho* effect". Although alternatively there could be a general tendency for inter-molecular interaction and that this could demand a specific conformation, but is thought to be unlikely, given the knowledge that there is a *cis* conformational preference. Nonetheless, because of the large range of *ortho* substituents, it is not expected that the inter-/intra-molecular interactions factor will have a large impact on the result. Any observable anomalies in the overall picture are not expected to account for the whole "*ortho* effect", although any observable effect would be examined to determine its significance. The search gives resulting data with a τ range $-180°$ to $180°$ and for the *o-o'*-substituted biphenyls the region 0 to $-180°$ is equivalent to 0 to $180°$, so the root mean square (R.M.S) is taken so τ for all angles so that they are positive. The resultant data are shown in Figure 10.3. There are a total of 91 observations for the *o-o'*-substituted biphenyl search, all τ are measured once. Of the 91 observations 52 (57.1%) are nearer *cis*, τ = 0-90, with the remaining 39 (42.9 %) nearer *trans*, τ = 90-180°. For the range $0 \leq \tau \leq 90$, the mean value for τ is 69.0°, and for $90 \leq \tau \leq 180°$ the mean is 112.67°. For this initial search, there is a large sharp peak at approximately 70°, with 22 observations (24.5%) lying between 67-76°, the equivalent peak does not occur in the $90 \leq \tau \leq 180°$ range of data. This peak does not consist of any specific *o,o'*-substituents and this indicates that there is a preferred τ value for *cis o,o'*-substituted biphenyls. The result shows a distinct tendency towards the *cis* conformation, which is what has been expected from a previous knowledge of the "*ortho* effect". This tendency however is not overly prominent and although the percentages that are *cis* are significant they do not dominate the picture as would be expected by a very strong effect. This then led to the speculation that the overall trend was not a trend that affected all *o,o'*-substituted-biphenyl compounds, but that it was the result of the influence of several separate factors, that would appear as subsets within the overall set. Inspection of the overall set showed that steric congestion has little to no effect on the conformational preference on all but the most extreme cases. This is also not expected, because it was thought that steric factors would at least have a significant role

in the "*ortho* effect". To this end the overall set was separated into several separate subsets; these subsets are not independent of each other and some of them overlap. The subsets were separated and examined to show the nature of any other factors influencing the conformational twisting of the *o,o'*-substituted biphenyls. Initially the separate subsets were determined based on where the substitutions occurred upon the rings, see Figure 10.3.

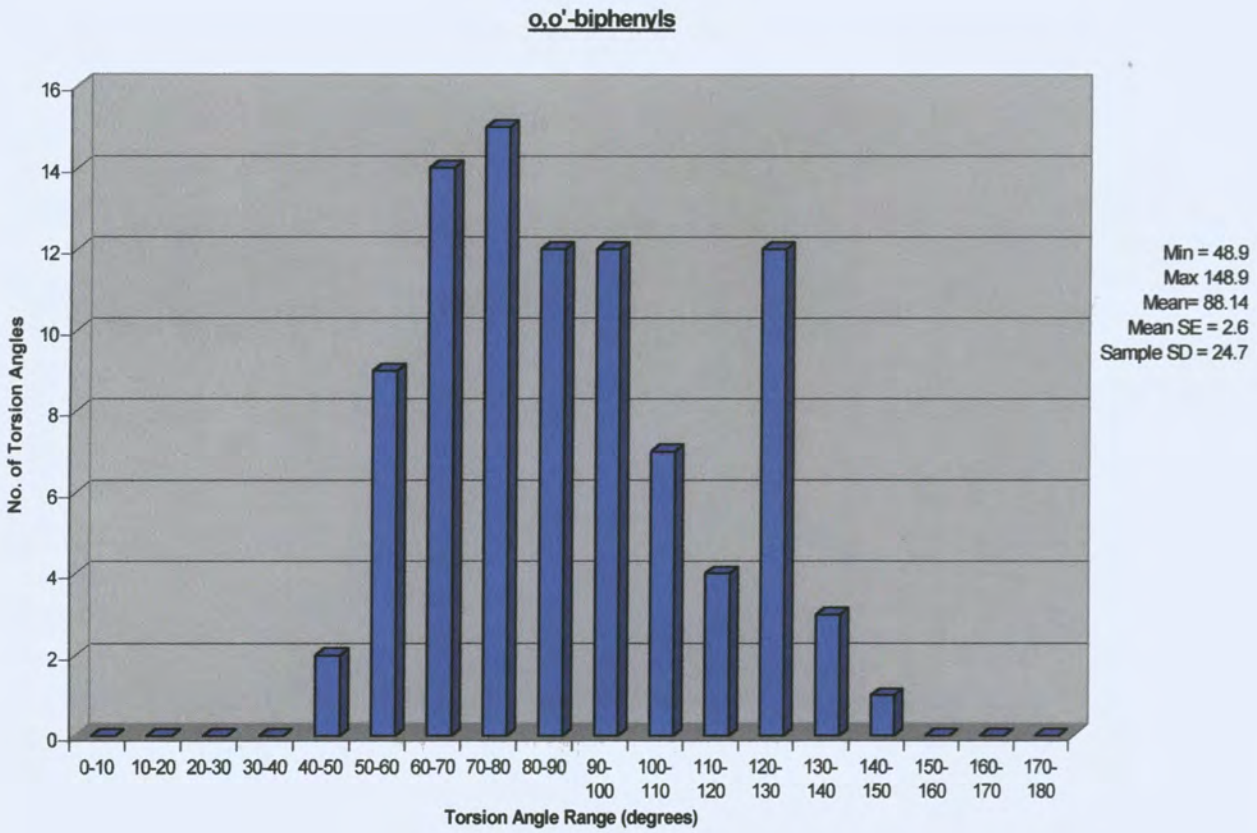

Figure 10.3 Dihedral angle distribution of all *o-o'*-biphenyls

10.2.2 Different Positional Substituents

10.2.2.a The effect of *ortho* substitution at 2 and 2' positions

In this subset there are 42 observations, of which 19 (45.0 %) are in the near *cis* region, and 23 (55.0 %) in the near *trans* (Figure 10.4). It is worth noting that in an initial analysis carried out with the previous version of the database (June 97 release), 29 observations were found, with a

ratio approximately 50:50. The trend here (with the April 1998 version) that more have been observed in the *trans* state, but the figures are inconclusive and if judged on the previous version of the CSD then the indication would be for no deviation away from a purely equal ratio. If a trend is present in the purely *ortho* set, it is not strong enough to show up conclusively and the observed trend in the newer version of the database can be put down to being a statistical anomaly. What can be seen here is that this set, however inconclusive, approximately mirrors the overall set of *o-o'*-substituted biphenyls. There is a strong peak at 68-70°, with 6 (20 %) observations, the nearest observation to this peak is at 59.8° and 76.9°, and this indicates a strong conformational preference for this specific region. The lack of any conformational preference in this set is unexpected because this now indicates that the "*ortho* effect" is independent of the *ortho* substituents and that these substituents have almost no bearing on the preferred conformation of either *cis* or *trans*. That *ortho* substituents have little bearing on the twisting is unexpected since it would be expected that the *ortho* substituents would have a great influence on the conformation of the rings relative to each other.

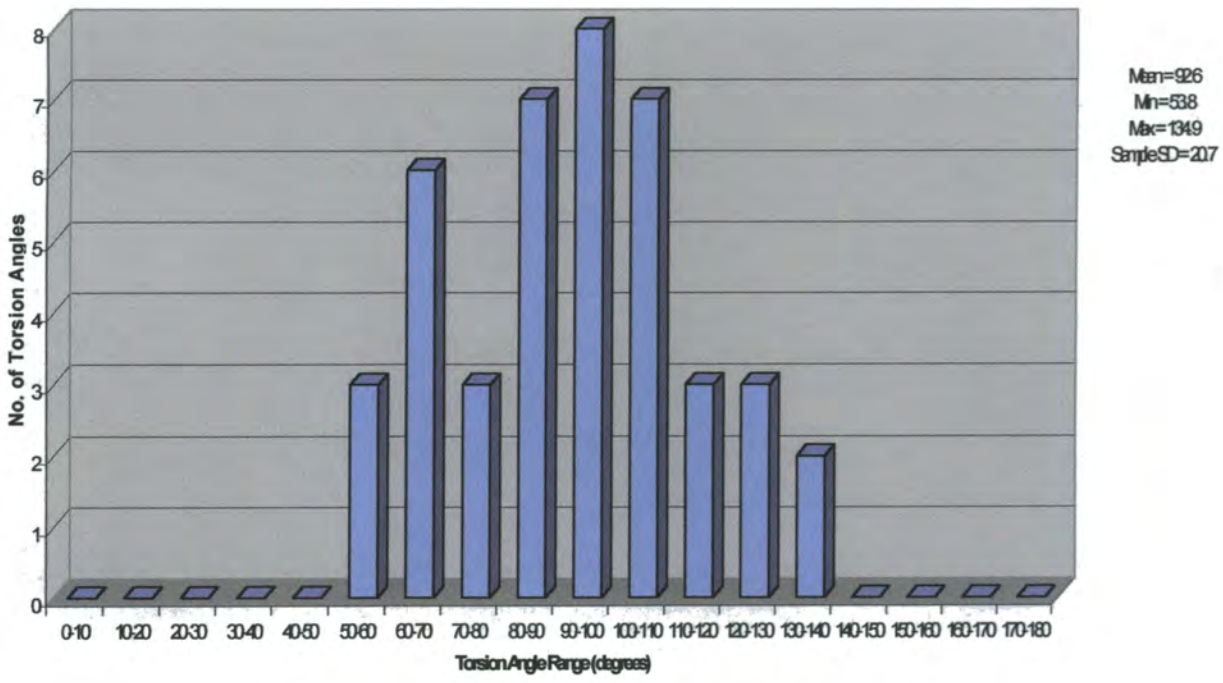

Figure 10.4 Biphenyls that contain *ortho* substituents only

10.2.2.b Purely *ortho/meta* set

This set consists of all *o-o'*-substituted biphenyls with 1 to 4 *meta* substituents present and hydrogen atoms at both *para* positions (Figure 10.5). To split the set into the individual subsets containing 1, 2, 3 and 4 reduces the data in each subset to sparse numbers and thus to an statistically unreliable extent. The alternative is to look at the larger set containing 1 to 4 *meta* substituents and attempt to make general deductions from this. This set is designed to examine the effect of *meta* substituents on the conformation. It can be reasoned that if the *ortho* substituents have no effect, then *meta* are the next most obvious candidate to examine. In this set there are only 12 observations and thus this set is statistically meaningless, but the results show a 50:50 ratio, which indicates that there is no distinct trend at least in this small number of data. The mean value for τ, 93.9°, is that which might be expected from initial ideas involving steric factors. The *meta* and *ortho* substituents have little to no effect on the system and this again is unexpected. It would be thought that given the lack of effect in the purely *ortho* set, that the *meta* would be influential even if this influence were small, due to possible stereochemical interaction.

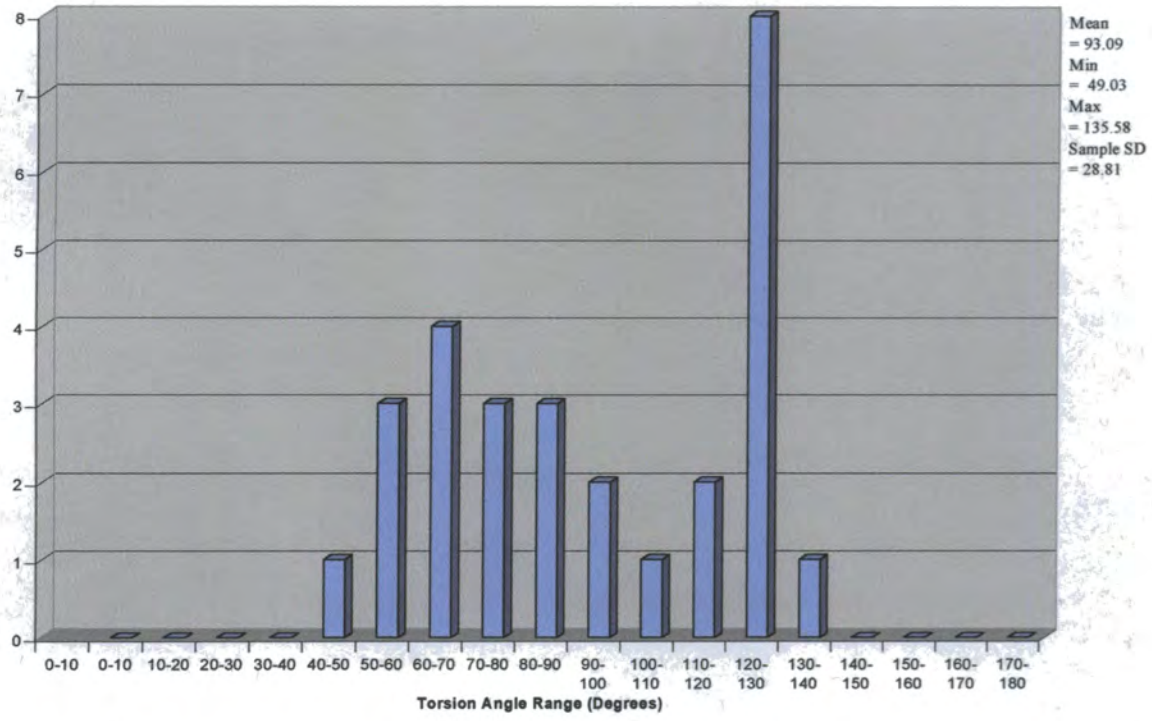

Figure 10.5 Biphenyls containing *ortho* and *meta* substituents

10.2.2.c The *o,o'*-biphenyls with *meta* and *para* substituents

This set consists of data comprising of at least one *meta* and one *para* substituent within the structure. This subset consists of only 21 observations, but shows a marked tendency towards the *cis* conformation, with a *cis:trans* ratio of 16:5 (76.2 %) (Figure 10.6).

This can be due to the effect of a series of one type of structures dominating the set, which can happen in the smaller sets. As it turns out, after examining the structures there is not a specific series of structures influencing this data set. The trend here is pronounced enough to indicate this is a true trend, strong enough to show up in the overall set and to account for a large proportion of the overall *cis* conformational preference. This leads to the conclusion that there is a conformational influence of *para* substituents for *o,o'*-substituted biphenyls. It is remarkable that the effect of the *para* substituents is observable, despite no distinction between separate *ortho* groups.

Para substitution has not been considered to be of very much influence in these systems in terms of the conformation, particularly the twisting conformation, due to the distance from the *ortho*

position and the C-C linkage bond. However, it is apparent that they do have an influence in the twisting of these systems. The substituents that are attached to the biphenyls at the *para* position are varied and there is not one specific type that shows up in this set and gives a conformational preference and indeed the substituents give a preference for the *cis* conformation, see Table 10.1.

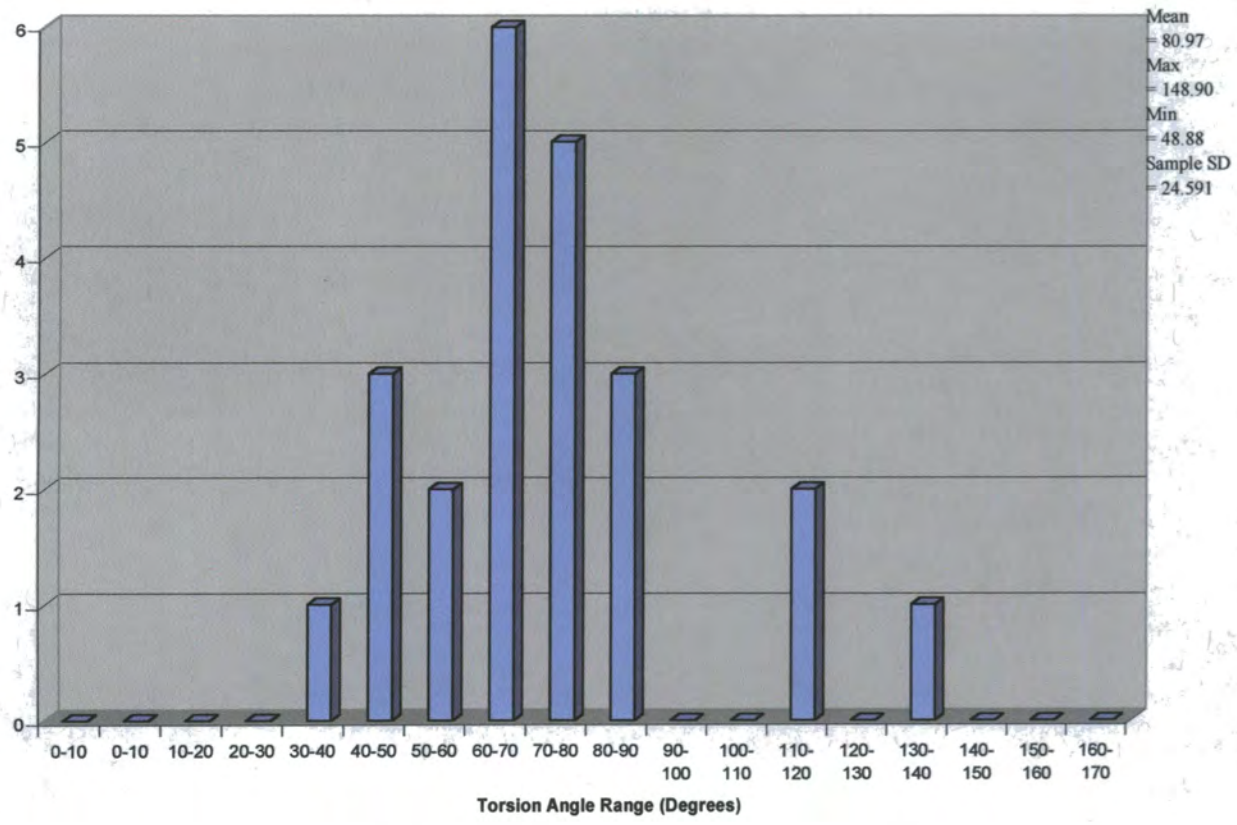

Figure 10.6 The dihedral angle range of *o,o'*-biphenyls with *meta* and *para* substituents

10.2.2.d The *o,o'*-biphenyls with *para* but no *meta* substituents

There are three structures that fit this criterion, not enough data for any real conclusions to be drawn. This is unfortunate since this data set would be extremely useful to examine and compare to the *para/meta* containing subset.

It would be expected, given the results found from the *para/meta* set that if there were more data in this group then it would show that there would be a large trend towards the *cis* conformer. What little data are present here have a strong preference towards the *cis* conformation (100%).

10.2.3 Different types of substituent on the *ortho* position

To examine the effect further the individual substituents and groups must be examined. Looking at both the *ortho* and *para* substituents enables this be done. The main problem with this set is the lack of structures with the required groups at the specific positions, which are needed to see any trend or effect that these structures exhibit. The effect will have to be very strong with a large percentage of the structures existing in these sets.

The next part of the overall set to examine is the individual substitutions, i.e., the structures with specific groups attached to the *ortho* positions of the biphenyls.

10.2.3.a Carbon at the *ortho* position

This set contains all structures with at least one carbon atom at the *ortho* position. There are 58 structures in this set (Figure 10.7). The conformation of the structures is 32 (55.2%) in the *cis* conformation. There is no apparent strong preference for the *cis* conformation.

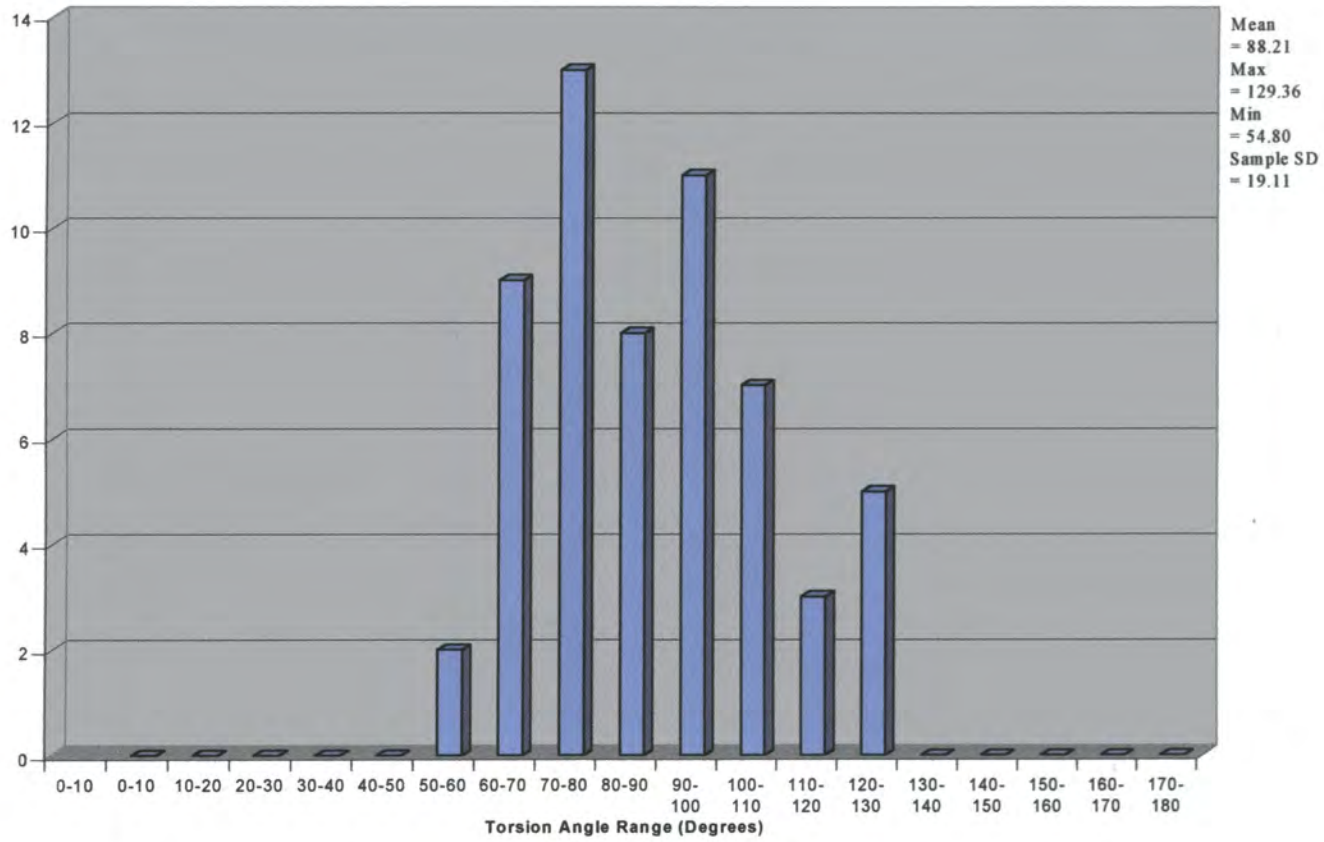

Figure 10.7 Carbon atom(s) at the *ortho* position(s) of *o,o'*-biphenyls

10.2.3.b COO substituent group at the *ortho* position

This set looks at COOR and COOH groups attached to the *ortho* position. Cases where there is a charge on the group, COO^- are also included in this examination. The -C=O are extremely likely to interact inter-/intra- molecularly with the correct orientation. In the case of -COOH there are many cases where the -C=O of one group forms hydrogen bonds with the -C-O-H group of another, a similar case is observed with 4-biphenylcarboxylic acid in chapter 5. There are a total of eight observations and of these five are the *cis* conformation. Again there is no clear preference for the *cis* conformation in this set.

10.2.3.c COR substituent group at the *ortho* position

In this set the -COR group is relatively unreactive and not be a source for intra-/inter- molecular interaction. However since the R group is not defined in the search criteria then atoms in the R groups may interact intra-/inter- molecularly.
Only 8 structures are present in this set and 7 are in the *trans* conformation. It is worth noting that none of these structures have *para* substituents.

10.2.3.d C=O substituent group at the *ortho* position

This set contains COR or COH groups at the *ortho* position, there is no distinction between these because in both cases the lone pair on the oxygen C=O should be available for interaction.
There are 11 observations, 5 of these are in the *cis* conformation. There is only one *para* substituted compound and in this case the conformation is *trans*, despite the strong possibilities of inter-/intra- molecular interaction, there is no apparent tendency for either.

10.2.3.e Oxygen at the *ortho* position

In this examination this set contains either –O-H or –O-R groups (Figure 10.8).
If there is an oxygen atom at the *ortho* position then what is seen is that out of a total of 23 observations, 16 (69.6%), are of the *cis* conformation. This is a large percentage and even though there is some overlap between this set and the *para* containing set (7 structures overlap, of which 5 are *cis* and 2 *trans*), the conformational preference for *cis* is independent of the presence of *para* substituents. These data show that with oxygen at the *ortho* positions there is a greater likelihood for the structure to adopt the *cis* conformation.

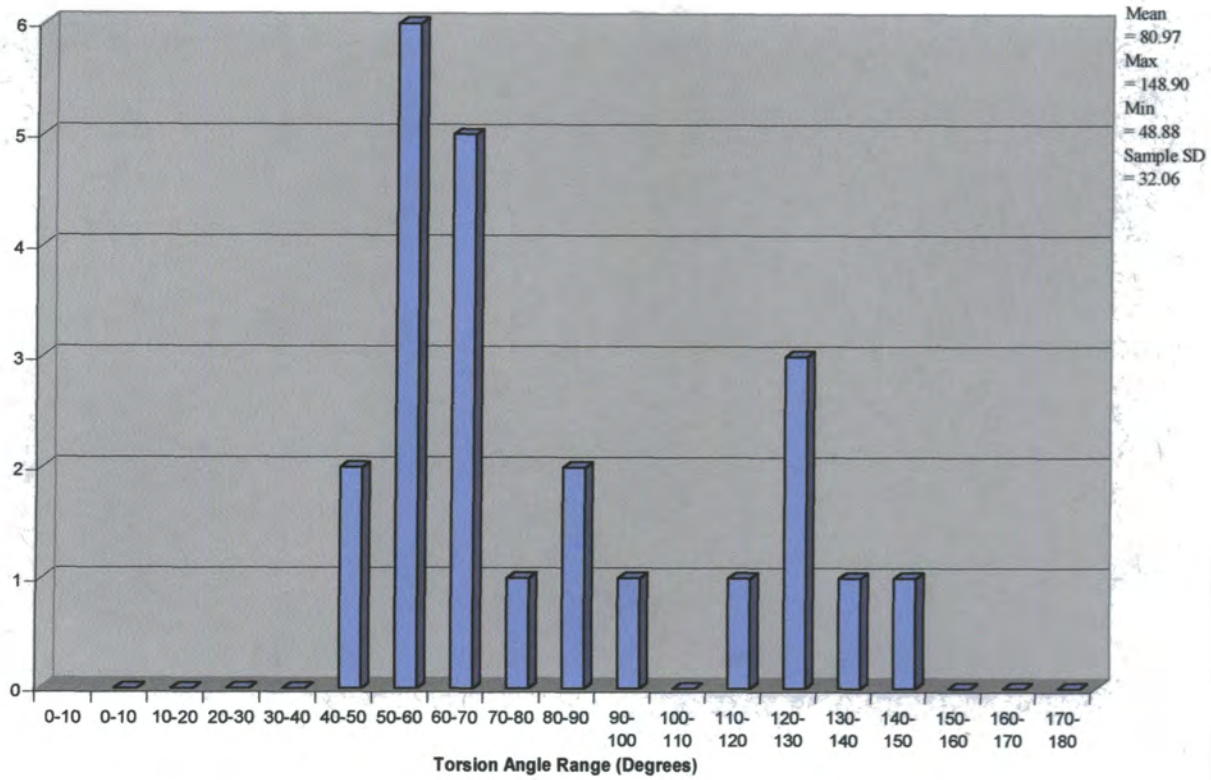

Figure 10.8 Oxygen atom(s) at the *ortho* position(s) of *o,o'*-substituted biphenyls

10.2.3.f O-H substituent group at the *ortho* position

In terms of hydrogen bonding O-H groups are susceptible to interaction, but would this make the *cis* conformer more preferable? The likelihood of the structure being intra-molecularly bonded depends on the other *ortho* substituent, but inter-molecular interaction is just as likely. The intra-molecular forms dominate and the *cis* conformer dominates, 10 of the 13 present are of the *cis* conformation. The ease by which these structures can intra-molecularly interact, when the two *ortho* positions have oxygen atoms, appears to be the reason for this. Only 3 of these structures have *para* substituents, 2 of which are *trans*. It would appear that when there are OH groups at the *ortho* position, then there is a distinct trend for the structures to adopt a *cis* configuration, and even when taking into consideration the *para* substituted structures, the two results (oxygen atoms at *ortho* and *para* groups present) are independent of each other.

10.2.3.g The X substituent group at the *ortho* position

Here the X group refers to any halogen atom and this examination is designed as a crude way to determine any effects halogen atoms have on *o,o'*-substituted biphenyls. In this set there are 9 hits, 6 *cis* (the structure with the CSD reference code RABREN (Jones *et al.*, 1996) accounts for 2 *cis* structures) and 3 *trans* (with the CSD reference codes DUXRAP and DUXRAP01 (Singh *et al.*, 1986) are essentially the same structure). If these are counted as one structure, then there are 7 structures, and 5 out of 7 are *cis*. Although the amount of data limits the accuracy, the result is similar to that which Bastiansen found. It is worth noting that of the four structures with chlorine at both *ortho* positions, only two are *cis*. The distances of the Cl···Cl for these structures is 3.33 to 3.50 which indicates probable Cl···Cl interactions (*c.f.* sum of vdw radii = 3.70 Å). Complications to this result are shown when considering the *para* substitution of these structures. Of the 7 structures, 5 have *para* groups attached and of these 5, 4 are in the *cis* conformation. This then is similar to the *para* substitution effect. It could be argued that it is the presence of *para* substituents that effect the conformation, rather than the halogen atoms. To see how the halogen atoms are affecting the group in detail, it is best to look at the halogen-halogen atom distances.

10.3 SUMMARY

There are several very interesting conclusions that can be drawn from the data available. There is indeed an overall tendency for the *o-o'*-biphenyls-type compounds to adopt the *cis* conformer rather than the *trans*, but further investigation reveals that the overall picture is clouded and influenced by separate subsets present in the overall set of all *o,o'*-biphenyls. Looking at *o-o'*-biphenyls with no *para* substituents it is found that there is in fact no discernable preference for either *cis* or *trans*. This includes *ortho* substituents alone and *ortho* with *meta* substituted and the likelihood of producing either conformer with no *para* substitution present in the solid state, will depend on that specific structure itself, the *ortho* substituent present and the inter-/intra-molecular interactions of these substituents. When *para* substituents are present however, there is a definite tendency towards the *cis* conformation, although with the available data, it is not conclusive as to whether the *para* substitution without any *meta* substitution present will also have this tendency. This does seem extremely likely, since *meta* on its own does not produce a specific conformational preference and the set with *para* substituents present, regardless of whether *meta* substituents are present or not, although limited in terms of different data, supports the trend. When describing this trend it is worth noting the structure of Secalonic acid (with the CSD code SECALA (Howard *et al.*, 1976)). This structure has both *meta* and *para* substituents and also has oxygen atoms at the *ortho* position, but this is not *cis* and further has an extremely large dihedral angle in the *trans* formation. When trying to find trends, including those in later chapters (chapters 11 and 12), this structure does not follow any of these trends. There is a large degree of hydrogen bonding, which accounts for the unusual stereochemical properties it has (Howard *et al.*, 1976).

When all the different positions are substituted on each ring there is a greater tendency towards the *cis*, and if Secalonic acid A is suppressed, which seems reasonable given its unusual twisting, then there are 100% *cis*. However, the lack of data on the exact tendency towards the *cis* conformer for these smaller subsets remain inconclusive.

It was thought possible that the effect of adding *para* substituents to biphenyl systems might lead to a change in the physical characteristics of the C-C bond between the rings, i.e. conjugation and bond length and the best way to investigate this is to look at the bond length, and to see whether it changes as a result of *para* substitution or twisting. The result showed that *para* substitution had no effect on the conjugation of the C-C bond (see chapter 13 for more detail). Whether the *para* substituent affects the *ortho* substituent and if this in turn determines whether the system becomes

near *cis* or *trans* is difficult to determine since the amount of *ortho* and *para* substituted biphenyls without *meta* substituents remains small.

One plausible explanation why the *cis* conformation is preferred with *para* substitution is that the *para* substituent itself will be likely to be involved in inter-molecular interactions and therefore creating long H-bonded chains. The intra-molecular interaction process necessitates the substituents being close enough to interact and this needs the conformation of the biphenyl to be nearer the *cis* conformation.

Bastiansen (Bastiansen, 1979) has indicated that there is a preference for the *cis* conformation in halogen *ortho* substituted biphenyls. His finding showed that in the gas phase, this is definitely true. In the search carried out on all *o,o*'-biphenyls in the CSD, there were only seven hits found for halo *ortho* substituted *o,o*'-biphenyls. Analysis does indeed indicate a possible preference for the *cis* conformation, but out of the seven, five have *para* substituents. Although this small selection of data cannot show much detail, it is interesting that they do follow the general trend found so far for the *para* substituted biphenyls.

Another structure that is purely an *o-o*'-halo substituted biphenyl (CSD with the reference code DCLBIP, (Rømming *et al.*, 1974)) is of the near *cis* conformation. In looking at the data for the solid state rather than the gas phase, as studied by Bastiansen, we find no specific evidence to support halogen-halogen interaction in the solid state. In 2,2'-dichlorobiphenyl (DCLBIP) the Cl···Cl distance is 3.418 Å, which is short and well within the vdw radii (3.70 Å) but the Cl···H inter-molecular distances are 2.879 and 2.952 Å, which are also well within the vdw radii (3.05Å), see Figure 10.9.

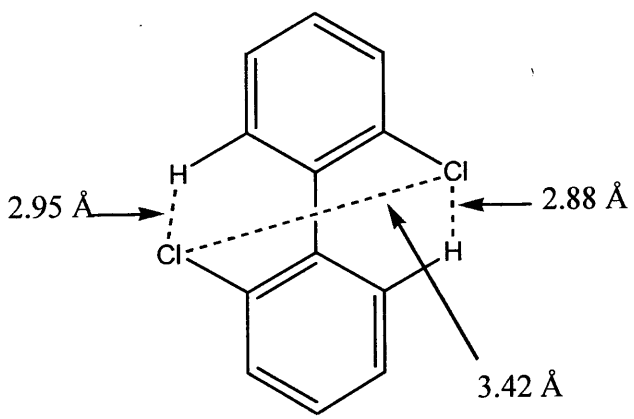

Figure 10.9 Representation of *intra*-molecular distances in 2, 2'-dichlorobiphenyl

This suggests that there is an *intra*-molecular interaction between chlorine atoms and this is governing the twisting of the structure (Rømming *et al.*, 1974), see Figure 10.9. This structure was the only one found in the CSD that has chlorine atoms at the 2 and 2' positions and has both Cl···Cl and Cl···H intra-molecular interactions possible. The packing of the *cis* conformation is favourable here, because the molecules can fit more neatly together. The main factors that govern these types of halogen-halogen distances are, possible halogen-halogen attractive forces, halogen-hydrogen hydrogen bonding and packing forces. In this study there is a lack of data to fully investigate this halogen attraction and so more is needed to investigate further, especially the Cl···Cl attraction forces, in the solid state.

To complicate the overall picture further, the presence of oxygen atoms at the *ortho* position also has a strong conformational effect, due to intra-molecular interaction. This effect is independent of the *para* substitutional effect and indeed when both oxygen *ortho* and *para* substituents are present there is no specific tendency towards *cis*. The presence of a conformational effect with oxygen atoms is not wholly unexpected, although interesting, but it is the *para* substitutional conformational effect that is of most interest. No specific *para* atom substitution is responsible (as no *ortho* atom substitution is either) when examining the interactions involved, so the reason must be more subtle. A fuller investigation into the effect of *para*, *ortho*, and *meta* substitutions is given in chapter 12. Tables 10.1 and 10.2 give a summary of subsets detailed in this chapter.

Section	Number	*ortho*	*meta*	*para*	Conformation (%age)
10.2.1	91	Yes	In Some	In Some	*Cis* (58.2)
10.2.2(a)	39	Yes	No	No	*Trans* (55.0)
10.2.2(b)	26	Yes	Yes	No	*Trans* (59.1)
10.2.2(c)	22	Yes	Yes	Yes	*Cis* (71.4)
10.2.2(d)	3	Yes	No	Yes	*Cis* (100)

Table 10.1 Summary of Biphenyl conformations with positional variation of substituents

Section	Substituent	Conformation	*Cis*:*Trans* ratio
10.2.3(a)	C	*Cis*	32:26
10.2.3(b)	COO	*Cis*	5:3
10.2.3(c)	COR	*Trans*	7:1
10.2.3(d)	C=O	*Trans*	5:6
10.2.3(e)	O	*Cis*	16:7
10.2.3(f)	O-H	*Cis*	10:3
10.2.3(g)	Halogen	*Cis*	5:2

Table 10.2 Summary of Biphenyl conformations with substitutional variation

10.4 REFERENCES

1. Bastiansen, O. *Acta Chem. Scand.* **1950**, *4*, 926.
2. Bastiansen, O.; Kveseth, K.; Møllendal, H. *Topics in Current Chemistry.* **1979**, 101.
3. Bastiansen, O.; Samdal, S. *J. Mol. Structure*, **1985**, 128, 115.
4. Brock, C. P.; Minton, R. P. *J. Am. Chem. Soc.* **1989**, *111*, 4586-4593.
5. Chen, X-M.; Luo, G-B.; Tong, M-L.; Zhou, Z-Y., *Acta Cryst.*, **1996**, C52, 1727.
6. Dynes, J. J.; Baudais, F. L.; Boyd, R. K. *Can. J. Chem.* **1985**, 63, 1292.
7. Fowweather, F.; Hargreaves, A.; *Acta Cryst.*, **1950**, 3, 81.
8. Fittig, R *Justus Liebigs Annalen Chemie*, **1862**, *121*, 361.
9. Howard, C. C.; Johnstone, R. A. W.; King, T. J.; Lessinger, L. *J. Chem. Soc, Perkin Trans 1*, **1976**, 1820.
10. Jones, G. P.; Heirtzler, F. P.; Hopf, H. *Z. Krystallogr.*, **1996**, 211, 213
11. Merritt, L. L. Jr.; Schroeder, E. D. *Acta Cryst.*, **1956**, 9, 801.
12. Reboul, J. P.; Pèpe. G.; Siri, D.; Oddon, Y.; Caranoni, C.; Rahal, H.; Soyfer. J. C.; Barbe, J. *Acta Cryst*, **1993**, C49, 735.
13. Roberts, R. M. G. *Magn. Res. Chem.*, **1985**, 23 52.
14. Rømming, C.; Seip, H. M.; Aanesen Øymo, I. M., *Acta Chem. Scand.* **1974**, *A28*, 507.
15. Shi, Y.; MacKinnon, A.; Howard, J. A. K.; Wan, P. *J. Photochemistry and Photobiology A:Chemistry*, **1998**, 113, 271.
16. Singh, P.; Pedersen, L. G.; M^{c}Kinney, J. D. *Acta Cryst*, **1986**, C42, 1172.
17. Smare, D. L. *Acta Cryst.*, **1948**, 1, 150.

CHAPTER 11:

THE TWISTING OF BIPHENYL COMPOUNDS WITH HYDROGEN ATOMS AT THE *ORTHO* POSITION

11.1 INTRODUCTION.

This section is primarily based on work that was done previously by Brock and Minton (Brock & Minton, 1989). In this paper the authors tried to fit the energy distribution curve of the dihedral twisting angle of solid state biphenyl compounds with hydrogen at all four *ortho* positions to a Boltzman distribution. This was done by analysing structures in the CSD, and plotting the torsion angle against the number of angles found. This was in an attempt to see if this distribution of data could be explained by the structure correlation method, which predicts the distribution of data should be given by the expression exp(-E/RT).

11.2 THE STRUCTURE CORRELATION METHOD

The structure correlation method has been a useful tool in terms of a prediction of a structure's energy distribution and the details of the method have been described in numerous places, but none so completely as in the two volumes edited by H. D. Burgi and J. D. Dunitz called "Structure Correlation" (Burgi & Dunitz, 1994). For this study it is not necessary to dwell on the fine detail of the method or to have an in-depth knowledge of all it entails, but rather just have an idea of how this method then pertains to the *ortho* unsubstituted biphenyls systems examined here. The structure correlation method is well described and summed up, although briefly, in the following short passage by J. D. Dunitz in his notes to the 27th course of the International School of Crystallography in Erice, Sicily, 1998. (Howard, Allen and Shields, 1999, In Press).

"*With the establishment of "standard" bond lengths and angles functional groups used to be characterized as having a more or less fixed structure. Gradually, it was recognized that this is not the case. For many groupings, structural changes occur in different crystals and molecular environments, and, moreover, the changes in individual structural parameters are often correlated in ways characteristic of the grouping itself. The connection with chemistry comes with the assumption that observed structures tend to concentrate in low lying regions of the potential energy surface, leading to what has been called the Principle of Structure Correlation:*
If a correlation is found between two or more independent parameters describing the structure of a given fragment in a variety of environments, then the correlation function maps a minimum energy path in the corresponding parameter space.
This approach thus provides a link between the "statics" of crystals and the "dynamics" of reacting chemical systems and has been applied to map reaction paths for several types of prototypical chemical reactions."

So how does the structure correlation method relate to the work conducted in this thesis? If a particular chemical substructure is specified as a query fragment to the CSDS then what it will retrieve depends largely on the type of fragment being investigated, but the number can amount to thousands of fragments and dozens of environments. Each fragment found represents a static three-dimensional snapshot of the fragment, all of which are under slightly different conditions. If there are n geometrical parameters to describe i examples, then a geometrical matrix G(i, n) is obtained; this matrix can then be examined for regularities, and for correlations involving some or all of the geometrical parameters, or between geometrical parameters and other chemical, physical and/or biological properties. This is the basic

fundamental principle of the structure correlation method. This method lends itself to the analysis of the twisting conformations of biphenyls.

11.3 NON *ORTHO* SUBSTITUTED BIPHENYLS AND THE STRUCTURE CORRELATION METHOD

The structure correlation method can be used in the case of non *ortho* substituted biphenyls, that is biphenyl compounds that have hydrogen atoms on all 4 *ortho* positions, see Figure 11.1, to study the energy of the twisting of the biphenyl rings about the single C-C bond. In this case this utilizes the Cambridge Structural Database to obtain data on these conformational twisting of all the non-*ortho* substituted biphenyls present in the CSD. In essence the structure correlation method relies upon the system in question following a path of the lowest energy. In the case of biphenyls with hydrogen atoms at the *ortho* positions, the theory would suggest that the twisting of the two rings relative to each other about the adjoining C-C bond would follow a Boltzman distribution from 0-90° with a maximum believed to be approximately 35° (Eaton & Steele, 1973), although the distribution is likely to be slightly distorted due the various temperatures that are sampled, for structures existing in the CSD. In comparison the gas phase maximum is shown to have an average torsional angle of 45° (Alminningen *et al.*, 1989) and the solid state phase of biphenyl, having a twist of less than 1° ((Charbonneau & Delugeard, 1976 & 1977) and Chapter 5). There are known to be differences between the solid state and gas and liquid phases of these compounds and biphenyl itself has been noted to have conformational differences between the gas and liquid compared to the solid phases. This leads to the speculation that biphenyl compounds may favour the planar conformations in the solid state and that the theoretical values based on gas and liquid phase information, which includes all the calculated predictions of biphenyls, can prove not to be transferable to the solid state. This is surprising but is an indication as to the different forces involved in the slid state.

What is seen in the case of non *ortho* substituted biphenyls is these systems do not fit in with the structure correlation method (Brock & Minton, 1989) and this has been used as a demonstration that the structure correlation method, although extremely useful, does have limits on its use. The study, by Brock and Minton, was conducted using a database analysis with the CSD. It was shown that the distribution of energy for these biphenyls is not a Boltzman distribution but a multi peaked distribution, with 2 or possibly 3 minima in energy from 0 to 90° of torsional motion. The main energy minima exists at;

1) approximately 30-40°, which is where the greatest number of structures are located
2) between 0-5°, the sharpest peak,
3) a third possible minimum is located at 15-20°.

Brock and Minton's study of this phenomenon came to three possible conclusions that could be derived from these findings. The explanation favoured most by the authors was that "the

solid state systematically favours nearly planar biphenyl fragments because they pack better", but it was also suggested "substitution in the *meta* or *para* positions have a much greater effect than expected on the preferred conformation". Since it has been shown that the *para* and *meta* substitution can be of influence in the *o,o'*-substituted biphenyl conformations (Chapter 10), it was considered worth investigating the effect that the *para* substitution, and indeed possibly *meta* substitution had on this similar type system. To this end, the original work was repeated with the latest available version of the CSD (April 1998). This was examined further with a view to discover any influence the *para* and *meta* substitution has on this type of system. Since the CSD has more than doubled since the previous work was carried out then any substitutional effects should be much clearer than in the original study and therefore they should be more prominent and easier to decipher.

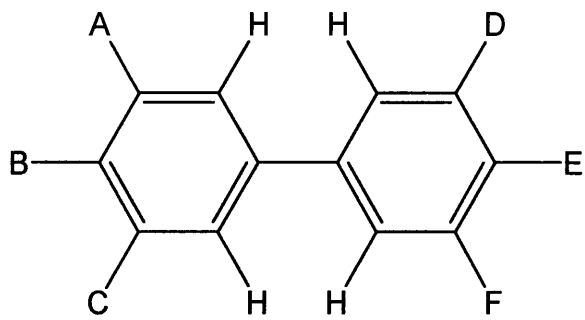

Figure 11.1. The non-*ortho* substituted biphenyl, A, B, C, D, E and F are any atoms (including hydrogen).

11.4 DATABASE STUDY OF NON-*ORTHO* SUBSTITUTED BIPHENYLS

While the original study produced a total of 101 torsion angles, there are now 268 observed torsion angles in the April 1998 version of the CSD. These angles being referred to are the same as defined in chapter 10 (i.e. the dihedral angle between the rings).

The overall histogram using this version, see Figure 11.2 is similar to the initial histogram by Brock and Minton, the difference being mainly the lack of the third independent peak that was seen between 15-20°. Here the main peak is a lot broader and starts at approximately 20°, therefore the peak observed previously has now been absorbed into the main broad peak at 20-45°, which resembles the Boltzman distribution, as would be expected if the structure correlation method were used to predict the outcome and the second peak which is much narrower and exists principally between 0-8°. The sharp peak is the highest with over 50 hits at between 0-5°, although this is the highest peak, when the data are segmented into sections of reasonable definition, two thirds of the torsion angles are situated in the larger, broader range (20-45°).

In an attempt to see what effect the substitutions at the separate positions have on the rings, the overall set of torsion angles was split into separate subsets. However, some of these subsets overlap, so are not entirely independent of each other.

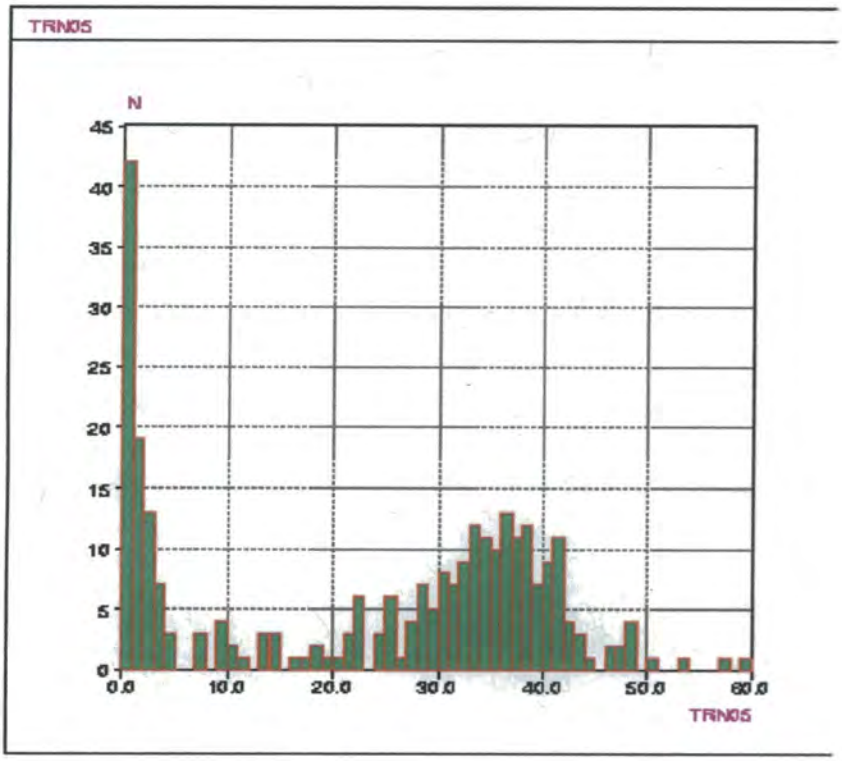

Figure 11.2 All non-*ortho* substituted biphenyls.
Mean = 23.52 and Sample SD = 18.68

11.4.1 *Para* Substituted Biphenyls

This set contains all non-*ortho* substituted biphenyls with one or both *para* positions substituted by any non-hydrogen atom. There are a total of 245 observed dihedral angles. In this case the effect of the *meta* substituents is not taken into account.

The *para* containing set is very similar to the overall set. The sharp peak at 0-5° is pronounced, containing 65 observed torsion angles. The peak at 20-45° contains a comparatively large percentage of data, with 144 observations, see Figure 11.2. This shows that the group containing *para* substituents has a greater tendency towards the ring co-planar structure. This could be that when *para* groups are present the likelihood of adopting an arrangement that these structures pack better. This is in keeping with the original studies of these types of structures (Brock & Minton, 1989), which thought that the herringbone pattern in biphenyls may be a strong factor for the conformational anomalies.

This *para* containing set can be split further into those biphenyls that have one or two *para* substituents and then these can be divided further into one and two *para* substituents with either *meta* or no *meta* substituents.

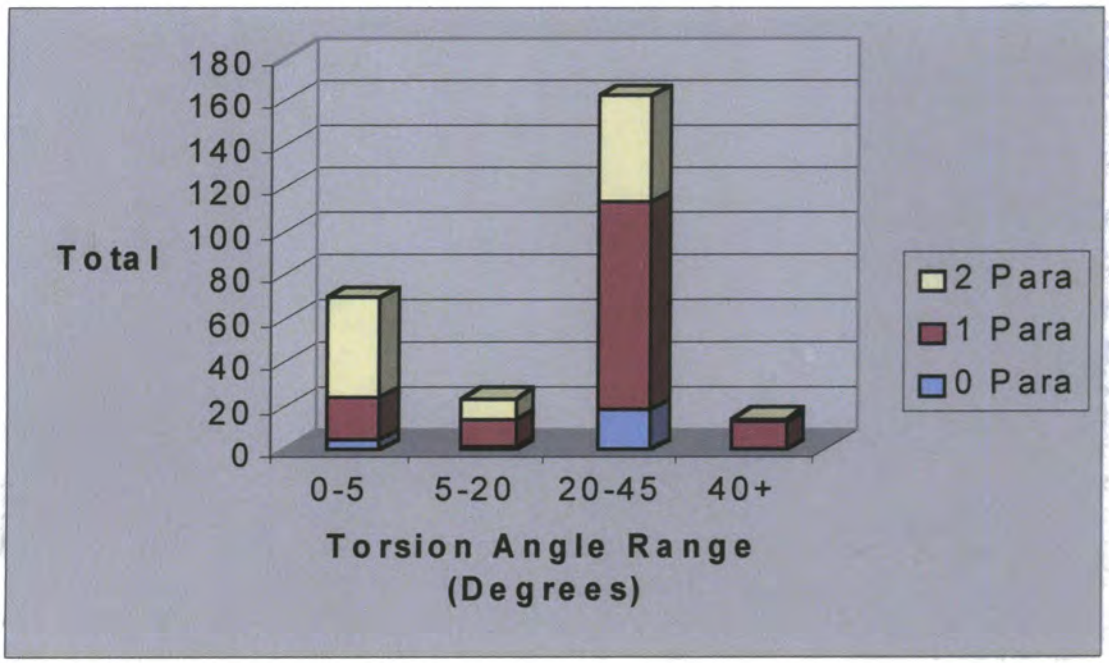

Figure 11.3 The distribution of torsion angles for 0, 1 and 2 *para* substituted biphenyls

11.4.1.a Biphenyls with two *para* substituents.

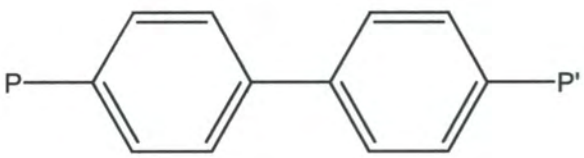

Figure 11.4 Bi-*Para* substituted Biphenyl, where P may equal P'

In this case the *para* containing group is split further into the biphenyls that have both *para* positions substituted, see Figure 11.4. The specific substituents on the *para* positions are varied, and no discernable pattern, regarding substitution type, was observed in the overall data. There are 106 observed dihedral angles, in the range 0-5°, giving a much more pronounced peak containing 45 structures and consequently the 20-45° peak becomes much less evident, see Figure 11.5, although this latter peak still exists and accounts for a large proportion of the torsion angles encountered. If trying to predict the conformation of a biphenyl with no *ortho* but two *para* substituents and based on the data in this chapter, then the conclusion would be an equal chance of either near 0° or twisted to 20-45°. Consequently,

if all that was known was that no *para* group was attached, the likely conformation should be 20-45°. The data from this set do fit approximately with the structure correlation method and are much closer to the predicted values than has been seen for structures that contain *para* substituents.

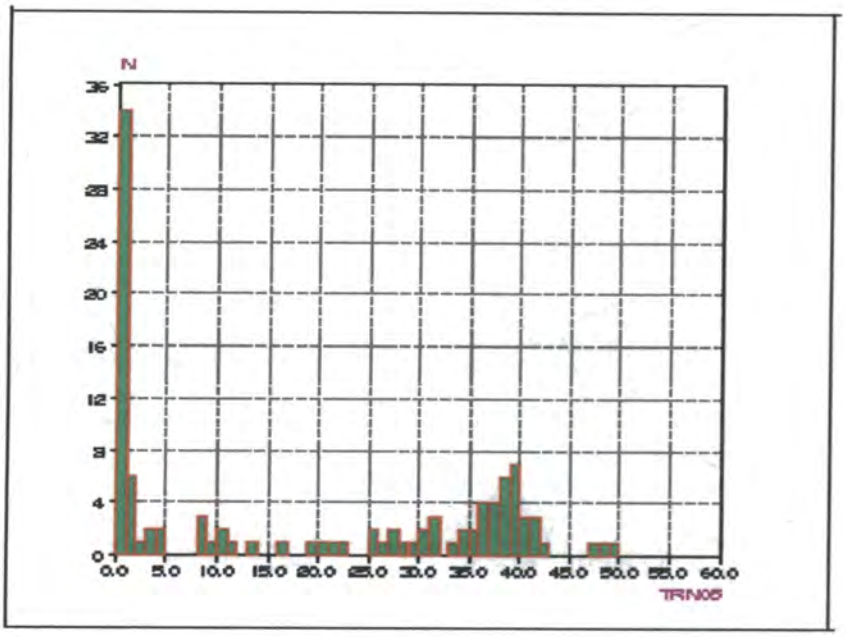

Total = 106, Range = 49.39
Mean = 18.56, Mean SE = 1.70, Sample SD = 17.50, Median =15.04

Figure 11.5 Biphenyls containing two *para* substituents.

11.4.1.a(i) Biphenyls with two *para* and no *meta* substituents

There are a total of 91 observed dihedral angles for this set. The distribution of the torsion angles is slightly higher in the 0-5° range than in the set with two *para* (with no distinction of *meta* substitution). There are 41 (45.1%) of the torsion angles existing in the 0 to 5°, and 45° (49.5%) in the 0-10° region, however there are slightly more in the 20-50° region. The torsion angles that lie outside the 0-5° region are extremely broadly distributed with no discernible peak in the distribution other than 28 (28.3%) structures in the 35-43° region, see Figure 11.6.

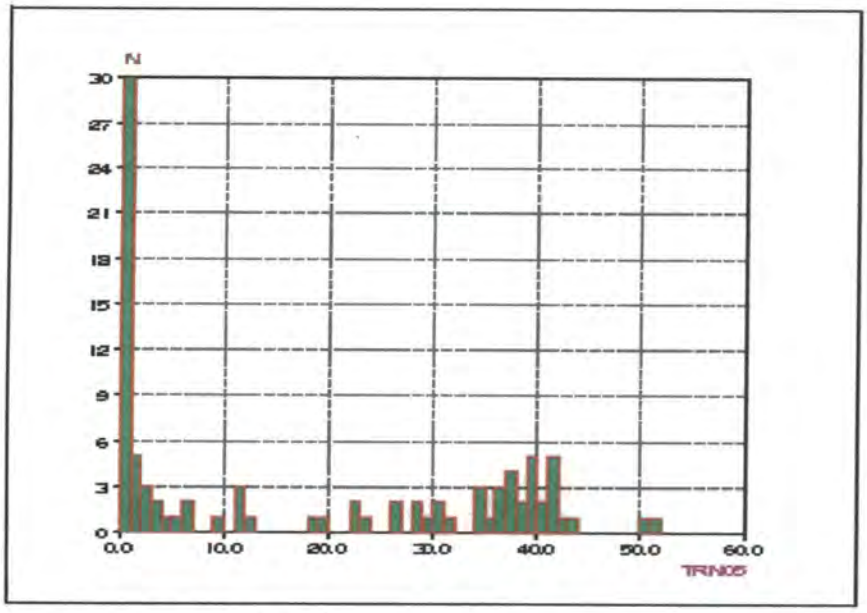

Total = 91, Range = 51.27
Mean = 17.52, Mean SE = 51.27, Sample SD= 17.63, Median = 11.04

Figure 11.6 Biphenyls with two *para* but no *meta* substituents

11.4.1.a(ii) Biphenyls with two *para* and some *meta* substituents.

There are 15 observations in this set. When there are two *para* and no *meta* substituents present then there is a distinct trend for planar conformations. A peak at near 0° contains four structural torsion angles. The other structures are distributed over a wide range of torsion angles, in the 25-45° range.

11.4.1.b Biphenyls containing one *para* substituent.

There are a total of 139 observations. The region at 0-5° contains 20 torsion angles, which is much lower than for the two *para* substituted set and the 20-45° region has 95 observed data, see Figure 11.3

These results indicate that although there is an effect with the *para* substitution, it is not as strong as when there are two *para* substituents present.

The effect of *para* substitution would seemingly be to increase the chance of planarity in the structure. However, this effect is relatively weak and is often outweighed by other factors and this is why there are non-planar structures in the *para* containing sets. Biphenyls with one *para* substituent can be divided further with no *meta* and *meta* either on the same ring as the *para* substituent or on the other ring.

11.4.1.b(i) Biphenyls containing one *para* and no *meta* substituents

This set is to investigate the effect of having no *meta* on a one *para* substituted structure. There are a total of 97 data present in this set. There are fewer structures adopting the 0-10° torsion angle range. The most noticeable feature here is the decrease in the number of structures in the 0-5° region. Consequently there is a relative increase in the distribution at 20-45°, with 48 structures in this region in a broad Boltzman type distribution. This shows that the introduction of *para* substitution causes structures to tend towards planarity and *meta* substitution seems to have the opposite effect. Whereas in the two *para* set, there is a broader distribution in this range with a much less pronounced peak, see Figure 11.7.

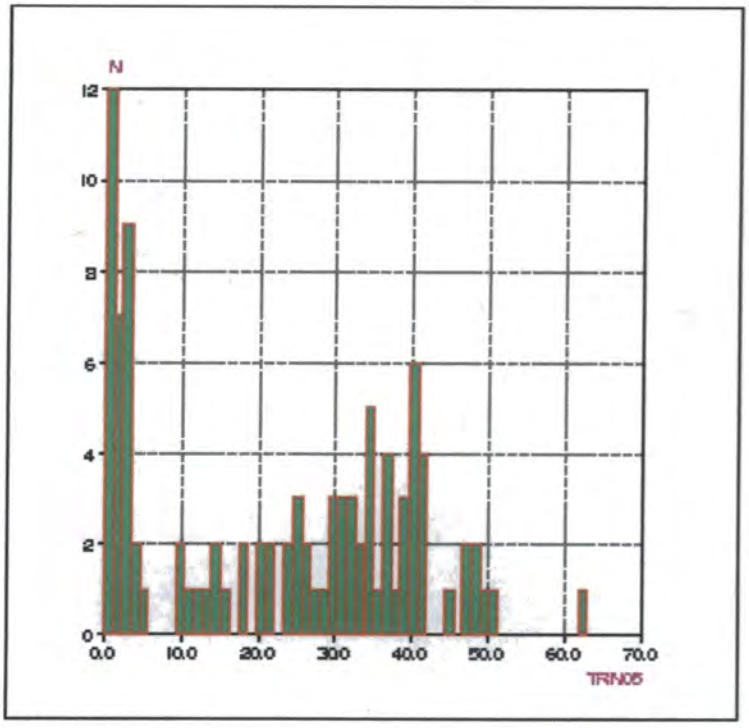

Total = 97, Range = 62.78
Mean = 22.38, Mean SE = 1.72, Sample SD = 16.89, Median = 24.98

Figure 11.7 Biphenyls with one *para* and no *meta* substituents

11.4.1.b(ii) Biphenyls containing one *Para* with *meta* substituents on the same ring

The number of data in this set is 41. There are a distinct lack of near planar structures. The data are distributed over a range of torsion angles from 16-51°. This gives the impression that *meta* substituents on the same ring are influential in a contrary manner to the effect of *para*, see Figure 11.8.

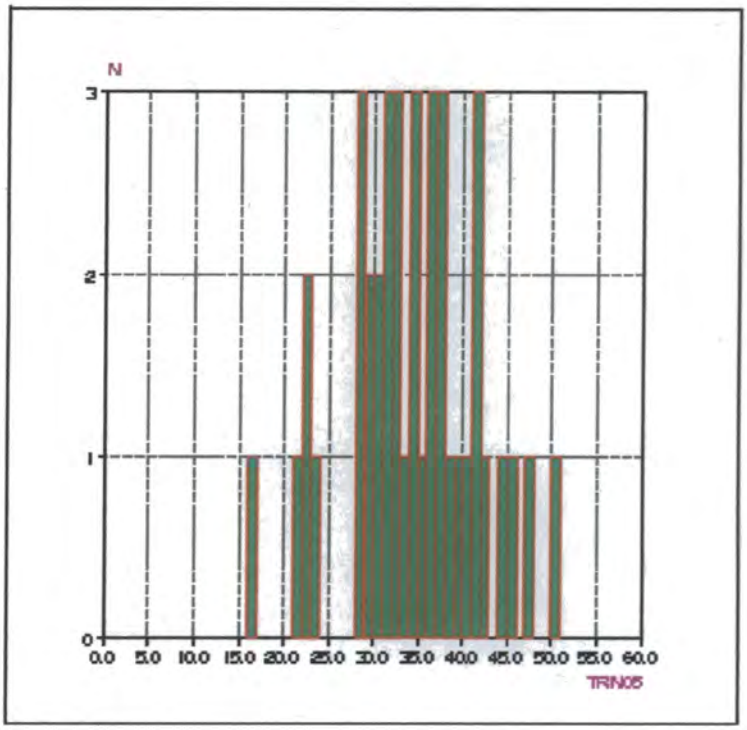

Total = 97, Range = 62.78
Mean = 34.22, Mean SE = 1.13, Sample SD = 7.23, Median = 34.29

Figure 11.8 Biphenyls with one *para* substituent with *meta* substituents on the same ring

11.4.1.b(iii) Biphenyls with one *para* and *meta* substituent, but occurring on different rings.

There are only 11 observations in this set. The data range from 28-52°, with the majority of structures between 21 and 36°. Again the most notable point is the lack of structures in the near planar region of the torsion angle distribution.

11.4.1.c The affect of *para* and *meta* substituents on biphenyl

Biphenyls with *para* substitution have a greater tendency to adopt a near planar conformation. What is seen is that structures with two *para* substituents have a greater tendency towards planarity than those with only one *para* substituent.
So the tendency for planarity can be represented as 2 *para* > 1*para* > non-*para*.

11.4.2 Biphenyls containing *meta* substituents

This group consists of non-*ortho* substituted biphenyls with some form of *meta* substitution present. There are five possible orientations of the *meta* substituents in this group, these are the substituents A, AA', ABA', AA'BB', see Figure 11.9. Unfortunately because of the lack of structures/data, division into the separate subsets can cause great inaccuracy. This group overlaps with those structures also containing *para* substituents and thus contains a great number of *para* containing structures. It would initially be expected that the *para* containing structures would have the same affinity to adopt a planar conformation unless the *meta* substituents are conformationally influential. What is seen is that there is a great tendency for these structures not to be planar. Of 86 torsion angles only 5 are in the 0-5° range, with 75 in the 20-45° region giving an adequate fit of the Boltzman distribution. This indicates that there is a distinctive effect that is caused by the addition of *meta* substituents, see Figure 11.10

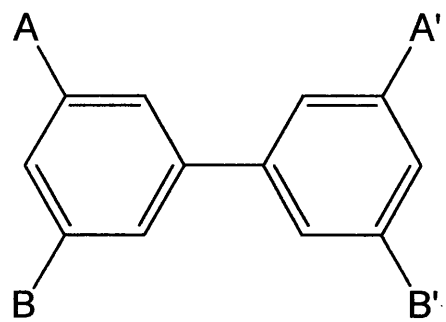

Figure 11.9 The *meta* substitution positions of biphenyl

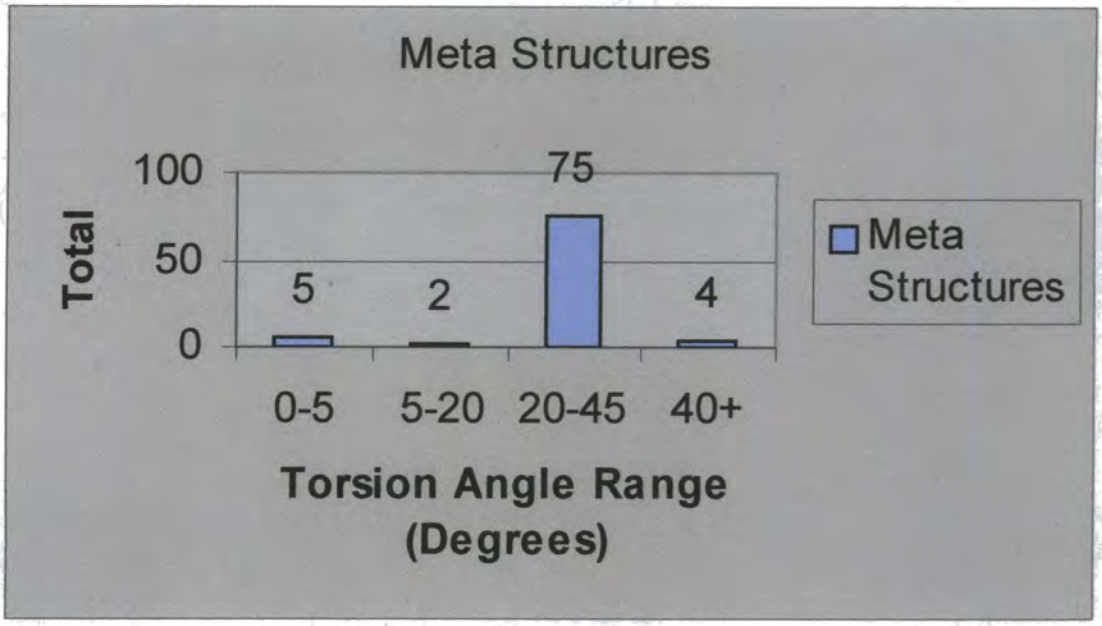

Figure 11.10 The distribution of torsion angles for biphenyls containing *meta* substituents

11.4.2.a Biphenyls with no *para* substituents; Biphenyls containing *meta* substituents only

There are 20 torsion angles present but eight of these angles come from the one structure (with the CCDC structure code HAXRED (Rabideau *et al*, 1993)). 18 of the 20 are in the 20-45° range while one is in the 0-5° range at 1.55°. This near planar structure is 2-Methyl-5-dimethylamino-8-(3,1', 5, 1''-terphenyl)-quinolinium picrate ((Manabe *et al*., 1993) and has two biphenyl fragments and so two dihedral angles with the other more twisted at 36.57°. This structure has a great deal of steric crowding and this is the reason why one of the biphenyl fragments of the structure is forced into the near planar geometry.

It would appear that the addition of two *para* substituents (and to a lesser extent one *para* substituent) leads biphenyl type compounds to favour a planar conformation. This would appear to be a major factor in the overall picture of these compounds not adhering to the structure correlation method. However, when all purely *meta* substituted biphenyls are investigated there is a definite similarity of the resultant data to the expected results of the structure correlation method. It appears the lack of *meta* substitutions causes the deviation of certain biphenyls from the theoretically predicted values.

When there are *meta* substituents and two *para* substituents present then the result is similar to that expected with adherence to the structure correlation method, thus *meta* substitution outweighs the effect of *para* substitution. The readon behind this is unclear and may be a

result of packing factors. *Meta* substituents are more likely to exhibit steric factors and with no *ortho* substituents present they are the only group able to sterically influence the dihedral angle of the rings. If one were trying to produce a non-*ortho* substituted biphenyl with a large twist out of the plane, then the addition of *meta* substitution would be a useful factor.

11.4.2.b Biphenyls with one *meta* substituent

There are 18 observed angles in this set; none have a torsion angle less than 23°, and all exist in the 22-41° region. The distribution could be a "Boltzman" form, but the data are too spread out to draw any useful conclusions.

11.4.2.c Biphenyls with two *meta* substituents on the same ring.

There are 54 structures in this subset with only two of them showing angles less than 20°, the rest are in the 20-52° region. This distribution is approximately a Boltzman type distribution, although over the large range involved the distribution is slightly sparse. The limited data is spread over too wide a range to give a conclusive picture.

11.4.2.d Biphenyls with two *meta* substituents on different rings

There are eight structures in this set with one in the near planar conformation. This is a binaphthal structure (with the CCDC reference code JAKROC (Chen Minqin *et al.*, 1987)) with different electronic properties to that of biphenyl which may explain why it adopts this conformation. The other seven torsion angles are in the 27-40° region.

11.4.2.e Biphenyls with three *meta* substituents

There are no structures with three *meta* but no *ortho* substituents.

11.4.2.f Biphenyls with four *meta* substituents

There are six data present. This set is different from the other *meta* containing sets, in that even though there are so few torsion angles present three of them are in the near planar range. This can be somewhat rationalized in terms of the *para* substitution: of the six structures five have two *para* substituents, the exception (CSD reference code WEPSAL (Guther *et al*, 1994)), has a torsion angle of 16.8°.

11.5 SUMMARY OF NON-*ORTHO* SUBSTITUTED BIPHENYLS

It is worth noting that generally the more *meta* substituents the more *para* substituents, this is not surprising because, the *meta* position is less likely to undergo an addition or substitution than the *para* and *ortho* positions. Given this, there is a lack of structures with one *meta* substituent in the near planar conformation. With two *meta* substituents on the same ring and none on the other ring, then often the other ring is purely a phenyl group. The situation is different when there are four *meta* substituents, when often both rings have *para* substituents. Those that are *meta* substituted, have a greater likelihood of not adopting the planar configuration. The influence of *meta* substitution is undoubtedly linked to that of *para* substitution and it is difficult to separate these two. It can be determined that *para* substituted structures tend to have a percentage of structures favouring planarity, but this can be somewhat diminished when there are also *meta* substituents present. Thus *para* and *meta* substituents both effect the twisting conformation. The distribution of torsion angles are given in Tables 11.1 and 11.2.

What can be deduced however is that these non-*ortho* substituted biphenyls do not conform to the structure correlation expected distribution, primarily due to the effect of the *para* substitutions.

When *para* substituted structures have no *meta* groups attached the percentage of planar structures remains approximately the same as when there are *meta* substituents present. However, when two *para* substituents are attached there are more planar structures.

Para substitution affects many of these structures, with two having a greater effect than one. The conclusion of this study is that the *para* substituted structures that do not adhere to the theory of the structure correlation method.

Why does *para* substitution affect these structures in this manner? There are several possible reasons;

(i) when packing, if there are *para* groups present then the crystal will form a planar configuration better. This could be a result of a tendency for *para* groups to interact with other *para* groups and form chains, which pack better when planar. Or possibly *para* substituted biphenyls simply fit together better when they are flat.

(ii) the *para* groups affect the electronic structure of the biphenyl in a way that the database analysis cannot determine. It is possible that *para* substituents give a greater delocalisation and/or conjugation (see chapter 13). To date no analysis has pointed to an electronic difference between *para* and non-*para* substituted structures, but since there has not been a large amount of study in this area then this is not surprising. Analysis of the structures does not show any specific type of *para* substitution occurring with specific stereochemisrty. Therefore an electronic effect is not obvious using this statistical database analysis.

(iii) biphenyls in the solid state prefer to be flat, *c.f.* biphenyl's differing configuration in both the solid and gaseous states. It is the presence of *meta* substituents that have a non-planar configuration effect.

This third possibility seems unlikely, although possible, and it could possibly be related to (i) or/and (ii) above.

To fully determine the difference between the various substituted biphenyls more analysis is needed. In chapters 12 and 13 an attempt to rationalize the biphenyls with database analysis and diffraction analysis has been conducted (*c.f.* chapters 12 and 13).

Table 11.1 The dihedral angle distribution of *para* substituted non-*ortho* biphenyls

Type	Total	0-5°	5-20°	20-45°	45°+
All non-*ortho* biphenyls	268	69	23	162	14
All Para	245	65	20	145	
2 *para*	106	45	10	48	3
2 *para* & no *meta*	91	41	10	38	2
2 *para* with *meta*	15	4	0	11	0
1 *para*	139	20	10	95	12
1*para* & no *meta*	97	20	11	48	8
1 *para* with *meta* on same ring	41	0	1	37	3
1 *para* with *meta* on different ring	11	0	0	10	1
No *para* substituents.	23	4	1	18	0

Table 11.2 The dihedral angle distribution of *meta* substituted non-*ortho* substituted biphenyls.

Meta					
Type	Total	0-5°	5-20°	20-45°	45°+
All *meta*	86	5	2	75	4
1 *meta*	18	0	0	18	0
2 *meta* on different rings	8	1	0	7	0
2 *meta* on the same ring	54	1	1	48	4
3 *Meta*	0	0	0	0	0
4 *Meta*	6	3	1	2	0

11.6 REFERENCES

1. Alminningen, A.; Bastiansen, O.; Gundersen, S.; Samdal, S. *Acta Chemica Scandanavica*, **1989**, 43, 932.
2. Brock, C. P.; Minton, R. P. *J. Am. Chem. Soc.* **1989**, *111*, 4586.
3. Burgi H.-B.; Dunitz, J.D, *Structure Correlation Volume 1* VCH Publishers, Inc., New York, NY (USA), **1994**.
4. Burgi H.-B.; Dunitz, J.D., *Structure Correlation Volume 2*,VCH Publishers, Inc., New York, NY (USA), **1994**.
5. Chen Minquin; Wu Guang; Zhuang Shanming; Huang Zuen; Qui Wenjie; Wu Wenling, *Chem. J. Chin. Uni.*, **1987**, 8, 556.
6. Charbonneau, G. P.; Delugeard, Y. *Acta Cryst.*, **1976**, B32, 1420.
7. Charbonneau, G. P.; Delugeard, Y. *Acta Cryst.*, **1977**, B33, 1586.
8. Eaton, V. J.; Steele, D. *J. Chem. Soc., Faraday Trans. 2.* **1973**, 69, 1601.
9. Guther, R.; Nieger, M.; Rissanen K.; Vogtle, F., *Chem. Ber.*, **1994**, 127, 743.
10. Howard, J.A.K.; Allen, F.H.; Shields, G.P (Editors), *Implications of Molecular and Materials Structure for New Technologies*, NATO Science Series E; Applied Sciences, Kluwer, Dordrecht, The Netherlands (In Press).
11. Manabe, K.; Okamura, K.; Date, T.; Koga, K., *J. Am. Chem. Soc.*, **1993**, 115, 5324.
12. Rabideau, P. W.; Sygula, A.; Dhar, R. K.; Fronzek, F. R., *J. Chem. Soc, Chem. Commun.*, **1993**, 1795.

CHAPTER 12:

THE OVERALL EFFECT OF *PARA* AND *META* SUBSTITUTION ON BIPHENYLS.

12.1 INTRODUCTION

In terms of the twisting of biphenyls the presence of *meta* and *para* substituents have not generally been considered to have much influence. Given the results seen from database studies already examined in this thesis, for these types of systems it is clear these substitutions may play a greater role in the overall stereochemistry than previously thought. Results from chapters 10 and 11 have shown that substitution is significant in conformational preferences. In general, it is difficult to determine the effects of these substitutions since there are a number of ways in which a biphenyl type structure can be substituted; i.e. it can have any combination of 0-4 *ortho* or/and *meta* substituents and/or 0-2 *para*. So when trying to analyze specific cases of substituted structure the number of structures of each type tends to be quite small and so it is often necessary to look for the more general features and trends. Initially, the specific atom type of *ortho* substitutions are generally only taken as a side issue, in order to determine what trends, if any, are purely due to the presence of *para* and *meta* substitutions.

In theory it is the *ortho* substituents that have the conformational effects and are generally thought to determine the amount of twisting that is involved in the system. The effect of *meta* and *para* substitution must in theory be of a much smaller magnitude in comparison. To determine the validity of these assumptions and for an investigation into the overall structural effect of *para* and *meta* substituents on the twisting of biphenyls, a database search was conducted using the CSD. This involved the complete search of biphenyls and only those structures where the rings were completely independent of each other (apart from the C-C ring linkage) were accepted, in the same manner as chapters 10 and 11. This set was split into subsets consisting of substituents at each position (*ortho*, *meta* and *para*) and the types of substituent atoms and/or groups at these positions.

The initial set includes all possible *ortho* substituted positions (0, 1, 2, 3, and 4). The effect of *para* and *meta* substitution here should be obscured by the effect of *ortho* substituted structures. The effect of having all the separate subsets of *ortho* substitution present in the one set is so dominating that the other smaller effects (such as *meta* or *para* substitution) are undetectable. In this set there are a number of structures with dihedral angles between 0-5° and relatively few between 5-25°. The number of structures rises for dihedral angles greater than 25°. This is somewhat expected and is due to the effect seen in chapter 11 concerning

biphenyls with *para* but no *ortho* substituents. From 25-90° the number of structures increases in an approximately linear fashion towards 90°; this is expected since this is the effect of progressive *ortho* substitution onto the rings and the subsequent effects of steric interaction.

This set is split into zero, 1 and 2 *para* substituents, and will subsequently be further divided into *para* substituted biphenyls with *meta* or *ortho* substituents. The subdivision into 0,1 and 2 *para* substituents will show if their effect is strong enough to be visible even in data containing all *ortho* substituents and if so, then how strong and how much of an effect the *para* substituents have on the biphenyls. Figure 12.1 shows the distribution of torsion angles for 0, 1 and 2 substituted biphenyls.

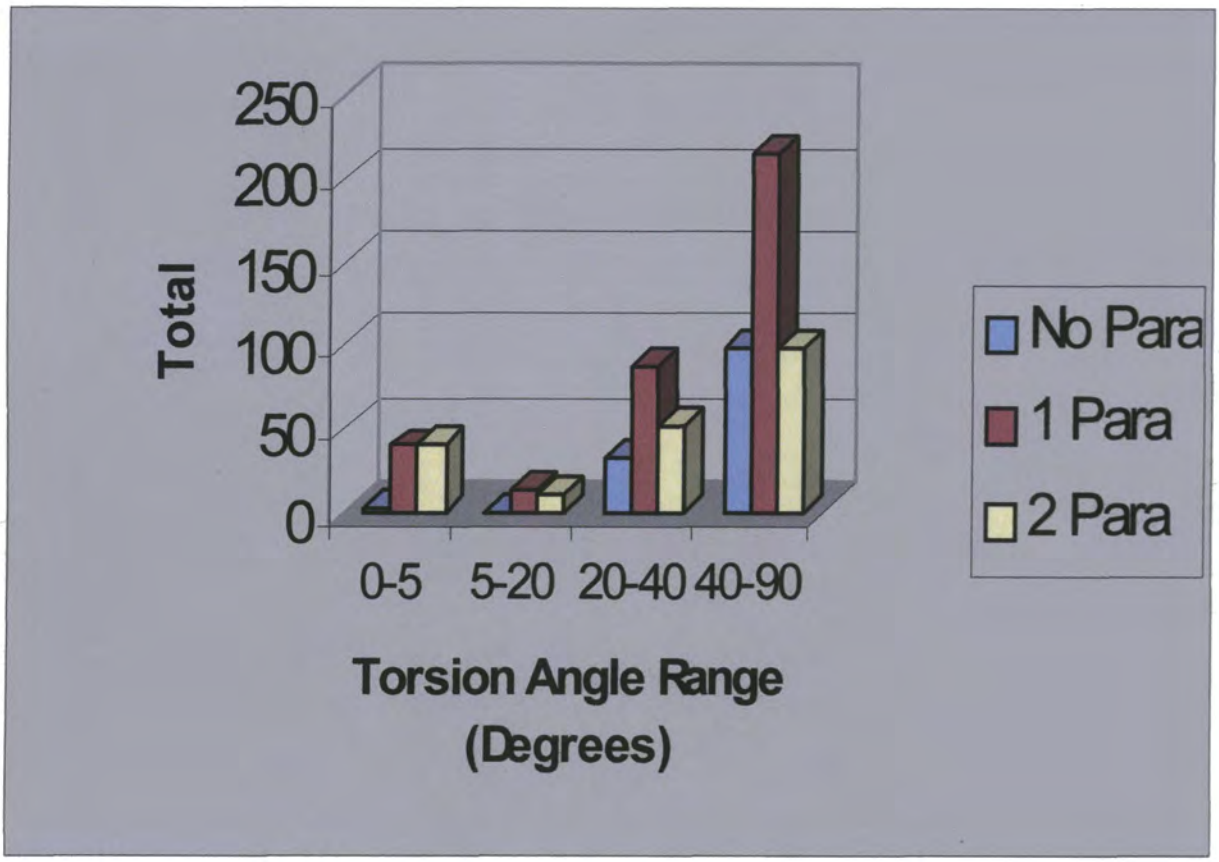

Figure 12.1 Biphenyls with *para* substituents

12.2 BIPHENYLS WITH NO *PARA* SUBSTITUENTS PRESENT ON THE RINGS

This set is used to examine the effect of having no *para* substituents present on the rings. It will also show the effect that *para* substituents have on the rings since it is a good comparison between itself and those sets that have *para* substituents present, see Figure 12.1. For *para* substituted biphenyls the set is further divided up to examine the effects of other positional substitution..

12.2.1.a Biphenyls with 0,1,2,3 or 4 *ortho* positions occupied, no *para* substituents

There are a total of 151 observed torsion angles. There is one near planar structures and then no structure until 20°, from where is a gradual increase in the number of structures for increasing torsion angles, similar to that seen for the set that contains all *para* substituted structures. There are only a few structures that have a torsion angle less than 25°, and a relatively large number of structures with an angle near 90°. The lack of structures with a torsion angle between 0-5° is an early indication that *para* substitution may have a considerable stereo-chemical effect. However, even without *para* substituents a small percentage of the structures are still planar. This shows that the effect of *para* substitutions on biphenyls is not exclusive, see Figure 12.2.

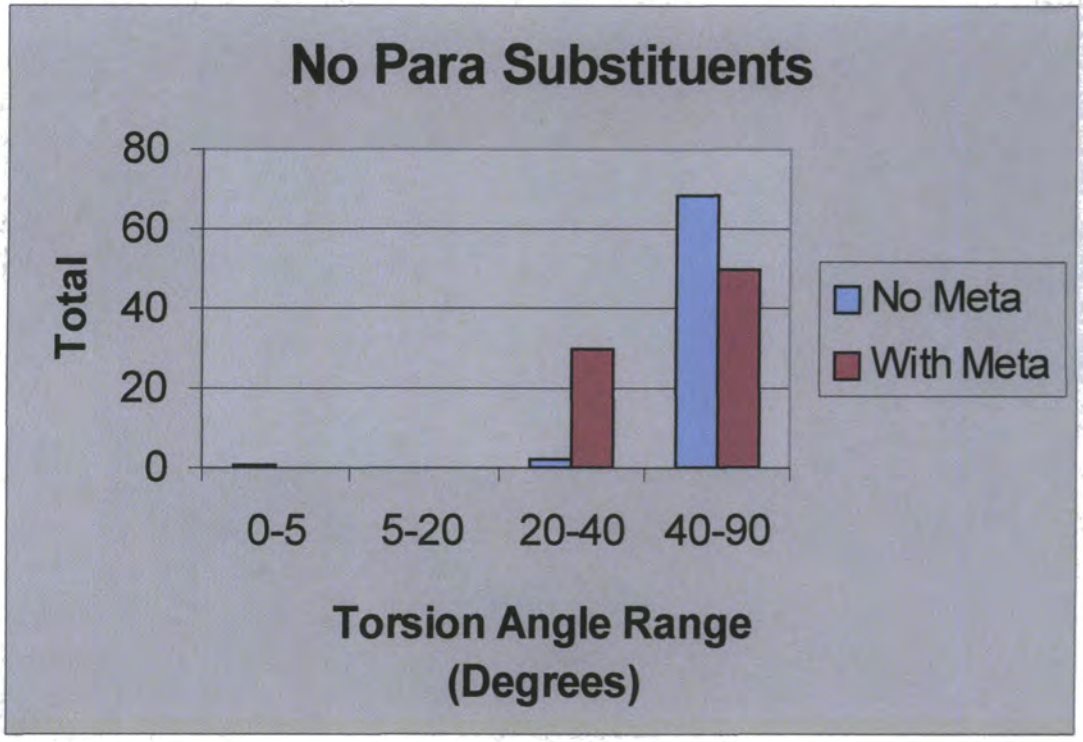

Figure 12.2 No *para* substituted biphenyls with and without *meta* substituents.

12.2.2 Non *para* substituted biphenyls with no *meta* substitution.

This set contains 71 structures and is used to study how much of an effect *meta* substitution has on the dihedral angle distribution of all biphenyls, see Figure 12.2. The main body of these data exists in the 40-90° region and there are distinctive peaks at 54° and 65°; this is in contrast to the overall non-para substituted set which has a gradual rise in the number of structures with increasing torsion angle up to 90°. This indicates that either without *meta* substituent present the biphenyls have a slight tendency towards the planar configuration, or *meta* substituents give a preference for non planarity .

12.2.3 Non *para*, *meta* substituted biphenyls with *ortho* substituents

The purpose of this set is to examine the effect that *meta* and *ortho* substituents have on the non-*para* substituted biphenyls, the set is split further into the separate subsets that depend solely on the number of *ortho* substituents. This gives an indication of how strong the steric effects of the *ortho* positions are and the relative magnitude of the dihedral angle that the substitutions demand.

12.2.3.a Non *para*, *meta* substituted biphenyls, no *ortho* substituents:

This set comprises the parent biphenyl compound, the twisting angle has been measured several times as approximately 0°. A number of the biphenyl structures are present in the data, for further details see chapter 5.

12.2.3.b Non *para*, *meta* substituted biphenyls, 1 *ortho* substituents,

There are 28 observations are present in this set, see Figure 12.3. The range is broad from 37.9-85.7°, with a mean at 57.9°. There are no structures that are close to planar.

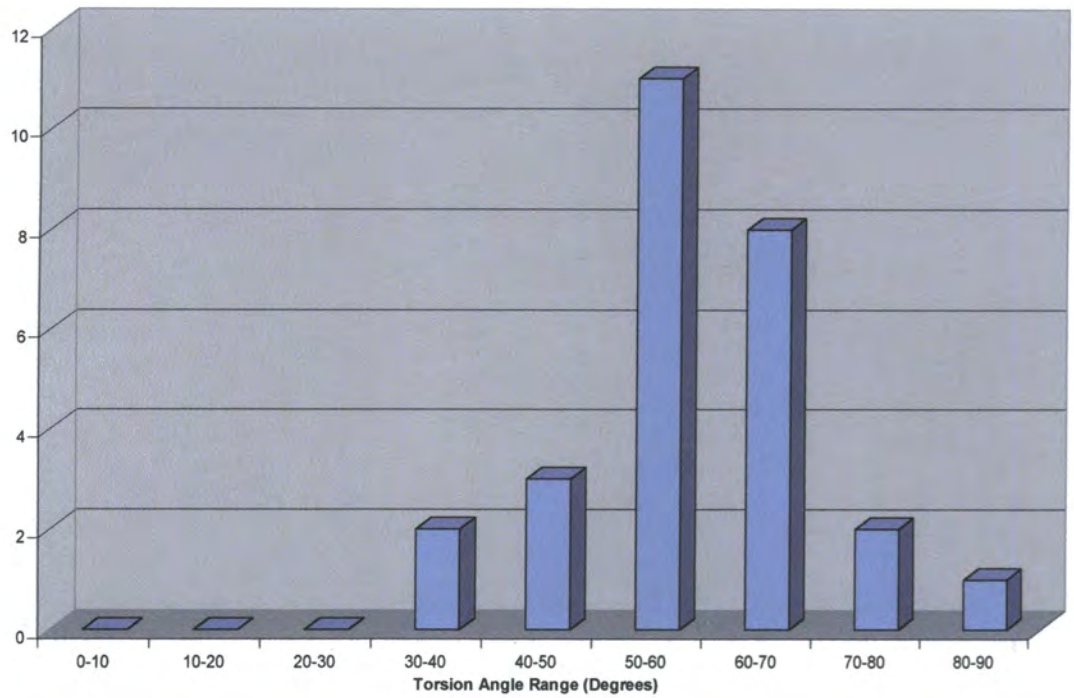

Figure 12.3 Non *para* and *meta* biphenyls with one *ortho* substituent

Mean = 57.95°, Max = 85.65°, Min = 37.98° and Sample SD = 10.11.

12.2.3.c Non *para*, *meta* substituted biphenyls, 2 *ortho* substituents

There are 35 structures in total, but these can be separated into two distinct parts, those with the *ortho* substituents on the same ring and those with the two on separate rings.

12.2.3.c(i) Non *para*, *meta* substituted biphenyls, two *ortho* substituents on the same ring

There are five structures with the *ortho* substituents on the same ring. These structures exist in the range 58-76°.

12.2.3.c(ii) Non *para*, *meta* substituted biphenyls, one *ortho* substituents on each ring

For the structures with one *ortho* substituent on each ring (Figure 12.4) there are 30 structures. This gives a more acceptable level for analysis and these structures are present in the range of 41.4 to 89.8°, with a mean of 67.62°. Again there are no structures with a dihedral angle ~0°.

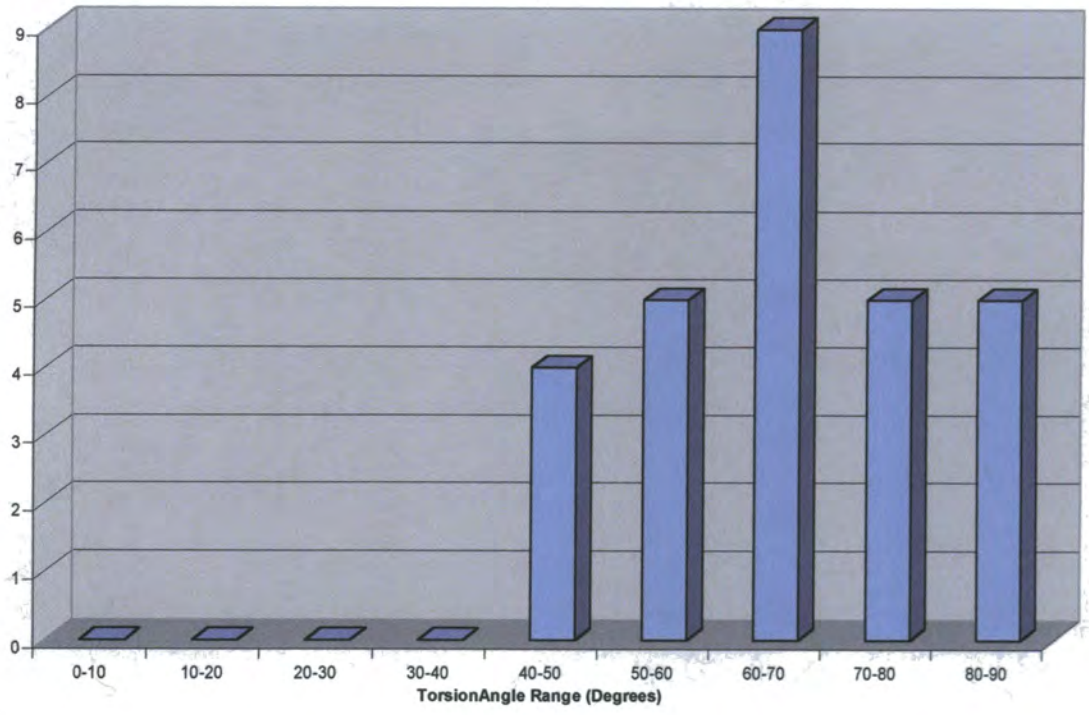

Figure 12.4 Non *para* substituted biphenyls with two *ortho* substituents on different rings. Mean = 67.62°, Max = 89.79°, Min = 41.43° and Sample SD = 13.64.

12.2.3.d Non *para*, *meta* substituted biphenyls, three *ortho* substituents

There are no structures without *para* or *meta* substituents but with three *ortho* substituents. This is not surprising considering the possible difficulties in synthesizing a structure with three rather than four substituents.

12.2.3.e Non *para*, *meta* substituted biphenyls, four *ortho* substituents

There are only seven structures here, so no real conclusions can be determined from this set. Six of the seven structures have dihedral angles in the 81-90° range, one is lower at 50.8°, which is due to intra-molecular interactions. Once again there are no structures with a near planar configuration, although in this case it is not surprising with the large steric hindrance present in these particular structures.

12.2.4 Non *para* substituted biphenyls with *meta* substitution

This set contains most of the data in the non-*para* substituted structures and therefore is similar to that set. It is evident that there is decrease in the near 0° angles and this again

indicates that both *ortho* and *meta* substituents can have an effect in the conformation. The presence of *meta* has the tendency for the conformation to be non-planar, see Figure 12.1

12.2.4.a Non *para* substituted biphenyls with *meta* substitution, no *ortho* substituents

There are 32 observations all of but one exist in the region of 25-43.3° dihedral angle, the one exception being almost planar with a 1.5° dihedral angle. The near planar structure here is the one structure present in the *meta*, but no *para* substituent, set that has a near planar structure, See Figure 12.5.

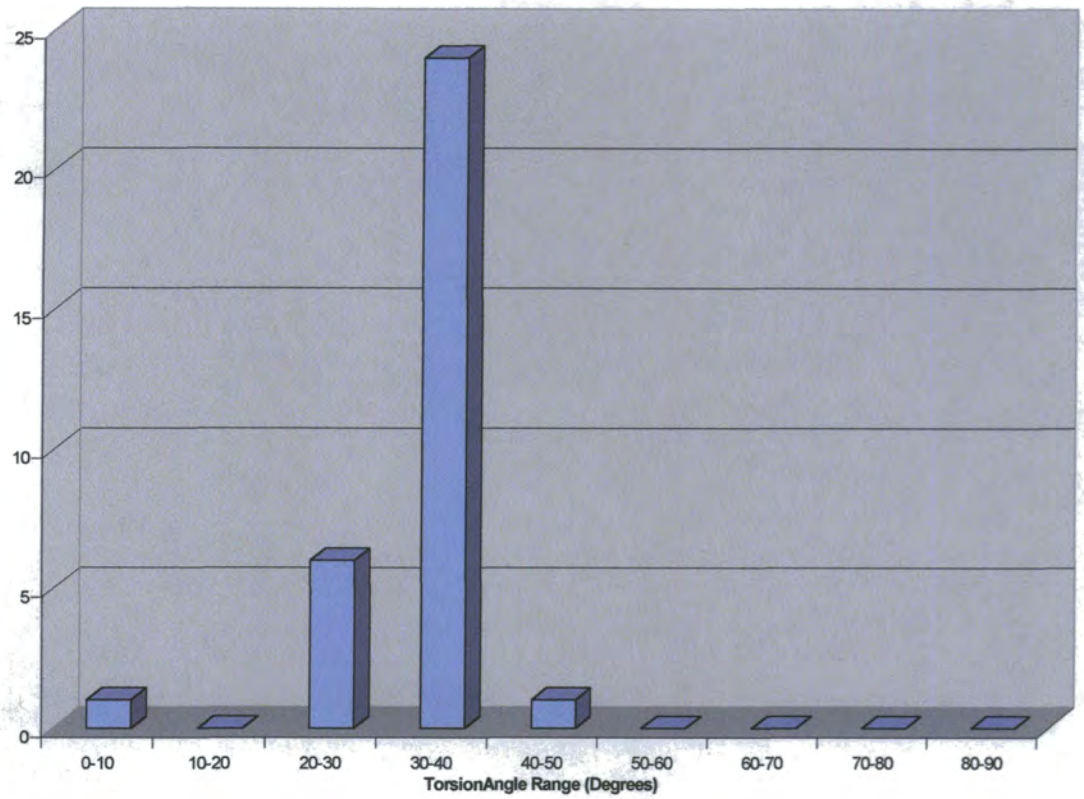

Figure 12.5 Biphenyls with *meta* but no *ortho* or *para* substituents
Mean = 41.69°, Max = 43.24° , Min = 1.55° and Sample SD = 6.99.

12.2.4.b Non *para* substituted biphenyls with *meta* substitution and one *ortho* substituent

There are 51 observations present and they lie in the range of 40-90°, 45 of these structures have dihedral angle in the 40-65° range, two structures are close to 90°, and four are in the 70-77° range. None of these distributions of dihedral angles resemble a Boltzman distribution, with the 40-65° range of structures, in what resembles a block of structures. It is

possible that with more observations this range of data would resemble a steep/narrow Boltzman distribution, since it has the general shape, but this is conjecture, see Figure 12.6.

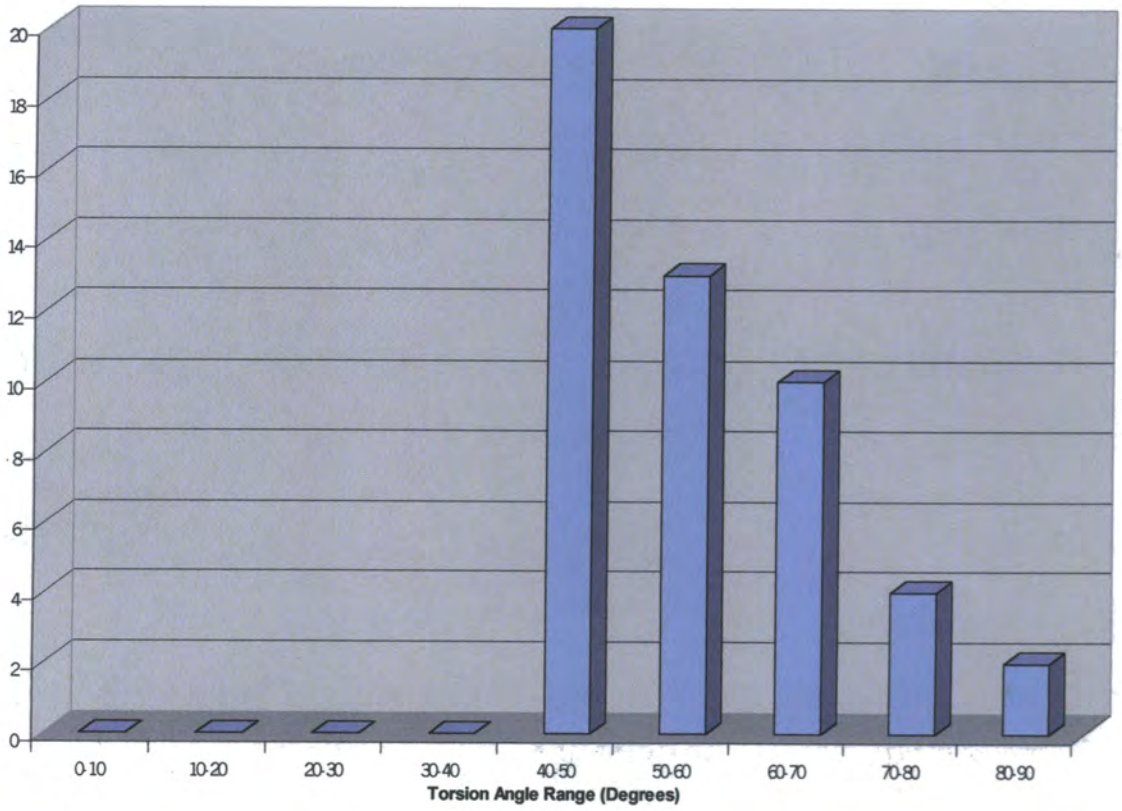

Figure 12.6 Biphenyls with *meta*, one *ortho*, and no *para* substituents Mean = 55.39°, Max = 89.45° , Min = 40.76° and Sample SD = 11.71.

12.2.4.c Non *para* substituted biphenyls with *meta* substitution, two *ortho* substituents:

With 26 observations present, there are few structures in this set. These are split into the structures with substituents on the same ring and those with the substituents on different rings, as described previously. Those structures that have substituents on different rings number 11 observations, 9 of these are between 44.4-63°, and the other two exist at 76 and 90°. For the structures with *ortho* substituents on the same ring (15 observations) there are two distinct regions of conformation, 53-72° and 82-90°. These two different types of structures exhibit the same magnitude and range of twisting, but they differ in the exact pattern that they adopt.

12.2.4.d Three and Four *ortho* substituents

For the compounds with three or four *ortho* substituents present there are only three structures, one with three and two with four. All the structures had a large amount of twisting (> 40°). Although there is not enough data in these sets to analyse, it would be expected that the effect of the *ortho* substituents would create large dihedral angles.

12.2.4.e Summary of non *para* with *meta* biphenyls

Since *ortho* substitution has a steric factor on the conformation of the rings, the more a structure is *ortho* substituted the more influence the *ortho* substituents have on the twisting of the biphenyl. When structures are grouped in terms of the number of *ortho* substitutions present then they tend to group into discrete regions. The effect of *ortho* substitution on non *para* substituted biphenyls is the main influencing factor on the dihedral angle. *Meta* substituted structures show a tendency towards non-planarity, although this effect is weak.

12.3 BIPHENYLS WITH ONE *PARA* SUBSTITUENT

This group shows the effect of having *para* substituents present as opposed to having none and examines the effect of *para* substitution in terms of one *para* substituent. The one *para* substituted case will fall into one of three separate outcomes;

1, It will be similar to the structures with no *para*, indicating the anomalies are due mostly to structures with two *para* groups present.

2, It will be more like the structures with both *para* positions occupied, indicating the presence of *para* is a factor to produce the anomalies.

3, The result will show the structures to be somewhere between zero and two substituents. Indicating that there is a trend present where one *para* has an effect that gets compounded when there are two *para* groups present, see Figure 12.7.

This group has a total of 352 observations. This group shows a distinct difference to the no *para* substituted set since here there are a number of structures that are near planar, with 39 structures being 0-5°. The area 20-90° is a large broad peak containing over three hundred structures, this peak follows an approximate Boltzman distribution. However it is probably several separate peaks amalgamated into the one large broad peak. Also noticeable is the lack of structures that have a torsion angle very close to 90°, 8/352 compared to 26/151 for the non-*para* substituted structures. The percentage of near planar structures is low, but when considering the large range of *ortho* position substitutions covered which should favour non-planar structures, it is still a noteworthy feature, see Figure 12.7.

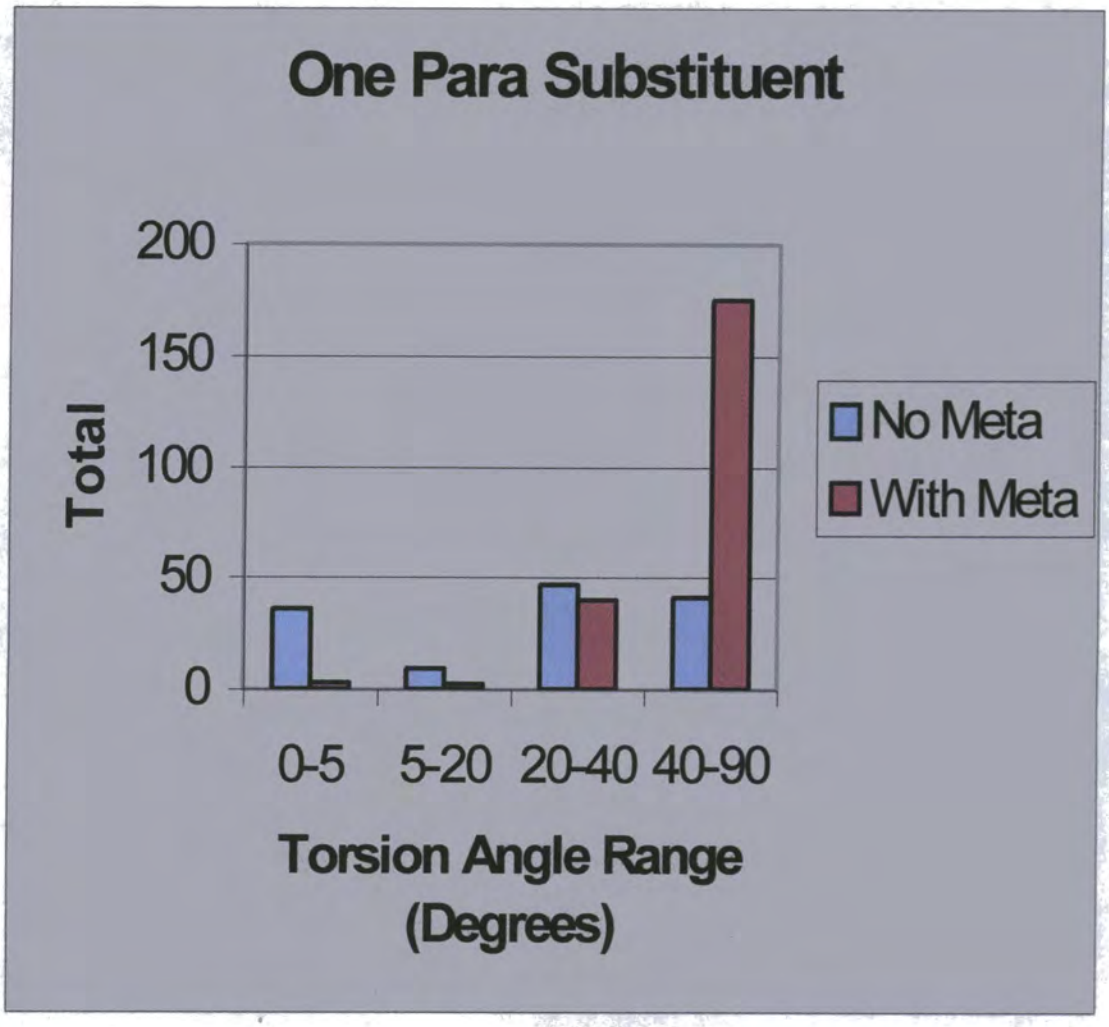

Figure 12.7 Biphenyls with one *para* substituent

12.3.1 One *para* substituent with no *meta* substituents

There are 132 observed data in this set. There is a large proportion of structures with a 0-5° torsion angle (~30%). The other features are the peaks at 30-45°, 48-50° and 60-70°, with that at 30-45° the most populated. There is an absence of structures after 55° except for a slight peak at 60-70°, with eight structures, see Figure 12.6.

12.3.1.a One *para* substituent with no *meta* substituents, no *ortho* substituents

There are 104 observations present ranging from almost planar to 60°. There are two distinct peaks present, the first from 0-6° contains 37 structures, the rest, from 9-60° follow an approximate Boltzman distribution, with the range between 32-42° also having 37 data. As this set contains 104 of the total 122 observations in the set with one *para* and no *meta*

substituents, it dominates this set. The peak at 0-6° is prominent and contains 36 % of the structures.

12.3.1.b One *para* substituent with no *meta* substituents, one *ortho* substituent

There are 24 observations here, the range is from 36-69.5° and follows an approximate broad Boltzman distribution. Although it can also be interpreted to consist of two narrow peaks (with apexes at 45° and 52° respectively), it is notable that there are no structures in the near planar region.

12.3.1.c One *para* substituent with no *meta* substituents and two, three and four *ortho* substituents:

Both three and four *ortho* substituted biphenyls with one *para* and no *meta* substituents produced no hits. There is one structure with two *ortho* substituents and this is a structure that contains four dihedral angles in the range of 58.9° to 64.6°. For no *meta* and one *para* substituted structures there is a distinct tendency for these structures not to have two, three or four *ortho* substituents. This is presumably due to difficulties in making structures with highly substituted *ortho* positions but with limited substitution at the other positions.

12.3.2 Biphenyls with *meta* and one *para* substituent

For one *para* and *meta* there are 220 structures, with two distinct peaks at 45-90° and 28-45°. To decipher the trends in this set it is necessary to look at the effect that *meta* substituents have with an increasing number of *ortho* substituents.

12.3.2.aOne *para* with *meta* substituents, no *ortho* substituents

There are 53 observations present here and of these, 52 exist in the main body of data with dihedral angles in the 21-52° range and this group forms an approximate steep Boltzman distribution. One observation which is not part of this data is that with a 0.084° dihedral angle. As already seen with the overall set (Figure 12.1), there are often structures that lie outside the general trend, see Figure 12.8.

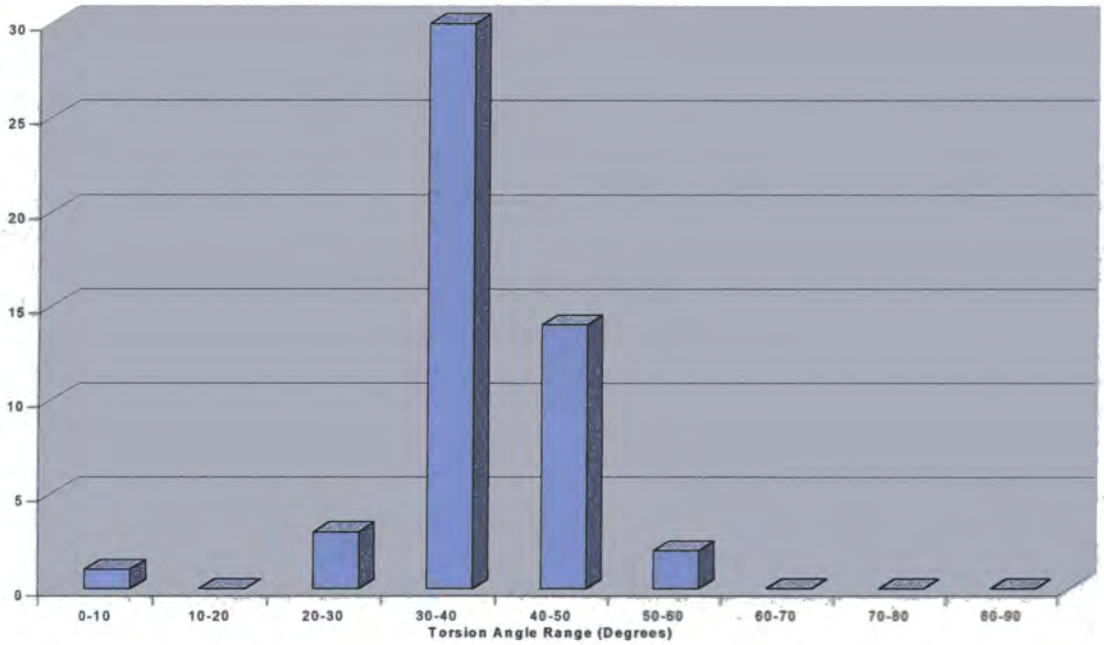

Figure 12.8 Biphenyls with one *para* and *meta* , but no *ortho*, substituents Mean = 35.72°, Max = 51.59° , Min = 0.08° and Sample SD = 8.16.

12.3.2.b One *para* with *meta* substituents, one *ortho* substituent

There are 57 observations present in this set, 52 have dihedral angles in the range 35-75°. The exceptions with these data are one observation at 89.45°, two structures at ~0° and two in the 8-12° range, see Figure 12.9.

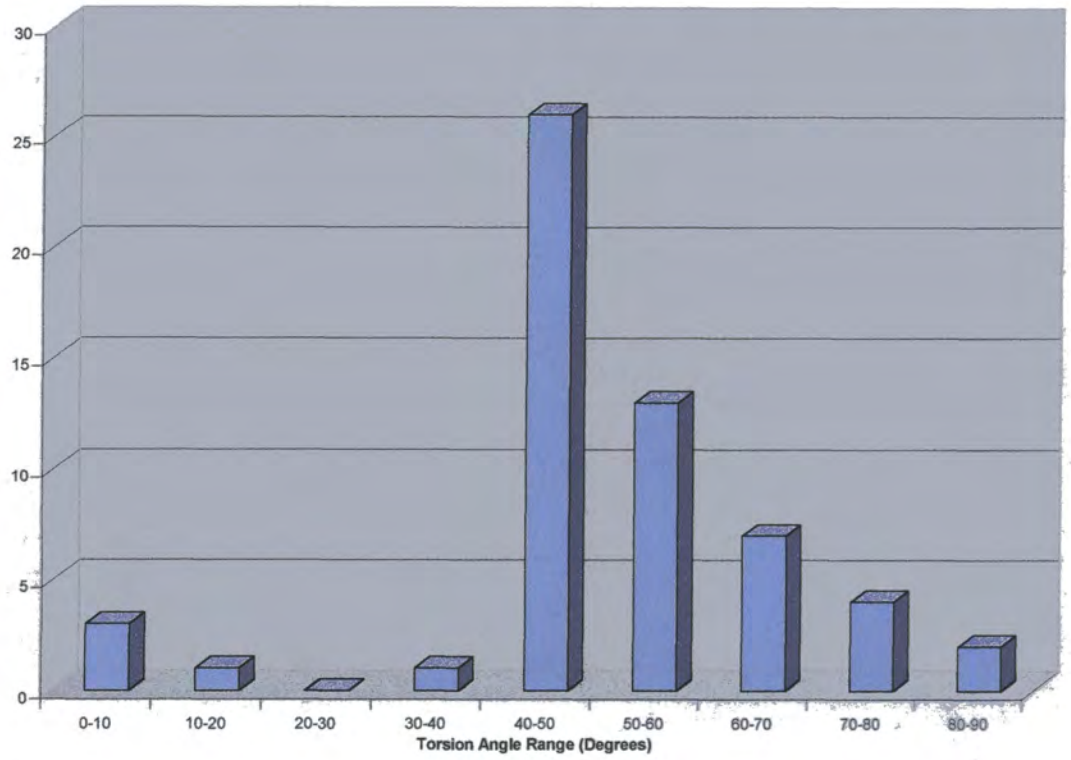

Figure 12.9 Biphenyls with one *ortho* substituent containing *meta* and one *para*. Mean = 51.32°, Max = 89.45° , Min = 0.69 ° and Sample SD = 16.49.

12.3.2.c One *para* with *meta* substituents and two *ortho* substituents.

There are 92 observations present, 91 of which exist in the main body of the histogram, in the range 53-90° in an approximate Boltzman distribution. The one observation that is not in this region is at 42.6°. In this set, the higher degree of twisting, and the lack of structures with a lower dihedral angle is noticable, see Figure 12.10.

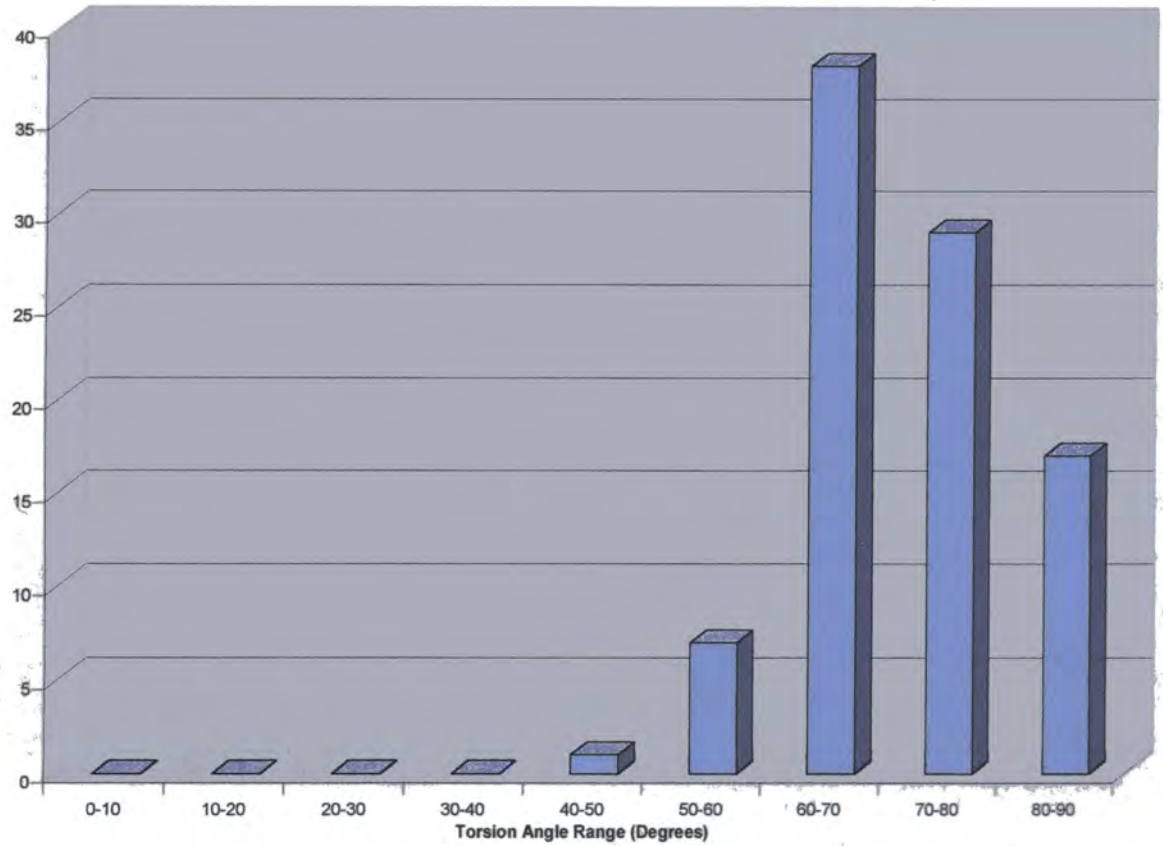

Figure 12.10 Mono *para* substituted biphenyl with *meta* and two *ortho* substituents Mean = 71.02°, Max = 89.93° , Min = 42.62 ° and Sample SD = 9.36.

12.3.2.d Three *ortho* substituents:

There are 18 observations in the range 58-90°. The limited data are spread out over too large a range to distinguish trends.

N.B. no structures have *meta*, 4 *ortho* and 1 *para* substituents.

12.3.3 Summary of one *para* substituted biphenyls;

It is observed that there is an effect of *meta* substitution on the structures with one *para* but no *ortho* substituents. The effect is manifest in that with *meta* substituents present there is a lack of structures with a close to planar configuration. This is in contrast with non-*meta* substituted structures when there is a large percentage of structures, although by no means dominant, that have a dihedral angle close to 0°.

12.4 DI-*PARA* SUBSTITUTION ON BIPHENYLS

This set is to examine the effect of both the *para* positions being substituted. This set should be the most informative since it will show just how strong the effect of *para* substitution is. It will also show how the "two *para*" relates to "one *para*" dataset, see Figure 12.1

12.4.1 Biphenyls with 0, 1, 2, 3 or 4 *ortho* positions occupied with two *para* positions occupied.

There are 199 observed torsion angles in this set. The most prominent peak is the sharp one at 0-5°, this contains 43 structures. In this set there are three peaks, the first is the 0-5° peak, the next a peak at 25-50° and the 3rd peak is from 60-90°, the number of structures gradually increases from 60-90°, which is similar to the pattern seen with previous sets. This second group contains the largest number of structures but the distribution is over a larger area and hence broader and does not have the same height as the 0-5° peak. Another similarity is the lack of structures observed between 10° and 20°, see Figure 12.11.

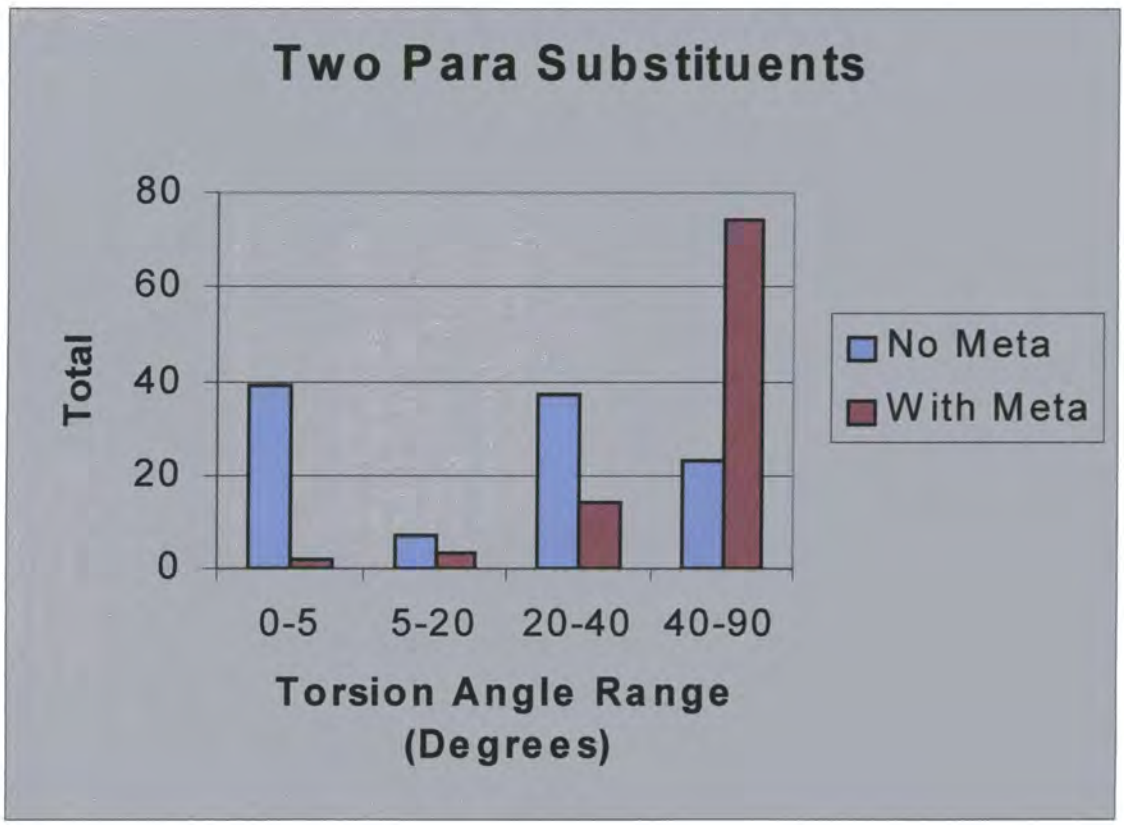

Figure 12.11 Two *para* substituted biphenyls

12.4.2 Two *para* positions occupied without *meta* substitution

In this set there is a peak at 0-5° containing 40% of the structures. This non-planar region dominates here more than any of the other sets. The peak at 35-40° is sharp. There is also a slight peak at 80-90°, and although it is small, this is in stark contrast to the set containing one *para* and no *meta* substituents that contained no structures in this region at all.

12.4.3 The effect of *ortho* substitution with two *para* and no *meta*

This set is used to examine the effect that *para* substitution has without any *meta* positions occupied, with increasing *ortho* substitution.

12.4.3.a Bi-*para* substituted biphenyls with no *meta* and no *ortho* substituents.

In this set the majority of structures, 92 of the 101 observations, have no *ortho* substituents, there are no data that have a dihedral angle greater than 50.42°, see Figure 12.12.

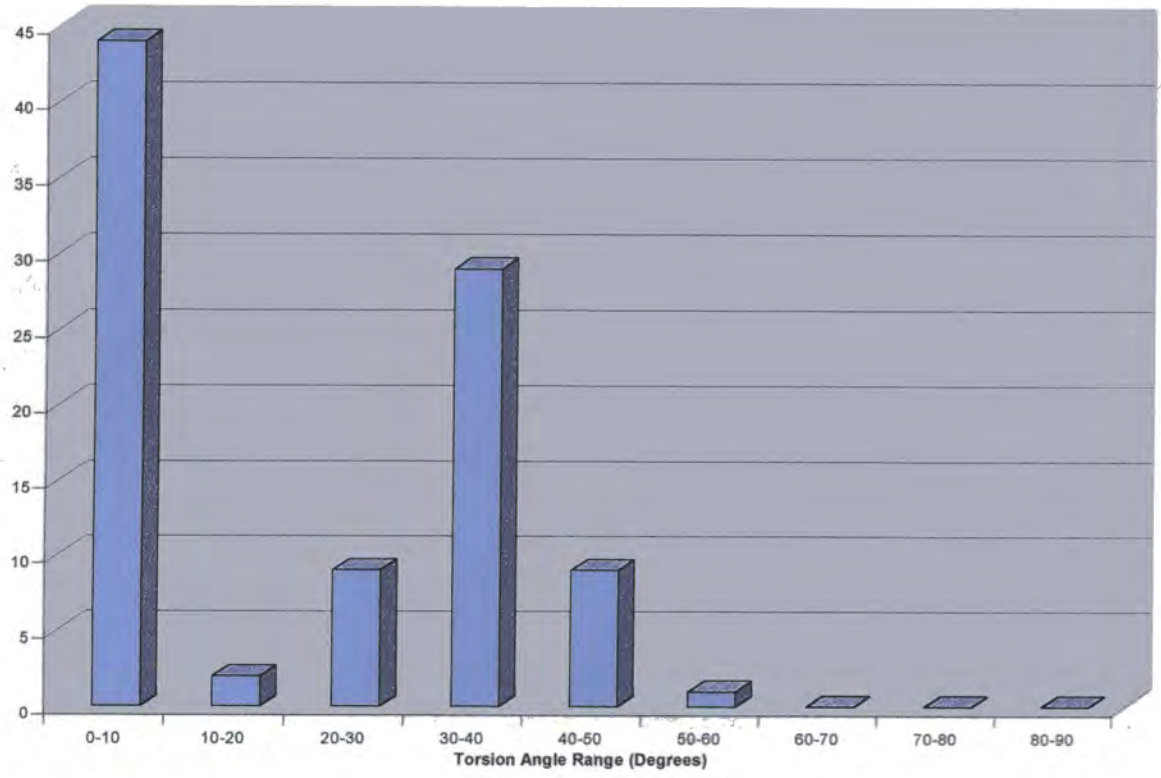

Figure 12.12 Two *para* substituted biphenyls with no *ortho* or *meta* substituents Mean = 18.99°, Max = 50.42° , Min = 0.03° and Sample SD = 17.69.

12.4.3.b Bi-*para* substituted biphenyls with no *meta* and one *ortho* substituent:

A single observation was found in this category with a dihedral angle 53°.

12.4.3.c Bi-*para* substituted biphenyls with no *meta* and two *ortho* substituents:

There are seven observations present, six with a range of dihedral angles of 78-90° and the other observation has an angle of 59.07°. The range here is larger than that with one *para* and no *para* substituents. There are no structures in the near planar configuration.

12.4.3.d Bi-*para* substituted biphenyls with no *meta* and three *ortho* substituents:

No observations present in this set.

12.4.3.e Bi-*para* substituted biphenyls with no *meta* and four *ortho* substituents:

There are only six observations, occupying two regions, two data at 48-52° and four at 82-90°. These are not enough observed data to determine if there are two distinct regions present or not.

12.4.4 Two *para* positions occupied with *meta* substitution

Here there are 93 data and their spread is very different to the set without *meta* substitution with a lack of data at the near planar range of torsion angles. There are several peaks, at approximately 10°, 30-40° and 45-90° (possibly consisting of two or three separate peaks). This result indicates that an effect of *meta* substituents on structures with two *para* substituted biphenyls is to stop the biphenyls is adopting smaller torsion angles.

12.4.4.a Bi-*para* substituted biphenyls with *meta* and no *ortho* substituents

There are 16 observations only, 15 of which lie in the range from 31-49° and one in the near planar conformation at 0.36°.

12.4.4.b Bi-*para* substituted biphenyls with *meta* and one *ortho* substituent

There are 11 observations in this set, all of which exist in the large range between 35.6-75.4°, there are too few observations spread out over too large a range to see any pattern that the distribution takes, but the lack of structures that are non planar is noticeable.
Unfortunately comparison between this set and the non-*meta* equivalent set is not possible because of the lack of data in the non-*meta* substituted set.

12.4.4.c Bi-*para* substituted biphenyls with *meta* and two *ortho* substituents:

With the *ortho* substituents on the different rings there are nine observations only, ranging from 31.6-83.1°, there are too few observations over too large a range to come to any conclusions.
With the *ortho* substituents on the same ring there are 14 observations, 12 of these are in the 55-90° range with 2 at 40-42° range.

12.4.4.d Bi-*para* substituted biphenyls with *meta*, three *ortho* substituents:

Only four observations, all of these have large dihedral angles, with a range from 70.83-81.80°.

12.4.4.e Bi-*para* substituted biphenyls with *meta*, four *ortho* substituents

With 39 observations present, this group has a more useful number of observations. The main body of observations, 35, occur in the region 50-90°. The structures that are outside this region are four observations, three of which at approximately 10° and one observation in the near planar configuration with 0.923°, see Figure 12.13.

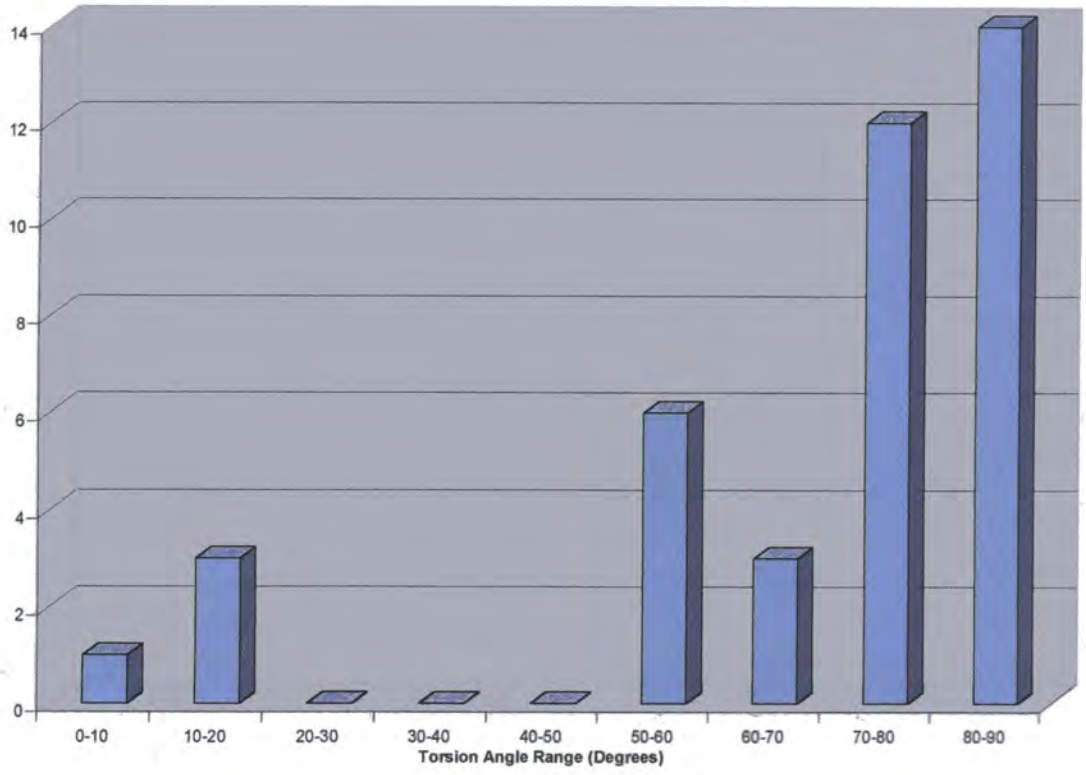

Figure 12.13 Bi-*para* biphenyls with *meta* substituents, with all four *ortho* positions occupied.

Mean = 68.76°, Max = 89.64° , Min = 0.92° and Sample SD = 23.38.

12.4.5 Summary of two *para* substituted cases

The conclusion from the two *para* substituted biphenyls is that as with one *para* substituted biphenyls, there is an effect from the *meta* substituents, compared to those with no *meta*. In the non *ortho* substituted case there are very few structures with a zero dihedral angle. There are a much greater number of such structures when there are no *meta* substituents present. As expected when *ortho* substituents are added the average dihedral angle increases, except in the four *ortho* substituted case when compared to the three, which is due to the greater ability of four to inter/intra-molecularly interact. The effect of *meta* and *para* substituents is relatively strong in non-*ortho* and singely *ortho*-substituted biphenyls when more are added but the effect of *para* and *meta* substituents is greatly reduced.

12.5 *META* SUBSTITUTED BIPHENYLS

The *meta* position can be substituted (1 to 4), regardless of the *ortho* and *para* substitution. If there is no *meta* substitution effect then the resulting histogram from three data should resemble approximately the set with all biphenyls present, since the *ortho* and *para* substitutional effects would obscure any *meta* effect present. What are seen though are certain slight differences. There is a lower percentage of structures at the near planar configuration, and also relatively fewer at the near 90° twist, with the distribution mainly at 25-90°, and peaks at 65°, 78° and 35°. In this histogram there are apparent multiple peaks, which is expected from the effects of the different number of *ortho* substituted structures present in this sample, although this may be a result of how many *meta* positions are substituted. Hence, this set needs to be divided further, to ascertain the effects that the different number of *meta* substituents has on the conformation.

12.5.1 Biphenyls with one *meta* substituent

In this set there are 85 observations. The most noticeable part of the resultant histogram is the broad general peak that exists at 30-90°. There is a narrow peak of nine structures that lies at 50-52° with a broad distribution, see Figure 12.14.

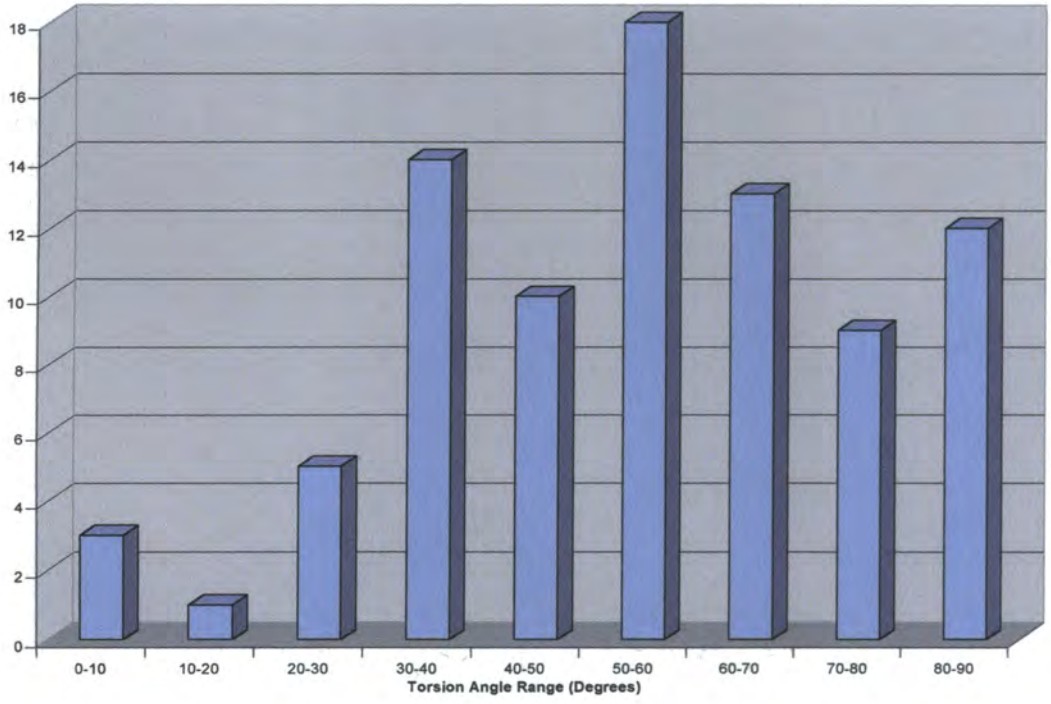

Figure 12.14 Biphenyls with one *meta* substituent

Mean = 53.77°, Max = 89.91° , Min = 0.69° and Sample SD = 20.85.

12.5.2 Biphenyl with two *meta* substituents

There are a total of 146 dihedral angles in this set. The histogram has similar peaks to that of the one *meta* substituted case, although the peaks at 60-70° and 75-90° appear to have been amalgamated into the one peak. There are also relatively more structures close to 90° and there is only one dihedral angle close to 0°, see Figure 12.15.

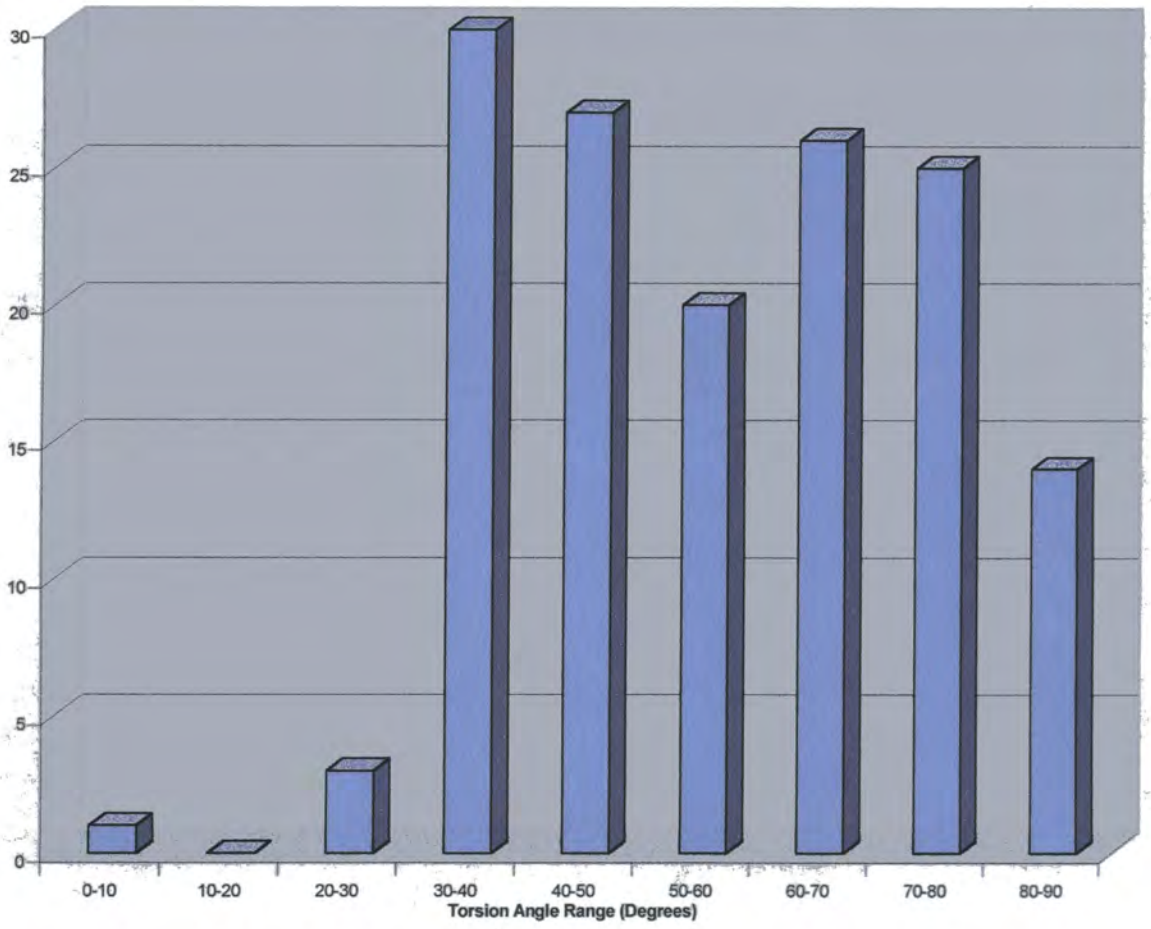

Figure 12.15 Biphenyls with two *meta* substituents

Mean = 53.77°, Max = 89.91° , Min = 0.69° and Sample SD = 20.85.

12.5.3 Biphenyls with three *meta* substituents.

There are a total of three dihedral angles in this set. There are relatively few structures probably because of the difficulty in synthesizing these compounds rather than compounds with either two or four substituents. Those that are in this group are found in the range from 40-90°.

12.5.4 Biphenyls with four *meta* substituents.

There are a total of thirty dihedral angles in this set. There are 3 distinct peaks, 0-12°, 50-65° and 70-90°.

12.5.5) Summary of *meta* substitution

In examining the *meta* substitution, there is no distinction made between the *para* substituted cases. The expected result is that with a *para* substituent present then there would be a distinct separation from the no *para* case. However, it is observed that in the one, two and four cases of *meta* substitution that are examinable most observations occur in the 20-90° range rather than the planar structures that may be expected with the *para* substituents present. This shows that *meta* substituents have an effect that is strong enough to be dominant when purely *meta* substituted biphenyls are examined. All the separate groups of *meta* substituted structures have more non planar structures and there is no trend for less planar structures with increasing *meta* substitution. So it appears that the presence of *meta* substitution causes a conformational effect, see Figure 12.16.

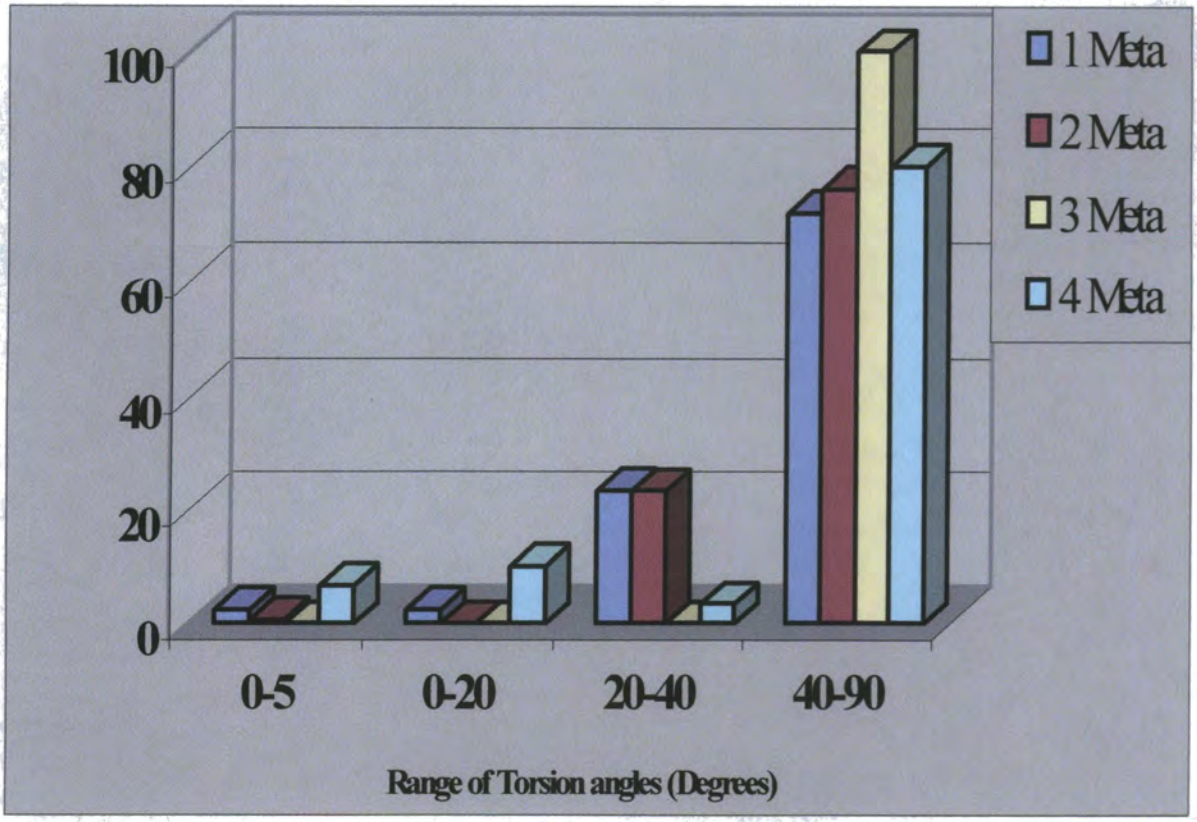

Figure 12.16 The percentage of biphenyls with 1-4 *meta* substituents within given ranges of torsion angles.

12.6 SUMMARY OF *ORTHO*, *META* AND *PARA* SUBSTITUTION ON BIPHENYLS

This chapter has concentrated on analyzing the three *para* substituted sets (zero, one and two *para* substituents) and the subsets with differing *meta* and *ortho* substituents. It is seen that the effect of *para* substitution is strong enough that even if the amount of *ortho* substitution is disregarded there are definite effects. The addition of *para* substituents influence biphenyl torsion angles towards a lower twisting angle and indeed planarity. When there are no *para* substituents then the torsion angle, tends to be greater than 30° and often greater than 70°, with a large percentage very close to 90°. With the addition of one *para* substituent, the profile changes and the near planar structures become more common, although only a small number of structures compared to the complete set including non-planar structures. The structures at close to 90° become less common, the peak in structural torsion angles is shifted towards 30-80°, with the main peak being at 50-60°. When a second *para* substituent is added the trend continues with approximately 20% of structures in the near planar region (0-5°). There are almost twice as many structures close to 0° with two *para* substituents than there are with one *para* substituent. The amount of structures with a torsion angle near 90° does not change from one *para* to two *para* substituents and the 85-90° region is approximately equal in these two sets. The effect of *para* substitution affects the range of torsion angles in the non-planar region of angles, the main body of dihedral angles moves to lower angles i.e. non-*para* 85-90°, one *para* 30-80° and two *para* 20-50°. In the substitution of *ortho* positions with no *para* attached the most common position substituted is the one *ortho*. For one *para* it is the non-*ortho* substituted structures that are the most common. The two *para* substituted structures have the largest percentage of structures as the non-*ortho* substituted region (see Table 12.1). Thus in the distribution of the non-planar region of torsion angles, the angles are controlled more by the amount of *ortho* substituents than by the *para* substitution. In both the cases of *para* substituted biphenyls, the effect of also having *meta* substituents present is to increase the torsion angles and to give a distinct tendency to move away from the near planar structures. What appears to happen is that when *para* substituents are added there is a tendency for them to adopt two conformations, one at near planar and another closer to 40°. However, when a *meta* substituent is also present structures with no twist become less prominent. In the case of all biphenyls, regardless of *ortho* substitution, there is an effect that is prominent and can be seen even though it would be expected to be masked by the different effects of the 0, 1, 2, 3 and 4 *ortho* substituted positions of the biphenyl. *Para* substituents have a great effect on the conformation but the effect of the *para* substituents is altered by the subsequent *meta* substituents. When considering these sets and subsets, it is worth noting the hugely dominating effect this

substitution has when the individual cases of *ortho* substitution are investigated and what is seen is the strength of the effect of *ortho* substitution. When there are *ortho* substituents present, then the steric effect of the groups at these positions comes into effect and the fraction of structures with dihedral angles close to the planar becomes much less. The addition of one or more *ortho* substituent dramatically decreases the likelihood of the structures being planar, regardless of other substituents. It is concluded that the *para* effect on the conformation is small when considering all biphenyls. In general the planarity effect of *para* substitution on biphenyls is only really evident when there are no *ortho* or *meta* substituents.

Meta substituents have an effect, which is that they counteract the effect of the *para* substitution, but this is less dramatic than the *para* substitution effect. *Para* substitution influences the biphenyls in the twisting conformation they adopt, and in many situations the theoretically ideal conformation is not adopted. Tables 12.1 and 12.2 give a summary of the spread of dihedral angles with respect to substitution.

SET	SUBSET	DIHEDRAL ANGLE (°)				
Meta		Total	0-5	5-20	20-40	40-90
	1 *Meta*	85	2	2	20	61
	2 *Meta*	146	1	0	34	111
	3 *Meta*	3	0	0	0	3
	4 *Meta*	30	2	3	1	24

Table 12.1 The distribution of *meta* substituted biphenyls

SET	SUBSET		DIHEDRAL ANGLE (°)			
		Total	0-5	5-20	20-40	40-90
No *Para*		151	1	0	32	98
No *Meta*		71	1	0	2	68
	0 *Ortho*	1	1	0	0	0
	1 *Ortho*	28	0	0	2	26
	2 *Ortho* (on the same ring)	5	0	0	0	5
	2 *Ortho* (on different rings)	30	0	0	0	30
	3 *Ortho*	0	-	-	-	-
	4 *Ortho*	7	0	0	0	7
With at least 1 *meta*		80	0	0	30	50
	O *Ortho*	32	0	0	30	2
	1 *Ortho*	51	0	0	0	51
	2 *Ortho* (on the same ring)	15	0	0	0	15
	2 *Ortho* (on different rings)	11	0	0	0	11
	3 *Ortho*	1	0	0	0	1
	4 *Ortho*	2	0	0	0	2
1 *Para*		352	39	12	87	215
No *Meta*		132	36	9	47	41
	0 *Ortho*	104	36	9	45	14
	1 *Ortho*	24	0	0	2	22
	2 *Ortho*	4				4
With at least 1 *meta*		220	3	2	40	175
	0 *Ortho*	53	1	0	39	13
	1 *Ortho*	57	2	2	1	52
	2 *Ortho*	92	0	0	0	92
	3 *Ortho*	18	0	0	0	18
	4 *Ortho*	0	0	0	0	0
2 *Para*		199	41	10	51	97
No *Meta*		106	39	7	37	23
	0 *Ortho*	92	39	7	37	9
	1 *Ortho*	1	0	0	0	1
	2 *Ortho*	7	0	0	0	7
	3 *Ortho*	0	0	0	0	0
	4 *Ortho*	6	0	0	0	6
With at least 1 *meta*		93	2	2	14	74
	0 *Ortho*	16	1	0	12	3
	1 *Ortho*	11	0	0	1	10
	2 *Ortho* (on the same ring)	14	0	0	0	14
	2 *Ortho* (on different rings)	9	0	0	1	8
	3 *Ortho*	4	0	0	0	4
	4 *Ortho*	39	1	3	0	35

Table 12.2 The distribution of *ortho* substituted biphenyls

CHAPTER 13:

THE INTRA-MOLECULAR BOND LENGTHS OF SUBSTITUTED BIPHENYLS

13.1 INTRODUCTION

In this thesis it has been shown that the addition of substituents to the *ortho*, *meta* and *para* positions of the rings of biphenyls has effects on the conformational effect on the rings relative to each other, especially in the *para* substituted case, see chapters 10, 11 and 12.
A database analysis of the dihedral angles does not give a full explanation. When examining the substituent types there is no pattern observed between different substituent types and the dihedral angle. Therefore the conformational preference may be as a result of positional substitution. To understand why *para*, *ortho* and *meta* substitution have this conformational effect, it is necessary to examine all the parts of the system affected by the addition of the *para* and/or *meta* and/or *ortho* substituents. Measurable parameters that are affected apart from the dihedral angles, should be the bond lengths. The initial expectation is that the most important bond length in the biphenyl system, in terms of the conformational twisting, is the carbon-carbon ring linkage bond, see Figure 13.1. Both the rings have influence on this bond and it is about this bond that the important relative orientation occurs. Since substitution effects the twisting, then it is a reasonable assumption that it may effect this C-C bond in some manner.

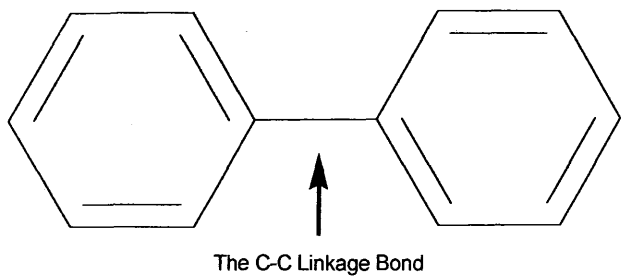

Figure 13.1 Biphenyl with the bond between the two rings illustrated

The linkage bond is known to be slightly conjugated and this is manifested in the length, which at approximately 1.49 Å is shorter than the 1.46 Å of the standard Csp^2-Csp^2 (conjugated C=C–C=C) single bond. It is longer than the standard double C=C bond (1.33 Å), and aromatic bonds (1.39 Å) (Handbook of Chemistry and Physics, 1995), see chapter 5 for more detail on the biphenyl molecule. The linkage bond distance approximates the

single bond distance rather than the aromatic bond distance, this shows that the conjugation in the bond is limited. Since the C-C link has conjugation present it can be considered an integral part of the aromatic system. Further evidence of conjugation in this bond is shown in IR and UV studies of the biphenyl type compounds (Roberts, 1985). It has been noted (Brock & Minton, 1989) that the conjugation about the C-C bond is not affected by the relative magnitude of the twisting of the rings. This was concluded because the C-C linkage bond generally has the same magnitude regardless of torsion angle. This is surprising since it would be expected that with an increase in the dihedral angle, would lead to a decrease in the conjugation. As with most aromatic structures a divergence from planarity greatly limits conjugation and they tend to remain planar. In the case of biphenyls the conjugation appears to be unaffected by this deviation from planarity (Brock & Minton, 1989), the reason for this is still unexplained.

13.2 THE C-C LINKAGE BOND

In this study the C-C ring linkage bond is inspected by analysis with the CSD (see chapter 5 for details) to investigate how it is affected by the addition of *para*, *meta* and *ortho* substitution. Initially, it might be expected that *ortho* substituents would show a stereochemical effect, by forcing the rings further apart therefore increasing the length of the C-C linkage bond. The substituents may also have an electronic effect, according to in which position the substituents are located and on the relative electron donating and withdrawing properties of these substituents. However, when comparing the C-C bond length with the position of the substituents, the electron donating and withdrawing groups effects should cancel, unless there are a large number of structures with specific substituents either electron donating or withdrawing. This will have a particular electronic effect and occupy very specific substitutional locations (i.e. the data are influenced by a series of similar structures), any disordered structures found in the search were screened out
The first set of data investigated the effect of the *para* substituents, since it is the *para* substitution that has the most notable effect. The biphenyl compounds were separated into three groups dependent on how the biphenyl was *para* substituted and these are;

(1) non-*para* substituted biphenyls,
(2) biphenyls with one *para* substituent and
(3) biphenyls with two *para* substituents.

These groups were then compared and the resultant figures were similar with C-C distances 1.48(2), 1.49(2) and 1.48(2) Å for non-*para*, one *para* and two *para* substituted biphenyls respectively. Some deviation occurs between the sets in terms of the outlying data in the histogram, for the non *para set* these are in the range of 1.446 to 1.532 Å. The outlying values for one *para* substituted structures range from 1.427 to 1.573 Å, this can be explained by the greater number of structures in this group compared to the "non *para*" set. When considering the case of "two *para*" the range is greater still, from 1.386 to 1.591 Å, this increase is due to increasing substitution on the system (i.e. the more *para* substituents generally the more *ortho* substitution) and so a greater steric effect on the C-C link, this is substantiated when the outlying structures are examined. In general there is no overall change in the nature of this bond with the addition of *para* substituents.

13.3 THE INTRA RING BOND DISTANCES

Although the C-C ring linkage bond is extremely important the other bonds within the rings will also be affected by the type and position of substituents. An electron withdrawing group on the *meta* position affects the reactivity of aromatic systems differently from an electron withdrawing group in the *ortho* and *para* positions and further an electron donating group is different than electron donating.

In the case of conformations of biphenyls the effect of *para* substitution on the systems is independent of the nature of the substituent. Also, as far as can be determined, there is a tendency for planarity in these systems and this is regardless of whether there are electron donating or withdrawing groups at the *para* position. This substitution may however have an effect on the bond lengths within the ring, and this subsequently affects the electronic structure of the aromaticity of the system. This may in turn also have a bearing on the ability of the compound to pack and therefore change the conformation of the compound. With a view to examining this further, a database search of all the significant bond lengths in a variety of substituted cases was conducted.

The search initially concentrated on the effect of *para* substitution on the bonds within the ring, since this appears to have a noticeable effect on the dihedral angle and twisting conformation of these systems. The bond lengths of the parent compound, biphenyl, were used for a comparison. Since there are several examples of biphenyl it is possible to get an average of the different bond lengths reported for biphenyl as well as for individual cases, and these can also be compared with the biphenyl results already studied, in relation to this thesis.

13.4 THE BOND DISTANCES OF BIPHENYL

Initially a search was conducted on biphenyl compounds that exist in the CSD. The result shows the C-C bond linkage in biphenyl is approximately equal that for the C-C bond linkages for all biphenyl type systems (Hargreaves & Rivzi, 1962 and Trotter 1961). This is as expected, although the C-C linkage may have been expected to be more conjugated due to lack of substitution. This conjugation was initially thought to have a bearing on the system, despite the results reported previously in this thesis (chapter 10 and 11) that disagree with this assumption. Despite the aromaticity of the compound, the bond lengths are slightly different, with the ipso-*ortho* length being at 1.40(2) Å, *ortho-meta* at 1.39(2) Å and the *meta-para* being even shorter at 1.38(2) Å, however, these differences are not significantly different. Obviously here the C-C bond distorts the ring from having identical bond lengths. This is not unexpected and the additions of substituents are well known to have an effect on the aromaticity of the ring. There is clearly a difference between the bond distances in the rings and this may have some bearing on the subsequent packing and twisting of the biphenyl and similar systems. In the analysis conducted on biphenyl in this thesis (see chapter 5), it was found that there was a large range of bond lengths present in the system. The C-C linkage bond was found to be long, with a database average of 1.499(2) Å, although this is shorter than the single C-C bond.

The study on biphenyl at low temperature shows that the *ortho-meta* bond is larger than *meta-para*. The *ortho-meta* distance varied from 1.372(6) to 1.411(6) Å and the reason for the large range is unclear although the closeness of the phase change and crystal packing may well be factors. The variation is large and is a lot greater than expected. Packing forces would not normally produce such a variation, so the probable reason for this larger than expected range of bond lengths is due to the structure beings so close to the phase change.

13.5 THE EFFECT OF *PARA* SUBSTITUTION ON THE INTRA RING DISTANCES OF BIPHENYLS

From hereafter the inter-ring bond distances of the bonds of *ipso-ortho*, *ortho-meta* and *meta-para* will be referred to as α, β, and γ respectively (see Figure 13.2). If initially the *meta* and *ortho* substituents are not taken into consideration then the *para* substituted biphenyls can be grouped into three sets, these contain no-*para*, one *para* and two *para* substituents. When the biphenyl has none or two *para* substituents then the system is symmetrical in terms of *para* substituents. So the relevant bond lengths are the α , β and γ bond lengths. If there is just one *para* substituent then the symmetry is lost and there are now the *ortho*, *meta* and *para* intra ring bond lengths on both the ring with the *para* substituent and the ring with just an hydrogen atom at the *para* position. With the unsymmetrical case (the mono *para* substituted biphenyl) the α, β and γ represent the *para* substituted ring while the α', β' and γ' represents the non-*para* substituted rings lengths (Figure 13.2). The C-C bond that is between the two rings is referred to as C-C.

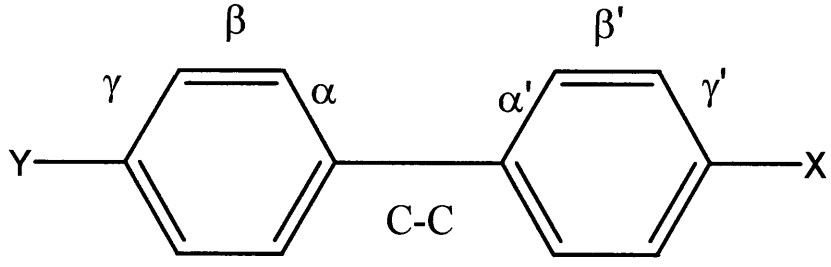

Figure 13.2 Biphenyl intra bond distances, when X=Y; α=α', β=β' and γ=γ'

The substituents labeled X and Y were allowed to be identical and any non-metallic group. No distinct pattern was observed in the data regarding the *para* substituents. So no specific type of substituent was overly common in the analysis.

It can be seen from the search is that there are small but significant differences in the bond lengths, (see Table 13.1). In general the α and β bond distance is reasonably consistent, although the X = H, Y ≠ H, (H represents an hydrogen atom) case is noticeable different from the X ≠ H and Y ≠ H and X = Y = H cases. The biggest observed differences are in the γ bond length as the *para* substituted rings have a larger γ bond length than the non-*para* substituted ring. This is seen especially with the X = H and Y ≠ H, where the γ' bond lengths are noticeably shorter than the γ. Also in X = H and Y ≠ H the γ distance is very

similar to the other intra ring distances. So when the biphenyl is doubly *para* substituted the bond lengths in the phenyl rings are more equal.

There are some anomalies in the bond lengths, firstly the bond lengths of the non-*para* ring for X = H and Y ≠ H is greater than the X = Y = H case. This is because in the X = H and Y ≠ H case there are other substituents present in many of the structures. With the mono *para* substituted case the ring with no *para* substituent is quite often a phenyl group with no other substituents attached. If a group is attached to a six-member aromatic ring then it is a biphenyl and it will be searched for and found in this analysis. This seems obvious but it is worth noting because it accounts for many biphenyls with one ring substituted and the other completely unsubstituted.

A similar case also occurs with the two *para* substituted case, X ≠ H, Y ≠ H, where the distances are shorter than the mono *para* substituted ring. This is due to the di-substituted *para* structures having a larger number of *ortho* and *meta* substituents compared to the mono *para* substituted case. A representation of the bond lengths of substituted biphenyls is given in Table 13.1 and Figures 13.3a, 13.3b, and 13.3c.

Intra Ring bond	0 *para* X = Y = H	1 *para*, X = H ≠ Y		2 *para*, X ≠ H ≠ Y
		Ring with no *para*	Ring with *para*	
α	1.392(18)	1.388(18) (α')	1.396(24)	1.394(18)
β	1.395(23)	1.388(18) (β')	1.396(22)	1.388(21)
γ	1.376(19)	1.372(20) (γ')	1.395(23)	1.389(20)
C-C	1.489(17)	1.491(17)		1.490(18)

Table 13.1 Mean bond lengths of *para* substituted biphenyls (All figures in Å).

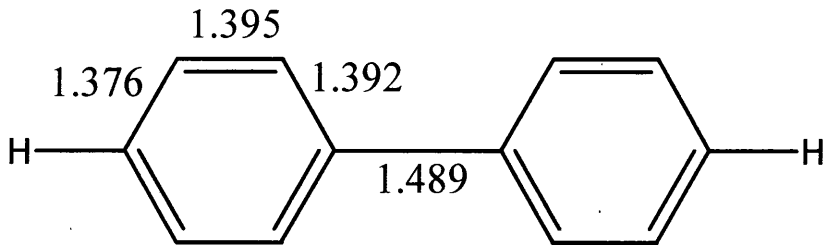

Figure 13.3a Representation of the mean values for non-*para* substituted biphenyls (All figures are in Å)

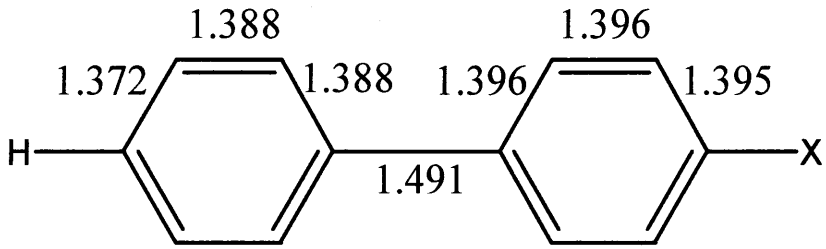

Figure 13.3b Representing the mean values for mono *para* substituted biphenyls (All figures in Å), where X ≠H

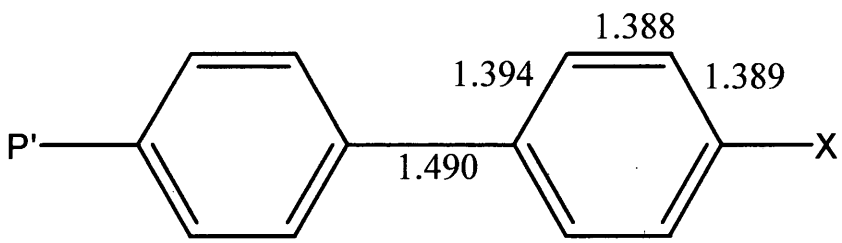

Figure 13.3c Representing the mean values for doubly *para* substituted biphenyls (All figures in Å), where X ≠ H and X' ≠ H (Note X may equal X').

13.6 THE EFFECT OF *META* SUBSTITUTION ON THE INTER RING DISTANCES OF BIPHENYLS

There are five possible ways in which *meta* substitution can occur on the biphenyl rings, either there can be no substitution, one, two, three, or four substitutions. Where there are two *meta* substituents, the substituents can be either on the same ring or one on each of the two rings. In the data search the presence of additional *ortho* and *para* substituents are not considered.

13.6.1 No *meta* substituents present

The average bond lengths when there are no *meta* substituents are very similar to that of biphenyl itself, although they are slightly shorter, this is a result of the different substitution patterns occurring, although they are not taken into account here, see Figure 13.4.

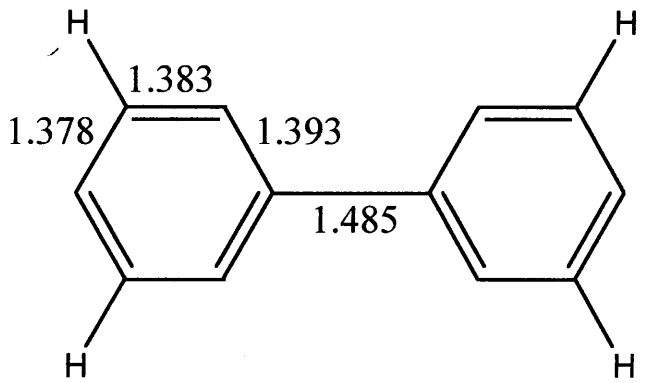

Figure 13.4 Representing the mean values for non-*meta* substituted biphenyls (All figures in Å)

13.6.2 One *meta* substituent present

When there is one *meta* substituent present there are 10 independent bond lengths, (see Figure 13.5). It would be possible to measure 13 bond lengths by taking account of the stereochemistry of the non substituted ring (*cis* or *trans*), however, in this analysis the relative stereochemistry of non-substituted rings are not considered. It can be seen that in the distribution of bond lengths on the ring with one *meta* substituents the bond lengths are similar to when there are no *meta* substituents present on the compound, with both the *o-m* and *m-p* bond lengths slightly longer. For the ring that contains the *meta* substituents the bond distances on the side opposite the *meta* substituent are similar to the non-*meta*

substituted ring, although the intra ring *para* distance is longer (1.397 Å compared to 1.379 Å). On the substituted *meta* side, the bond lengths are significantly longer. This is due to the *meta* substitution and so it is seen that the effect of one *meta* substituent is an increase in the bond lengths of the adjacent bonds, although it must be considered that for many of the structures studied the presence of one *meta* substituent means that the adjacent position may also be occupied.

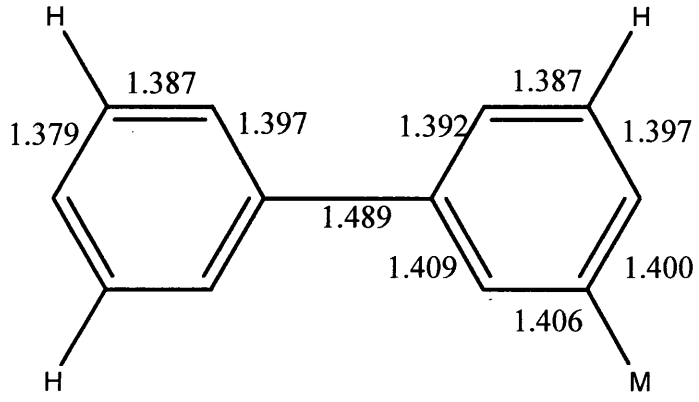

Figure 13.5 Representing the mean values for mono-*meta* substituted biphenyls (All figures in Å)

13.6.3 Two *meta* substituents present

As indicated earlier the di-*meta* substituted biphenyls fall into two categories, those with the substituents on the same ring and those on different rings, see Figures 13.6 and 13.7, with M representing the substituent.

The bond lengths in the two *meta* substituted case with substituents on different rings is similar to those of the substituted ring in the one *meta* substituted case, see 13.6.2. The bond lengths on the *meta* substituted side are slightly longer. So there appear to be a pattern.

When there are two *meta* substituents on the same ring then the bonds on the *meta*-substituted ring are affected in a similar manner. Thus the pattern seen that with a *meta* substituent then α, β and γ bond lengths increase to a similar value, although with the two *meta* substituents on the same ring the value is slightly larger, presumably because of the double effect of the *meta* substituents. It is interesting that the bond lengths on the non-*meta* substituted ring are shorter than the completely non-*meta* substituted compounds.

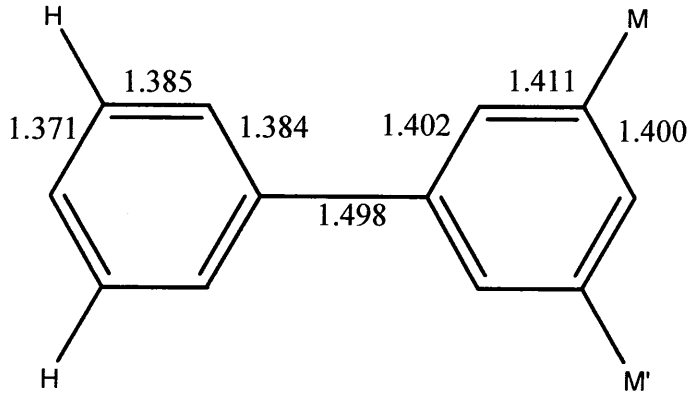

Figure 13.6 Representing the mean values for bi-*meta* substituted biphenyls, with the *meta* substituents on the same ring (All figures in Å)

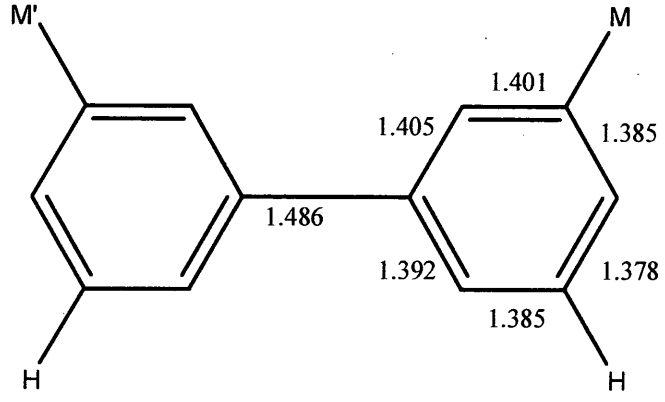

Figure 13.7 Representing the mean values for bi-*meta* substituted biphenyls, with the *meta* substituents on different ring (All figures in Å)

13.6.4 Three *meta* substituents present

If the observed pattern of the *meta* substituents is the same in this case, the doubly substituted ring will have $\alpha \approx 1.40$ Å, $\beta \approx 1.40$ Å and $\gamma \approx 1.39$ Å.

With three *meta* substituents the mono *meta*-substituted ring is similar to the one-substituted rings seen previously, although the value of the γ parameter at 1.369 Å is much shorter than would be expected, see Figure 13.8. The two-substituted ring is very similar to that of the two *meta* on the same ring substituted type and in general, the predicted values occur.

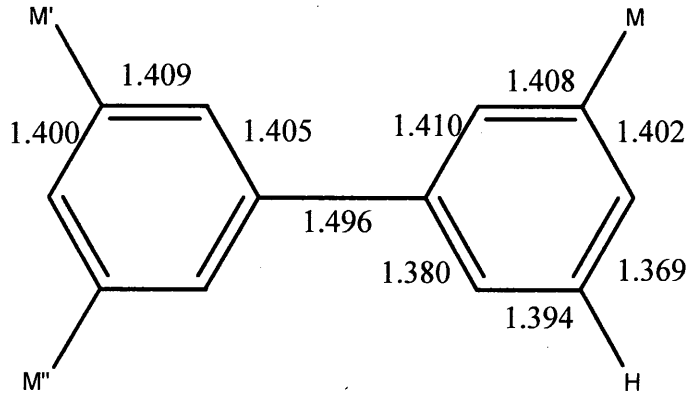

Figure 13.8 Representing the mean values for tri-*meta* substituted biphenyls (All figures in Å)

13.6.5 Four *meta* substituents present

There is a similar pattern to that already seen but there is a subtle difference; the β bond tends to be longer and the γ and α lengths tend to be shorter than the average with two *meta* substituents. There are a large number of structures with four *meta* substituents and no others, this could be a reason for this bond length pattern. This difference is slight and in general these values are as expected.

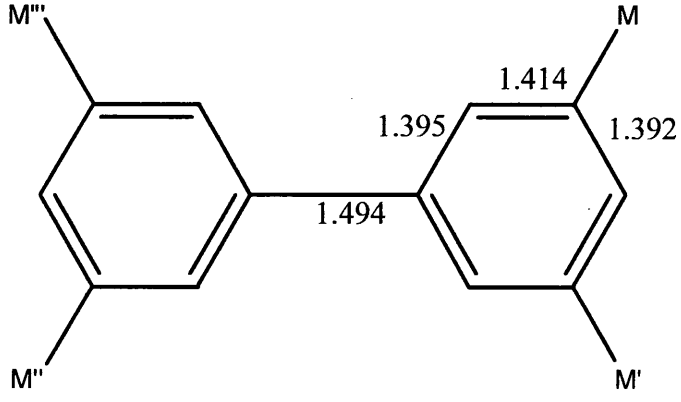

Figure 13.9 Representing the mean values for tetra-*meta* substituted biphenyls (All figures in Å)

13.6.6 Summary of structures with *meta* substituents present

The C-C bond lengths in all these cases are very similar although there are slight difference between them, and the C-C bond length tends to increase slightly as there are more *meta* substituents. This is probably due to the fact that an increase in the *meta* substitution of a structure tends to increase the *ortho* substituents present. The lengths of the bonds increase when there are *meta* substituents present. This lengthening occurs on the side where the substitution occurs and when there is one *meta* on each side this tends to make the length on each side of the ring longer. Thus *meta* substituents have an effect on the system and it is possible to predict these bond lengths. This is in contrast to that which occurs when *para* substituents are present. Tables 13.2 and 13.3 give the list of biphenyls with *meta* substituents bond lengths with standard deviation.

	Bond Lengths (Å)		
	Ipso-ortho	*Ortho-meta*	*Meta-para*
Biphenyl with no *meta* substituents	1.393(14)	1.383(16)	1.378(18)
Biphenyl with four *meta* substituents	1.395(24)	1.414(30)	1.392(23)

Table 13.2 The average bond lengths of the symmetrically substituted *meta* biphenyls with zero and four substituents.

Meta substituted biphenyls	ring with 0 *meta* substituents			ring with 1 *meta* substituent on the same side as the substituent			ring with 1 *meta* substituent on the opposite side as the substituent		
	i-o	*o-m*	*m-p*	*i-o*	*o-m*	*m-p*	*i-o*	*o-m*	*m-p*
1 *meta*	1.394 (14)	1.387 (14)	1.379 (14)	1.409 (20)	1.406 (20)	1.400 (19)	1.392 (17)	1.387 (17)	1.397 (21)
2 *meta* (on different ring)				1.405 (17)	1.401 (20)	1.385 (19)	1.392 (15)	1.385 (19)	1.378 (20)
				ring with 2 *meta* substituents					
2 *meta* (on same ring)	1.384 (14)	1.385 (16)	1.371 (22)	1.402 (24)	1.411 (26)	1.400 (26)			
	ring with 2 *meta* substituents			ring with 1 *meta* substituent on the same side as the substituent			ring with 1 *meta* substituent on the opposite side as the substituent		
3 *meta*	1.405 (25)	1.409 (19)	1.400 (23)	1.410 (21)	1.408 (23)	1.402 (18)	1.380 (14)	1.394 (14)	1.369 (19)

Table 13.3 The average bond lengths of the asymmetrically substituted biphenyls.

13.7 THE EFFECT OF *ORTHO* SUBSTITUTION ON THE INTRA BOND LENGTHS OF BIPHENYLS

The permutation in which *ortho* substituents bond to biphenyl is similar to that of the *meta* substituents, so there are five possible ways in which the *ortho* substituents can bond. The main difference is the closer proximity of the *ortho* substituents to one another: if more than one is present, this creates a scenario where there can be a steric interaction between the *ortho* substituents. The steric effects of the substituents, intra-molecularly, may affect the subsequent bond distances of the biphenyl rings, especially the C-C link and the intra ring α bond.

What is seen by the analysis is that the average for the C-C link does indeed increase when *ortho* substituents are added, although this increase is relatively small, and ranges from 1.486 Å for no *ortho* substituents to 1.495 Å for three. The bonds for the di-*ortho*-substituted biphenyls are an anomaly. The two substituents on the same ring result in an average C-C bond distance of 1.498 Å, which is the largest of all the cases investigated so far and the C-C bond distance for substituents on the different rings may be as low as the non-*ortho* substituted case at 1.486 Å. What is happening here is that with two substituents on the same ring there is a distinct lack of any intra molecular interaction between *ortho* substituents. For the case when substituents are on the opposite rings there is a large number of these structures involved in intra molecular *ortho* interaction it will generally be between only two in the three *ortho* substituted case and therefore the other *ortho* substituent will tend to repel the other ring. For the same reason the lengths of the three substituents are slightly greater than that for the four substituents For four substitutions there is a likelihood that all four will be involved in intra-molecular interaction.

For the other bonds within the ring there is a similar pattern to that which is seen when adding the *meta* substituents. The lengths of all the bonds on the same side increases, although the γ bond is not affected as much as with the *meta* case because of the distance separating the bonds.

13.8 OTHER RING SUBSTITUTION

Often where one ring is more substituted the comparison between the lengths with the non *para* substituted ring is useful as it shows how often the lengths are the same. Comparing the results here to the case when there are *ortho*, *meta* and *para* substituents on the ring, shows just how much the addition of substituents affects the bond distances in the ring. The bond lengths in the substituted case are all greater by approximately 0.03 Å, this is a small but significant difference. In comparison the linkage bond does not greatly change in any cases.

The addition of just one substituent onto the ring shows just how much an effect these substituents. It can be seen in the *ortho* and *meta* cases there is an increase in the adjacent bond lengths, and in both cases the β bond on the opposite side to the substituent decreases in length to a value lower than that of the hydrogen only case. A *meta* substituent affects the adjacent bonds resulting in an increase in length, but the adjacent γ bond length increases to more than the *para* substituted case with 1.398 Å compared to 1.383 Å respectively. This means that the addition of the *meta* substituent has a substantial effect, the ring becomes distorted and the bond lengths differ to a greater extent. The *para* substituent has an effect on the α bond, with the length increasing from 1.382 Å in the non bonded ring, to 1.391 Å. This is interesting given the *para* effect on the *o-o'*-substituted biphenyls, since the increase in the α bond length will lower the energy barrier between the two conformations without adding any steric hindrance and increase the chances of the conformation being able to adopt an energy minimum *via* rotation.

To see the combined effect of substitution on the rings, a search was carried out on the combinations of two substituents per ring. The results are as expected, *i.e.* with the addition of substituents there is an increase on the adjacent bond lengths within the ring. It is noticeable in the *para/ortho* and *para/meta* cases that the ring distances are much more similar with 0.009 and 0.006 Å difference between the bond lengths, respectively. The similarity in these bond distances will make the system within the ring more aromatic, although the C-C bond distances are similar it is only a small increase in aromaticity within the system. It is noticeable that when the *para* substituent is present there would seem to be an effect on the ring in a way that equalizes the bond distances and so therefore must increase the aromaticity of the ring itself.

13.9 SUMMARY AND CONCLUSION

From this study of bond lengths, it is observed that much of the phenomena are directly related to *para* substitution and to the related effects, which are to;

a) even up the *intra*-bond lengths and therefore make the system more aromatic,
b) generally increasing the *intra*-ring *ipso-ortho* bond length, α, and lower the barrier to rotation.

This may be due to the *para* substituents allowing more electron movement in the system, *i.e.* with the addition of *para* substituents the ring, and the structure, become more aromatic and consequently become planar. P*ara* substitution has an effect on the bond lengths, albeit not a great one and this can explain why *para* substituted biphenyls often act conformationally in the same manner as the parent biphenyl compound. How this effects the packing of the *o,o'*-substituted biphenyls needs to be investigated. The barrier to rotation will be smaller with *para* substituents. If an effect of the *para* substituent is to increase the length of the α bond, then when the compound is crystallizing, the structure will be able to adopt a more suitable conformation for packing and any slight attractive or repulsive forces will then have an influence on the crystal structure of the compound. This does not fully explain why *cis* is preferred to *trans* but it does give an explanation as to why the conformation in the solid state can differ from the gas phase.
It is believed that the effect of *para* substitution on the bond lengths of biphenyls gives an indication as to why *o,o'*-biphenyls have the predominantly *cis* conformation (Chapter 10) and show non-adherence to the "Structure Correlation Method" (Chapter 11) as well as general conformational anomalies of biphenyl (chapter 12).
Meta substitution tends to have the effect of make the rings more distorted. The effect of *meta* substitution is also an important, although less dramatic, factor. The *meta* substituents act almost in an opposite manner to the addition of *para* substitution, i.e. they have little effect on the α bond and they make the bond lengths unequal and therefore decrease the aromaticity of the ring. This can be seen in seen chapters 10, 11 and 12.

The reason for the effect of *para* and *meta* substitution twisting effect is not entirely clear, but one explanation relates to the symmetry of the substitution. The phenyl ring has a substituent in the form of the other phenyl ring which distorts both of the rings slightly, but when there is a *para* substituent this has the same effect on the opposite side of the ring. Since this is symmetrical it has the effect of equalising the bond distances of the ring and therefore increasing the aromaticity of the rings. In the same manner *meta* has an unsymmetrical effect on the ring of the substituted phenyl group. This does not explain why

the average α bond length also increases with *para* substitution but this may be due to the types of groups associated with the *para* position. A group attached to the *para* position effects the *meta-para* bond lengths, but the extent depends on the type of substituent, and it will have a greater effect on these bond lengths compared to a phenyl group. The *ipso-ortho* bonds may compensate for this and increase slightly in length to retain a level of aromaticity and symmetry.

Since this analysis is using the database and is therefore statistical, initially no account was taken for different types of substitutional groups (*i.e.* electron withdrawing/donating groups, charged groups, steric factors, *etc*) at the *meta* and *para* positions. Closer inspection of the types of groups involved shows that no specific type predominates any specific stereochemistry, and indeed the distribution for different stereochemistries has a large range of substitutional types attached. So any electronic effect effecting the data is not obvious and must therefore be more subtle than substitutional effects.

Studies into Non Linear Optics and Liquid Crystals often use biphenyl structures and these studies often investigate the electronic properties. These structures and properties that may have a bearing on the structures analysed in this study.

In conclusion, in this chapter it has been shown that *para* substitution affects the ring differently from *meta*, which manifests itself in the effects seen in chapters 10-12. A possible explanation of the conformational effect of these substituents in terms of effecting the bond lengths has also been given.

13.10 REFERENCES

1. Brock, C. P.; Minton, R. P. *J. Am. Chem. Soc.*, **1989**, *111*, 4586.
2. Hargreaves, A.; Rizvi, S. H. *Acta Cryst.*, **1962**, 15, 365.
3. Lide, D. R. (Ed), *Handbook of Chemistry and Physics*, **1995**, CRC Press.
4. Roberts, R. M. G. *Magn. Res. Chem.*, **1985**, 23, 52.
5. Trotter, T.; *Acta Cryst.*, **1961**, 14, 1135.

CHAPTER 14:

AN INTRODUCTION TO CARBABORANES

14.1 INTRODUCTION

Borane hydrides and carbaboranes, which are commonly referred to as carboranes, are classified as being cluster compounds. The use of the term cluster compounds covers a variety of different types of compounds. Other cluster compounds range from homonuclear charged or uncharged species such as Buckminsterfullerenes (e.g. C_{60}), to the heteroatomic species like the boron hydrides (e.g. $B_6H_6^{2-}$). These boron hydrides where there is a central core of boron atoms surrounded by bound hydrogen atoms are the types of compounds that are discussed in this and subsequent chapters. A large number of cluster compounds are electron deficient species and the bonding is different to the valency model and popular convention. Study of these types of compounds has increased the knowledge and general understanding of bonding in such compounds and their use has created many novel and unusual molecular architectures.

In this thesis the study of these types of compounds has concentrated on the icosahedral carboranes, $C_2B_{10}H_{12}$, and derivative compounds. The following chapter will give an introduction and overview of the interesting peculiarities of this group of compounds, discussing their history and what has led to the development of the field of study, and the understanding of their structures and bonding. Their properties and many applications are also reviewed, in section 14.5. This chapter will give an overview of this class of compounds to show the vast applications but will not thoroughly examine the chemistry or give fine detail of the theory involved.

14.2 THE BONDING OF BORON HYDRIDE CLUSTERS

The first synthesis of these types of compounds was between 1912 and 1936 by A. Stock. He made and isolated many different boron hydrides, including those of formulae B_2H_6, B_4H_{10}, B_5H_9, B_5H_{11}, B_6H_{10} and $B_{10}H_{14}$, ((Stock, 1933) & (Cross, 1993)), see Equation 14.1.

$$MgB_2 + HCl \rightarrow B_4H_{10}, B_5H_9, B_5H_{11}, B_6H_{10}, B_{10}H_{14}$$
$$3NaBH_4 + 4BF_3.OEt_2 \rightarrow 2B_2H_6 + 3NaBF_4 \qquad \text{Equation 14.1}$$

Stock knew the molecular formulae of these compounds but did not know much about the structures, since the then current bonding theories would not give reasonable models based on the formulae. The structure of diborane was later deduced by Longuet-Higgins (Longuet-Higgins, 1949) and through the concept of three-centre-two-electron (3c2e) bonds and the extension of this idea from Lipscomb, the bonding of diborane, B_2H_6, could be rationalised. In understanding the bonding of these compounds the use of (3c2e) bonds has to be accepted and this rationalises the bonding in dicarba-*closo*-dodecaborane, with an electron pair being shared between three atoms. The cluster structure permits the maximum use of 3c2e bonds, and so gives the most efficient distribution of electron pairs. Thus when examining the atoms contained in these cages, it is worth remembering that the edges of the carborane polyhedra shown in this thesis do not represent formal bonds. They merely represent connectivities, with the two distance between the two atoms being smaller than the combined van der Waals radii of the two atoms.

The simplest such compound, and easiest to describe, is diborane, B_2H_6. Each boron atom donates two of its three electrons to form σ-bonds with two terminal protons. This leaves each boron atom with two orbitals and one electron. The two boron atoms and two bridging hydrogen atoms use four electrons (one from each boron, one from each hydrogen) and six orbitals (two from each boron atom, one from each hydrogen) to form two bonds (see Figure 14.1).

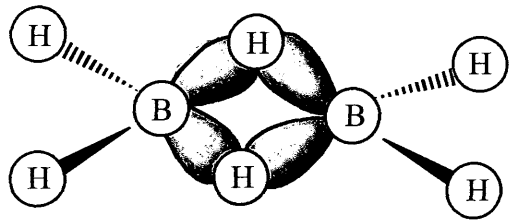

Figure 14.1 The bonding in diborane

The electron density in these boron hydrides and similar types of structures is delocalised, so they can be portrayed in terms of molecular orbitals. Each cage boron atom is attached to one hydrogen atom by an *exo* bond radially outwards. Each boron atom is *sp* hybridised, with one *sp* hybrid orbital used in bonding to a hydrogen atom and the other *sp* hybrid, along with the two unhybridised *p* orbitals involved in cluster bonding (Cotton and Wilkinson, 1988). Thus each boron uses one electron in *exo* bonding to the hydrogen atoms, and contributes the other two to cluster bonding.

The structures of these polyhedral compounds are determined by the number of electrons involved in cluster bonding. The number of vertices of the polyhedron (each occupied by a cluster atom) will be one less than the number of electron pairs participating in cluster bonding (Wade, 1976). This arrangement results in all the molecular orbital bonding levels being filled within the structure. The delocalised nature of the bonding in these clusters causes them to behave, in many respects, like organic aromatic compounds, and they are often considered to have 3-dimensional 'pseudo-aromatic' character.

With the removal of a BH unit from the cluster, whilst its cluster bonding electrons remain behind, i.e. it is removed as a BH^{2+} fragment, then the resultant new cluster will have the same electronic structure as the original but will have one vertex missing (see Figure 14.2).

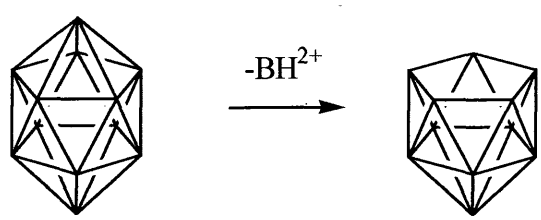

Figure 14.2 The removal of a BH^{2+} vertex

The term 'carborane' is used to describe mixed hydrides of boron and carbon where the polyhedral boron skeleton contains at least one carbon atom. There is a large variety of different carboranes and many have well documented derivative chemistries (Grimes, 1970). Unmarked carborane cage vertices represent BH units, see Figures 14.2 to 14.4. The CH fragments are identified. In this thesis it is carboranes rather than pure boron hydrides that are examined.

A structure in which every vertex is occupied is known as *closo* (meaning 'cage-like'), with a single vertex unoccupied known as *nido* ('nest-like'), and one with two unoccupied vertices this is known as *arachno* ('web-like'). A vertex atom may be replaced by another atom, whilst retaining the cluster structure, providing that the number of atomic orbitals and cluster-bonding electrons remain the same. A BH^- unit may be replaced by an isoelectronic CH (or CR) unit, giving rise to families of structurally similar, isoelectronic clusters (Figure 14.3) When carbon atoms are contained within the cage the structure is called a carbaborane, which is commonly referred to as a carborane.

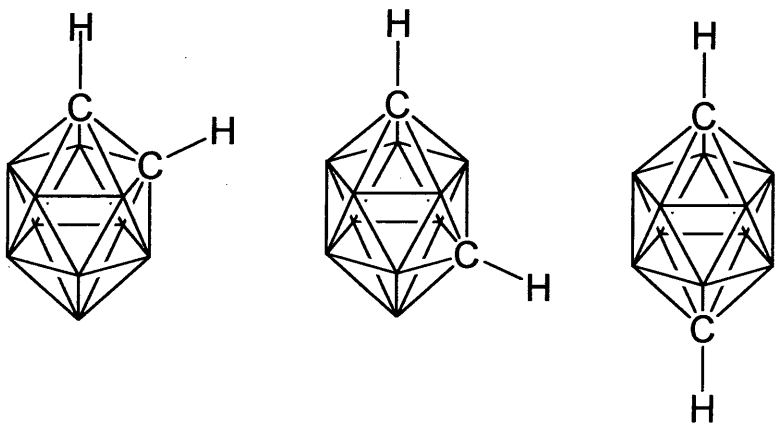

Figure 14.3 The isomers of $B_{10}C_2H_{12}$. a = *ortho*, b = *meta* and c = *para*

Boron hydrides (and carboranes) are deltahedral fragments, originating from a closed deltahedron, i.e. all the faces are triangular. For example, the *arachno* species, decaborane, $B_{10}H_{14}^{2-}$, can be viewed as a fragment of *nido*-$B_{11}H_{12}^-$, which is in turn a fragment of the parent deltahedral icosahedron dodecaborane, *closo*- $B_{12}H_{12}$.

14.3 THE ELECTRONIC DISTRIBUTION

When the polyhedral structures are closed, the electrons occupy the skeletal bonding orbitals, this effectively forms a pseudo-spherical distribution of electron density over the atoms which are relatively evenly spread over the deltahedral surfaces defining the twelve vertex icosahedron (see Figure 14.3). However when heteroatoms, such as carbon, are incorporated into the cage structure, the electron distribution is necessarily altered.

The hydrogen atoms attached to the carbon sites of the carborane are more electropositive (acidic) than the boron-attached hydrogen atoms. It is for this reason that when a metallating reagent is introduced to the parent carborane compound, $C_2B_{10}H_{12}$, the protons of the carbon atoms, being the most acidic, are metallated preferentially. Following this reasoning, the boron atom of the BH vertex most highly connected to a CR (R=H, alkyl or aryl) vertex is the most electropositive boron, and this explains its preferential removal by a strong nucleophile during deboronation reactions. The twelve vertex "B_{12}" icosahedron has maximum symmetry (I_h), but as the icosahedron is altered to incorporate heteroatoms, two carbons in the case of the icosahedral carboranes, $C_2B_{10}H_{12}$, the cage symmetry is reduced. The differing electronegativities of the cluster atoms leads to distortions in the cage geometry and as a result to a redistribution of electron density. As the carbon atoms are further substituted, the distortions increase, the nature of which is dependent upon the specific substituent. Modern X-ray diffraction analysis allows these distortions to be quantified. Using diffraction data it is possible to get all the B-B and B-C distances and angles in the cage, as well as to define accurately the substituents present. It is only with diffraction data that inter and intra-molecular interactions can be completely determined.

14.4 NOMENCLATURE

A standard nomenclature concerning carboranes is important since there can be a reasonably large number of atoms in the structures and the three dimensional cage geometry can be rather confusing.

When discussing these systems in this thesis, it is in reference to the 12-vertex-*closo*, 11-vertex-*nido* and 10-*arachno* (11-vertex *nido* with the 11th vertex missing) species. The nomenclature for these systems is different for each type of cage. The amount by which the cage is opened is described by a prefix *closo*, *nido*, *arachno* or *hypho* as in Table 14.1. In the borane and carborane structures, an apical atom is labeled atom 1. Successive belts of cage atoms are numbered in a clockwise manner, with carbon atoms having a numbering priority over boron vertices (see Figure 14.4)

Structure Type	Number of Skeletal Electron Pairs
Closo (Cage-Like)	n+1
Nido (Nest-Like)	n+2
Arachno (Web-Like)	n+3
Hypho (Net-Like)	n+4

Table 14.1 The cage structure types and related number of skeletal electron pairs

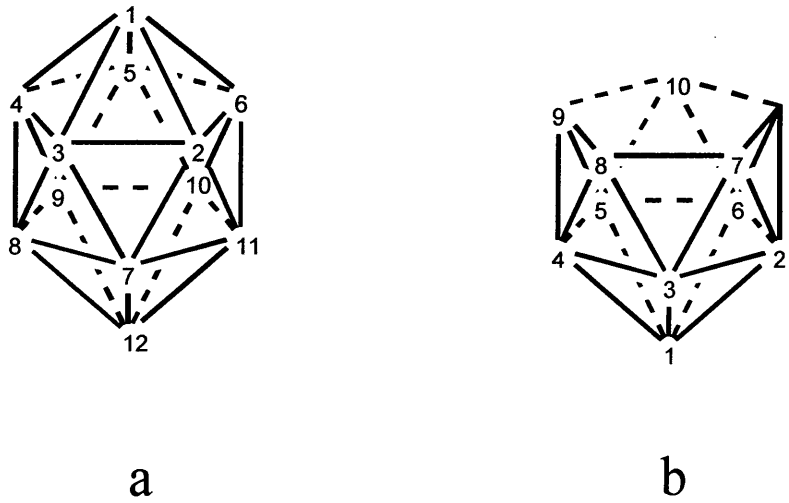

Figure 14.4 The numbering scheme of boron hydride cages, with a = the *closo* cage and b = *nido*.

14.5 PROPERTIES OF CARBORANES

Neutral carboranes containing two carbon atoms are derived from the polyhedral boron hydride species, $B_nH_n^{2-}$, and have the general formula $C_2B_nH_{(n+2)}$ (n=5-12). The carborane of interest in this thesis is dicarbadodecaborane, $C_2B_{10}H_{12}$, and derivatives thereof, which exists as an icosahedron with twenty deltahedral faces. The connectivities which would illustrate a two-centre two-electron bond in a "normal" compound herein are not indicative of a formal bond. They simply illustrate the shape and connectivities within the cluster for visual convenience.

During the 1960's boron hydrides were investigated as potential rocket fuels, due to their being pyrophoric and then having a very high heat of combustion (the B=O bond is extremely strong). Decaborane, $B_{10}H_{14}$, was produced on a multi-ton scale for the investigation into this and the icosahedral carboranes $C_2B_{10}H_{12}$ are readily accessible from decaborane. Boron hydrides proved to be unusable for rocket fuels and research in this area was abandoned relatively quickly although an interest in the chemistry was retained. The carboranes can undergo substitution reactions at cage carbon and boron sites without cage degradation occurring. The predominant feature of carboranes is that they have remarkable chemical and thermal stability: *ortho*carborane is stable up to 400°C and retains its structure in the presence of oxidising agents, alcohols and strong acids. However, above 400°C isomerisation can occur to the *meta* and then the *para*-isomer. The *ortho* to *meta* transformation is quantitative at 460°C and at 620°C isomerisation to *para*carborane occurs, but this has a tendency to be inefficient. Various mechanisms have been postulated for the rearrangement ((Wu and Jones, 1989), (Edvenson and Gaines, 1990), (Wales, 1993) and (Johnson and Roberts, 1993; 1994)) including diamond square-diamond, rotation of a triangular face and rotation of two pentagonal faces. The driving force for the isomerisation is proposed to be the reduction in the overall dipole of the carborane upon increased separation of the carbon atoms.

The reverse isomerisation from *meta* to *ortho*-carborane has also been achieved and this is done by isomerisation of the *meta*-carboranyl dianion, followed by oxidation of the *ortho*-carborane dianion to the neutral close species (Zakharkin *et al.*, 1967). The carborane cage has strong electron withdrawing effects and tends to "pull" any available electron density into its delocalised electronic system. This electron-withdrawing effect decreases as the isomers are progressed from *ortho* through to *para*, in both the *closo* and *nido* species.

Pyrolysis of carborane (or boron hydrides) containing polymers often leads to the formation of thermally stable coatings (Packerisamy *et al.*, 995) and ceramic materials ((Bucca and Keller, 1997) and (Sneddon *et al.*, 1991)). As carborane compounds contain essential elements for the

formation of thin boron carbide films, they have potential as source materials for chemical vapour deposition technique (Hitchcock *et al.*, 1997).

Boron compounds have found application in the field of medicine as a treatment for tumours. Boron Neutron Capture Therapy relies upon the decay of the $^{10}_{5}B$ nucleus when bombarded with a neutron, to give an *in situ* dose of radiation to the tumour. Compounds with a high boron content which are stable under physiological conditions and which have tumour targeting selectivity are required for this treatment, and much effort is being expended in this field (e.g. Dahlhoff *et al.*, 1993). The synthesis of compounds which have a large difference between the ground and excited state dipole moments, which are not highly coloured, and which crystallise in a non-centrosymmetric space group leads to materials which are of interest in the field of non-linear optics. Derivatives of *ortho*-carborane and other carborane isomers have been investigated as potential non-linear optical materials (Murphy *et al.*, 1993).

Unlike many salts of organic and inorganic acids, salts of polyborates dissolve readily in organic solvents. This allows their extraction from the aqueous to the organic phase. Using this principle, metallacarboranes of the type $[(C_2B_9H_{11})_2\text{-}3\text{-}M^{III})]^-$ have been used to aid the extraction of metals including radionuclides from spent nuclear fuels (Chetcuti *et al.*, 1995).

14.6 CARBORANE SYNTHESIS

Ortho-carborane (1,2-dicarbadodecaborane) can be prepared by the reaction of ethyne with Lewis base adducts of decaborane. The *meta* and *para* isomers are usually prepared by thermal isomerisation of *ortho*carborane at 460° C and 620° C respectively (Grafstein and Dvorak, 1963) and (Papetti and Heying, 1964)). This isomerisation occurs because the most thermodynamically stable isomer is the *para* (relative thermodynamic stability is *para* > *meta* > *ortho*), which has been attributed to the minimisation of the dipole moment brought about by separation of the carbon atoms (Olah *et al.*, 1991). The problem with isomerising carboranes possessing organic substituents is that it generally results in decomposition of these substituents (Grafstein and Dvorak, 1963) and (Papetti and Heying, 1964)). Substituted *ortho*carboranes may be prepared by reaction of the appropriately substituted ethyne with $B_{10}H_{14}$ in the presence of a suitable Lewis base.

Substituents can be attached to both the carbon and boron atoms of the cage by several different methods. In this thesis substituents on the boron atom are not encountered and so will not be detailed further. However, typical reactions include chlorination, alkylation, mercuration, oxidation and metallation, and these reactions usually proceed *via* a photochemically induced radical mechanism, or by attack by electrophilic reagents. There has been a considerable amount of study into carbon-substituted clusters, and a huge number derivatives are known. The most common method of preparing these compounds is *via* C-lithiated intermediates. The hydrogens on the cluster carbon atoms are acidic, and so can participate in C-H···X hydrogen bonding.

Nido species can be prepared by selective removal of a BH^{2+} unit from a *closo-ortho* or *meta*carborane, by a process commonly called 'deboronation' (this is also possible for *para*carborane, but the conditions are very forcing and little studied). The most widely used reagent for deboronation is KOH dissolved in either MeOH or EtOH, giving the appropriate alkoxide ion.

14.7 APPLICATIONS OF CARBORANES

There has been a lot of interest in icosahedral carboranes concerning their application to polymers and there are a large range of carborane-containing polymers already known, e.g. polyesters (Lebedev *et al.*, 1974), polyazomethines (Rabilloud *et al.*, 1990) and polysiloxanes (Heying *et al.*, 1968) known under the trade name 'Dexsil'.

The incorporation of carborane units (usually *ortho* or *meta*) into the silicone polymers greatly increases their thermal stability (Finch, 1970), particularly at high temperatures (450° C), and lead to a large reduction in loss of mass through degradation at high temperatures. Hydrogen elimination from carborane BH bonds, at high temperature, can lead to the formation of crosslinking bonds (Stanko *et al.*, 1977) which gives the prospect of high-performance ceramic materials (Kabachi and Valetskii, 1990). Carborane polymers are used in such diverse applications as high temperature fittings, oils, adhesives and fire retardants.

Carborane derivatives have a potential application in the use of metallacarboranes as catalysts. Metallacarboranes, have been the subject of intense study since the 1960's (Zakharkin *et al*, 1965; 1967; 1972; 1973).

14.8 CARBORANES IN THIS THESIS

As already mentioned in this chapter, the carboranes in this thesis are mostly of the *closo* type. Carboranes, or at least those in this thesis, do not tend to form regular crystals, with multiple twinning a common occurrence, and often the X-ray diffraction experiment involves the laborious task of sampling many possible candidate crystals until an adequate one has been found. Often the carboranes are air or moisture sensitive and so data collection and preparation are conducted using the appropriate equipment and procedures, see chapter 2.

The carboranes in this thesis have varied applications and properties but are linked *via* their association with hydrogen bonding and inter- and/or intra-molecular interactions, with the exception of those in chapter 17, which are examined because of their non hydrogen bonding properties.

14.9 REFERENCES

1. Bresadola, S. in *"Metal Interactions with Boron Clusters"*, ed. Grimes, R. N., **1982**, Plenum Press, New York, 175.
2. Bucca, D.; Keller, T. M., *J. Polymer Science A, Polym. Chem.*, **1997**, 35, 1033.
3. Chetcuti, P. A.; Hofherr, W.; Liégard, A.; Rihs, G.; Rist, G., *Organometallics*, **1995**, 14, 666.
4. Cotton, F. A.; Wilinson, G., *Advanced Inorganic Chemistry, Fifth Ed.*, Wiley-Interscience. John Wiley & Sons, New York Edvenson, G. M.; Gaines, D. F., *Inorg. Chem.*, **1990**, 29, 1210.
5. Grimes, R. N., *Carboranes*, **1970**, Academic Press, New York.
6. Finch, R. W., *Analabs Research Notes*, **1970**, 3, 10.
7. Grafstein, D.; Dvorak, J., *Inorg. Chem.*, **1963**, 2, 1128.
8. Heying, T. L.; Papetti, S.; Schaffling, O. G., U.S. Patent, **1968,** 3388, 090,.
9. Hitchcock, A. P.; Urquhart, S. G.; Wen, A. T.; Kilcoyne, A. L. D.; Tyliszczak, T.; Rühl, E; Kosugi, N.; Bosek, J. D.; Spencer, J. T.; M^{c}Ilroy, D. N.; Dowben, J., *J. Phys. Chem. B*, **1997**, 101, 3483.
10. Johnson, B. F. G.; Roberts, Y. V.; Parsini, E., *Inorganica Chem. Acta*, **1993**, 115, 1557.
11. Johnson, B. F. G.; Roberts, Y. V., *J. Chem. Soc.,Dalton Trans.*, **1994**, 759.
12. Lebedev, V. P.; Babchinister, T. M.; Bekasova, N. I.; Komarova, L. G.; Tsvankin, D. Y.; Korshak, V. V., *Vysokamol. Soedin. Ser. A*, **1974**, 16, 987.
13. Longuet-Higgins, H. C., *J. Chem. Phys.*, **1949**, 46, 275.
14. Murphy, D. M.; Mingos, D. M. P.; Forward, J.M. *J. Mater.Chem.*, **1993**, 3, 139.
15. Murphy, D. M.; Mingos, D. M. P.; Haggitt, J.L.; Powell, H. R.; Westcott, S.A.; Marder, T. B.; Taylor, N. J.; Kanis, D. R., *J. Mater.Chem.*, **1993**, 3, 139
16. Olah, G. A.; Wade, K.; Williams, R. E., **1991**, John Wiley & Sons, New York.
17. Packirisamy, S.; Schwam, D.; Litt, M. H., *Material Science*, **1995**, 30, 308.
18. Papetti, S.; Heying, T. L., *J. Am, Chem, Soc.*, **1964**, 86, 2295.
19. Rabilloud, G.; Sillion, B., *Eur. Polym. J.*, **1990**, 26, 967.
20. Sneddon, L. G.; Mirabelli, M. G. L.; Lynch, A. T.; Fazen, P. J.; Su, K.; Beck, J. S., *Pure and Appl. Chem.*, **1991**, 63, 407.
21. Stanko, V. I.; Valetskii, P. M.; Klimova, A. I.; Klimova, T. P., *Gen, Chem. USSR*, **1977**, 47, 369.
22. Wade, K., *Adv. Inorg. Chem. Radiochem.*, **1976**, 18, 1.

23. Wales, D. J., *J. Am. Chem. Soc.*, **1993**, 115, 1557.

24. Wu, S. –H.; Jones Jnr, J., *J. Am. Chem. Soc.*, **1989**, 111, 5373.

25. Yu, A. Kabachii; Valetskii, P. M., *Intern. J. Polymeric Mater.*, **1990**, 14, 9.

26. Zakharkin, L. I.; Bregadze, V. I.; Okhlobstin, O. Y., *J. Organomet. Chem.*, **1965**, 4, 211.

27. Zakharkin, L. I.; Kalinin, V. N.; Podvisotskaya, L.S., *Bull. Acad. Sci. USSR*, **1967**, 2212.

28. Zakharkin, L. I.; Kalinin, V. N.; Rys, E. G., *Zh. Obsch,. Khim.*, **1972**, 42, 477.

29. Zakharkin, L. I.; Kalinin, V. N.; Rys, E. G., *Zh. Obsch,. Khim.*, **1973**, 43, 847.

CHAPTER 15:

DEFINITIVE CRYSTAL STRUCTURES OF *ORTHO*, *META* AND *PARA* CARBORANES: SUPRAMOLECULAR STRUCTURES DIRECTED SOLELY BY C-H···O HYDROGEN BONDING.

15.1 INTRODUCTION

This study involves the analysis of three similar carborane cages with an interaction between the C-H units and an hexamethylphosphoramide (HMPA) molecule. The study relies mostly on X-ray diffraction analysis for full characterization but also incorporates the use of some other analytical techniques, (e.g. NMR, IR, *etcetera*). The co-crystallisation of *ortho*, *meta* and *para* carboranes with HMPA results in the isolation of 1:1 carborane: HMPA adducts which provide the first definitive X-ray diffraction analysis of the unsubstituted carboranes as part of three very different C-H···O hydrogen-bonded supramolecular structures.

The study of the supramolecular structure of solids is currently undergoing a great deal of intensive research (Desiraju, 1995) in general chemistry and not just in the crystallographic world (although crystallography has a particular association because of its ability to give defining structural analyses). Primarily it is hoped and expected to be able to predict and control the supramolecular structure of a large number of organic solids (Aakeröy and Seddon, 1993) by consideration of the molecular units employed, this is commonly referred to as crystal engineering, and this will provide an ingredient into the designing of optically and electronically active organic solids. The major factor that drives the assembly of a particular supramolecular structure in organic compounds is commonly inter-molecular interaction and in particular that of "hydrogen bonding" has been shown to be extremely influential. A strategy that has been employed to elucidate the molecular factors that govern supramolecular structure is to co-crystallise two or more components that possess potential hydrogen-bonding functional groups and to compare structures in which the orientation of these groups has been systematically varied at the molecular level (Etter and Reutzel, 1991).

While this approach has been successful for a number of the "strong" hydrogen-bonded systems e.g. X···H-Y (X, Y = N, O), its application to weaker C-H···X interactions has been far more limited, mainly because they are weak. In recognizing the high C-H acidity of carboranes ((Grimes, 1970) & (Onak, 1995)) and therefore their potential for hydrogen bonding (Leites, 1992), and the ready availability of *ortho*, *meta* and *para* derivatives, which possess C-H groups in well defined but differing orientations within the same pseudo-spherical molecular frame-work, it was speculated that the $C_2B_{10}H_{12}$ cluster may be a good molecular unit with which to

apply this strategy to a system containing only C-H···X hydrogen bonds as directors of supramolecular structure. The molecular rigidity and topological versatility of carboranes has already been exploited in other molecular design contexts ((Clegg *et al.*, 1993), (Hawthorne and Mortimer, 1996) & (Armspatch *et al.*, 1996)), a feature of this work was to use the hydrogen bond acceptor to fix the carborane cage in the crystal. It is common for carboranes to have disorder in the cages particularly when the cage has the "freedom" to move or rotate. The C-H units of the structure can easily become disordered with the B-H units, this could be caused by a number of rotations of the cage about the adjacent carbon atom twist (i.e. 180°, 90°, 62°, *etcetera.*) or the cage can be completely disordered at all atom positions. The similarity in electron density between the carbon and boron atoms can be problematic when trying to locate the carbon atoms in the cage, particularly when the C-B and C-C bond distances have become distorted or non-characterisable, usually due to disorder, but also can be due to electronic effects that alter the C-C, C-B and/or B-B distances).

A feature of great importance in this study is that despite having been studied extensively for over 30 years the precise bond lengths and angles for the parent carboranes remain unknown. This is due to disorder of the carborane icosahedron that has been already mentioned.

Previous attempts to get around this problem by substituting the hydrogen atoms the boron or carbon atoms for any R groups have only been partially successful, due to the electron-withdrawing and highly delocalised nature of the cages. This alters the electron density within the cluster and thus all the bond lengths and angles. Gas-phase electron diffraction studies of the three carborane isomers did give individual bond length/bond angle values but the errors on the values were notably larger than typical X-ray diffraction errors, particularly for *ortho-* and *meta-*carborane. It was hoped that the relatively weak C-H···O interactions predicted for carborane/HMPA co-crystals would locate the cluster carbon atoms without the perturbation of the cage, which occurs upon substitution (Davidson *et al*, 1996).

15.2 CHARACTERISATION

15.2.1 Introduction

In this study it was hoped that the HMPA structure would hydrogen bond to the C-H units of the cage and so fixes the cage into a rigid non-disordered structure. This was done by co-crystallising carboranes with hexamethylphosphoramide (HMPA). Slow evaporation of these solutions yielded crystalline solids which were shown by ^{1}H NMR to contain carborane and HMPA in a 1:1 stoichiometry (the presence of an excess of HMPA in solution was found not to affect the stoichiometry of the solids isolated).

15.2.2 Crystallographic Experiments

For the three carborane adducts studied in this chapter, all the data sets were collected at 150(2) K using the SMART CCD (see Chapter 2), with Mo-Kα radiation (λ = 0.71073 Å).

15.3 PRELIMINARY CHARACTERISATION

15.3.1 *Ortho*carborane / HMPA co-crystallisation

The slow evaporation of the solvent over a period of three days gave a crop of colourless crystals, of *ortho*carborane and HMPA.

15.3.1.a Infra Red Spectroscopy

The solid state IR spectrum of these crystals showed that they contained both *ortho*carborane and HMPA. However, the C-H stretching frequency of the *ortho*carborane had either disappeared or shifted to below 3000 cm^{-1}, and thus been subsumed by the C-H absorptions (compared to $\bar{\nu}_{max}$ = 3073 cm^{-1} for pure *ortho*carborane).

15.3.1.b NMR

^1H NMR spectroscopy of the crystals in C_6D_6 showed a mixture of *ortho*carborane and HMPA signals (unshifted - the hydrogen bonding is not evidenced in solution), the integrals of which suggested a 1:1 ratio of *ortho*carborane to HMPA. This 1:1 ratio was confirmed by elemental analysis. Subsequent repetition of this reaction using a 2:1 ratio of HMPA to *ortho*carborane gave an identical product (plus unchanged HMPA).

15.3.2 *Meta*carborane/HMPA co-crystallisation

Slow evaporation of the solution, toluene, over a period of 18 hours gave a crop of colourless crystals.

15.3.2.a Infra Red Spectroscopy

The solid state IR spectrum of these crystals showed that they contained both *meta*carborane and HMPA, and again the C-H stretching frequency of the *meta*carborane was absent, with no peaks being present above 3000 cm^{-1} (compared to $\bar{\nu}_{max}$(CH) = 3062 cm^{-1} for pure *meta*carborane), indicating the presence of hydrogen bonding.

15.3.2.b NMR

The ^1H NMR spectrum of the crystals in C_6D_6 showed a mixture of unshifted *meta*carborane and HMPA signals, again integrating to a 1:1 ratio of *meta*carborane to HMPA, which was confirmed by elemental analysis. Repetition of this reaction using a 2:1 ratio of HMPA to *meta*carborane gave an identical product (plus unchanged HMPA). This preliminary characterisation of *meta*carborane suggested close similarity to the *ortho*carborane analogue.

15.3.3 *Para*carborane / HMPA co-crystallisation

Addition of one equivalent of HMPA to one millimole of *para*carborane partially dissolved in toluene, caused complete dissolution of the *para*carborane. Slow evaporation of the toluene solution over a period of 18 hours gave a crop of colourless crystals.

15.3.3.a Infra red Spectroscopy

The solid state IR spectrum showed that they contained both *para*carborane and HMPA, and the C-H stretching frequency of the *para*carborane had either disappeared or shifted to below 3000 cm^{-1}, and thus been subsumed by the C-H absorptions (compared to $\bar{\nu}_{max}$ = 3053 cm^{-1} for pure *para*carborane), indicating the presence of hydrogen bonding.

15.3.3.b NMR

The 1H NMR spectrum of the crystals in C_6D_6 showed a mixture of unshifted *para*carborane and HMPA signals.

15.4 THE X-RAY DIFFRACTION ANALYSIS OF THE *ORTHO*, *META* AND *PARA* CARBORANE MOLECULES WITH HMPA.

15.4.1 *Ortho*carborane

X-ray diffraction studies of the colourless crystals showed a dimeric structure, with C-H···O hydrogen bonds linking the HMPA molecules to two similar but crystallographically distinct *ortho*carborane units (see Figure 15.1). The C-C bond length in *ortho*carborane (av. 1.63 A) is shorter than for structurally characterised substituted *ortho*carboranes, thus providing a quantitative benchmark for the study of the effects of substitution on the structure of carboranes. The packing of this structure is illustrated in Figure 15.2,.

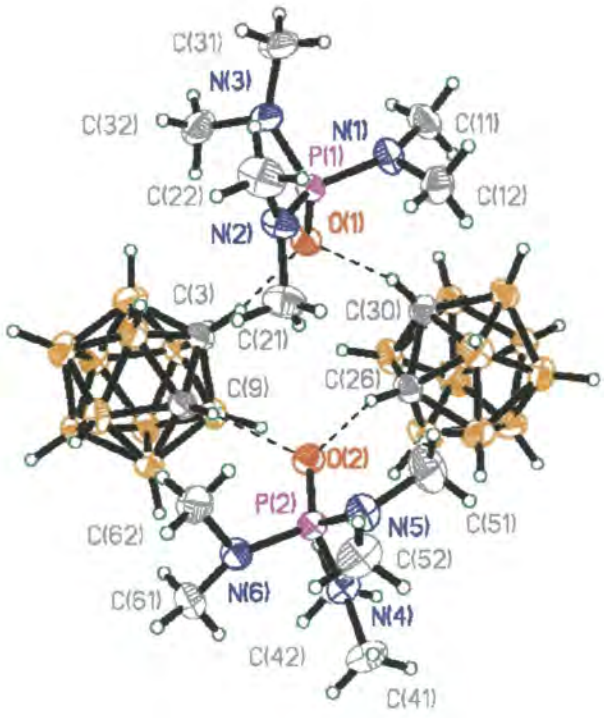

Figure 15.1 Molecular structure of the dimer unit of *ortho*carborane/HMPA, with 50% thermal ellipsoid probability

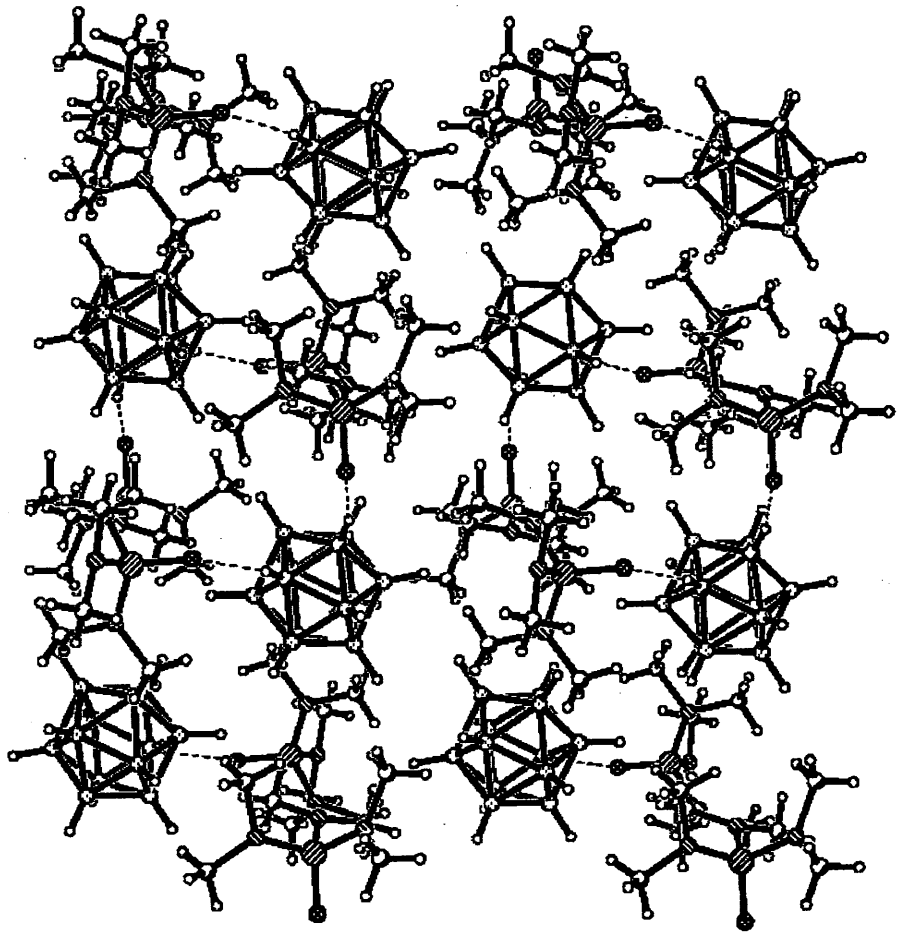

Figure15.2 The packing of *ortho*carborane/HMPA

15.4.2 *Meta*carborane

X-ray diffraction studies of the colourless crystals showed a very new form. In contrast to the discrete dimers of the *ortho* system, possesses a one-dimensional polymeric structure (see Figure 15.2), with the *meta*carborane and HMPA units arranged in parallel 'tramlines'. All the *meta*carboranes are equivalent, each contributing to one near linear and one more bent C-H···O hydrogen bond.

The polymeric nature is explained by the greater separation of the C-H units, favouring the formation of a polymer over an oligomer. It is interesting to note that *meta*carborane precipitates from toluene solution appreciably faster than *ortho*carborane, presumably due to the much greater mass of the polymeric unit. This feature has the potential for exploitation as a means of separating the *ortho* and *meta* isomers of the carborane. The packing of the structure is illustrated in Figure 15.4.

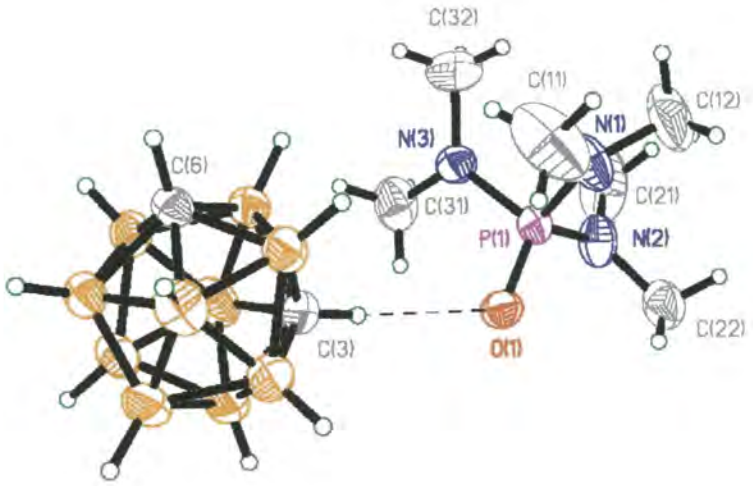

Figure 15.3 Molecular structure of *meta* carborane/HMPA, 50% thermal ellipsoid plot

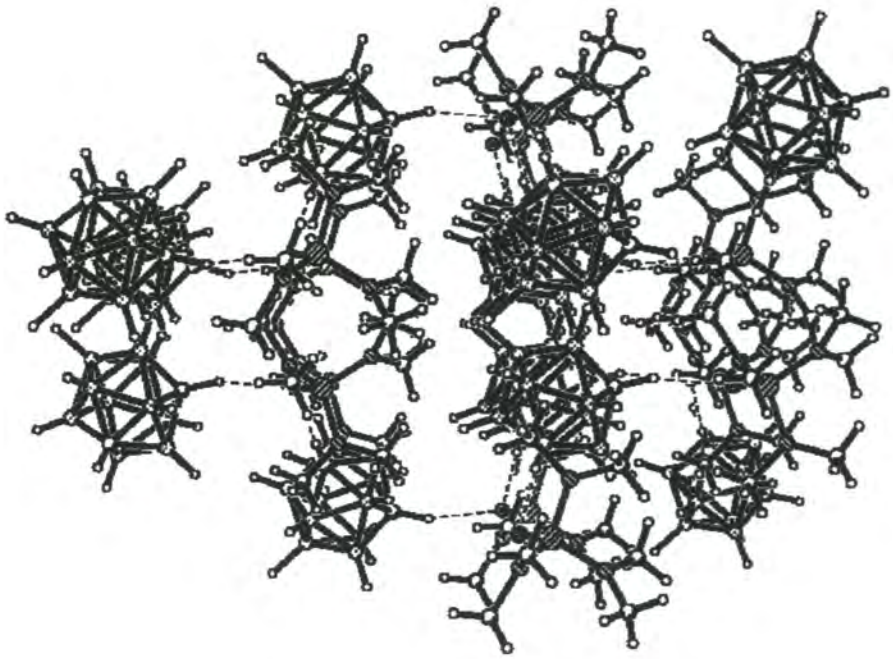

Figure 15.4 The polymeric structures of *meta* carborane with HMPA.

15.4.3 *Para*carborane

The X-ray analysis of the co-crystal adduct *para*carborane (see Figure 15.5) showed a polymeric structure, but one substantially different from that of the *meta*carborane. The polymeric chains in *para*carborane adopt a zigzag formation in which the HMPA molecules alternate on each side along the chain. As in *meta*carborane, each HMPA takes part in one near-linear and one more acute hydrogen bond, but unlike *meta*carborane there are two inequivalent carborane molecules: one involved solely in near-linear C-H···O interactions, the other only forming more acute C-H···O hydrogen bonds (see Table 15.1)

Though crystallographically inequivalent, these two independent *para*carborane molecules in the asymmetric unit have identical bond lengths and angles. The packing is illustrated in Figure 15.6. and a summary of crystallographic data for *ortho*, *meta* and *para* carboranes is given in Table 15.2.

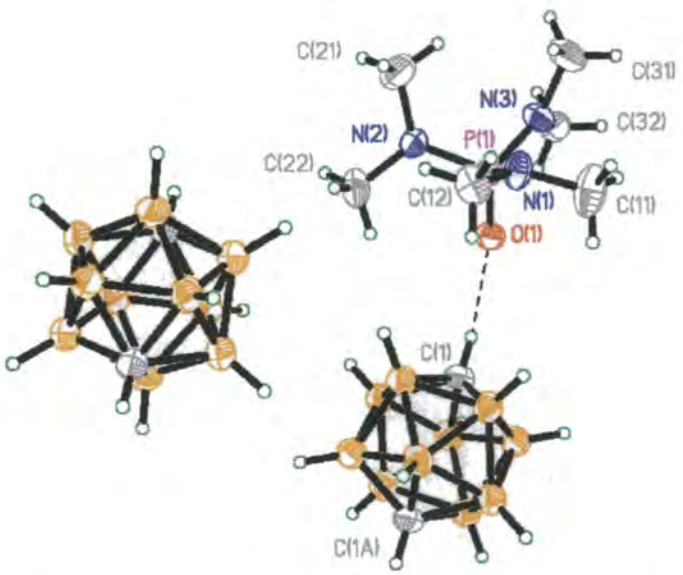

Figure 15.5 X-ray structure of *para*carborane/HMPA, 50% thermal ellipsoid plot

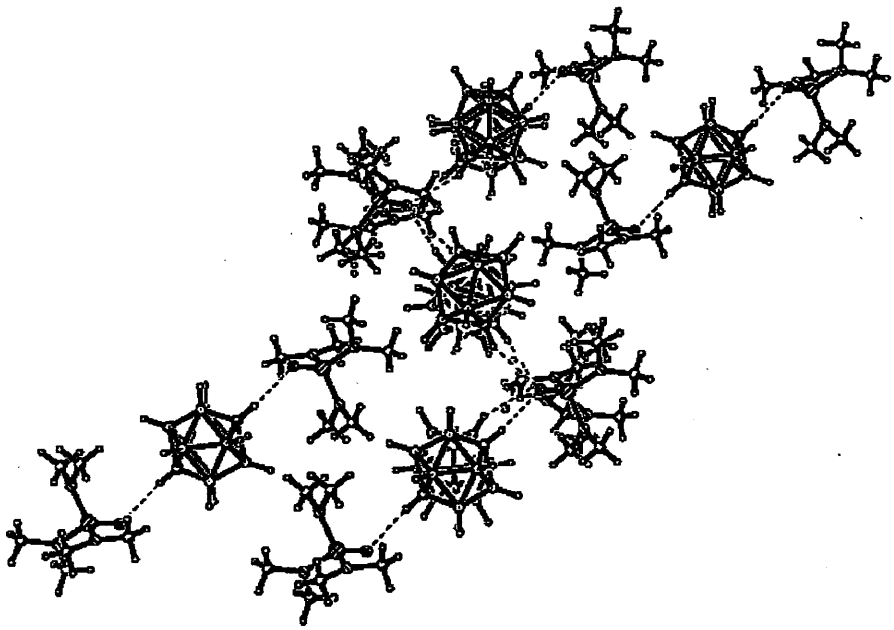

Figure 15.6 The polymeric structures of *para* carborane with HMPA.

	H-bond	Distances, (Å)	Angle, (°)
*Meta*carborane/HMPA	C(3)···O(1)	3.328(6)	-
	C(6)···O(1)	3.234(5)	-
	C(3)-H(3)···O(1)	-	175(4)
	C(6)-H(6)···O(1)	-	164(4)
*Para*carborane/HMPA	C(1)···O(1)	3.132(4)	-
	C(2)···O(1)	3.378(4)	-
	C(1)-H(21)···O(1)	-	173(2)
	C(2)-H(22)···O(1)	-	152(3)

Table 15.1 Selected inter-molecular bond lengths and angles of *meta* and *para* carboranes/HMPA.

	*Ortho*carborane/ HMPA	*Meta*carborane/ HMPA	*Para*carborane/ HMPA
Formula	$C_8H_{30}B_{10}N_3OP$	$C_8H_{30}B_{10}N_3OP$	$C_8H_{30}B_{10}N_3OP$
Formula Weight	323.42	323.42	323.42
Crystal Colour	Colourless	Colourless	Colourless
Crystal Description	Block	Block	Block
Crystal Dimensions (mm)	0.2 x 0.3 x 0.3	0.3 x 0.4 x 0.5	0.4 x 0.4 x 0.4
Crystal System	Triclinic	Monoclinic	Monoclinic
Space group	P-1	Cc	$P2_1/c$
Unit Cell a = (Å) b = (Å) c = (Å) α = (°) β = (°) γ = (°)	 10.662(2) 10.890(2) 17.078(3) 90.59 (3) 91.97 (3) 92.23 (3)	 12.86(4) 14.713(8) 11.100(2) 90 111.41(3) 90	 10.234 (2) 14.338 (3) 13.531 (3) 90 102.81 (3) 90
Volume ($Å^3$)	1980.1 (6)	1956.24 (6)	1936.1 (7)
Z	4	4	4
Calculated Density (Mg/m^3)	1.085	1.10	1.11
Absorption Coefficient (mm^{-1})	1.37	1.39	1.40
F (000)	860	688	688
θ Range for Collection (°)	1.19 – 25.53	2.19 - 26.22	2.04 - 25.64
Reflections Collected	9691	4632	8235
Independent reflections	6413	2682	3294
Goodness-of-fit on F^2	1.22	1.20	1.08
Final R indices [I>2sigma(I)]	0.077	0.051	0.060
wR indices (all data)	0.188	0.135	0.139
Extinction coefficient	0.0019(4)	0.0014(4)	0.0032(6)
Largest diff. Peak and hole.	0.375 & -0.401	0.198 & -0.200	0.262 & -0.251

Table 15.2 Summary of crystallographic data of the three datasets

15.5 CONCLUSION

The structures of these adducts represent the first observations of the unsubstituted parent carboranes in a crystal lattice (search of October 1995 version of the CSD). The C-H···O hydrogen bonds lock the clusters in specific orientations and so allow unambiguous location of the two carbon atoms within the C_2B_{10} clusters. Their location *via* weak inter-molecular interactions, rather than by substitution of the carborane at either a boron or carbon atom, causes minimum electronic perturbation of the cluster and one can assume, therefore, that the structural parameters derived from the adducts provide a very close approximation to those of the carboranes themselves. As such, these structures provide a useful benchmark from which to judge the effect of substitution on bonding within the cluster. For example, the C-C distances of [*ortho* carborane:HMPA)]$_n$, 1.630(6), 1.629(6) Å for C(3)-C(9).

The effect due to electron-donating carbon substituents, all structurally characterised examples of which exhibit longer cage carbon bond distances than are found in (*ortho*carborane···HMPA)$_n$ (Coult, 1992). Similarly, the cross polyhedral (antipodal) C-C distances in (*para*carborane:HMPA)$_{\infty n}$ 3.052(7), 3.059(8) Å for C(l) C(la), C(2)···C(2a), respectively may be compared with intra-cage distances ranging between 3.01 (3) and 3.22 (1) Å for a series of boron-iodo derivatives of (*para*carborane:HMPA)$_n$ (Jiang, 1995).

15.6 REFERENCES

1. Aakeröy, C. B.; Seddon, K. R. *Chem. Soc. Rev.*, **1993**, 397.
2. Armspatch, D.; Constable, E. C.; Housecroft, C. E.; Neuburger, M.; Zehnder, M. *New J. Chem.*, **1996**, 20, 331.
3. Clegg, W.; Gill, W. R.; MacBride, J. A. H.; Wade, K. *Angew. Chem. Int. Ed. Engl.*, **1993**, 32, 1328.
4. Davidson, M. G.; Hibbert, T. G.; Howard, J.A. K.; MacKinnon, A.; Wade, K.,*J. Chem., Soc., Chem. Commun.*, **1996**, 2285
5. Desiraju, G. R., *Acc. Chem. Res.*, **1991**, 24, 290.
6. Desiraju, G. R. *Angew. Chem., Int. Ed. Engl.*, **1995**, 34, 2328.
7. Etter, M. C.; Reutzel, S. M. *J. Am. Chem. Soc.*, **1991**, 113, 2586.
8. Grimes, R. N. *Carboranes*, **1970**, Academic Press, New York,.
9. Hawthorne, M. F.; Mortimer, M. D. *Chem. Br.*, **1996**, 32, 4, 32.
10. Leites, L. A. *Chem. Rev.*, **1992**, 92, 279.
11. Jiang, W.; Knobler, C. B.; Curtis, C. E.; Mortimer, M. D.; Hawthorne, M. F., *Inorg. Chem.*, **1995**, 34, 3491.
12. Onak, T. *Comprehensive Organometallic Chemistry II*, **1995**, Pergamon Press, Oxford, 1, Chapter 6.

CHAPTER 16:

HYDROGEN BONDING IN HETEROAROMATIC CARBORANES

16.1 INTRODUCTION

A non-bonding interaction involving inter and/or intra-molecular interaction with a central hydrogen atom involved is generally referred to as an hydrogen bond. The idea of the 'hydrogen bond' has been a concept that has been around now for a considerable time, but exactly what are and what are not hydrogen bonds has never been completely singularly defined and is often defined by the researcher. For clarity the bonding of the carborane structures in this thesis will be given a definition. This definition will detail what is meant by the term hydrogen bond purely in terms for the carboranes in this thesis, it must be stressed that this is not a definition of hydrogen bonding outside of carboranes in this thesis. So this definition of hydrogen bonding, is defined as a bonding interaction between an electropositive hydrogen atom and one (or more) electronegative atoms with which it does not form a 2-centre-2-electron bond. Some of these bonds are of the "weak" variety (10-65 $kJmol^{-1}$ for the neutral species (Zeegers-Huyskens, 1991) but despite the term weak these interactions are still much stronger than van der Waals forces and often influence the solid state, both in conformation and packing.

Infrared spectroscopy is an extremely valuable tool in the elucidation of hydrogen bonding interactions. In the solid state, the molecules cannot move as much as when in solution, so by recording one sample in the solid state (KBr disc) and another in solution (CCl_4) the type of hydrogen bonding interaction can be deduced. If the bonding-mode is inter-molecular, the N···H interaction will be removed in solution and changes the stretching frequency of the C-H bond. If it is intra-molecular, the carboranyl C-H stretching frequency will remain the same in both the solid and solution state. The best way to observe hydrogen bonding is to use diffraction analysis, as with this method any debate over the bond is resolved in all but the more extreme cases, where the length and strength of the interactions is in the debatable range. There can be complications when the hydrogen bonding is close to the limits of what would be considered the norm, and in such circumstances there is often a debate over whether there is an interaction or not. However in the majority of structures, crystallographic means identify the possible existence of hydrogen bonds.

This study was conducted to investigate the inter- and intra-molecular hydrogen bonding, if any, present in carborane systems and to establish how the molecules pack, with a view to studying how the π-systems are involved with each other especially in the form of π-stacking. If these

structures are of predictable orientation then these structures may be used as an aid in crystal engineering.

16.2 THE STRUCTURE OF 1-(2-PYRIDYL)-*ORTHO*CARBORANE

The compound 1-(2-pyridyl)-*ortho*carborane (see Figure 16.1) appeared worthy of further investigation.

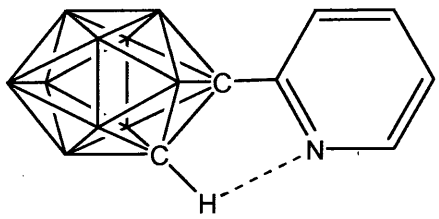

Figure 16.1 The structure of 1-(2-pyridyl)-*ortho*carborane (for clarity hydrogen atoms not shown)

In principle the structure may adopt either inter- or intra-molecular hydrogen bonding, but it was envisaged that it would make use of the suitable stereochemistry and would become intra-molecularly bonded, *via* the cage C-H and the nitrogen of the pyridyl. Synthesis *via* the reaction of decaborane with (2-pyridyl)ethyne proved only partially successful with the reaction low-yielding and requiring a tedious and very time-consuming work-up (Yang *et al.*, 1992). This is believed to be due to the pyridyl moiety interaction with the open face of the decaborane, and this deters any reaction with the acetylenic triple bond. Attempts to prepare 1-(2- pyridyl)-*ortho*carborane yielded only the disubstituted product (1,2-bis-(2-pyridyl)-*ortho*carborane) and unchanged *ortho*carborane. This disubstitution is believed to arise from activation of the second carboranyl C-H hydrogen atom by the newly-added pyridyl group (in the form of a C-H···N hydrogen bond), thus transferring the copper moiety to the unsubstituted carboranyl carbon and facilitating further attack by pyridyl halide (Müller *et al.*, 1992).

Using X-ray diffraction analysis this compound was shown to exhibit intra-molecular activity (see Figure 16.2). It is assumed that the conformation being intra- rather than inter-molecularly bonded is at least partially due to the added ability of the structure to pack with π-stacking in the intra-molecular bonded conformer, the distance between the rings is 3.47(1) Å at the closest, see Figure 16.2. The interaction of the C-H···N is manifest in a slight bending of the C(2)-C(1)-C(12) and C(1)-C(12)-N(1) angles between the ring and the cage, the angles are 116.0(2)° and 115.1(2)° respectively. The atoms C(1) and C(2) lie in the same plane as the pyridyl ring. It is the combination of the intra-molecular interaction and the π-stacking that gives this conformational preference. The bulk of the carborane cage hinders the ability of the structure to

be involved in π-stacking with inter-molecular interactions (see Figure 16.3). A similar packing arrangement has also been noted in a related structure (Alekseyeva *et al.*).

Given the importance of the hydrogen bonding in determining solid state structures, and the possibility of preparing new carboranyl ligands possessing pendant Lewis bases (and thus potential chelation sites), it was decided to prepare novel carboranyl derivatives containing Lewis basic groups, themselves capable of participation in C-H···X hydrogen bonds.

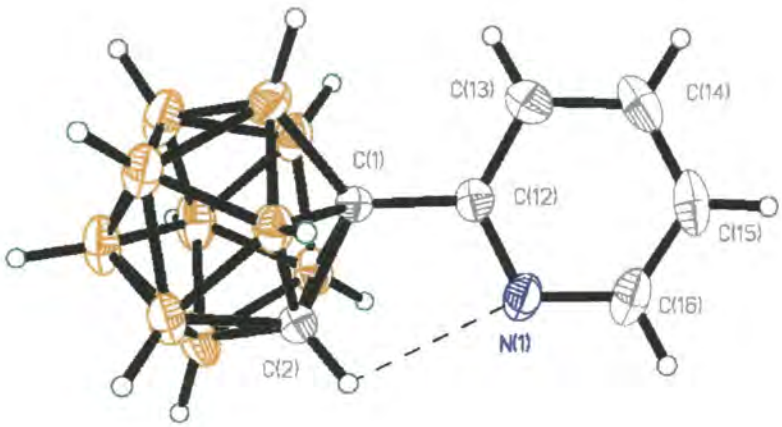

Figure 16.2 The crystal structure of 1-(2-pyridyl)-*ortho*carborane, with 50% probability ellipsoids)

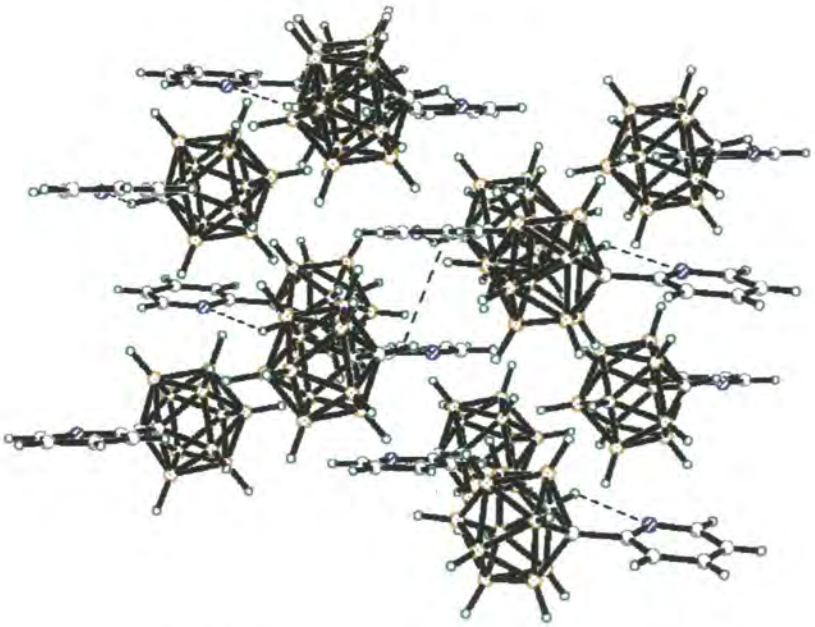

Figure 16.3 Packing diagram of 1-(2-pyridyl)-*ortho*carborane

16.3 THE STRUCTURE OF 1-(3'-PYRIDYL)-*ORTHO*-CARBORANE.

For this structure, the possibility for intra-molecular hydrogen bonding is greatly reduced to the point of being almost impossible due to the positioning of the nitrogen atom in the pyridyl ring (see Figure 16.4). As a consequence of this the structure should be forced to adopt an inter-molecular contact, assuming interaction is present.

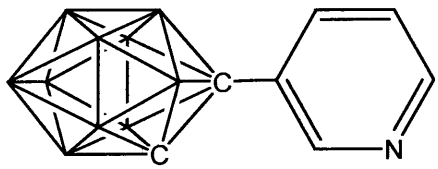

Figure 16.4 The structure of 1-(3'-pyridyl)-*ortho*-carborane (hydrogen atoms not shown)

The crystals used for the diffraction experiment were grown from ethanol/water. [1-(3'-pyridyl)-*ortho*-carborane] is different than the 2'-pyridyl analogue, already seen in section 16.2 and Figure 16.1, the X-ray diffraction structure intra-molecularly hydrogen bonds to give the dimer in the solid state, see Figures 16.5 and 16.6. In this structure there is hydrogen bonding present but as predicted, and unlike the 2' analogue, here the hydrogen bonding is in the form of intra-molecular C-H···N hydrogen bonds, with a distance of 2.544 Å. This is of similar magnitude to the 2'-pyridyl analogue. This intra-molecular hydrogen bonding creates a dimer. The inter-molecular C-H···N bond is impossible without creating a huge bending of the C-C bond or massive ring distortion. Atom C(10) does not lie on the plane of the aromatic ring, due to the twisting necessary to form the hydrogen bond. The bending caused by the intra molecular interaction in the 2'-pyridyl analogue is also not present in this structure with the C(1)-C(2)-C(3) and C(7)-C(2)-C(3) angles being 121.1(1)° and 121.0(1)° respectively, see Figure 16.5.

Another difference between the two structures is that with the 2' pyridyl analogue there is π-stacking present in the crystal lattice, but this is absent in the 3' pyridyl analogue. This is probably due to the bulk of the dimer preventing the rings becoming proximal enough to allow them to be involved in π-stacking, with a minimum distance between the rings of 7.8Å, see Figure 16.6.

X-ray diffraction analysis has been used to observe the hydrogen bonding in 1-(3'-pyridyl)-*ortho* -carborane, but although the IR spectroscopy determines the existence of the hydrogen bond it does not tell us anything about the character of the interaction. The same type of inter-molecular hydrogen bond characteristics in the IR are also present in the *meta*- isomer, although the

crystallographic structure has not been studied. The reason for this is due to the difficulties in obtaining suitable crystalline specimens for diffraction analysis.

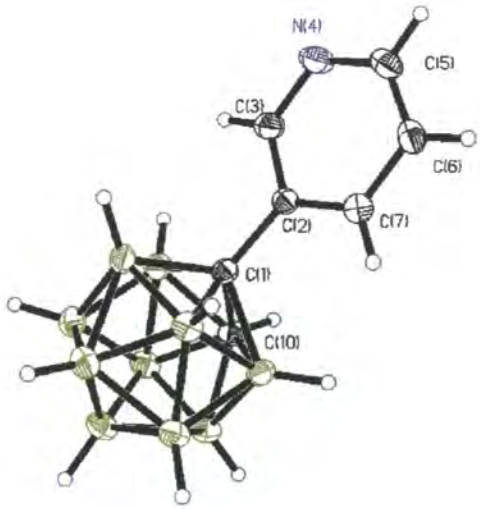

Figure 16.5 The structure of 1-(3'-pyridyl)-*ortho*-carborane

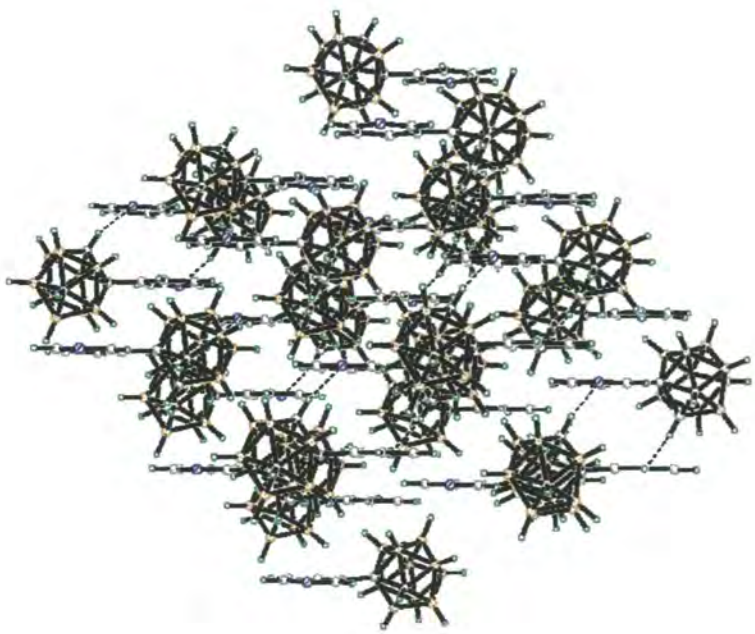

Figure 16.6 The packing of 1-(3'-pyridyl)-*ortho*-carborane

16.4 THE STRUCTURE OF 1-(2'-THIOPHENYL)-*ORTHO*-CARBORANE.

This compound has a similar structure to the 2'-pyridyl analogue and was envisaged to have similar interactions, with the sulphur atom undergoing the same form of hydrogen bonding with the cage C-H as the nitrogen atom, albeit possibly not as strongly, see Figure 16.7.

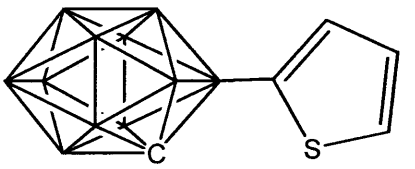

Figure 16.7 The structure of 1-(2'-thiophenyl)-*ortho*-carborane (hydrogen atoms not shown)

For 1-(2'-thiophenyl)-*ortho*-carborane an intra-molecular hydrogen bonding interaction was anticipated, in a similar manner to that seen in the 2'-pyridyl system. Although an alternative possibility of an inter-molecular interaction was postulated for the *meta*-isomer, in which both compounds should display inter-molecular hydrogen bonds, see Figure 16.8. Crystals of 1-(2'-thiophenyl)-*ortho*-carborane were grown from chloroform as clear colourless square platelets.

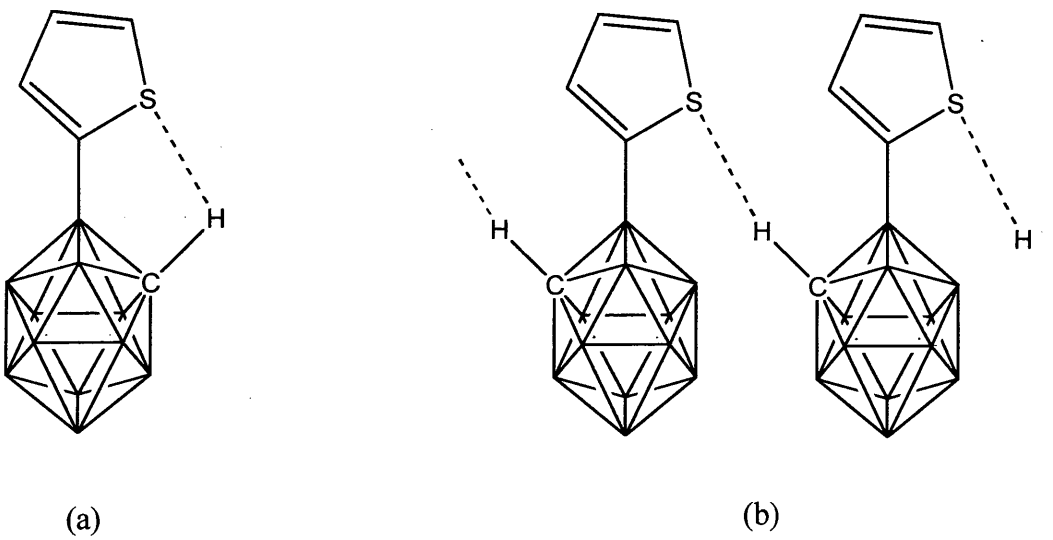

Figure 16.8 The envisaged hydrogen bonding of 1-(2'-thiophenyl)-*ortho*-carborane (a) intra-molecular and (b) inter-molecular hydrogen bonding

The resultant model created from the diffracted data shows that in the packing model of this compound, there are no interactions between the carbon and sulphur atoms at the S(1)/S(2) or C(1Y)/C(2Y) and the hydrogen atoms attached to C(3), see Figure 16.9.

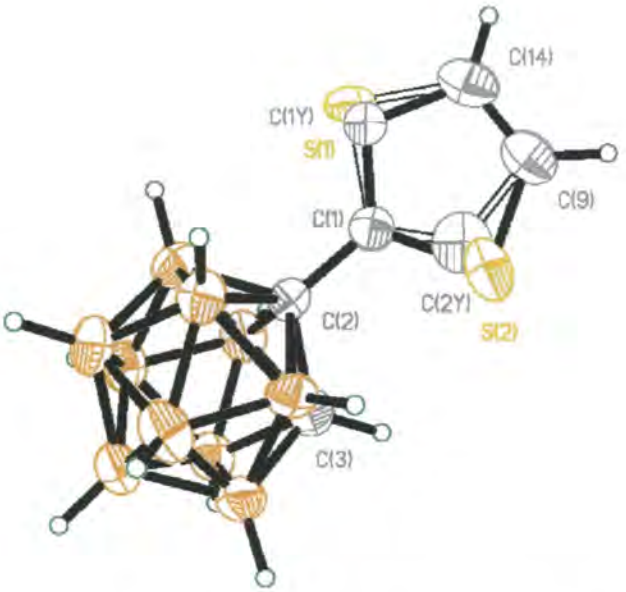

Figure 16.9 The structure of 1-(2'-thiophenyl)-*ortho*-carborane

Like the 3-pyridyl analogue of this compound, no π-stacking can be seen in the crystal lattice between thiophenyl rings, see Figure 16.10. This would suggest that, contrary to IR spectroscopic evidence, no inter-molecular interactions are present in this compound. However, the structure is highly disordered and inter-molecular interactions have been postulated as likely hydrogen bonding possibilities (see Figure 16.8). This presents a slight conundrum, on one hand the presence of hydrogen bonding would generally create a non-disordered structure because the H-bonds would reduce the motion, but on the other hand if disorder were present then it would disguise much of the hydrogen bonding interaction. So, given that the IR information points towards the presence of hydrogen bonding, then it must be assumed that the hydrogen bonding is present, but this interaction must be weak, and must be a resultant of another force, otherwise the conformation would be fixed by this interaction. There is also the possibility of intra-molecular interactions competing against the inter-molecular and so causing this. The crystal has probable twinning with both conformers existing within the twinned crystal. The intra-molecular interaction has a similar magnitude to the inter-molecular interaction with a length of 2.79(5) Å. This gives a disordered result when solving the structure with the X-ray diffraction data. Therefore it can be speculated that there is both inter- and intra-molecular hydrogen

bonding present. The position of each sulphur atom corresponds to the opposite side of the ring and so the interaction involving the sulphur atoms are mutually exclusive and the structure is disordered at both the sulphur sites.

The hydrogen bond lengths present in the structure of are 2.81(4)Å and 2.79(5)Å for the intra- and inter-molecular hydrogen bonds respectively and this is indicative of strong hydrogen bonding interaction, in both these scenarios. For the modeled compound, a cage C-C distance of 1.65(4) Å is measured since this distance is the shortest of the cage bonds, it indicates that it is the C-C cage bond. This is greater than a single C-C distance but is within the limits for cage bond bonds, see chapter 14. It can be seen that there is some disorder in the cage itself, but this disorder is not large and the carbon atoms within the cage can be distinguished because of the shorter bond length. This means that the C-H part of the cage is not disordered and is fixed, this concurs with the envisaged inter-molecular interaction, see Figure 16.8, where both inter and intra-molecular interactions occur with the cage in the same relative geometry.

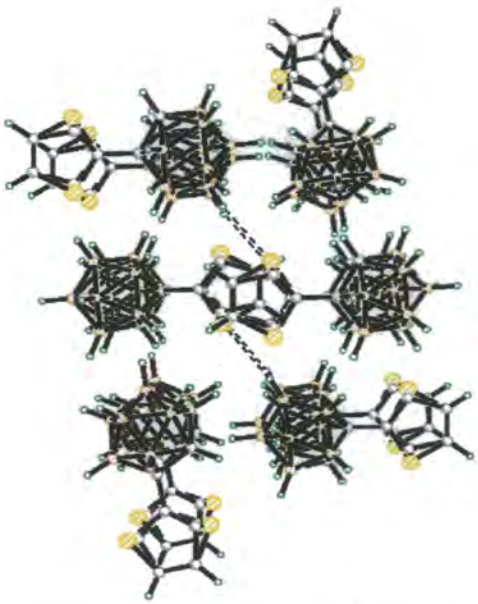

16.10 The packing structure of 1-(2'-thiophenyl)-*ortho*-carborane viewed down the rings

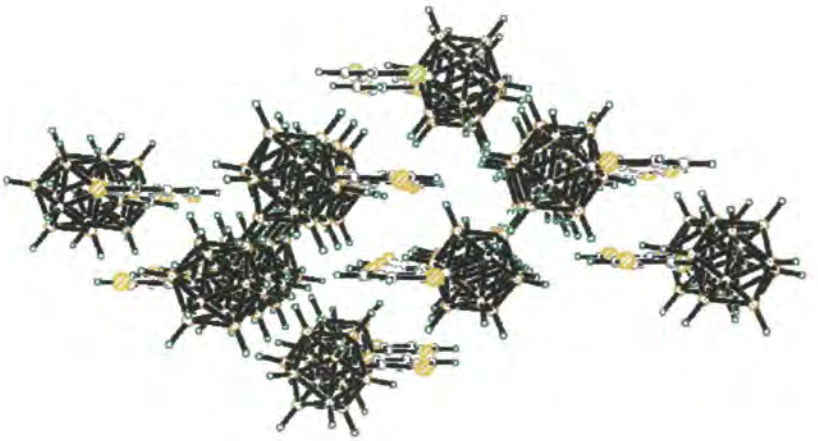

16.11 The packing structure of 1-(2'-thiophenyl)-*ortho*-carborane, viewed with rings side on

It is concluded that the structure is twinned and contains two separate conformers, with both inter- and intra-molecular interactions. This creates a disordered result when solving the X-ray diffraction data. Since this does not occur in the pyridyl analogues, it indicates the relative strengths of the C-H···N in comparison to the C-H···S hydrogen bonds, i.e. the strength of the C-H···N bond ensures no ambiguity for hydrogen bonding. However it must be noted that the assumption that both the structures will undergo intra-molecular interaction, is based on the similarity of the thiophenyl to the pyridyl. However the exact analogue of the 2'-pyridyl structure would be a 2'-thiozine structure. Unfortunately the 2'-thiozine structure was not determined in the course of this thesis.

16.5 THE STRUCTURE OF 1-(2-PYRIDYL)-2-(TRIMETHYLSTANNYL) *ORTHO*CARBORANE /$SnMe_3$

This structure is similar to the 2'-pyridyl compound, see section 16.1, in that is has both the carborane cage and the pyridyl ring in the same orientation. However there is a large difference between the structures, with the C-H group of the pyridyl in section 16.1 being replaced with the large bulky group $SnMe_3$ (see Figure 16.12).

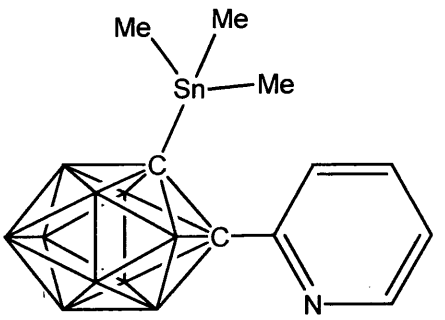

Figure 16.12 the structure of 1-(2-pyridyl)-2-(trimethylstannyl) *ortho*carborane /$SnMe_3$

This compound does not contain the C-H part of the cage with which to form hydrogen bonds and it is envisaged that the structure may have a N···Sn intra-molecular interaction.

1-(2-pyridyl)-2-lithio-orthacarborane was initially prepared from n-BuLi and l-(2-pyridyl)-*ortho*carborane under a dry nitrogen atmosphere. This l-(2-pyridyl)-2-lithio-orthocarborane was then allowed to react *in situ* with Me_3SnCl in Et_2O. Filtration, by purification gave l-(2-pyridyl)-2-(trimethylstannyl)-*ortho*carborane in 74% yield. The product had some structural aspects characterised by IR, NMR and elemental analyses. The characterization found no appreciable inter-molecular interaction. NMR spectroscopy was the next step wto try to identify a lithiated carborane derivative which contained a pendant pyridyl group.

Large, colourless crystals were grown from Et_2O and X-ray diffraction revealed a monomeric structure (see Figure 16.13). The structure appears to be a weak intra-molecular N···Sn interaction present (although the distance is long at 3.2 Å, given the combined Van der Waals radius for tin and hydrogen is approximately 3.4 Å).

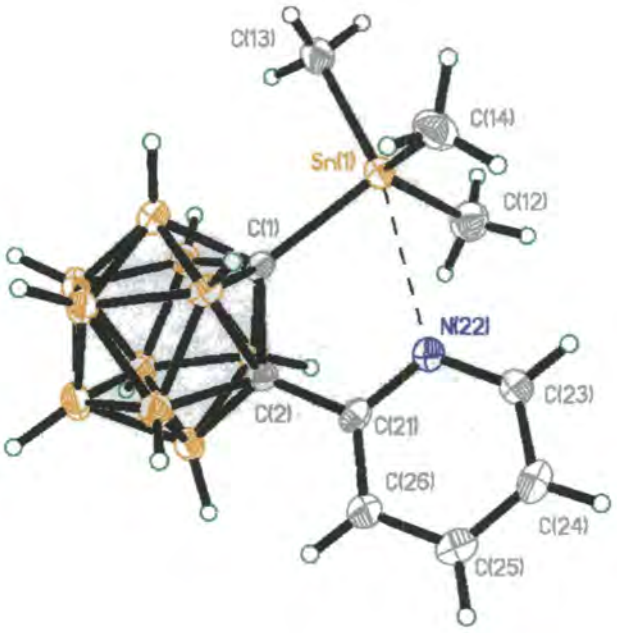

Figure 16.13 The X-ray diffraction structure of 1-(2-pyridyl)-2-(trimethylstannyl) *ortho*carborane /$SnMe_3$, with a probability of 50%.

Extra credence is given to the intra-molecular interaction because the pyridyl ring is positioned so that it minimises this distance. There is also a slight angling of the C_{cage}-Sn and C_{cage},-C_{ring} bonds toward each other. The bending in this structure is not large with the angles of C(21)-C(2)-C(1) and C(2)-C(1)-Sn(1) being 117.4(3)° and 123.9(2)° respectively. The interaction is difficult to determine since the orientation of the ring and the $SnMe_3$ group would adopt a similar conformation because of the steric strain. As expected there is no π-stacking in the crystal so the ring does not adopt this conformation for π-stacking reasons, see Figure 16.14. The IR indicates a possible intra-molecular bond but is inconclusive in this respect. It is concluded that although the structure does have an intra-molecular interaction this is due to the forced conformation due to steric factors and it is therefore relatively weak. There is no evidence for a strong inter-molecular interaction if there is an interaction then this is somewhat forced. The definition of the methyl groups is interesting, these groups are well defined and free of disorder. This indicates how sterically hindered the group is, both in the monomeric and packing senses (see Figures 16.13 and 16.14).

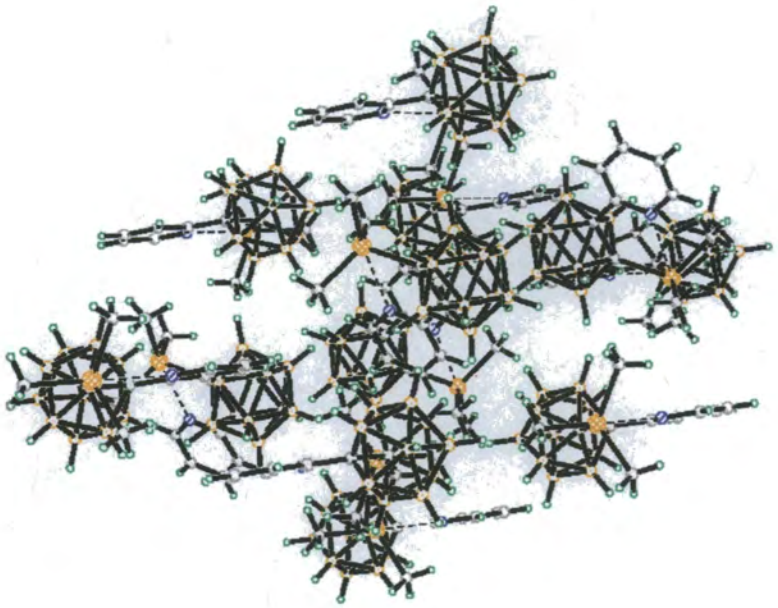

Figure 16.14 The packing structure of 1-(2-pyridyl)-2-(trimethylstannyl) *ortho*carborane /$SnMe_3$

16.6 SUMMARY

In this study several similar structures were investigated to study the inter- and intra-molecular hydrogen bonding, it is seen that there is a great variety amongst these structures with reasonably slight alterations to the molecular structure. Given the dissimilarity in the hydrogen bonding it is not reasonable to use these structures to determine the exact arrangement of similar type systems, and problems may occur when trying to predict definite hydrogen bonding motifs. However in terms of simple prediction the results are encouraging and it would be reasonable to use these inter-molecular interactions to assist in the prediction of structures and so help in the scope of crystal engineering. This was illustrated in sections 16.1 and 16.2 with the 2'- and 3'-pyridyl structures respectively, where the hydrogen bonding characteristics were correctly predicted before structural determination.

All the structures seen exhibit hydrogen bonding characteristics to some extent, although with the Sn···H-N structure this appears to be minor. However the range, strengths and nature of these bonds are varied. Infrared spectroscopy gave an indication of the *ortho*-derivative 1-(3'-pyridyl)-*ortho*, and the X-ray structure analysis found the inter-molecular C-H···N contact of 2.11(3) Å. Their IR spectra suggested that 1-(2'-thiophenyl)-*ortho* and *meta*–carboranes should both have inter-molecular hydrogen bonds, although an intra-molecular interaction would have been expected from the *ortho* case. The X-ray analysis shows a possible C-H···S intra-molecular interaction at 2.79(10) Å. However, this interaction is long and not determinable by I.R.. It is speculated that this disorder is caused by a form of twinning, however attempts to model this twinning have been unsuccessful. Overall the prediction of hydrogen bonding characteristics in these structures have only been somewhat successful. The presence of the carborane cage has a relatively large steric factor and this has an influence on the hydrogen bonding motifs. The steric effects of the carborane cages are predictable.

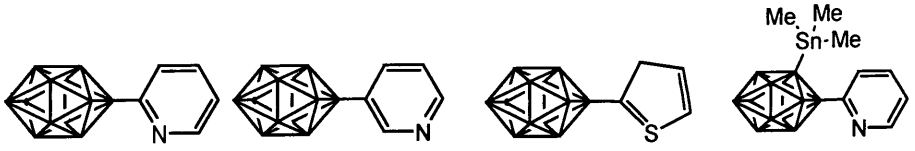

Formula	$C_7H_{15}B_{10}N$	$C_7H_{15}B_{10}N$	$C_6H_{14}B_{10}S$	$C_7H_{14}B_{10}NSn(Me)_3$
Formula Weight	221.30	221.30	214.32	384.08
Crystal Colour	COLOURLESS	COLOURLESS	COLOURLESS	COLOURLESS
Crystal Description	Needle	Wedge	Needle	Block
Temperature (K°)	150(2)	150(2)	150(2)	150(2)
Wavelength (Å)	1.54184	0.71073	0.71073	0.71073
Crystal System	Monoclinic	Triclinic	Monoclinic	Monoclinic
Space group	P2(1)/n	P-1	P2(1)/c	P2(1)/c
a= (Å) b= (Å) c= (Å) α= (°) β= (°) γ= (°)	7.0570(10) 18.029(4) 9.899(2) 90 92.54 (3) 90	7.238(1) 7.699(1) 11.197(2) 100.053(1) 92.303(1) 90.572(1)	7.172(2) 9.014(2) 18.635(4) 90 93.122(30) 90	10.0093(2) 13.5441(3) 13.5157(2) 90 107.2800(10) 90
Volume ($Å^3$)	1258.2(4)	613.94(2)	1203.0(4)	1749.58(6)
Z	4	2	4	4
Calculated Density (Mg/m^3)	1.168	1.197	1.183	1.458
Absorption Coefficient (mm^{-1})	0.390	0.057	0.221	1.446
F (000)	456	228	440	760
θ Range for Collection	4.91 to 73.65	1.85 to 27.48	2.19 to 27.42	2.13 to 27.89
Index Ranges	0<=h<=7, 0<=k<=22, -12<=l<=12	-9<=h<=9, -9<=k<=8, -14<=l<=14	-9<=h<=9, -4<=k<=11, -24<=l<=22	-12<=h<=11, -15<=k<=16, -15<=l<=17
Reflections collected	1985	4529	7641	8410
Independent reflections	1781	2783	2728	3149
Data/restraints/parameters	1781/0/168	2782/0/208	2728/0/167	3149/0/217
Goodness-of-fit on F^2	1.034	1.039	1.201	1.090
Final R indices [I>2sigma(I)]	0.0472	0.0454	0.0780	0.0310
WR^w indices (all data)	0.1433	0.1315	0.2210	0.0715
Extinction coefficient	0.0055(7)	None	None	None
Largest diff. Peak and hole. ($eÅ^{-3}$)	0.206 -0.179	0.284 -0.241	0.336 -0.370	0.408 -0.613

Table 16.1 Crystallographic data for the structures in this chapter

16.7 REFERENCES

1. Aleskseyeva, E. S.; Hibbert, T. G.; Howard, J. A. K.; Wade, K., Unpublished Results.
2. Müller, J.; Base, K.; Magnera, T. F.; Michl, J., *J. Am. Chem. Soc.*, **1992**, 114, 9721.
3. Yang, X.; Jang, W.; Knobler, C. B.; Hawthorne, M. F., *J. Am. Chem. Soc.*,**1992**, 114, 9719.
4. Zeegers-Huyskens, T.; Huyskens, P.L. *Intermolecular Forces –An Introduction to Modern Methods and Reselts*, Ed. Huyskens, P. L., Berlin, 1991, 1.

CHAPTER 17:

NON HYDROGEN BONDING CARBORANES.

17.1 INTRODUCTION

In the previous chapters the carboranes studied have all been concerned with hydrogen bonding and the subsequent possibilities of crystal engineering. For these studies the structures have had groups incorporated into them that greatly increase the likelihood of inter/intra molecular interaction and in particular hydrogen bonding. Of course not all carboranes contain such groups and many do not contain groups that would be considered likely to be involved in any hydrogen bonding. However as seen in chapter 15 the carborane units within a structure may be involved in hydrogen bonding without having any normal hydrogen bonding groups attached.

The following chapter gives examples of structures that do not contain hydrogen-bonding groups and are not candidates for inter-molecular interactions.

17.2 THE DEBORANATION OF *ORTHO*-CARBORANE BY AN IMINOPHOSPHORANE: A NOVEL CARBORANE AND THE BORENIUM ADDUCT.

17.2.1 Introduction

The conversion of *closo*-1,2-$C_2B_{10}H_{12}$ into the *nido*-7,8-$C_2B_9H_{12}^-$ anion by bases is a well-known reaction. In this study X-ray diffraction analysis has for the first time structurally determined the carborane intermediate in this reaction.

The *closo*-icosahedral carboranes of the structure $C_2B_{10}H_{12}$ have an extensive three dimensional aromatic chemistry, they are of interest in neutron scattering, metal extraction, supra-molecular chemistry and catalysis. They are useful for materials thermally stable or conducting or otherwise electronegative oligomers and polymers (Plešek, 1992). They are also extremely resilient to both high temperature and oxidizing agents. It has been shown that these structures have an important degradation reaction, being susceptible to nucleophilic attack by a select few powerful Lewis bases (e.g. fluorine amines) (Hawthorne *et al*, 1965). These can remove one of their BH units and become *nido*-shaped $C_2B_9H_{11}^{2-}$ (or $C_2B_9H_{12}^-$) anionic residues, see Figure 17.1, these can bind metal ions strongly to the open C_2B_3 faces. However, although these base deboration reactions have been known for 35 years the mechanistic details have until now remained elusive. The X-ray diffraction studies of an adduct, $C_2B_{10}H_{12}HNP(NMe_2)_3$ formed in the nucleophilic attack by the novel deboronating base $HNP(NMe_2)_3$ on *ortho* carborane, 1,2-$C_2B_{10}H_{12}$, and of the novel dication, $[(Me_2N)_3PNHBNP(NMe_2)_3]_2O^{2+}$, (which is an unexpected product when there are traces of water present) shown here have been used to shed more light on the mechanism.

17.2.2 Experimental and Results

For the conversion of the carborane anion *nido*-7,8-$C_2B_9H_{12}^-$ from *closo*-$C_2B_{10}H_{12}$, imino-tris(dimethylamino)phosphorane ($HNP(NMe_2)_3$ has proven to be effective, see Figure 17.2. For this reaction the NMR (^1H, ^{11}B and ^{10}B) spectra of the product revealed that it was present as a 1:1 mixture of salts. These mixtures contained the expected $H_2NP(NMe_2)_3^+$ as well as the novel protonated tris(imino)borane $B[(NP(NMe_2)_3)_2(HNP(NMe_2)_3)]^+$ cations. The protonated tris(imino)borane is probably generated *via* the bis(imino)borane $HB[NP(NMe_2)_3]_2$ which is observed to occur, briefly, as a doublet in the ^{11}B NMR.

With the addition of dry $HNP(NMe_2)_3$ in toluene to the resultant product, a single crystal was formed. X-ray structure of this crystal was investigated by X-ray diffraction analysis and was found to be the novel carborane adduct $C_2B_{10}H_{12}.HNP(NMe_2)_3$.

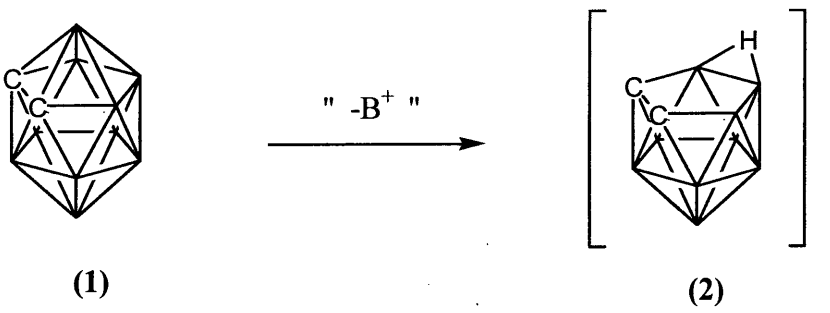

(1) (2)

Figure 17.1 Scheme 1, The reaction of (1) to (2)

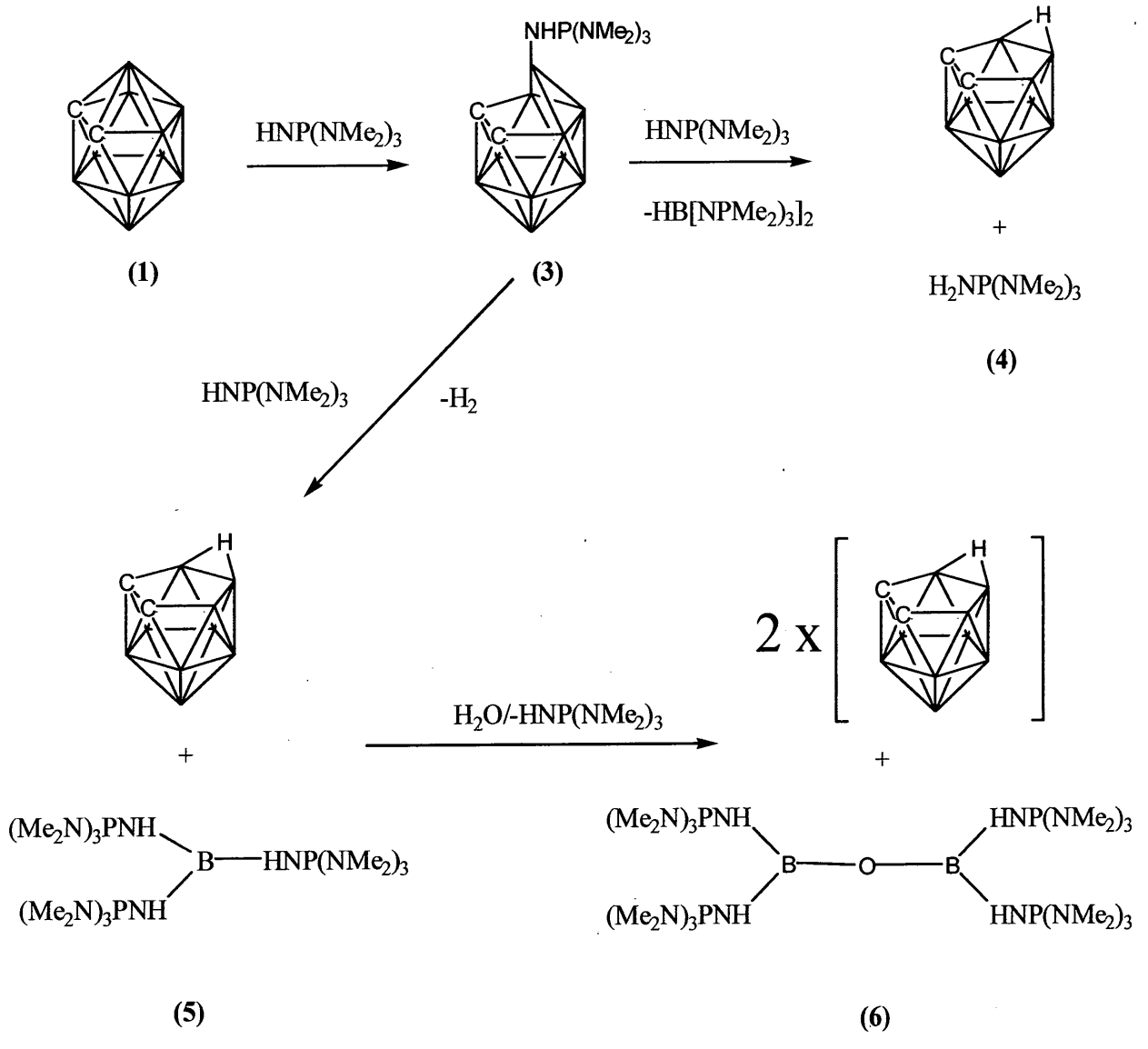

(1) (3) (4)

(5) (6)

Figure 17.2 Scheme 2, The reaction scheme from structure (1) to (3), (4), (5) and (6)

17.2.3 The X-ray Diffraction analysis of (3)

The X-ray diffraction model is in good agreement with the intermediate observed in the NMR-scale reactions and so this leads to the conclusion that this adduct is indeed the first structurally characterized intermediate in the conversion of the carborane anion *nido*-7,8-$C_2B_9H_{12}^-$ from *closo*-$C_2B_{10}H_{12}$. With the diffraction analysis it can be seen that the first step in the *closo* to *nido* reaction is when the base becomes attached to the most positively charged boron atom near the two neighboring carbon atoms. This cleaves the two B-C bonds and subsequently the length of the two B-B bonds to B(9) and B(11) is increased.

Diffraction data for **(3)**, were obtained on the Seimens SMART CCD diffractometer under a nitrogen atmosphere, see chapter 2 for details. The crystals produced were not of good quality and much time was spent on finding crystals suitable. The resultant diffraction and subsequent model from the diffraction analysis is of a reasonable high quality when considering how poorly the crystals appeared to diffract. It is seen from the model that the structure of **(3)**, is the combination of $HNP(NMe_2)_3$ and $B_{10}C_2H_{12}$. The representation of **(3)** in Figures 17.2 and 17.3 has atom B12 with 5 bonds (3 boron, 1 carbon and 1 hydrogen), this however is not simple with only B12-B10 being within the normal B-B distance range. The other represented B-B bonds, B12-B9 and B12-B11, are 2.099 Å and 2.091 Å respectively. Perhaps a more correct representation would be for B12-B9 and B12-B11 to be considered as non-bonded interactions. The other B-B bond lengths are within the standard range of such bonds, see Table 17.1. There are no inter-molecular interactions present in the packing of this structure (if not considering the possible non-bonding interaction between B9 and B12), this is not unexpected since there is no ideal hydrogen donor groups.

Bond	Length (Å)	Bond	Length (Å)
N(1)-B(12)	1.50 (1)	B12-B9	2.099(6)
B12-B10	1.761(4)	B12-B11	2.091(6)
C8-C7	1.529(7)	P1-N1	1.650(4)
P1-N2	1.630(4)	P1-N3	1.623(4)
P1-N4	1.623(4)		

Table 17.1 Selected bond lengths of (3)

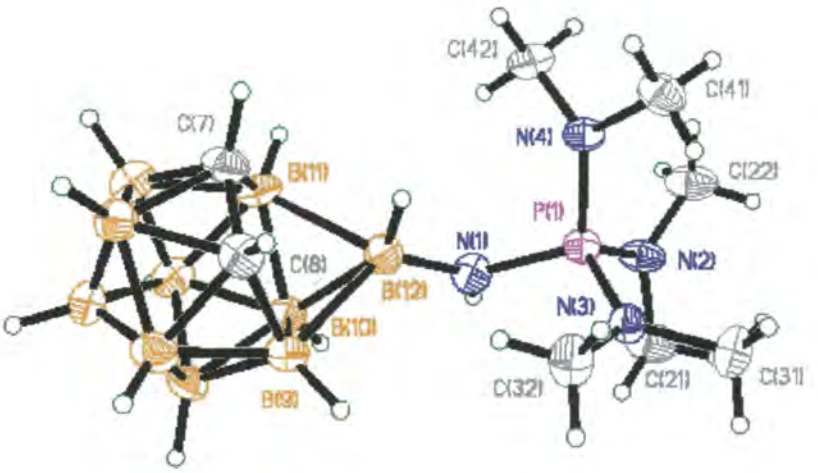

Figure 17.3 X-ray diffraction structure of (3), with 50% probability

17.2.4 The structure of the two carborane anions and the dication (6)

In a similar way to the structure of **(3)**, the crystals of **(6)** could not be produced of a high quality and degraded in air, but the subsequent diffraction analysis yielded data that, if not of the highest quality, gave an accurate representation of the structure.

The diffraction model of **(6)** is dominated by the dication $[(Me_2N)_3PNHBNP(NMe_2)_3]_2O^{2+}$. As well as pure size of the dication, the dication contains much heavier and therefore higher electron density atoms than the two anions. There are no inter-molecular interactions in this structure and the cage carbon atoms could be distinguished and identified with relative ease.

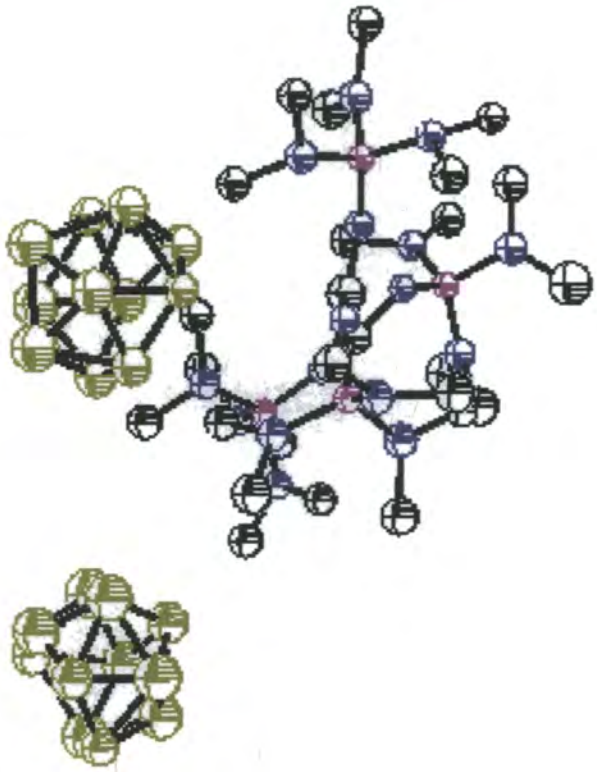

Figure 17.4 the X-ray structure of (6), with 50% probability ellipsoids

17.3 CARBORANES WITH NO INTER-MOLECULAR INTERACTIONS PRESENT.

17.3.1 The structure of 1,2-bis({1,2-diphenyl})*ortho*carborane (7)

To a suspension of 1,2-dilithio*ortho*carborane in Et_2O at -78°C was added, under dry nitrogen atmospheric conditions, two equivalents of benzyl chloride. Swift, exothermic reaction followed, precipitating LiCl, which was removed by filtration. Removal of *ortho*carborane by vacuum sublimation, followed by further purification gave 1,2-bis-((1,2-diphenyl)ethyl)*ortho*carborane **(7)** (See Figure 17.5), in 39% yield. The reason why **(7)** is obtained rather than 1,2-dibenzyl*ortho*carborane is believed to be analogous to that for **(8)** (See Figure 17.5). Crystals of **(7)** suitable for X-ray diffraction were grown from a toluene solution. The crystal structure is shown in Figure 17.6 and 17.7. The structure of **(7)**, does not contain any inter-molecular interactions, this is despite the presence of phenyl rings, which can be envisaged to π-interact. The lack of intermolecular interaction is due to the lack of suitable groups and the steric bulk of the units hinders any π-interaction from the rings.

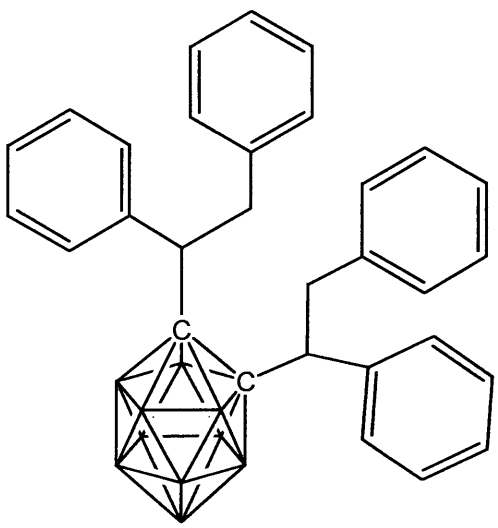

(7)

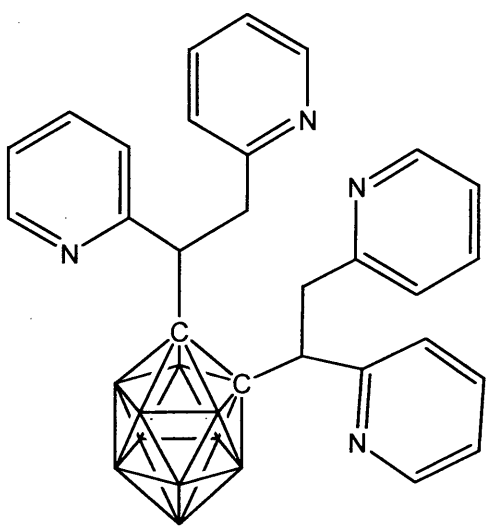

(8)

Figure 17.5 1,2-bis({1,2-diphenyl})*ortho*carborane (7) and 1,2-bis({1,2-di-2'-picolyl}ethyl)*ortho*carborane (8)

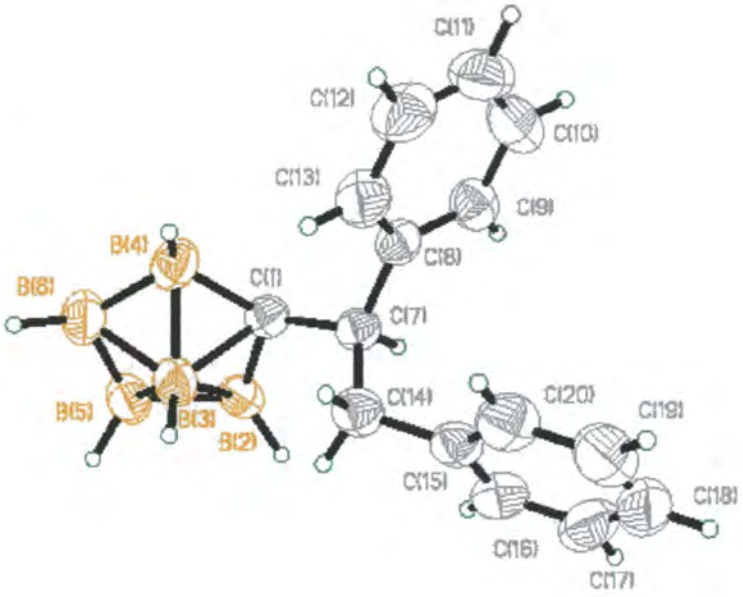

Figure 17.6 The asymmetric unit of (7)

Figure 17.7 The structure of (7)

17.3.2 The structure of 1,4-di(phenyl*ortho*carboranyl)benzene (9)

1,4-di(phenyl*ortho*carboranyl)benzene **(9)**, see Figure 17.8, was prepared by the reaction of two equivalents of $B_{10}H_{12}$ with 1,4-di(phenylethynyl)benzene in toluene. The reaction required two days at 90 °C (yield was 77%). Crystals suitable for X-ray diffraction were grown from cyclohexane. The bond lengths and angles in **(9)**, see Figure 17.9 and 1,3,5-tris(phenyl*ortho*carboranyl)benzene are similar. In both cases the carboranyl C-C distance is appreciably longer than that in *ortho*carborane (1.630(6) Å) (Davidson *et al.*, 1996); this is believed to be due to the steric repulsion of the phenyl/phenylene rings. The bond lengths and angles in **(9)** correlate well with those found in the X-ray structures of the related compounds, i.e. 1,4-bis-l-(2-methyl*ortho*carboranyl)benzene (Henly *et al.*, 1992). There are no inter-molecular interactions in this structure. The lack of hydrogen bonding in this structure is not surprising since there are no groups within this structure that have typical hydrogen bonding groups. There is a centre of inversion in the middle of the joining phenyl ring in the solid state. This means that the *ortho* bonded rings are at 180° to each other.

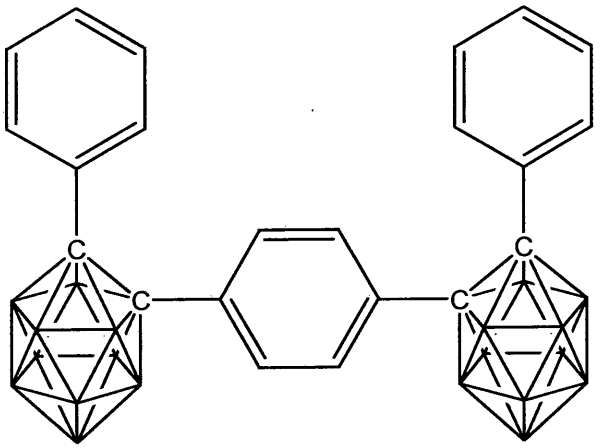

(9)

Figure 17.8 The structure of 1,4-di(phenyl*ortho*carboranyl)benzene (9)

Figure 17.9 The X-ray diffraction structure of (9)

17.3.3 The structure of 1, 2-diphenyl*ortho*carborane (10)

Two independent conformations of **(10)** exist as the structure. Both of these conformers are extremely similar with small differences in the bond lengths and slight deviations in the phenyl ring twisting. This structure does contain phenyl rings and these rings can be envisaged to be involved in π-stacking type interactions and therefor influence the packing. Given that there are two independent conformers, these may be as a result of this π-stacking. What is seen is that there is the closest link between two rings is quite long at 4.679 Å. The long distance and lack of π-interaction may be due to the steric bulk of the carborane cage, as can be seen from Figure 17.10 the cage would limit how close the rings can be to each other. There are no other inter-molecular interactions.

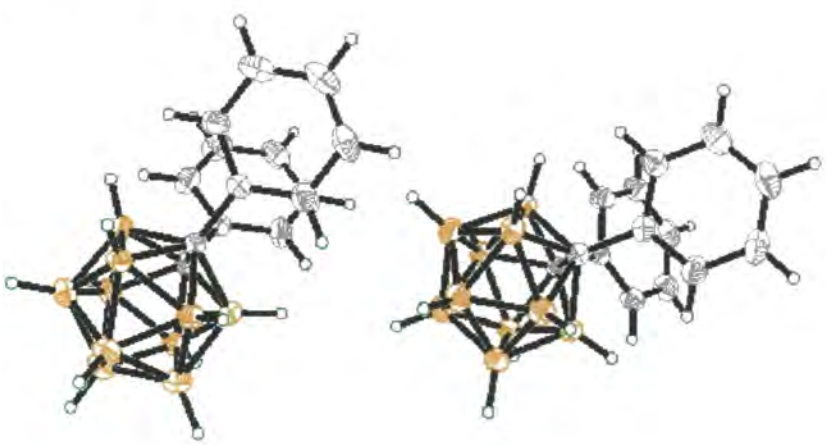

Figure 17.10 The X-ray structure of (10)

17.4 SUMMARY

This shows that the structures in the previous chapters, which have used these groups to facilitate hydrogen bonding within the structures, are necessary in many cases to create hydrogen bonding within the structure. As expected the interaction between the structures is minimal with no sign of any π-interactions occurring. The relative orientation of these structures within the solid state is determined by crystal packing forces and as a result are not as predictable as if there were hydrogen bonding groups were present to direct inter-molecular interactions.

17.5 REFERENCES

1. Davidson, M. G.; Hibbert, T. G.; Howard, J.A. K.; MacKinnon, A.; Wade, K.,*J. Chem. Soc., Chem. Commun.*, **1996**, 2285.
2. Henly, T. J.; Knobler, C. B.; Hawthorne, M. F., *Organometallics*, **1992**, 11, 2313.
3. Hawthorne, M. F.; Young, D. C.; Wegner, P. A., *J. Am. Chem. Soc.*, **1965**, 87, 1818.
4. Plésék, J., *Chem. Rev.*, **1992**, 92, 269.
5. Thomas, R. L. I.; Welch, A. J., *Acta Cryst.*, **1996**, C52, 1689.

CHAPTER 18:

AN INVESTIGATION INTO SYMMETRICAL TRIAZINES

18.1 INTRODUCTION

This chapter investigates triazine compounds with carborane cages attached. The principal multi-carboranyl system that will be discussed is the tri-carboranyl triazine assembly. These are compounds which have three nitrogen and three carbon atoms joined together to form a six membered aromatic ring. In this study there are carborane cages attached to the carbons on the ring. There are three possible types of triazine systems possible, illustrated in Figure 18.1. Considering the bulk of the carborane unit, the 1,3,5-triazine isomer was chosen as the most suitable of the three isomers. It is also the most readily available, the most stable and the most readily derivatised (Boyd, 1997).

There are many applications of triazines, and 1,3,5-triazines are commonly used as resins, herbicides and as constituents of dyestuffs. Certain derivatives have explosive properties, whilst others are fire retardants (Boulton and M^{c}Killop, 1984). Some substituted triazines have also shown clathrate behavior ((Jessiman *et al.*, 1990) and (Henderson *et al.*, 1995)) to be exhibited in forming a Piedfort-based host lattice to small molecules like 1,4-dioxane and isopropanol. The aromatic rings (1,3,5-triazines) lie above each other and play host to a small solvent molecule.

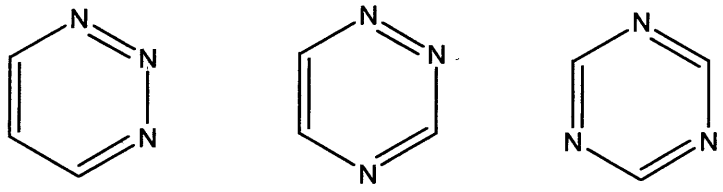

a) 1,2,3-triazine b) 1,2,4-triazine c) 1,3,5-triazine

Figure 18.1: The three triazine isomers, a) 1,2,3-triazine, b) 1,2,4-triazine and c) 1,3,5-triazine

Structures in the solid state with nitrogen heterocyclic chemistry often have hydrogen bonded lattices and with triazine chemistry this is also the case. This property has been shown to be useful in the field of crystal-engineering as a stabilizer in polymers which would otherwise be degraded by ultraviolet radiation (Keck *et al.*, 1996).

Certain 1,3,5-triazines have terpyridine-like ligands (Chan *et al.*, 1995) and have been used to create luminescent complexes (Yang *et al.*, 1996).

As with icosahedral carboranes, 1,3,5-triazine derivatives have been shown to have second harmonic generation properties (Yonehara *et al.*, 1994). The tri-carboranyl benzenes have been studied previously (Schöberl *et al.*, 1997)), and it was of interest to make a comparison in reactivity, structure and electronic properties. The family of 1,3,5-triazines, are often referred to as s-triazines, and they can be synthesized by a variety of methods depending on which moieties are required in the ultimate triazine.

18.2 SYMMETRICALLY SUBSTITUTED TRIAZINES

18.2.1 Synthesis

The chosen starting material was chosen to be cyanuric chloride $C_3N_3Cl_3$, since this was the most obvious and convenient material from which to begin the derivatisation of the triazine ring. Cyanuric chloride is relatively inexpensive, and the chlorine atoms can be substituted without much difficulty, since the carbon atoms are activated by the adjacent nitrogen atoms. The same activation is observed for all six-membered nitrogen heterocyclic rings as all the carbons at positions *ortho-* and/or *para-* to the nitrogen atom are activated. This activation is ascribed to a lowering of the energies in the *p*-orbitals that form the heterocycle and the energy becomes lower each time the nitrogen atoms are incorporated into the six-membered ring. Consequently nucleophilic attack on the carbons is much easier. Cyanuric chloride will readily lose its chlorine substituents, by nucleophilic substitution, to another substituent that may or may not help to stabilize the aromatic C_3N_3 ring. The final structure of the triazine formed is dependent upon the nature of the substituent introduced. Where the proposed substituent, R, is electron donating, mono substitution is favoured as electron density is pushed into the ring, stabilizing the aromatic system and subsequently reducing the ability of the other chlorines to react further. Alternately if R is electron withdrawing, the reverse is true and trisubstitution is favoured.

18.2.2 THE ASSEMBLY OF VARI-SUBSTITUTED TRIAZINES

When the substituents are the same on tri-substituted, 1,3,5-triazines, cyanuric chloride then it is the perfect starting material, particularly when the R group is electron withdrawing. However, in order to synthesize mono- or di-functionalised triazines with either reactive sites for further substitution, or already usefully functionalised remaining carbons, the triazine needs to be built. There are various ways in which this can be done, e.g. by reduction (i.e. $LiAlH_4$) to remove unwanted chlorines (Smolin and Rapoport, 1959).

The process involved to synthesis tri-carboranyl benzenes has already been generally discussed, however, in altering the chemistry of the central moiety from a carbocycle to a heterocycle, it is worth reviewing the synthetic strategies to such multi-carboranyl systems. Substitution of 1,3,5-triazines is very much dependent on the nature of the introduced substituent, with tri-substitution being favoured with electron withdrawing moieties. Carboranes are strong electron-withdrawing groups, with *ortho*-carborane having the greatest electron withdrawing potential, followed by *meta* then *para*. It is possible to use the substitution of cyanuric chloride by R groups to slow

down and subsequently to control or tailor the degree of substitution, to give for example, a mono-substituted product. When the R functionality is a carborane, however, tri-substituted triazine was found to be the only multi-carboranyl product in the reaction between lithio-carborane and cyanuric chloride. This was independent of the ratio of reagents, solvent, temperature, reaction time and whether the lithio-carborane was added to the cyanuric chloride or *vice versa*. The reaction itself was immediate, even when the reaction was conducted at –78°C. Although *para*-carborane is significantly less electron withdrawing than *ortho*-carborane for all three isomers, either substituted or containing a carboranyl C-H functionality, trisubstituted triazine was the only new carboranyl product. Any unreacted carborane was reclaimed unchanged, and unreacted cyanuric chloride was converted into cyanuric acid, which is in equilibrium with its keto tautomer, in the aqueous work-up (Horribin, 1963).

Solid State NMR spectroscopy has been a very useful technique in the characterization of these products from the reactions between lithio-*meta*- and lithio-*para*-carborane and cyanuric chloride when the reactants were in the ratios 1:1, 2:1 and 3.1. The subsequent NMR studies (^{11}B, ^{13}C and ^{1}H) on these insoluble products showed that this was indeed the case. If mono- and di-substituted carboranes were formed then more than one nitrogen environment would be present. However it was seen was that only one signal was detected in each attempt, indicating that only one carboranyl-triazine product to be formed. Conversely, when a two-fold excess of cyanuric chloride was added to dilithio-*ortho*-, *meta*- or *para*-carborane it resulted in an insoluble pale yellow solid whose composition could not be determined.

18.3 PROPERTIES OF TRIAZINE COMPOUNDS

18.3.1 Degradation of multi-carboranyl triazines

In the chemistry of classical 1,3,5-triazines, the heterocyclic ring is often susceptible to attack by various compounds, including hydrazines, (Grundmann and Kreutzberger, 1957) which bring about either ring-degradation or ring-opening reactions. With the reaction of s-triazine with N,N-dimethylhydrazine the ring is cleaved forming 1-formyl-2,2-dimethylhydrazine 2',2'-dimethylhydrazone (Grundman, 1963).

If this were a viable synthetic alternative, the chemistry of these compounds could have been investigated more eagerly and, given their nature, may have usefully led to novel polymeric and non-linear optical materials. There was an alternative possible outcome to the reaction between the tricarboranyl triazines and the hydrazine group of compounds, this reaction involves deboronation of the carborane cage. Hydrazine is electron-rich so there was always the possibility that the carborane cage, particularly *ortho*- although to a lesser extent *meta*-carborane, would be attacked and deboronated as a result of the basicity associated with the hydrazine functionality. The predominant result of reactions between carboranyl triazines and hydrazine derivatives is deboronation.

18.3.2 Thermal Stability of tri-carboranyl triazines

Carboranes are reasonably thermally stable but they have been shown to undergo thermal rearrangement to higher isomers, and reverse isomerisation from *para* to *meta*. (Zakharkin *et al.*, 1967). Unsubstituted carboranes have been shown to transform to higher isomers at 723 K and 893 K for the *ortho* to *meta* and the *meta* to *para* conversions, respectively. The first of these is quantitative, but the *meta* to *para* rearrangement is relatively inefficient, and there a large amount of cage degradation also occurs.

Para-carboranyl derivatives cannot be converted to a higher isomer, and are known to be thermally stable. To investigate its thermal stability, 1,3,5-tri-(*para*-carboranyl)-benzene , which has been shown to pack in sheets, was heated in a furnace to 1473 K under a flow of argon, to give a clear, colourless hard film on the surface of the quartz sheet used to support the sample. On exposure to air over prolonged periods of time (3days or more), this film became opaque, white and began to flake.

X-ray photoelectron spectroscopy (X.P.S.) conducted on the film produced after heating to 1473 K, as a clear, colourless film on quartz and on tape had observed peaks attributable to oxygen 1s, carbon 1s, boron 1s and silicon 2p. Unfortunately the elemental analysis of the product could not be calculated accurately, as it was unknown what percentage of the oxygen was attributable to the silica of the quartz plate or tape from which the measurement was recorded. The presence of carbon suggested that boron oxide was not the unique product. The carbon trace showed a "hump", indicative of bound carbon, possibly to boron. Boron was represented by a small peak. In XPS, the peak heights are not indicative of the quantity of each element present, as different nuclei have varying sensitivities. The elemental composition of a sample can be obtained by the multiplication of peak area by the relative sensitivity.

Two experiments were also conducted on 2,4,6-tri-(*para*-carboranyl)-1,3,5-triazine at elevated temperature and pressure. The first raised the temperature of the autoclave to 623 K and a pressure of 70 bar for 12 hours, the second to 673 K and 63 bar for 15 hours. (The melting point of the compound was 649 K.) No change in the compound was observed on either occasion. Graphite, which has a similar layered sheets structure is converted to diamond at 1000 K and 104 bar.

18.4 DIFFRACTION STUDIES OF TRIAZINES

18.4.1 X-ray structure of 2.4.6-tris-(2'-Phenyl-*ortho*-carboranyl)- 1.3.5-triazine

If the orientation of the R group itself is not taken into account then there are two possible isomers of this compound in the solid state, one in which two phenyl groups are directed upwards and the other down relative to the plane, and one in which all three phenyl groups face upwards, see Figure 18.2. In this case consideration of the phenyl groups twisting or the degree at which they are directed up or down is not taken into account, if it were there would be an infinite number of possibilities. The isomer with "three up" is the structure that has been seen. This isomer has been solved previously for the benzene analogue, 1,3,5-tri-(2'-phenyl-*ortho*-carboranyl)-l ,3,5 benzene (II), of this compound (Herbertson, 1995).

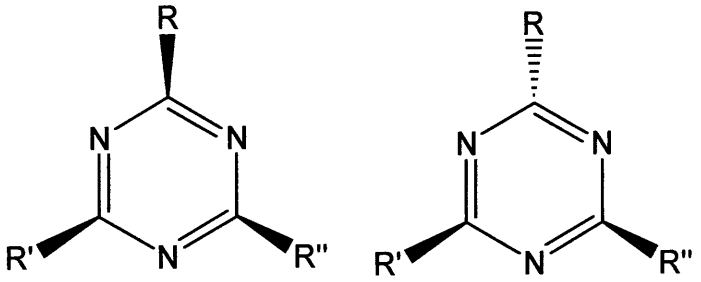

Figure 18.2 The two possible isomers of trisubstituted 1, 3, 5-triazines

This compound crystallizes in the space group R-3, which is the same as its benzene analogue. The unit itself is shown in Figure 18.3, and the three-fold symmetry is easily seen in the structure (see Figure 18.4). All three phenyl groups face upwards, lying above and leaning in towards the plane of the central triazine ring.

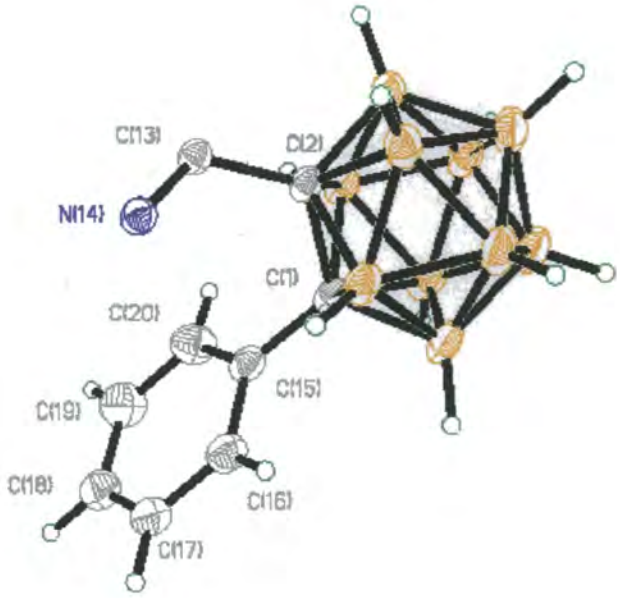

Figure 18.3 The asymmetric unit of 2,4,6-tris-(2'-diphenyl-*ortho*-carboranyl)- 1,3,5-triazine, with thermal ellipsoid probability of 50 %

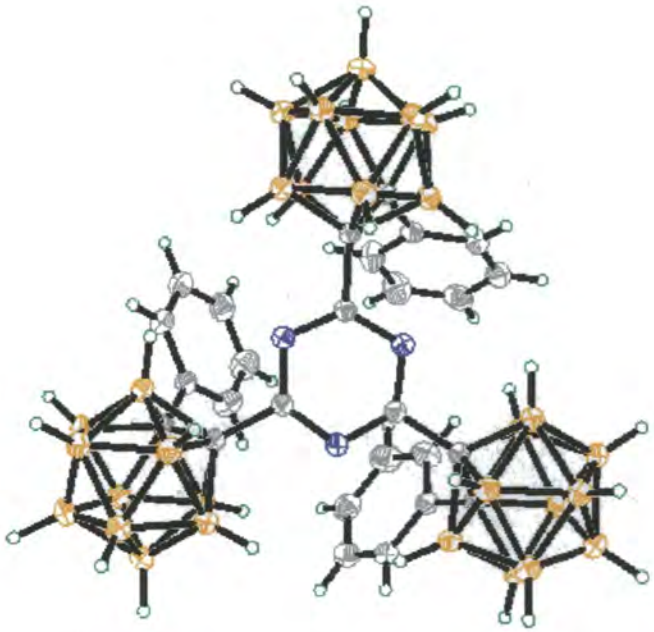

Figure 18.4 The structure of 2,4,6-tris-(2'-diphenyl-*ortho*-carboranyl)- 1,3,5-triazine expanded for the whole molecule, clearly showing the three fold symmetry.

Since the electron withdrawing influence of the carborane cage is the same on each carbon of the triazine ring, no C_3N_3 ring distortion was expected or observed. The (C-N) bond lengths within this ring were found to be standard for any symmetrically substituted 1,3,5-triazine in the range of 1.336(2) Å and 1.340(2) Å. The C-N-C internal ring angle was smaller than the N-C-N ring angle due to the external lone pair on the ring nitrogen. It is clear that the ring is not uniform in the distribution of bond lengths and angles and as a result some of the aromaticity must subsequently be lost. Due to the steric bulk of the carborane groups, the triazine ring distances and angles could quite easily be distorted,. What is seen is that the angles observed were typical of symmetrically substituted 1,3,5-triazines, where the internal ring angles C-N-C and N-C-N are usually within the ranges 112-117° and 123-128° respectively ((Belitskus *et al.*, 1965), (Bullen *et al.*, 1972) and (Brown, *et al.*, 1976)).

The carboranyl cage carbon to triazine ring bond length showed no deviation, at 1.510(2) Å, from the cage carbon to central benzene ring, (1.509(3) Å). The cage carbon to phenyl ring distance typically varies only slightly with a second substituent on phenyl-*ortho*-carboranyl derivatives, with the second substituent having very little influence on the *exo* cage C-phenyl bond length, (see table 18.1, for a summary of the bond lengths and angles).

Bond	Length (Å)
C1-C2	1.686(2)
C1-C15	1.511(2)
C2-C13	1.510(2)
C13-N14	1.336(2); 1.340(2)
Torsion Angles	(°)
N14,C13,C2,C1	63.8
C13,C2,C1,C15	0.2

Table 18.1 Summary of selected bond lengths and torsion angles

As discussed previously the cage carbon-carbon distances can indicate of the amount of electron density available for cage bonding. Typically, if the cage is electron rich, the cage C-C distance will lengthen and the cage will become more open. If electron density is drawn out of the cage by an exo substituent, the opposite is true. In the crystal structure the cage C-C distance for the triazine derivative was 1.686(2) Å. This is in contrast to diphenyl-*ortho*- carborane where the cage C-C bond was lengthened as a result of steric repulsions between the two phenyl groups (Lewis and Welch, 1993), the tri-(phenyl-*ortho*-carboranyl)-benzene and triazine derivatives were

twisted and so these types of repulsions were kept to a minimum. However, comparison with 1-phenyl-*ortho*-carborane, where the cage C-C bond was 1.640(5) Å (Brain *et al.*, 1996) showed there was possibly a degree of steric repulsion present which could break bonds and open the cage. Within the cage itself, the only bond found to be reduced with respect to diphenyl-*ortho*-carborane is the cage C-C distance. Although, the distances from the triazine substituted carbon to the upper CB4 face layer were more or less the same as those of the diphenyl-*ortho*-carborane, every other cage connectivity was longer. This gave a larger cage size and was consistent with the VSEPR bonding principle of less electron density forming a longer, weaker bond. Generally, there is less electron density available for cage bonding, although the electronic distribution may have the most density focused on the cage carbons and the least on the antipodal atoms, resulting in very slight cage distortion.

Within the crystal lattice, the molecules packed in pairs with the C_3N_3 rings lying in parallel planes and with the phenyl groups of one molecule all oriented upwards, whilst those of the second molecule face down. Layers of these pairs formed stacks with the C_3N_3 rings forming a channel surrounded by phenyl-carboranyl groups.

18.4.2 X-ray structure of 2,4,6-tris-(2'-phenyl-*para*-carboranyl)-1,3,5-triazine.

This compound was expected to follow previous examples already discussed and crystallize from $CDCl_3$ as solvent, with three fold, R-3 space group as might have been expected. However this is not the case and it crystallized in the P-1 space group where one of the three phenyl groups was twisted at 90° to the other two, which lie in the plane of the C_3N_3 central ring. This configuration is common with molecules with a C_{3v} symmetry. The main reason for the lack of symmetry in the structure is due to the presence of disordered solvent molecules in the unit cell. These are situated in such a position that all potential space group symmetry of the triazine molecule is lost.

All of the B-B and C-B connectivities were within accepted ranges, from 1.75(2)-1.82(2) Å and 1.686(13)-1.749(13) Å, respectively. Perturbations were not observed in the phenyl groups. There are no significant differences observed between the bond lengths of the three cages.

The structure of 2,4,6-tri-*para*-carboranyl-1,3,5-triazine has been shown, by means of X-ray powder diffraction, to pack in sheets. The phenyl-*para*-carboranyl derivative also packs in sheets, with the perpendicular phenyl group slotted in between the other two phenyl-*para*-carboranyl groups of the next molecule in a head-to-tail manner, the layers above and below running in the opposite direction. (see Figure 18.5)

The dissimilar electron withdrawing potentials of the two carborane isomers are manifested in the crystal structures of the two tri-(carboranyl)-triazines studied. Comparison of this structure with that of the *ortho*-isomer showed virtually no difference in the bond lengths and angles of the central C_3N_3 ring. Since the triazine was symmetrically substituted in each example, this was perhaps not surprising.

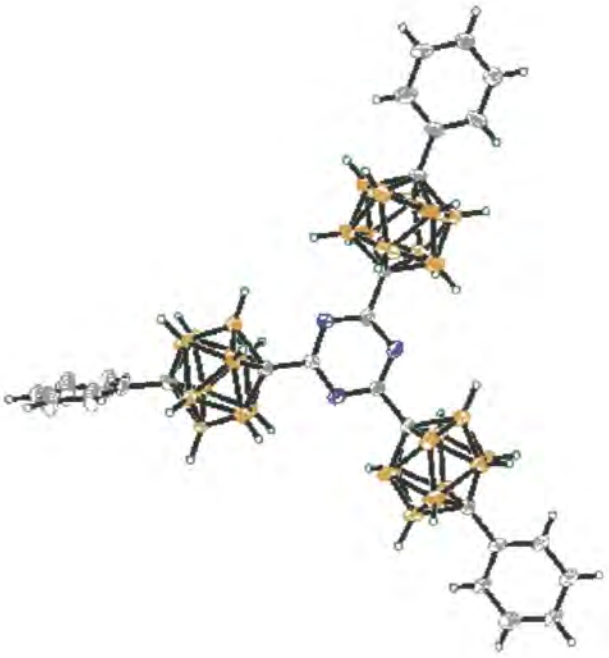

Figure 18.5 The structure of 2,4,6-tris-(2'-phenyl-*para*-carboryl)-1,3,5-triazine with 50% thermal ellipsoids. Disordered solvent is not shown.

18.5 HIGH PRESSURE EXPERIMENTS

Two experiments were carried out under the supervision of Mr. D. Hunter of Durham University, with 2,4,6-tri-*para*-carboranyl)-1 ,3,5-triazine. In both the sample was placed inside a glass sleeve inside an autoclave under a positive nitrogen pressure. The sample (0.1079g) was taken to a maximum pressure of 70 bar at 623 K for 15 hours. The final product was slightly yellow compared to the white starting material, but no change in the compound was noted.

The run was repeated with a pressure of 63 bar and a temperature of 673 K. Again, no change was observed.

18.6 SUMMARY

The synthesis, properties and structures of a novel group of compounds, the mono-, di- and tri-(carboranyl)-1,3,5-triazines, have been investigated in this chapter.

The synthesis of 2,4,6-tri-(carboranyl)-1,3,5-triazines has been shown to be facile, this being the unique multi-carboranyl product from the reaction of lithio-*ortho*-, *meta*- or *para*- substituted or unsubstituted carborane with cyanuric chloride. Their synthesis has been shown to be far simpler and higher yielding than the analogous benzene derivatives, where the products are obtained from reaction of a decaborane adduct with an acetylene, or through copper- or palladium-catalyzed coupling reactions. Carboranyl triazines were synthesized by first derivatising the triazine, and mono-carboranyl triazines often were formed from reaction of a triazinyl-acetylene with a decaborane adduct. In these compounds, the presence of inter-molecular hydrogen bonding interactions was postulated. A structural investigation of these insoluble compounds, namely 2,4,6-tri-(*meta*- and *para*-carboranyl)-1,3,5-triazines, has shown them to pack in planes. The same layers were observed for 1,3,5-tri-(*para*-carboranyl)-benzene, which has no potential to hydrogen bond. This suggested it was the size and shape of the molecules, and not the hydrogen bonding interactions, which directed the packing arrangement.

An X-ray diffraction study of 2,4,6-tri-(2'-phenyl-*ortho*-carboranyl)-1,3,5-triazine has shown the crystal structure to be of the same nature as the benzene analogue. Crystals of the *para*-isomer reveal it to pack as interlocking molecules in a layer arrangement.

The tri-carboranyl triazines were stable compounds, both thermally and chemically. The triazine ring remained intact when the compound was reacted with hydrazine derivatives. Similar conditions were known to cleave the C_3N_3 ring in organic systems. The transformation of 1,3,5-triazine to the *meta* isomer occurs at 673 K. The *para* isomer has disordered solvent present in the X-ray structure and therefore has high experimental error. The absorption coefficient is much greater for the *para* isomer and this is due to the presence of the solvent and the solvent dramatically decreases the quality of data, this is seen when comparing to the *ortho* isomer. The crystallographic data is summarised in Table 18.2. However the structure is of high enough resolution to compare it with the analogous structures in this chapter.

	2.4.6-tris-(2'-triphenyl-*ortho*-carboranyl)- 1.3.5-triazine - (I)	**2,4,6-tris-(1, 2'-phenyl-*para*-carboranyl)-1,3,5-triazine**
Formula	$C_{27}H_{45}B_{30}N_3$	$C_{31}H_{13}B_{30}N_3O_2$
Formula Weight	735.96	783.64
Crystal Dimensions (mm)	0.4 x 0.35 x 0.35	0.4 x 0.2 x 0.1
Temperature (K°)	150(2)	293(2)
Wavelength (Å)	0.71073	0.71073
Crystal System	Trigonal	Triclinic
Space group	R-3	P-1
a= (Å) b= (Å) c= (Å) α= (°) β= (°) γ= (°)	19.815(1) 19.815(1) 18.159(1) 90 90 120	7.24(14) 15.95(3) 20.93(4) 78.06(3) 80.50(3) 81.55(3)
Volume (A^3)	6175.2(7)	2319.1(8)
Z	6	2
Calculated Density (Mg/m^3)	1.187	1.223
Absorption Coefficient (mm^{-1})	0.058	0.720
F (000)	2268	838
θ Range for Collection (°)	1.63 to 27.47	1.00 to 30.51
Index Ranges	-17<=h<=25, -25<=k<=23, -22<=l<=23	-10<=h<=10, -22<=k<=21, -29<=l<=16
Reflections collected	14445	19334
Independent reflections	3147	12364
Data/restraints/ Parameters	3107 / 0 / 241	12364 / 0 / 588
Goodness-of-fit on F^2	1.143	1.570
Final R indices [I>2sigma(I)]	0.0433	0.2257
R indices (all data)	0.1411	0.4475
Largest diff. Peak and hole ($e.A^{-3}$)	0.241 and -.246	1.423 and -0.500

Table 18.2 X-ray diffraction data

18.7 REFERENCES

1. Boyd, L., *PhD. Thesis*, University of Durham, **1997**.
2. Boulton A.J.; McKillop A., *Comprehensive Heterocyclic Chemistry*, **1984**, Pergamon Press.
3. Henderson, K.; MacNicol, D. D.; Mallinson P.R., Valiance, I., *Supramolecular Chem.*, **1995**, 5, 301.
4. Keck, J.; Kramer, H.E.A.; Port, H.; Hirsch, T.; Fischer, P.; Rytz, G., *J. Phys. Chem.*, **1996**, 100, 14368.
5. Chan, C.-W.; Mingos, D.M.P.; White, A.J.P.; Williams, D.J., *J. Chem. Sec., Dalton Trans.*, **1995**, 2469.
6. Yang, C.; Chen, X.-M.; Zhang, W.-H. J. Chen, Y.-S. Yang, M.-L. Gong, J. *Chem. Soc., Dalton Trans.*, **1996**, 1767.
7. Yonehara, H.; Kang, W.-B. ; Kawara, T.; Pac, C., *J. Mater. Chem.*, **1994**, 4, 1571.
8. Smolin, E.M.; Rapoport, L., *Chem. Heterocyclic Compounds*, **1959**, 13, 1.
9. Horrobin, S., *J. Chem. Soc.*, **1963**, 4130.
10. Herbertson, P.L., PhD Thesis, University of Durham, **1995**.
11. Belitskus, D.; Jeffrey, G.A., *Spectrochim. Acta*, **1965**, 21, 1563.
12. Bullen, G.J.; Corney, D.J.; Stephens, F.S., *J. Chem. Soc., Perkin Trans. 2*, **1972**, 642.
13. Brown, D.S.; Lee, J.D.; Russell, P.R., *Acta Cryst.*, **1976**, B32, 2101.
14. Lewis, Z.G.; Welch, A.J., *Acta Cryst.*, **1993**, C49, 705.
15. Brain, P.T.; Cowie, J.; Donohoe, D.J.; Hnyk, D.; Rankin, D.W.H.; Reed, D.; Reid, B.D.;
16. Robertson, H.E.; Welch, A.J.; Hofmann, M.; Schleyer P.v.R., , *Inorg. Chem.*, **1996**, 35, 1702.
17. Grundmann, Ch.; Kreutzberger, A.; *J. Amer. Chem. Soc.*, **1957**, 79, 2839.
18. Grundmann, Ch., *Angew. Chem., Int. Ed. Engl.*, **1963**, 2, 309.
19. Zakharkin, L.I.; Kalinin, V.N.; Podvisotskaya, L.S., *Bull. Acad. Sci. USSR*, **1967**, 2212.

POST GRADUATE COLLOQUIA, LECTURES AND SEMINARS FROM INVITED SPEAKERS

1995

October 11 Prof. P. Luger, Frei Univ Berlin, Germany
Low Temperature Crystallography

October 13 Prof. R. Schmutzler, Univ Braunschweig, Germany.
Calixarene-Phosphorus Chemistry: A New Dimension in Phosphorus Chemistry

October 18 Prof. A. Alexakis, Univ. Pierre et Marie Curie, Paris,
Synthetic and Analytical Uses of Chiral Diamines

October 25 Dr.D.Martin Davies, University of Northumbria
Chemical reactions in organised systems.

November 1 Prof. W. Motherwell, UCL.
New Reactions for Organic Synthesis

November 3 Dr B. Langlois, University Claude Bernard-Lyon
Radical Anionic and Psuedo Cationic Trifluoromethylation

November 8 Dr. D. Craig, Imperial College, London
New Stategies for the Assembly of Heterocyclic Systems

November 15 Dr Andrea Sella, UCL, London
Chemistry of Lanthanides with Polypyrazoylborate Ligands

November 17 Prof. David Bergbreiter, Texas A&M, USA
Design of Smart Catalysts, Substrates and Surfaces from Simple Polymers

November 22 Prof. I Soutar, Lancaster University
A Water of Glass? Luminescence Studies of Water-Soluble Polymers.

November 29 Prof. Dennis Tuck, University of Windsor, Ontario, Canada
New Indium Coordination Chemistry

December 8 Professor M.T. Reetz, Max Planck Institut, Mulheim
Perkin Regional Meeting

1996

January 10 Dr Bill Henderson, Waikato University, NZ
Electrospray Mass Spectrometry - a new sporting technique

January 17 Prof. J. W. Emsley , Southampton University
Liquid Crystals: More than Meets the Eye

January 24 Dr Alan Armstrong, Nottingham Univesity
Alkene Oxidation and Natural Product Synthesis

January 31 Dr J. Penfold, Rutherford Appleton Laboratory,
Soft Soap and Surfaces

February 7 Dr R.B. Moody, Exeter University
Nitrosations, Nitrations and Oxidations with Nitrous Acid

February 12 Dr Paul Pringle, University of Bristol
Catalytic Self-Replication of Phosphines on Platinum(O)

February 14 Dr J. Rohr, Univ Göttingen, Germany
Goals and Aspects of Biosynthetic Studies on Low Molecular Weight Natural Products

February 21 Dr C R Pulham , Univ. Edinburgh
Heavy Metal Hydrides - an exploration of the chemistry of stannanes and plumbanes

February 28 Prof. E. W. Randall, Queen Mary & Westfield College
New Perspectives in NMR Imaging

March 6 Dr Richard Whitby, Univ of Southampton
New approaches to chiral catalysts: Induction of planar and metal centred asymmetry

March 7 Dr D.S. Wright, University of Cambridge
Synthetic Applications of Me_2N-p-Block Metal Reagents

March 12 RSC Endowed Lecture - Prof. V. Balzani, Univ of Bologna
Supramolecular Photochemistry

March 13 Prof. Dave Garner, Manchester University
Mushrooming in Chemistry

April 30 Dr L.D.Pettit, Chairman, IUPAC Commission of Equilibrium Data
pH-metric studies using very small quantities of uncertain purity

1996

October 9 Professor G. Bowmaker, University of Auckland, NZ
Coordination and Materials Chemistry of the Group 11 and Group 12 Metals : Some Recent Vibrational and Solid State NMR Studies

October 14 Professor A. R. Katritzky, University of Gainesville,University of Florida, USA
Recent Advances in Benzotriazole Mediated Synthetic Methodology

October 16 Professor Ojima, Guggenheim Fellow, State University of New York at Stony Brook
Silylformylation and Silylcarbocyclisations in Organic Synthesis

October 22 Professor Lutz Gade, Univ. Wurzburg, Germany
Organic transformations with Early-Late Heterobimetallics: Synergism and Selectivity

October 22 Professor B. J. Tighe, Department of Molecular Sciences and Chemistry, University of Aston
Making Polymers for Biomedical Application - can we meet Nature's Challenge?
Joint lecture with the Institute of Materials

October 23 Professor H. Ringsdorf (Perkin Centenary Lecture), Johannes Gutenberg-Universitat, Mainz, Germany
Function Based on Organisation

October 29 Professor D. M. Knight, Department of Philosophy, University of Durham.
The Purpose of Experiment - A Look at Davy and Faraday

October 30 Dr Philip Mountford, Nottingham University
Recent Developments in Group IV Imido Chemistry

November 6 Dr Melinda Duer, Chemistry Department, Cambridge
Solid-state NMR Studies of Organic Solid to Liquid-crystalline Phase Transitions

November 12 Professor R. J. Young, Manchester Materials Centre, UMIST
New Materials - Fact or Fantasy?
Joint Lecture with Zeneca & RSC

November 13 Dr G. Resnati, Milan
Perfluorinated Oxaziridines: Mild Yet Powerful Oxidising Agents

November 18 Professor G. A. Olah, University of Southern California, USA
Crossing Conventional Lines in my Chemistry of the Elements

November 19 Professor R. E. Grigg, University of Leeds
Assembly of Complex Molecules by Palladium-Catalysed Queueing Processes

November 20 Professor J. Earnshaw, Deptartment of Physics, Belfast
Surface Light Scattering: Ripples and Relaxation

November 27 Dr Richard Templer, Imperial College, London
Molecular Tubes and Sponges

December 3 Professor D. Phillips, Imperial College, London
"A Little Light Relief" -

December 4 Professor K. Muller-Dethlefs, York University
Chemical Applications of Very High Resolution ZEKE Photoelectron Spectroscopy

December 11 Dr Chris Richards, Cardiff University
Sterochemical Games with Metallocenes

1997

January 15 Dr V. K. Aggarwal, University of Sheffield
Sulfur Mediated Asymmetric Synthesis

January 16 Dr Sally Brooker, University of Otago, NZ
Macrocycles: Exciting yet Controlled Thiolate Coordination Chemistry

January 21 Mr D. Rudge, Zeneca Pharmaceuticals
High Speed Automation of Chemical Reactions

January 22 Dr Neil Cooley, BP Chemicals, Sunbury
Synthesis and Properties of Alternating Polyketones

January 29 Dr Julian Clarke, UMIST
What can we learn about polymers and biopolymers from computer-generated nanosecond movie-clips?

February 4 Dr A. J. Banister, University of Durham
From Runways to Non-metallic Metals - A New Chemistry Based on Sulphur

February 5 Dr A. Haynes, University of Sheffield
Mechanism in Homogeneous Catalytic Carbonylation

February 12 Dr Geert-Jan Boons, University of Birmingham
New Developments in Carbohydrate Chemistry

February 18 Professor Sir James Black, Foundation/King's College London
My Dialogues with Medicinal Chemists

February 19 Professor Brian Hayden, University of Southampton
The Dynamics of Dissociation at Surfaces and Fuel Cell Catalysts

February 25 Professor A. G. Sykes, University of Newcastle
The Synthesis, Structures and Properties of Blue Copper Proteins

February 26 Dr Tony Ryan, UMIST
Making Hairpins from Rings and Chains

March 4 Professor C. W. Rees, Imperial College
Some Very Heterocyclic Chemistry

March 5 Dr J. Staunton FRS, Cambridge University
Tinkering with biosynthesis: towards a new generation of antibiotics

March 11 Dr A. D. Taylor, ISIS Facility, Rutherford Appleton Laboratory
Expanding the Frontiers of Neutron Scattering

March 19 Dr Katharine Reid, University of Nottingham
Probing Dynamical Processes with Photoelectrons

1997

October 8 Prof. E. Atkins, Department of Physics, University of Bristol
Advances in the control of architecture for polyamides: from nylons to genetically engineered silks to monodisperse oligoamides

October 15 Dr. R. Mark Ormerod, Department of Chemistry, Keele University
Studying catalysts in action

October 21 Prof. A. F. Johnson, IRC, Leeds
Reactive processing of polymers: science and technology

October 22 Prof. R.J. Puddephatt (RSC Endowed Lecture), University of Western Ontario
Organoplatinum chemistry and catalysis

October 23 Prof. M.R. Bryce, University of Durham, Inaugural Lecture
New Tetrathiafulvalene Derivatives in Molecular, Supramolecular and Macromolecular
Chemistry: controlling the electronic properties of organic solids

October 29 Prof. Bob Peacock, University of Glasgow
Probing chirality with circular dichroism

October 28 Prof. A P de Silva, The Queen's University, Belfast
Luminescent signalling systems

November 5 Dr Mimi Hii, Oxford University
Studies of the Heck reaction

November 11 Prof. V Gibson, Imperial College, London
Metallocene polymerisation

November 12 Dr Jeremy Frey, Department of Chemistry, Southampton University
Spectroscopy of liquid interfaces: from bio-organic chemistry to atmospheric chemistry

November 19 Dr Gareth Morris, Department of Chemistry, Manchester Univ.
Pulsed field gradient NMR techniques: Good news for the Lazy and DOSY

November 20 Dr Leone Spiccia, Monash University, Melbourne, Australia
Polynuclear metal complexes

November 25 Dr R. Withnall, University of Greenwich
Illuminated molecules and manuscripts

November 26 Prof. R.W. Richards, University of Durham, Inaugural Lecture
A random walk in polymer science

December 2 Dr C.J. Ludman, University of Durham
Explosions

December 3 Prof. A.P. Davis, Department. of Chemistry, Trinity College Dublin.
Steroid-based frameworks for supramolecular chemistry

December 10 Sir Gordon Higginson, former Professor of Engineering in Durham and retired Vice-Chancellor of Southampton Univ.
1981 and all that.

December 10 Prof. Mike Page, Department of Chemistry, University of Huddersfield
The mechanism and inhibition of beta-lactamases

1998

January 14 Prof. David Andrews, University of East Anglia
Energy transfer and optical harmonics in molecular systems

January 20 Prof. J. Brooke, University of Lancaster
What's in a formula? Some chemical controversies of the 19th century

January 21 Prof. David Cardin, University of Reading

January 27 Prof. Richard Jordan, Dept. of Chemistry, Univ. of Iowa, USA.
Cationic transition metal and main group metal alkyl complexes in olefin polymerisation

January 28 Dr Steve Rannard, Courtaulds Coatings (Coventry)
The synthesis of dendrimers using highly selective chemical reactions

February 3 Dr J. Beacham, ICI Technology
The chemical industry in the 21st century

February 4 Prof. P. Fowler, Department of Chemistry, Exeter University
Classical and non-classical fullerenes

February 17 Dr S. Topham, ICI Chemicals and Polymers
Perception of environmental risk; The River Tees, two different rivers

February 18 Prof. Gus Hancock, Oxford University
Surprises in the photochemistry of tropospheric ozone

February 24 Prof. R. Ramage, University of Edinburgh
The synthesis and folding of proteins

February 25 Dr C. Jones, Swansea University
Low coordination arsenic and antimony chemistry

March 4 Prof. T.C.B. McLeish, IRC of Polymer Science Technology, Leeds University
The polymer physics of pyjama bottoms (or the novel rheological characterisation of long branching in entangled macromolecules)

March 11 Prof. M.J. Cook, Dept of Chemistry, UEA
How to make phthalocyanine films and what to do with them.

March 17 Prof. V. Rotello, University of Massachusetts, Amherst
The interplay of recognition & redox processes - from flavoenzymes to devices

March 18 Dr John Evans, Oxford University
Materials which contract on heating (from shrinking ceramics to bullet proof vests)

ACKNOWLEDGEMENTS

Chapters involving carboranes were conducted in collaboration with Thomas Hibbert, Lynn Boyd, Mark Fox, Hugh M^{ac}Bride, Mathew Davidson and Kenneth Wade of the University of Durham and it has been their synthesis of the carbaborane compounds and spectroscopic analysis I have used in chapters 14-18. I would further like to give thanks to the "Wade group" for their help and endeavor.

Chapters 6-8 were conducted in collaboration with Peter Wan, Li Daio, Z. Chen and Jijian Shi of the University of Victoria, BC, Canada and the synthesis of these compounds, photochemistry and spectroscopic analysis was conducted by them, many thanks to them for letting me be part of this research. I would especially like to thank Peter Wan for his help and advice, specifically with chapters 10-13.

Synthesis of compounds and spectroscopic analysis, in chapter 9, was conducted by Otto Meth-Cohn and Nicola J. R. Williams.

Thanks to Peter Ford for his help with the computers, Mike Leech for his help with the low temperature experiments and the computers, Roy Copley, Andrei Batsanov and Vanessa Hoy for help solving those difficult structures, Clair Bilton for helping with the database searches and results, Dima Yufit for loads.
And for advice, help and guidance a big Thankyou to everybody in the lab.

For help when I first arrived and the times in the bridge Garry Thomas Smith.
Desmasiados Gracias a Carl M^{c}Bride for those times in numerous establishments as well as the house and much more.
Thanks to Dave Tottman for his help with the graphs and spreadsheets.

I am indebted to Judith A. K. Howard for her belief, guidance, friendship and support, especially when times were difficult.

More thanks than I can possibly express on a page of paper to Heather Sutton for absolutely everything.

And finally I would like to thank my father who made everything I have achieved and will continue to achieve possible. I am forever indebted.